Pulsation of Solar-type Stars

Dissertation

Zur Erlangung des Doktorgrades an der
Formal- und Naturwissenschaftlichen Fakultät der
Universität Wien

Eingereicht von

Günter Houdek

Institut für Astronomie
Türkenschanzstr. 17
A-1180 Wien

Dezember 1996

meinen Eltern

1. Introduction

It has been one of the most exciting and challenging tasks for humanity to understand the nature of the Universe. Modern astronomy revealed us the existence of myriad of Galaxies and that each of them are comprised of billions of stars. Our chronological perception of the Universe depends crucially on the history of Galaxies and thus on the evolution and age of stars. Moreover, the vast progress in modern astrophysics has led us to the common belief that the synthesis of almost all chemical elements is supposed to take place inside the stars. We may therefore indeed call ourself 'Children of the Universe' as it is mentioned in the beautiful poem *Desiderata*[1] and which has been set to music by many composers. Furthermore, the study of stellar structure and evolution will provide us with a deeper insight into the physical properties of the matter prevailing in stars by comparing theoretical models with observations. However, stellar models are not well constrained by the usual observational quantities such as apparent brightness and surface values of gravity, temperature and composition. In particular, the present state of stellar modelling suggests that there is still an uncertainty of a factor of at least 2 in the rate of heavy element production, for example.

To obtain a better understanding of the physical processes in stellar interiors we need additional observational informations about the inner structure of stars at different stages of evolution. Interestingly, in the nineteenth century, Auguste Comte[2] argued that humanity would never gain the knowledge of the internal structure of the stars. Because they are so far beyond our earthly grasp, these celestial worlds would forever remain unfathomable and mysterious. In spite of this strong pronouncement, stars with periodically varying luminosity, which were already discovered in the sixteenth century[3], have inspired astronomers to investigate this phenomena in more detail; this has led to a relatively small, but highly important, area of modern stellar astrophysics: the study of pulsating stars. At the beginning of this century, astronomers have been able to understand the observed variations in such stars, the so called classical pulsating variables, in terms of periodic expansions and contractions of the stellar matter itself and that the observed pulsation period corresponds to the fundamental radial mode. Moreover, the pulsation period can be defined by means of the basic stellar parameters and essentially provides an estimate of the star's mean density, an intrinsic property, which may not have been obtained from the usual observational quantities. Some of those classical pulsating variables, such as the double-mode Cepheids, are pulsating in two different modes, and then the stellar mass can be determined as one more item of information from the pulsations in addition to the mean density. Thus the amount of information derived from the pulsation increases with the observed pulsating modes in the star. Obviously, the observed amplitudes of these classical pulsating variables are large, a property which has led to their early detection. With the rapid progress in observation techniques, low amplitude pulsations were discovered in the Sun in the early sixties and were identified, a few years later, as global non-radial oscillations with high spherical harmonic degree l and with many thousands of periods (this

[1] "...you are a child of the Universe, no less than the trees and the stars...";
the text was found in the Church of St. Paul in Baltimore in 1692.

[2] French philosopher (1798-1857), from his notes about *Cours de philosophie positive* (1830-1842).

[3] the Mira *o* Ceti in 1596 by Fabricius (Ledoux & Walraven 1958)

particular new discipline in astrophysics has been given the name *helioseismology*). The richness of non-radial modes compared with radial pulsation has made it possible to measure properties of the solar interior with unprecedent detail providing an excellent check of the theory of solar structure and evolution. Since the Sun represents only one particular star with a relatively simple structure, the possibility of a seismological approach to stars in general is a very powerful potential tool to obtain similar information about the internal structure of other stars and represents the new field of *asteroseismology*.

In addition to the observed frequencies, measurements of amplitudes, line widths (or damping rates) and phases between various types of oscillations provide important information about the underlying mechanism responsible for the excitation of the observed pulsations. The excitation mechanisms for various types of pulsating stars are of different physical nature. Solar-type stars and red giants, for example, exhibit very huge convectively unstable surface layers. These layers are believed to be responsible for driving the pulsation to the comparatively small amplitudes in the very broad frequency-domain, as observed in the Sun.

It is the main subject of this thesis to investigate the properties of solar-like oscillations. In particular the theoretical estimates of damping rates and pulsation amplitudes of main-sequence stars with masses of $(0.9 - 2.0)\, M_\odot$ could aid the selection process of solar-type stars to observe. Moreover, if one day unambiguous amplitude measurements of solar-like oscillations in other stars will be available, the data may help constrain and improve prescriptions for convection. Of particular interest will be a better understanding of the physics describing the interaction between pulsation with the turbulent velocity field as considered in the present computations by means of a non-local, time-dependent mixing-length theory.

1.1. Overview

In the following I shall give a brief overview of the fundamental mechanisms of stability relevant for the star's equilibrium state and the basic properties of stellar pulsations. As important, however, is the mechanism of convective heat transport and its interaction with the oscillations for the stability analyses of solar-type stars and for classical pulsation variables with relatively low surface temperatures. Thus in Section 2 various formulations of turbulent flow and their assumptions are reviewed as they are implemented in many of todays available stellar evolution codes and in particular in the computations used in this thesis. Section 3 investigates the physical processes which are responsible for pulsational damping and driving in stars with distinctive convection zones in the outer layers as well as their influence upon the oscillation frequencies. In addition, theoretical damping rates and their dependence on pulsation frequency and model parameters are discussed. The results of the theoretical amplitude predictions for velocity and luminosity variations are presented in Section 4 for stars evolving along the main-sequence. Also discussed are overstable modes, as observed in the classical pulsating variables of δ Scuti stars, and their dependence on the control parameters used in stellar evolution theory. Section 5 considers amplitude ratios and phases between various types of oscillations in the solar atmosphere by comparing model results with observations. Finally, implementation details of the model computations are addressed in the Appendix.

1.2. A Short Historical Review on Helioseismology

The epoch-making discovery of the five-minute oscillations in the Sun was reported more than thirty years ago by Leighton, Noyes & Simon (1962). They observed periodic Doppler velocity signals obtained from spectroheliograms recorded simultaneously in the red and blue wings of spectral lines. Since then many attempts have been made to explain the observed oscillations. The correct nature of the oscillations was first proposed by Ulrich (1970a) and Leibacher & Stein (1971), who suggested that the oscillations are acoustic modes trapped in the outer layers of the Sun. The observational confirmation for this physical picture was given first by Deubner (1975). He demonstrated that the power in the five-minute oscillations of high-degree modes ($l \gtrsim 200$) are indeed concentrated along slanted ridges (showing modes with like radial order n) when plotted as function of the horizontal spatial wavelength, and the temporal frequency, ν, representing the so-called diagnostic diagram.

It became evident that the observed frequencies of the oscillations can be used as a diagnostic tool of the Sun's interior, which led to the first tentative comparisons of measured frequencies with those of solar models (e.g. Scuflaire *et al.* 1975; Christensen-Dalsgaard & Gough 1976). The definite confirmation that solar oscillations are normal modes of the whole Sun was demonstrated by Claverie *et al.* (1979) who observed low degree modes ($l \lesssim 3$) in the integrated sunlight of whole-disk Doppler measurements. The individual modes in the observed power spectrum were resolved by Grec, Fossat & Pomerantz (1980) obtained from about 120 hours of continuous time-series measurements at the geographical South Pole.

The gap between low-degree and high-degree oscillation measurements was filled by Duvall & Harvey (1983, 1984) with observations of intermediate degree modes ($3 \lesssim l \lesssim 200$). These measurements provided data accurate enough for individual mode identifications of radial and low-degree oscillations and for crude estimates of line widths, as obtained from fitting line-profile functions to the individually resolved modes in the power spectrum. More thorough measurements of line widths and amplitudes were reported by Libbrecht (1988) and Libbrecht & Woodard (1991) for low-degree l modes and by Elsworth *et al.* (1990) for the $l = 0$ mode.

A major progress in obtaining high-precision data was accomplished with the establishment of networks of observing stations, suitably placed around the world. Such networks enable us to obtain continuous observations over very long periods, which are in particular required for accurate measurements of mode properties at relatively low frequencies. Several of such networks have been established (e.g. Pallé 1996). One of it, the GONG[4] project, involves six observing sites and became operational in October 1995. Additional high quality data of low-order and high-degree modes are expected from the GOLF[5] (Gabriel *et al.* 1991) and SOI-MDI[6] (Scherrer, Hoeksama & Bush 1991) instrument, respectively, mounted on the SOHO[7] spacecraft, which was launched in December 1995.

[4] Global Oscillation Network Group

[5] Global Oscillations at Low Frequency

[6] Solar Oscillations Investigation-Michelson Doppler Imager

[7] SOlar and Heliospheric Observatory

1.3. Stability and Oscillation of Stars

This section gives a short overview of the fundamental mechanisms of stability relevant for stars and a brief discussion of the physical properties of solar and stellar oscillations. A more complete and detailed discussion of the theory of stellar pulsations may be found in the monographs of Cox (1980) and Unno *et al.* (1989). Recent reviews on solar and stellar oscillations are given for example by Gough & Toomre (1991), Christensen-Dalsgaard & Berthomieu (1991) and Christensen-Dalsgaard (1996).

1.3.1. Stellar stability

During its life a star experiences different stages of evolution at which small perturbations applied to its equilibrium state may grow or decay rapidly in time compared to the evolutionary changes of the star's characterizing parameters (e.g. its chemical composition). The equilibrium state of a star is determined by three fundamental stability criteria: the dynamical stability, the thermal (secular) stability and the vibrational (pulsational) stability. Dynamical stability is governed by gravitational forces working against the pressure forces of the gas in the absence of any heat exchange. Thus dynamical stability is maintained if the pressure gradient increases more rapidly during an accidental compression of the star than the gravitational forces, leading to an oscillatory motion. Convectively unstable layers in a star, for example, represent local dynamical instability against non-radial perturbations, where buoyancy is the responsible mechanism for driving the motion. Indeed, there is a close relation between convective motion, which can be described by a superposition of Fourier modes in the theory of linear stability (e.g. Ledoux, Schwarzschild & Spiegel 1960), and non-radial oscillations of gravity modes in convectively stable layers (see below).

Non-adiabatic effects influence thermal and vibrational stability, which are usually determined by a much longer time scale relative to the dynamical time scale. Thus the latter two types of stability are reasonably defined only in a dynamically stable system. The state of thermal stability is closely connected with the virial theorem (e.g. Collins 1978), which relates the gravitational and thermal properties of the star. An arbitrary small heat excess in an ideal gas sphere leads to an expansion of the sphere. However, more energy is needed by this expansion process than was originally available by the heat excess and has therefore to be taken from the internal energy of the gas. This leads to a decrease of the temperature and thermal stability is obtained. In degenerate matter an excess of thermal energy, such as through the ignition of helium in a degenerate core, leads to a thermal runaway, known as the flash phenomenon (helium flash). Such a thermal runaway is also observed in non-degenerated shell sources, where the hydrostatic adjustment to a heat excess in a thin shell provides only a negligible change in the pressure promoting a further temperature increase.

In a dynamically stable system an induced perturbation results in an oscillatory motion around the equilibrium configuration, as already stated before. Heat exchange with the surroundings alters the kinetic energy of this oscillatory motion and thus its amplitude. If the amplitude grows in time, the oscillation of a system is said to be overstable or pulsationally (vibrationally) unstable and to be damped if the amplitude declines with time. The investigations of the physical processes responsible for damping and driving of these oscillations in stars with convective outer layers are the main subject of this thesis.

1.3.2. Basic theory of solar-like oscillations

The patterns of the velocity field as observed on the solar surface result from the interference between $\sim 10^7$ resonant global oscillation modes. Each of these modes can be interpreted as a resonant standing wave whose oppositely directed traveling constituents propagate in a well defined resonant cavity beneath the photosphere. Outside these resonant cavities the modes tunnel through evanescent regions such as the visible atmosphere where they can be observed. The amplitudes of the observed oscillations are rather small and may therefore be described by a linear theory. Thus assuming further spherical symmetry and a time-independent background state, the modes can be written as the product of a function describing the spatial variation by means of a radial function and spherical harmonics, and a sinusoidal function of time t with frequency ω. For a linearly damped or excited mode the velocity field can be written as

$$V_{nlm} = \hat{V}_{nlm}\,\mathrm{Re}\left\{\left[\xi_{r,nl}\left(r\right)\mathbf{a}_r + \xi_{h,nl}\left(r\right)\left(\frac{\partial}{\partial\theta}\mathbf{a}_\theta + \frac{\partial}{\sin\theta\,\partial\varphi}\mathbf{a}_\varphi\right)\right] Y_l^m\left(\theta,\varphi\right)e^{-i\omega_{nl}t}\right\}, \quad (1.1)$$

where Re{} denotes the real part of a complex function, θ and φ are the co-latitude and longitude, $Y_l^m(\theta,\varphi)$ is a spherical harmonic of degree l and azimuthal order m, ξ_r and ξ_h are the radial and horizontal displacement eigenfunctions, and $\mathbf{a}_r$, $\mathbf{a}_\theta$ and $\mathbf{a}_\varphi$ are unit vectors in r-, θ-, and φ- directions. The spherical degree l can be interpreted as the total number of nodes around the surface, whereas the number of nodes along the equator is given by m and along the meridian by $l-m$. Since we assumed spherical symmetry, the physics of the oscillations must be independent of the choice of the axis $\theta = 0$, and thus the eigenfunctions ξ_r and ξ_h and the complex eigenfrequency ω are independent of, but degenerate by $(2l+1)$-folds in m. The complex eigenfrequency ω is written as $\omega = \omega_r + i\eta$, where ω_r and η are real. The damping or growing rate η can be interpreted as a characteristic time, $|\eta|^{-1}$, the so-called mode lifetime, at which the mode amplitude changes its value by a factor e.

Non-radial modes are governed by two physical processes which can act as restoring forces for the oscillations: gas pressure and buoyancy. Waves whose restoring force is predominantly the gas pressure are acoustic or pressure waves with normal modes called p modes. These acoustic waves propagate in well defined spherical shells (resonant cavities). The upper boundary of such a cavity is located near the surface, where an incident wave is reflected back downward by the steep density gradient there. Above a certain frequency, the so-called acoustical cut-off frequency, ω_{co} (Lamb 1909), the wavelength of the incident sound wave becomes smaller than the length-scale associated with density changes of the background medium, and the wave propagates outward into the atmosphere. Thus p modes with frequencies above ω_{co} are no longer trapped inside the star. The lower boundary or turning point of trapped acoustic waves depends on their cyclic frequency $\nu = \omega/2\pi$ and degree l. Purely radial modes penetrate to the centre, whereas non-radial modes are reflected upward at a point where the waves are propagating horizontally. This comes about because the deeper portions of the wavefronts are traveling at a faster sound speed $c \propto \sqrt{T}$ (and the temperature T increases with depth), causing a downward propagating wave to be progressively refracted around until it is once more headed upward. The lower turning point r_t can be derived from the dispersion relation for a sound wave and occurs a the depth $r_t = c(r_t)L/\omega$, where $L = \sqrt{l(l+1)}$. Thus modes with like ν/L penetrate to like depths. The period of a trapped sound wave is determined by its travel time between

the turning points, and this is controlled by the varying sound speed c at which that wave propagates. The observed cyclic frequency ν of p modes therefore provides a mean measure of c within the depth range of the cavity.

Resonant cavities also exist for internal gravity waves. The restoring force of gravity waves is predominantly buoyancy, acting on the density perturbation, and whose normal modes are therefore called g modes. The boundaries of the region where gravity waves can propagate are determined by the local buoyancy (or Brunt-Väisälä) frequency N. This is the adiabatic frequency at which a displaced fluid element would oscillate vertically without displacing its environment horizontally and which remains in pressure balance with the background fluid. In other words, the shape of this fictitious fluid element would be that of an infinitely thin needle. In reality, however, matter has to be pushed sideways accompanied by a pressure perturbation to provide place for the vertically moving fluid element, which results in a reduction of its oscillation frequency. Moreover, buoyancy can therefore not be a restoring force for purely radial oscillation. The buoyancy frequency is positive in convectively (dynamically) stable zones and imaginary in regions where buoyancy acts to enhance the motion of the displaced fluid parcel, forcing it away from equilibrium. For this case $|N|$ is approximately the reciprocal turn-over time of a convectively unstable fluid element. Thus the upper and lower reflection points of trapped g modes are defined only in purely radiative regions and at a depth where their oscillation frequencies are less then the local buoyancy frequency N. The travel time of a g mode within the resonant cavity and thus its oscillation period depend on the variation of N with depth. In convection zones g modes are evanescent and their amplitudes decay more rapidly with increasing degree l. Thus only modes with low degree are likely to be detectable in the observable layers of stars with distinctive outer convection zones.

The measured frequencies of p modes and g modes of different degree l provide us with detailed information about the variation of c and N over different regions in the star. For the solar case several thousands of p modes have been identified and measured with a relative standard deviation of less than 5×10^{-6} and from which the sound speed variation has been determined with an accuracy of better than 0.5% (e.g. Basu *et al.* 1996). From the observed power spectrum one may obtain yet more information than just the absolute values of the frequencies. The visible peaks in a seismic spectra appear to be almost uniformly spaced, and can be identified as a sequence of $l = 1$ p modes alternating with closely spaced double peaks arising from $l = 2$ and $l = 0$ p modes. From asymptotic theory applied to the frequency set (e.g. Tassoul 1980) one can obtain two parameters describing the so-called large separation of the cyclic frequency $\nu_{n,l}$ of modes of like degree l and adjacent order n and the small frequency separation of the closely spaced peaks which measures $\nu_{n,0} - \nu_{n-1,2}$. These seismic parameters essentially provide information about the gross structure of the star and about the inhomogeneities in the core due to the changes in the mean molecular weight with depth and in particular with age. Obviously, these parameters may help to determine mass and age of solar-type stars (Christensen-Dalsgaard 1988), and are also the most likely obtained parameters from full-disk measurements in integrated light. Observations in light integrated over the stellar disk, as it has to be done for distant stars, provide only information of low degree modes (modes with $l \gtrsim 4$ are canceled out in full-disk measurements). It is, however, the vast number of stars which provides a powerful potential for testing stellar evolution theory by means of a statistical approach (e.g. Fridlund *et al.* 1995).

2. Convection

2.1. Introduction

The temperature in a star is determined by the balance of energy and its gradient depends on the details how energy is transported through out the stellar interior. Red giants and solar-like stars exhibit in the outer layers a substantial convectively unstable zone, where hot elements of gas rise and cold elements sink, dominating the energy transport.

Thermal heat transport is governed by turbulent motion of the underlying fluid or gas. To determine the average of vertical velocity, temperature and momentum fluctuations, the full turbulent flow is needed. This is up today not a tractable theoretical problem without the introduction of some hypothetical assumptions in order to close the system of equations describing the turbulent flow. Such closure models can be classified basically into four categories: the *algebraic model* including the mixing-length approach (e.g. Prandtl 1925), the *one-equation model*, which uses a modified turbulent kinetic energy equation along with a prescribed mixing-length (e.g. Rodi 1976, Ljuboja & Rodi 1981), the *two-equation model* like the so-called $k - \epsilon_k$ model with k standing for the turbulent kinetic energy and ϵ_k representing the turbulent viscous dissipation (Jones & Launder 1972), and finally the *Reynolds stress model*, using transport equations for the Reynolds shear stresses (e.g. Rotta 1951; Launder *et al.* 1975).

Theories based on the mixing-length formalism (Prandtl 1925) still represent the main method used for computing the stratification of convection zones in stellar models. However, through the advent of more sophisticated model prescription of turbulence, Canuto & Mazzitelli (1991) recently introduced an alternative convection formulation based on the Eddy-Damped Quasi-Normal Markovian approximation to turbulence (Orszag 1977). This approximation is characterized as a two-equation model and is sometimes referred to as two-point closure, since it is dealing with correlations in two different points of space, or two different wave numbers $\mathbf{k}$ and $\mathbf{k}'$ in the Fourier space. Although two-equation models have a reasonable degree of flexibility, they are restricted by the assumption of a scalar turbulent viscosity and the assumption that the stresses are proportional to the rate of mean strain. The above mentioned Reynolds stress models are free of these restrictions and were recently discussed by Canuto (1992, 1993) for the application in stellar convection.

The present unprecedented computer revolution enables us to perform fully hydrodynamical simulation of the large scales of turbulent flow (Large Eddy Simulation) of solar near-surface convection (e.g., Stein & Nordlund 1989, Kim *et al.* 1995). Such numerical simulations represent a fruitful tool for investigating the accuracy and hence the field of application of phenomenological prescription of convection like the mixing-length approach.

In this Section I try to emphasize the different approximations and simplifications inherent in the mixing-length formalism and its various guises from the fluid dynamics point of view, starting off the continuity- and Navier-Stokes equations. An overview of Gough's time-dependent formulation by means of a local and non-local mixing-length prescription (Spiegel 1963, Gough 1976) will be given in the subsequent paragraphs with reference to Balmforth (1990), followed by a short discussion of other formulations of convection relevant for stellar models.

2.2. Local mixing-length theory

The simplest closure model of turbulence is the early one of Boussinesq (1877), who suggested that turbulent flow could be considered as having an enhanced viscosity, a turbulent (or eddy) viscosity ν_t. Boussinesq assumed ν_t to be constant, in which case the equations of mean motion become identical in structure with those for a laminar flow. This assumption however, will break down describing appropriate the turbulent fluctuations at the boundary layers, where they must be zero, and hence also ν_t.

The simplest turbulence model able to account for the variability of the turbulent mixing with the use of only one empirical constant is the mixing-length idea, introduced independently by Taylor (1915) and Prandtl (1925). Based on Boussinesq's approach and considering the turbulent fluid decomposed into so called eddies, parcels or elements ("Flüssigkeitsballen"), Prandtl obtained for the case of shear flow by dimensional reasoning an expression for the turbulent viscosity or exchange coefficient of momentum ("Austauschkoeffizient"). This expression is in the form of a product of the velocity fluctuation perpendicular (transverse) to the mean motion of the turbulent flow and the mixing-length ℓ. The latter length ℓ is characterized by the distance in the transverse direction which must be covered by a fluid parcel traveling with its original mean velocity in order to make the difference between its velocity and the velocity in the new laminar equal to the mean transverse fluctuation in the turbulent flow. Inherent in this physical picture is the major assumption, that the momentum of the turbulent parcel is assumed to be constant along the travel-distance ℓ, which is analogous to neglecting the streamwise pressure forces and viscous stresses. Prandtl's concept of a mixing-length may be compared, up to a certain point, with the mean free path in the kinetic theory of gases. A somewhat different result was obtained by Taylor (1932) who assumed that the rotation (vorticity) during the transverse motion of the parcel remains constant, yielding a mixing-length which is larger by a factor $\sqrt{2}$ compared with Prandtl's momentum-transfer theory.

Neglecting rotation and magnetic fields, thermal heat transport in stars corresponds to the case of free convection where there is no externally imposed velocity scale as in shear flow. Hence, it is necessary to consider the dynamics of the turbulent elements in greater detail. The imbalance between buoyancy forces, pressure gradients and non-linear advection processes causes the turbulent elements to accelerate during their existence. Ignoring different combinations of these processes and approximating the remaining terms in different ways, various phenomenological models can be established. In the astrophysical community basically two physical pictures have emerged which were first applied to stellar convection by Biermann (1932, 1937, 1943) and Siedentopf (1933, 1935).

The first interprets turbulent flow by direct analogy with kinetic gas theory, where one imagines the fluid parcel to accelerate from rest followed by an instantaneously breakup after the element have traveled approximately one mixing-length. Within this picture the evolution of the fluid properties carried by the turbulent parcels can be approximated by linear growth rates. The nonlinearities that occur in the equations governing the turbulent fluctuations are assumed to be taken into account by the instantaneously breakup of the element (Spiegel 1963, Gough 1977).

In the second physical picture the turbulent element is considered as a convective cell, having a characteristic vertical length of ℓ. It evolves out of some chaotic state

and loses its kinetic energy, working against turbulent drag, after having turned over a distance of about one mixing-length. In this picture the fluid element maintains exact balance between buoyancy force and turbulent drag by continuous exchange of momentum with other elements and its surrounding (Prandtl 1932). Thus the acceleration terms are neglected (i.e. the inertia is unimportant) and the non-linear advection terms (i.e. momentum exchange) are approximated appropriately (e.g. Kraichnan 1962, Unno 1967).

If the mixing-length represents both the element size and the mean-free path the two pictures are complementary in envelopes that do not pulsate. However in a time-dependent theory additional information is required how the initial state of a convective element depends on conditions at the time of its creation. Hence, the different versions of mixing-length theories yield different formulae for the turbulent heat and momentum fluxes when applied to pulsating stars (Unno 1967, Gough 1977).

In the above discussed models, the overturning fluid parcels were still considered to travel adiabatically. Öpik (1950) suggested to treat radiative heat-exchange between the element and the background fluid in a similar way as for the momentum exchange. Based on this assumptions Vitense (1953) and Böhm-Vitense (1958) established a mixing-length description which is still widely used for calculating the convective heat flux in stellar models.

For simplicity, we shall already now introduce the first assumptions describing turbulent convective motion . We assume the considered layer to be plane parallel, with infinite horizontal extent. The fluctuations in the gravitational acceleration g arising from the motion will be neglected, so that g is a function only of height. Additionally, magnetic fields, rotation and the energy generation due to nuclear reactions will be neglected. With respect to inertial rectangular co-ordinates (x_1, x_2, x_3), the fluid dynamic equations for studying convective motion are

$$\frac{\partial \rho}{\partial t} + \frac{\partial}{\partial x_i}\left(\rho u_i\right) = 0\,, \tag{2.1}$$

$$\rho\left(\frac{\partial u_i}{\partial t} + u_j \frac{\partial u_i}{\partial x_j}\right) = \rho g_i - \frac{\partial p}{\partial x_i} + \frac{\partial \tau_{ij}}{\partial x_j}\,, \tag{2.2}$$

$$\rho\left[\frac{\partial}{\partial t}\left(U + \frac{u^2}{2}\right) + u_i \frac{\partial}{\partial x_i}\left(U + \frac{u^2}{2}\right)\right] = \rho u_i g_i - \frac{\partial}{\partial x_i}\left(F_{r,i} + p u_i - u_i \tau_{ij}\right)\,, \tag{2.3}$$

where ρ is the density, u_i the velocity, p the gas plus radiation pressure, U the internal energy by unit mass, $F_{r,i}$ the combined heat flux by conduction and radiation and $g_i = (0, 0, -g)$. The viscous stress tensor τ_{ij} for a Newtonian fluid may be written in the form (Batchelor 1967)

$$\tau_{ij} = \mu\left[\left(\frac{\partial u_i}{\partial x_j} + \frac{\partial u_j}{\partial x_i}\right) - \frac{2}{3}\frac{\partial u_k}{\partial x_k}\delta_{ij}\right]\,, \tag{2.4}$$

where μ is the coefficient of molecular shear viscosity or just the dynamic viscosity, and δ_{ij} is the Kronecker delta. Following Reynold's approach, each flow variable of the turbulent

motion may be separated into its average and fluctuating part, as indicated here for the velocity field

$$u_i \;=\; \overline{u_i} + u_i' \,, \tag{2.5}$$

where the overbar should ideally represent an ensemble average (or moment) of the particular field variable, but it is computationally more convenient to use averages over horizontal surfaces. For constructing the mean-flow equations the following identities (Reynold's rules of averages) may be useful where $a = \overline{a} + a'$ and $b = \overline{b} + b'$ represent fluctuating quantities

$$\overline{a+b} \;=\; \overline{a} + \overline{b} \,, \qquad \overline{ab} \;=\; \overline{a}\,\overline{b} + \overline{a'b'} \,, \qquad \overline{\frac{\partial a}{\partial x}} \;=\; \frac{\partial \overline{a}}{\partial x} \,, \qquad \overline{a'} \;=\; \overline{b'} \;=\; 0 \,. \tag{2.6}$$

Applying these rules first on the continuity equation (2.1) we obtain for the mean and fluctuating parts

$$\frac{\partial \overline{\rho}}{\partial t} + \frac{\partial}{\partial x_i}\left(\overline{\rho u_i} + \overline{\rho' u_i'}\right) \;=\; 0 \,, \tag{2.7}$$

$$\frac{\partial \rho'}{\partial t} + \frac{\partial}{\partial x_i}\left(\rho' \overline{u_i} + \overline{\rho} u_i' + \rho' u_i'\right) \;=\; 0 \,. \tag{2.8}$$

Defining the viscous stress tensor for a Newtonian fluid, and since Stokesian fluid is essentially non-elastic, we may apply the anelastic approximation (Gough 1969) to the fluid equations, which renders the equations (2.7) and (2.8) into

$$\frac{\partial \overline{\rho}}{\partial t} + \frac{\partial}{\partial x_i}\left(\overline{\rho u_i}\right) \;=\; 0 \,, \tag{2.9}$$

and

$$\frac{\partial}{\partial x_i}\left(\overline{\rho} u_i'\right) \;=\; 0 \,. \tag{2.10}$$

Additional to the last two equations, the anelastic approximation treats the thermodynamic fluctuating quantities as perturbations of the mean ones, linearizing the equations in the fluctuating parts and neglecting the pressure fluctuations except in the momentum equation. This is equivalent to filter out high-frequency phenomena such as sound waves, expressed by the suppression of the time derivative of the density fluctuation in the continuity equation Eq. (2.8). This approximation is certainly not valid in the upper layers of the convective domain, where there is a substantial superadiabatic region in solar-type stars and red giants and where the Mach numbers of the convective motions may become considerable. Or expressed in terms of time scales, when the turnover-time of a fluid parcel becomes such small, that it is comparable with the time-scale associated with the local

speed of sound of the background fluid. Through the generation of sound waves kinetic energy from the turbulent motion will be converted into acoustic radiation hence, neglecting this mechanism will overestimate the predicted convective velocities and the resulting temperature profile will become too flat. Within this approximation the mean-fluid equations for the velocity and total energy may be written as

$$\frac{D\overline{u_i}}{Dt} = g_i - \frac{1}{\overline{\rho}}\frac{\partial \overline{p}}{\partial x_i} - \frac{\partial}{\partial x_j}\overline{u_i' u_j'} + \frac{1}{\overline{\rho}}\frac{\partial \overline{\tau_{ij}}}{\partial x_j}\,, \tag{2.11}$$

and

$$\begin{aligned}\overline{\rho}\frac{D}{Dt}\left(\overline{U} + \frac{1}{2}\overline{u'^2}\right) = &- \frac{\partial \overline{F_{r,i}}}{\partial x_i} - \frac{\partial}{\partial x_i}\left(\overline{(\overline{\rho}h)'\, u_i'} + \overline{\frac{1}{2}\,(\overline{\rho}u'^2)'\, u_i'} - \overline{u_i'\tau_{ij}}\right) \\ &- p\frac{\partial \overline{u_i}}{\partial x_i} + \overline{\left(\tau_{ij} - \overline{\rho}u_i'u_j'\right)}\frac{\partial \overline{u_i}}{\partial x_j}\,,\end{aligned} \tag{2.12}$$

where

$$\frac{D}{Dt} = \frac{\partial}{\partial t} + \overline{u_i}\frac{\partial}{\partial x_i}\,, \tag{2.13}$$

and $h = U + p/\rho$ is the specific enthalpy. The second term of the right hand side of equation (2.12) represents the sum of the gradients of the specific enthalpy flux, the turbulent energy flux and the flux of kinetic energy due to molecular viscosity. For stars the estimations of the Reynolds number suggest a value in the order of 10^{10} (e.g. Spiegel 1966), which implies a very small molecular viscosity. It is therefore usual to neglect in the computations all the terms which become small due to the vanishing molecular shear viscosity. However, some terms including the molecular viscosity may remain finite, as shown below for the dissipation of turbulent kinetic energy. For equation (2.12) this means the neglect of $\overline{u_i'\tau_{ij}}$ and of the viscous stress tensor τ_{ij} compared to the turbulent energy flux and Reynolds stress, respectively.

The second-order moment $\overline{u'^2/2}$ is the mean specific turbulent energy and represents a new field variable, demanding an additional equation for it. This equation, the transfer equation for the kinetic energy, may be obtained by taking the scalar product of the momentum equation (2.11) with the velocity u_i' and then taking the average of the result. This expression exhibits a term describing the rate of dissipation of turbulent kinetic energy, ϵ, including the molecular kinetic shear viscosity $\nu = \mu/\overline{\rho}$, and must not be neglected in order to maintain energy conservation (Canuto 1993). In particular, this quantity ϵ may be defined as the trace (contraction) of the expression (e.g. White 1991)

$$\epsilon_{ij} = 2\nu\overline{\left(\frac{\partial u_i'}{\partial x_k}\right)\left(\frac{\partial u_j'}{\partial x_k}\right)}\,, \tag{2.14}$$

and which will not vanish even for ν approaching to zero. This comes about, because the mean-square vorticity, which is proportional to $\overline{(\partial u_i'/\partial x_j)^2}$, varies inversely as the

molecular kinetic shear viscosity under almost all circumstances. Therefore ϵ is essentially independent of viscosity and remains finite for $\nu \to 0$. This effect hinges on the property that most of the turbulent effects and energy are associated with the largest, energy-bearing eddies, which decay first by cascading to smaller eddies before converting to thermal energy. The energy which is fed into the system is conserved during its distribution to the whole spectrum of eddies by the non-linear fluctuation interactions and the viscosity describes the scale at which the dissipation into heat takes place.

Similar as for the Reynolds stresses, the energy dissipation term ϵ has to be modelled by introducing proper assumptions. In one-equation models for instance (e.g. Taylor & Gent, 1974), ϵ is estimated in terms of an energy dissipation length scalar ℓ_ϵ, as

$$\epsilon \equiv \frac{\left(\overline{u'^2}\right)^{3/2}}{\ell_\epsilon}\,, \tag{2.15}$$

representing a local approximation and which has been considered in stellar convection by, e.g. Shaviv & Chitre (1968) and Xiong (1986). They assumed $\ell_\epsilon = \ell/D$, where ℓ represents the usual mixing length and D, being a constant in the order of unity, a drag coefficient.

In stellar model calculations it is usual to neglect the mechanical (kinetic) flux in the treatment of the total energy flux *viz.*, the mechanical part arising from the momentum equation is subtracted from the total energy equation (2.3), which renders indistinguishable from the thermal energy equation

$$\rho c_p \frac{\partial T}{\partial t} - \delta \frac{\partial p}{\partial t} + \rho u_i \left(\frac{\partial h}{\partial x_i} - \frac{1}{\rho} \frac{\partial p}{\partial x_i} \right) = -\frac{\partial F_{r,i}}{\partial x_i} + \tau_{ij} \frac{\partial u_i}{\partial x_k}\,, \tag{2.16}$$

where the following thermodynamic relation has been used

$$\rho c_p \, dU - \frac{p}{\rho} \, d\rho = \rho \, dh - dp = \rho c_p \, dT - \delta \, dp\,, \tag{2.17}$$

and c_p represents the specific heat at constant pressure. The thermodynamic quantity δ is defined as

$$\delta\,(\rho, T) = -\left(\frac{\partial \ln \rho}{\partial \ln T} \right)_p . \tag{2.18}$$

In the anelastic approximation the mean density may vary as function of time and space as shown by the equations (2.9) and (2.10). An even simpler approximation with $\overline{\rho}$ variable is the incompressible approximation in which the velocity divergence (i.e. expansion or contraction of a parcel having constant mass) is set to zero or according to Eq. (2.1): $\partial\rho/\partial t + u_i \partial\rho/\partial u_i = 0$. Boussinesq (1903) assumed that in thermal convection the only density variations which have to be taken into account are the one which are responsible for the differential buoyancy forces driving the convective motion. Thus, he neglected density fluctuations in the continuity and momentum equations except when they were

coupled to the gravitational acceleration and considered the mean density to be constant as well. This approximation can be justified only when the vertical dimension of the fluid, represented in the mixing-length approach by the mixing-length ℓ, is much less than the pressure and density scale heights of the considered layer and the amplitudes of the motion-induced variations in density and pressure are much smaller than the static one (Spiegel & Veronis 1960). The latter approximation combined with the anelastic approximation constitutes the so called *Boussinesq approximation* which is used in almost all attempts to model stellar convection and particular in the mixing-length approach. Using again Reynold's separation Ansatz, the mean- and fluctuating fluid equations in the Boussinesq approximation for a Newtonian Fluid with a constant uniform dynamic viscosity μ may be written as

$$\frac{\partial \overline{u_i}}{\partial x_i} = 0\,, \tag{2.19}$$

$$\frac{\partial u_i'}{\partial x_i} = 0\,, \tag{2.20}$$

$$\frac{D\overline{u_i}}{Dt} = g_i - \frac{1}{\overline{\rho}}\frac{\partial \overline{p}}{\partial x_i} - \frac{\partial}{\partial x_j}\overline{u_i' u_j'}\,, \tag{2.21}$$

$$\frac{Du_i'}{Dt} = \frac{\rho'}{\overline{\rho}} g_i - \frac{1}{\overline{\rho}}\frac{\partial p'}{\partial x_i} - \frac{\partial}{\partial x_j}\left(u_i' u_j' - \overline{u_i' u_j'}\right) - u_j'\frac{\partial \overline{u_i}}{\partial x_j} + \nu\frac{\partial^2 u_i'}{\partial x_j^2}\,, \tag{2.22}$$

$$\frac{D\overline{T}}{Dt} - \frac{\overline{\delta}}{\overline{\rho}\,\overline{c_p}}\frac{D\overline{p}}{Dt} = -\frac{1}{\overline{\rho}\,\overline{c_p}}\frac{\partial}{\partial x_i}\left(\overline{F_{r,i}} + \overline{\rho}\,\overline{c_p}\overline{u_i' T'}\right) + \frac{\epsilon}{\overline{c_p}}\,, \tag{2.23}$$

$$\frac{DT'}{Dt} = -\frac{\partial}{\partial x_i}\left(u_i' T' - \overline{u_i' T'}\right) + u_i'\beta - \frac{1}{\overline{\rho}\,\overline{c_p}}\frac{\partial F_{r,i}'}{\partial x_i} + \frac{\nu}{\overline{c_p}}\left[\left(\frac{\partial u_i'}{\partial x_j}\right)^2 - \overline{\left(\frac{\partial u_i'}{\partial x_j}\right)^2}\right]\,, \tag{2.24}$$

where

$$\beta = -\frac{1}{\overline{c_p}}\left(\frac{d\overline{h}}{dx_3} - \frac{1}{\overline{\rho}}\frac{d\overline{p}}{dx_3}\right) \approx -\left(\frac{d\overline{T}}{dx_3} - \frac{\overline{\delta}}{\overline{\rho}\,\overline{c_p}}\frac{d\overline{p}}{dx_3}\right)\,, \tag{2.25}$$

and the perturbations in c_p and δ have been neglected.

The viscous stress tensor, Eq. (2.4), has been retained in the derivation of these equations in order to demonstrate which additional terms should be taken into account for maintaining energy conservation even in the limit of a vanishing kinematic viscosity (Canuto 1993). These additional terms (last term on the right hand side of (2.22), (2.23) and (2.24)), which describe the dissipation of momentum and energy by molecular processes, remain finite in this limit since they are also proportional to the divergence of the mean-squared vorticity, as already discussed before.

In modelling stellar convection, using the mixing-length approach, it is usually assumed, that ϵ and terms including the molecular shear viscosity can be neglected. Beside the fact, that this is a violation of the energy conservation, as discussed before, the excess of energy through the neglect of this sink will be used up by other processes leading to an overestimation of the turbulent heat and momentum fluxes (similar as in the case of the anelastic approximation where the generation of acoustic radiation is neglected).

In turbulent thermal convection we do not have a mean horizontal velocity, hence $\overline{u_i} = 0$. Moreover, we may adopt the widely held belief that under stationary external conditions the mean quantities are also stationary, at least in turbulent convection. Thus, the mean-fluid equations (2.21) and (2.23) are simplified to

$$\frac{d}{dz}\left(\overline{p_\mathrm{g}} + \overline{p_\mathrm{t}}\right) = -g\overline{\rho}\,, \tag{2.26}$$

and

$$\frac{d}{dz}\left(\overline{F_{r,z}} + \overline{F_{c,z}}\right) = 0\,, \tag{2.27}$$

where z is the vertical co-ordinate ($z = x_3$), p_g the gas plus radiation pressure (was p so far) and $F_{r,z}$ the vertical component of the radiative and conductive energy flux. With w representing the vertical velocity fluctuation ($w = u_3'$) the convective momentum and heat fluxes may be approximated as

$$\overline{p_\mathrm{t}} \equiv \overline{\rho w^2} \approx \overline{\rho}\,\overline{w^2}\,, \tag{2.28}$$

and

$$\overline{F_{c,z}} \equiv \overline{\rho h' w} \approx \overline{\rho}\,\overline{c_p}\,\overline{wT'}\,, \tag{2.29}$$

where the mean thermodynamical state variables are considered to be constant over the scale ℓ of motion, in accordance with the Bousinesq approximation. Moreover, in a local mixing-length theory the superadiabatic lapse-rate, Eq. (2.25) in the fluctuating thermal energy equation is treated as though it were constant either, which is certainly violated in the upper layers of the convection zone, where β varies on a scale much shorter than ℓ. However all these approximations enables one to compute the turbulent fluxes solely in terms of the mean quantities, describing a particular level in the stratified envelope, for which the theory is called local. The equations for the fluctuations become then

$$\frac{\partial u_i'}{\partial t} + \frac{\partial}{\partial x_j}\left(u_i'u_j' - \overline{u_i'u_j'}\right) = -\frac{1}{\overline{\rho}}\frac{\partial p_\mathrm{g}'}{\partial x_i} - g_i\frac{\overline{\delta}}{\overline{T}}T'\,, \tag{2.30}$$

and

$$\frac{\partial T'}{\partial t} + \frac{\partial}{\partial x_i}\left(u_i'T' - \overline{u_i'T'}\right) - \beta w = -\frac{1}{\overline{\rho}\,\overline{c_p}}\frac{\partial F'_{r,i}}{\partial x_i}\,, \tag{2.31}$$

where we used the Boussinesq equation of state

$$\frac{\rho'}{\overline{\rho}} = -\overline{\delta}\frac{T'}{\overline{T}}\,. \tag{2.32}$$

The non-linear advection terms in the right hand sides of equations (2.30) and (2.31) have to be modelled. According to Prandtl's mixing-length theory the Reynolds stresses are modelled as

$$-\rho\overline{u_i'u_j'} \approx \rho\nu_t\frac{dw}{dz}\,, \tag{2.33}$$

with

$$\nu_t = w\ell\,, \tag{2.34}$$

Prandtl's (1925) definition for the turbulent viscosity ν_t. Thus, the non-linear advection terms can be written in the form (e.g. Unno 1967)

$$\frac{\partial}{\partial x_j}\left(u_i'u_j' - \overline{u_i'u_j'}\right) \approx \nu_t\frac{d^2w}{dz^2} \approx \frac{2w^2}{\ell}\,, \tag{2.35}$$

and

$$\frac{\partial}{\partial x_i}\left(u_i'T' - \overline{u_i'T'}\right) \approx \kappa_t\frac{d^2w}{dz^2} \approx \frac{2wT'}{\ell}\,, \tag{2.36}$$

where

$$\kappa_t = \frac{\nu_t}{P_{\mathrm{r_t}}}\,, \tag{2.37}$$

represents an eddy diffusivity accounting for the turbulent heat exchange, proposed first by Öpik (1950), which may be determined using ν_t and the turbulent Prandtl number $P_{\mathrm{r_t}}$ of nearly unity (Launder 1978). Additionally, we replaced the spatial derivatives of the fluctuating quantities by ℓ^{-1}, i.e. $\partial^2/\partial x_i^2 \approx \ell^{-2}$ (Kraichnan 1962). A typical parcel at any instant might have travelled say half the distance ℓ at which the typical values for the velocity and temperature fluctuations are taken into account in the equations (2.35) and (2.36), which yields the additional factor 2.

For simplicity overbars for mean quantities are omitted from now on. In the physical picture of continuous turbulent exchange of heat and momentum the time derivatives in (2.30) and (2.31) are ignored and the non-linear terms are replaced by the appropriate mixing-length models, Eq. (2.35) and Eq. (2.36). Ignoring further the coupling between vertical and horizontal motion by neglecting the pressure fluctuations in the momentum equation the expression for the convective velocity and temperature fluctuation may be written as

$$w^2 = \frac{1}{2} g \frac{\delta \ell}{T} T' \,, \tag{2.38}$$

and

$$T' = \frac{1}{2} \left(\beta - \frac{\kappa}{\ell^2} \frac{T'}{w} \right) \ell \,. \tag{2.39}$$

For the radiative transfer we applied the diffusion approximation

$$F_r = -K dT/dz \,, \tag{2.40}$$

where $K = \rho c_p \kappa$, κ is the thermal diffusivity. Thus the momentum flux may be estimated as

$$p_{\rm t} \approx \frac{1}{4} \rho \frac{g\delta}{T} \ell^2 \beta \,. \tag{2.41}$$

The expression for the turbulent heat flux is generally more involved but becomes quite simple in the two extremes, when convection is either very efficient or very inefficient. In the former limit this is equivalent for a pure adiabatically motion of the fluid parcels, hence, the thermal diffusion term in equation (2.39) may be neglected. In this limit, the convective heat flux may be approximated as

$$F_c \approx \frac{1}{4} \rho c_p \left(\frac{g\delta}{T} \right)^{1/2} \ell^2 \beta^{3/2} \,. \tag{2.42}$$

The numerical factors (1/4) depend on the geometry of the considered fluid parcel and on possible introduction of additional factors of order unity to account for the coupling between vertical and horizontal motion as well as for imperfect correlation in terms with second order moments (e.g. wT'). Thus these factors may differ between the different physical pictures and derivation of the fluxes in the various guises of mixing-length prescriptions.

In the second phenomenological picture the non-linear advection terms are neglected during the fluid element's life-time and are to be taken into account by its instantaneous disruption after it has travelled through a distance ℓ. Thus, the time-dependence of the velocity and temperature fluctuations are retained and the equations become

$$\frac{\partial w}{\partial t} = g\frac{\delta}{T}T' , \tag{2.43}$$

and

$$\frac{\partial T'}{\partial t} - \beta w = -\frac{\kappa}{\ell^2}T' . \tag{2.44}$$

Assuming the coefficients in these equations to be constant not only over the distance ℓ but also in time, the fluctuating quantities may be solved as function of time, using the Ansatz w and $T' \propto \exp(\sigma t)$, where σ is in general a complex quantity, depending on the induced boundary conditions. The real part of it, $\mathrm{Re}(\sigma)$ describes the growth (or decay) of convection and hence, is to be known as the convective growth rate. The characteristic equation may then be written as

$$\sigma^2 + \frac{\kappa}{l^2}\sigma - \frac{g\delta}{T}\beta = 0 . \tag{2.45}$$

The last term in (2.45) represents the well known characteristic frequency in the theory of pulsating stars and other fields: the *Brunt-Väisälä frequency* N defined as

$$N^2 \equiv -\frac{\delta}{T}g\beta . \tag{2.46}$$

For the case of convective instability, $N^2 < 0$ and the quantity $1/|N|$ may be interpreted as a free fall time under reduced gravity $(\ell\beta\delta/T)g$, *viz.* representing a time scale for the convective dynamics. The coefficient of the second term of (2.45) indistinguishable accounts for the radiative cooling time. Thus the square of the ratio of these time-scales will give us a measure of the convective efficacy

$$S = -\frac{N^2\ell^4}{\kappa^2} = \frac{g\,(\delta/T)\,\beta\ell^4}{\kappa^2} , \tag{2.47}$$

which may be interpreted in terms of parameters common in fluid mechanics as the product of the Prandtl number and locally defined Rayleigh number. The convective heat flux in the two asymptotic limits may be easily estimated in terms of the growth rate σ. The solutions of the fluctuating velocity and temperature for a fluid parcel having travelled half the mixing-length are

$$w = \frac{1}{2}\sigma\ell , \tag{2.48}$$

and

$$T' = \frac{1}{2}\frac{\sigma^2}{|N^2|}\beta\ell\,. \tag{2.49}$$

For the limit of efficient convection with $S \gg 1$, the solution of (2.45) for the growth rate yields $\sigma = |N|$, i.e., dominated by the buoyancy time scale. Thus the convective heat flux becomes with the help of equation (2.29)

$$F_c = \frac{1}{4}\rho c_p S^{1/2}\kappa\beta\,, \tag{2.50}$$

which is identical to the result (2.42) obtained from the phenomenologically picture operating with continuously momentum-exchange. For the case of inefficient convection, where $S \ll 1$, the convective growth rate is dominated by the thermal diffusion time and we obtain from (2.45), using equation (2.47), an expression for $\sigma = |N|S^{1/2}$. The convective heat flux becomes in this limit

$$F_c = \frac{1}{4}\rho c_p S^2\kappa\beta\,. \tag{2.51}$$

As Gough and Weiss (1976) indicate, every formulation of local mixing-length theory is an interpolation formula between the two limits of efficient and inefficient convection. The transition between these two limits occurs in solar-type stars in a very thin layer on the top of the bulk of the convection zone, where the temperature gradient is substantially superadiabatic.

Although conceptually the two phenomenological models are rather different, their mathematical representations for non-pulsating stars are identical. Moreover, Gough and Weiss pointed out, that the various guises of local mixing-length prescriptions (e.g. Öpik 1950; Vitense 1953; Henyey, Vardya; Bodenheimer 1965; Ulrich 1970b) are essentially similar with appropriate calibrations of the various parameters inherent in these theories.

2.3. Gough's local mixing-length formulation

In this section a brief discussion of a specific mixing-length model introduced by Gough (1965, 1976) should be given, since this is the basis for the generalization to the time-dependent theory (Gough 1977) and a non-local prescription (Gough 1976), which have been applied to our model calculations.

2.3.1. Theory in a static envelope

In the upper parts of the convection zone, the convective fluid parcels may become optically thin. Moreover, radiative equilibrium is no longer sustained in the region, where there is the transition from convective to radiative heat transport and hence the treatment of

radiation through the diffusion approximation is no longer valid. Vitense (1953) studied the case when fluid parcels are optically thin by adjusting proper numerical constants such, that the optically thick and and thin formulae gave same results at unit optical thickness. A more accurate transition between these two limits may be obtained by using the Eddington approximation to radiative transfer (Unno & Spiegel 1966) which was also applied by Gough (1977) in his local mixing-length prescriptions.

Based on the physical concept of linear growth rates the basic equations of the fluctuating quantities for a spherical symmetric star and of the Eddington approximation to radiative transfer may be written in the following form

$$\boldsymbol{\nabla} \cdot \mathbf{u}' \;=\; 0\,, \tag{2.52}$$

$$\frac{\partial \mathbf{u}'}{\partial t} \;=\; -\frac{1}{\rho}\boldsymbol{\nabla} p'_{\mathrm{g}} + g\,\frac{\delta T'}{T}\hat{\mathbf{r}}\,, \tag{2.53}$$

$$\frac{\partial T'}{\partial t} \;=\; -\frac{1}{\rho\, c_p}\boldsymbol{\nabla}\cdot\mathbf{F}'_r + \beta w\,, \tag{2.54}$$

$$\boldsymbol{\nabla}\cdot\mathbf{F}'_r \;=\; 4\pi\varkappa\rho\left[B' - J' + (\varkappa_{\mathrm{T}} - \delta)\,(B-J)\,\frac{T'}{T}\right]\,, \tag{2.55}$$

$$\boldsymbol{\nabla}\, J' \;=\; -\frac{3\varkappa\rho}{4\pi}\left[\mathbf{F}_r{}' + (\varkappa_{\mathrm{T}} - \delta)\,F_{r,\mathrm{r}}\frac{T'}{T}\hat{\mathbf{r}}\right]\,, \tag{2.56}$$

where $\hat{\mathbf{r}}$ is the unit-vector in radial direction, $F_{r,\mathrm{r}}$ the radial component of the radiative flux, B the integrated Planck function, J the mean intensity and $\varkappa$ the Rosseland-mean opacity with its logarithmic derivative $\varkappa_{\mathrm{T}} = (d\ln\varkappa/d\ln T)_{p_{\mathrm{g}}}$. The pressure fluctuations are only present in the momentum equation. Thus they have no significance to the thermodynamic structure and may be eliminated by taking the double curl of equation (2.53)

$$\frac{\partial}{\partial t}\boldsymbol{\nabla}^2 w - \frac{g\delta}{T}\boldsymbol{\nabla}_h^2 T' \;=\; 0\,, \tag{2.57}$$

where

$$\boldsymbol{\nabla}_h^2 = \frac{1}{r^2\sin\theta}\frac{\partial}{\partial\theta}\left(\sin\theta\frac{\partial}{\partial\theta}\right) + \frac{1}{r^2\sin^2\theta}\,\frac{\partial^2}{\partial\varphi^2}\,. \tag{2.58}$$

Equation (2.57) together with (2.54) describe the linear stability problem and admit separable solutions (Chandrasekhar 1961) with horizontal variations of $\mathbf{u}'$ and T' satisfying the planform $f(\theta,\varphi)$

$$\boldsymbol{\nabla}_h^2 f \;=\; -k_h^2 f \qquad \overline{f^2} \;=\; 1\,. \tag{2.59}$$

Thus the fluctuating quantities may be expanded as

$$\mathbf{u}' = -k_h^{-2}\partial_r W \boldsymbol{\nabla}_h f + W f \hat{\mathbf{r}}\,, \tag{2.60}$$

$$T' = f\,\Theta\,, \tag{2.61}$$

where the separation constant k_h represents the horizontal wavenumber of the motion and W and Θ are sinusoidal in r and functions of time. With the advent of the horizontal wavenumber we cannot longer assume that there is only one single length scale associated with the fluid parcel, which brings its shape into play. This coupling between vertical and horizontal motion is due to the inclusion of the pressure fluctuations in the momentum equation, diverting the vertical motion into horizontal flow and thus reducing the efficacy with which the motion might otherwise have released potential energy gained by the buoyancy forces. Perhaps this might be explained in an even more obvious way in the physical picture of a convective cell. The vertical motion in such a convective cell, typically up near the central axis, is governed by buoyancy, however the horizontal flow, across the top of the cell to its edge, experiences only damping forces due to dissipative processes without any compensation. Hence, in both pictures the horizontal motion is considerably wasteful. The simplest way to account for this effect without changing the functional form of the equation of motion, is to introduce an additional parameter which effectively increases the inertia of the vertically moving fluid. This parameter, the shape factor Φ, may be expressed in view of equation (2.60) as

$$\Phi = 1 + \frac{k_v^2}{k_h^2}\,, \tag{2.62}$$

where the vertical wave number will be associated with the vertical scale of a fluid parcel of size ℓ, expressed as

$$k_v \equiv \pi/\ell\,. \tag{2.63}$$

In this view, convective motion becomes most efficient for parcels with a geometry of tall thin needles, where $\Phi \to 1$. Similar argumentation may be applied for the definition of the Brunt Väisälä frequency N, Eq. (2.46), which is the frequency of a convectively stable, oscillating fluid parcel with vanishing horizontal extent, i.e. $k_h \to \infty$ (Christensen-Dalsgaard 1994), thus representing the highest frequency of gravity modes.

The differential equation for the horizontal structure of the convective fluctuations (2.60) and (2.61) can be solved with subject to proper periodic boundary conditions in the domain described by the planform $f(\theta, \varphi)$ being a spherical surface (Spiegel 1963). Thus the horizontal wavenumber k_h can take any value from an infinite discrete set of eigenvalues. Assuming the eigenvalue spectrum to be dense for relatively high harmonics and since the motion is unlikely to be coherent over the whole spherical surface, it might be a reasonable approximation to consider Φ as continuous. Within this approximation,

Gough (1977) has chosen a value for k_h that maximizes the convective velocity at fixed k_v. This is equivalent to selecting the most rapidly growing mode in the theory of linear stability (Spiegel 1963). Another possibility might be to chose the mode that maximizes the convective heat flux (Balmforth & Gough 1990a), or to describe the total heat flux by averaging over an ensemble of different eddies, determined with the help of a distribution function for the eddy-shape Φ. With the latter method, Balmforth (1989) obtained in the limit of efficient convection ($S \gg 1$) a maximal value for Φ of 5/3.

In order to account for the optical thin and thick limit in the treatment of the radiative heat loss of the fluid parcels, one may obtain for the radiative flux in the general Eddington approximation (Unno & Spiegel 1966) an expression of the form

$$\boldsymbol{\nabla} \cdot \mathbf{F}_r{}' \;=\; \phi K k^2 \Theta \,, \tag{2.64}$$

where

$$\phi \;=\; \frac{\left[1 + 1/4\,(\varkappa_{\mathrm{T}} - \delta)\,(1 - J/B)\right]}{\left[1 + \Phi\Sigma/\,(\Phi - 1)\right]} \,, \qquad\qquad \Sigma \;=\; \frac{1}{3}\frac{\pi^2}{(\rho\varkappa\ell)^2} \,, \tag{2.65}$$

providing a smooth transition between these two limits, $K = 4a_r c T^3/(3\rho\varkappa)$ is the radiative conductivity and

$$k^2 = k_h^2 + k_v^2 \,. \tag{2.66}$$

The fluctuating equations (2.53) and (2.54) may now be reduced to

$$\Phi \frac{\partial W}{\partial t} \;=\; \frac{g\delta}{T}\Theta \,, \tag{2.67}$$

$$\left(\frac{\partial}{\partial t} + \frac{\phi K}{\rho c_p} k^2\right) \Theta \;=\; \beta W \,, \tag{2.68}$$

where the vertical derivatives have been replaced by ik_v. Assuming again that the solutions of W and Θ to be proportional to $\exp(\sigma t)$, the characteristic equation for the convective growth rate may be written as

$$\sigma^2 + \frac{\phi K}{\rho c_p} k^2 \sigma - \frac{g\delta\beta}{\Phi T} \;=\; 0 \,. \tag{2.69}$$

This expression is essentially equation (2.45), when the thermal diffusion κ is multiplied by the factor ϕ, accounting for the partial optical transparency and dividing the square of the Brunt Väisälä frequency by the shape factor Φ, thus reducing N accordingly through the virtual increase of the inertia of the fluid parcel. Its solutions yields

$$\sigma \;=\; \eta^{-1} S^{-1/2} \left(\frac{g\delta\beta}{\Phi T}\right)^{1/2} \left[\left(1+\eta^2 S\right)^{1/2} - 1\right] , \qquad\qquad S \;=\; \frac{g\,(\delta/T)\,\beta l^4}{\left(\phi K/\rho c_p\right)^2} , \tag{2.70}$$

where $\eta \;=\; 2\pi^{-2}\Phi^{-3/2}(\Phi - 1)$ represents a geometrical factor.

In order to construct the expressions for the turbulent fluxes, we should perhaps have the following specific model in mind. The growth of the fluid parcels can be considered to be linear, at least initially, whereas non-linear processes may become important at the end of the parcel's lifetime and eventually responsible for its breakup. If however, this final stage of the parcel's existence is treated as occurring instantaneously, then we may approximate the entire evolution of the parcel by its linear growth rate, and use some mathematical device to account for the non-linear destruction of the fluid parcel. Such a mathematical device can be established in terms of an eddy survival probability $\mathscr{P}(r,t,t_0)$, where t_0 is the time at which the eddy was created. Depending on the cause what may break up an eddy, different probabilities can be derived (Gough 1978). Here we may follow Spiegel's (1963) idea, where the probability of disruption of an eddy that is displaced by a distance dx along its trajectory of length ℓ is dx/ℓ. Thus the probability that the eddy will survive until a time t, can be set to

$$\mathscr{P}\,(r,t,t_0) \;=\; \exp\left[-\int_{t_0}^{t} \frac{W\,(t';t_0)\,dt'}{\ell}\right] . \tag{2.71}$$

Assuming that the initial conditions, or convective fluctuations at the parcel's creation time, do not significantly contribute to the final heat flux, the time dependence of W and Θ may be described only by the linear growth rates

$$W = \hat{W}_0 \exp\left[\sigma\,(t-t_0)\right] , \qquad\qquad \Theta = \hat{\Theta}_0 \exp\left[\sigma\,(t-t_0)\right] , \tag{2.72}$$

hence, the probability may be approximated as

$$\mathscr{P}\,(r,t,t_0) \;=\; \exp\left[-\frac{\hat{W}_0 e^{\sigma(t-t_0)}}{\sigma\ell}\right] , \tag{2.73}$$

where $\hat{W}_0$ and $\hat{\Theta}_0$ are determined by the equations (2.67) and (2.68), respectively.

The turbulent fluxes may be constructed in terms of the probability of survival by the following integral expressions

$$F_c \;=\; nmc_p \int_{-\infty}^{t} W\Theta\mathscr{P} dt_0 \,, \tag{2.74}$$

$$p_{\mathrm{t}} \;=\; nm \int_{-\infty}^{t} W^2\mathscr{P} dt_0 \,, \tag{2.75}$$

where n is the creation rate per unit volume of the convective eddies, each having a mass m. In a statistically steady state, where as many eddies are created as destroyed, the following relation holds

$$nm \int_{-\infty}^{t} \mathscr{P} dt_0 \, = \, \rho \, . \tag{2.76}$$

Since the initial conditions of the eddies are unimportant, i.e. the amplitudes of W_0 and Θ_0 are small compared to the average values of W and Θ, and $\exp(\sigma\tau) \gg 1$, τ being the mean lifetime of the eddy. Using equation (2.73), the eddy creation rate gives

$$nm \, = \, \rho\tau^{-1} \, = \, \rho\sigma\chi \, , \tag{2.77}$$

where χ is a numerical constant, which can be calibrated with the expressions for the fluxes, obtained by solving the equations Eq. (2.67) and (2.68), yielding $\chi = 1/2$. Hence, the fluxes can be approximated by

$$F_c \, = \, \frac{1}{4} \frac{\rho c_p \Phi T \ell^2}{g\delta} \sigma^3 \, , \tag{2.78}$$

$$p_{\rm t} \, = \, \frac{1}{4} \rho \ell^2 \sigma^2 \, . \tag{2.79}$$

2.3.2. Time-dependent theory

The next paragraphs provide a short overview of Gough's (1977) prescription of a time-dependent mixing-length theory. In the derivation of the mean- and fluctuating fluid equations in the Boussinesq approximation, equations (2.19)–(2.24), we assumed that the horizontal mean quantities of ρ, c_p and δ, appearing as coefficients, are independent of time, thus describing a static atmosphere. In order to study the coupling between convection and a pulsating atmosphere one has also to consider the time-dependence of these quantities (note however, that ρ is independent of height in the Boussinesq approximation). Thus the linearized equations for the convective fluctuations in a pulsating atmosphere become

$$\left[\frac{\partial}{\partial t} - \frac{1}{\Phi} \frac{\partial \ln \left(r^2 \rho \right)}{\partial t} \right] W - \frac{g\delta}{\Phi T} \Theta \, = \, 0 \, , \tag{2.80}$$

$$\left[\frac{\partial}{\partial t} + \left(c_{p_T} - \delta \right) \frac{\partial \ln T}{\partial t} - \delta_{_T} \nabla_{\rm ad} \frac{\partial \ln p}{\partial t} \right] \Theta - \beta W + \frac{\phi K}{\rho c_p} k^2 \Theta \, = \, 0 \, , \tag{2.81}$$

where c_{p_T} and $\delta_{_T}$ are the logarithmic derivatives with respect to temperature of c_p and δ, and

$$\nabla_{\rm ad} = \delta p_{\rm g} / \left(\rho c_p T\right) \ . \tag{2.82}$$

In a static atmosphere the evolution process of a convective element is described by the linear growth rate, and the element itself is characterized by its wave number $\mathbf{k}$, Eq. (2.66), and thus by the constant values of the mixing-length ℓ, Eq. (2.63), and shape-parameter Φ, Eq. (2.62), at each point in the atmosphere. These latter parameters, however, are no longer constant in a pulsating atmosphere, because of the locally changing environment. The eddies are advected by the pulsating flow, and in a Lagrangian frame moving with the pulsation they deform as they grow. Thus the evolution of the convective elements becomes influenced by the temporal behaviour of the atmosphere. In the mixing-length prescription by Unno (1967), the time dependence of the fluctuating quantities W and Θ was taken to be proportional to $\exp(-i\omega t)$, where ω denotes the complex pulsation frequency, and hence, were independent from the initial conditions at the time t_0 the element was created. However, if we apply the time-dependent equations (2.80) and (2.81) to a static mean-atmosphere, one may obtain an estimation for the time taken to achieve a steady state (i.e. constant velocity fluctuation), which turns out to be in the order of the characteristic life-time of a convective element. In a moving atmosphere therefore, the phase between pulsation and the turbulent perturbations at the instant t_0 substantially influences the stability of pulsation. The dependence on the initial conditions at t_0 can be taken into account by linearizing the variation of the atmosphere about its equilibrium state, denoting the instant t_0, which provides an expression for the wave number as function of the pulsation frequency ω in the form

$$k_h \ = \ k_{h,0} \left(1 + k_{h,10} e^{-i\omega t_0} + k_{h,11} e^{-i\omega t}\right) \ , \tag{2.83}$$

$$k_v \ = \ k_{v,0} \left(1 + k_{v,10} e^{-i\omega t_0} + k_{v,11} e^{-i\omega t}\right) \ , \tag{2.84}$$

where $k_{h,0}$ and $k_{v,0}$ are the wave numbers characterizing a convective element in a static atmosphere, and $k_{h,10}$, $k_{h,11}$, $k_{v,10}$, $k_{v,11}$ take the time-dependence upon the pulsation into account.

Combining the equations (2.80) and (2.81) and linearizing the result, provide us a differential equation of second order for the evolving velocity fluctuations with coefficients depending on k_h and k_v. The coupling of this equation with the pulsation is achieved by expressing these coefficients in the form, such as given here for the shape parameter Φ using Eq. (2.62), (2.83) and (2.84)

$$\Phi \ = \ \Phi_0 \left(1 + \Phi_{10} e^{-i\omega t_0} + \Phi_{11} e^{-i\omega t}\right) \ , \tag{2.85}$$

which represents the influence of the pulsating atmosphere on the shape of the eddy. The resulting expression becomes, to first order in pulsational perturbations

$$\frac{\partial^2 W}{\partial t^2} + 2\kappa\phi k^2 \left(1 + \kappa_{10} e^{-i\omega t_0} + \kappa_{11} e^{-i\omega t}\right) \frac{\partial W}{\partial t} + \frac{N^2}{\Phi} \left(1 + 2\mu_{10} e^{-i\omega t_0} + 2\mu_{11} e^{-i\omega t}\right) W \;=\; 0\,, \tag{2.86}$$

where the coefficients are given in the Appendix B according to Gough (1977). This equation can be solved exactly and may be written for the convective elements travelled about one mixing-length approximately as

$$W \;=\; W_0 \left[1 + W_{10} e^{-i\omega t_0} + W_{11} e^{-i\omega t} + \sigma\,(t - t_0)\, W_{12} e^{-i\omega t_0}\right]\,, \tag{2.87}$$

where $W_0 \approx \hat{W}_0 \exp[\sigma(t - t_0)]$ represents the evolving convective velocity fluctuation in a static atmosphere as given by equation (2.72). A similar expression results for the convective temperature fluctuation Θ. Thus the pulsationally induced perturbations of the convective fluxes may be obtained, with the help of Eq. (2.71), by substituting these solutions into the integral expressions (2.74) and (2.75) which become to first order in the relative perturbations

$$\frac{\delta F_c}{F_{c,0}} \;=\; \frac{\delta\rho}{\rho_0} + \frac{\delta c_p}{c_{p,0}} + W_{11} + \Theta_{11} + W_{21} + (W_{10} + \Theta_{10})\,\mathscr{F} + (W_{12} + \Theta_{12})\,\mathscr{F}\mathscr{G} + \mathscr{H}\,, \tag{2.88}$$

$$\frac{\delta p_{\rm t}}{p_{\rm t,0}} \;=\; \frac{\delta\rho}{\rho_0} + 2W_{11} + W_{21} + 2\,(W_{10}\mathscr{F} + W_{12}\mathscr{F}\mathscr{G}) + \mathscr{H}\,, \tag{2.89}$$

and for the linearized perturbation of the shape parameter Φ one obtains

$$\frac{\delta\Phi}{\Phi_0} \;=\; \Phi_{11} - \Phi_{10}\mathscr{F}\,, \tag{2.90}$$

where δX is the perturbation to the quantity X in a Lagrangian frame of reference arising from the pulsations. The subscript zero denotes the value in the static equilibrium model. The coefficients W_{1i}, Θ_{1i} and W_{12}, as well as the functional expressions $\mathscr{F}, \mathscr{G}$ and $\mathscr{H}$ are reproduced in the Appendix B according to Baker & Gough (1979). The expressions $\mathscr{F}, \mathscr{G}$ and $\mathscr{H}$ account for a statistical averaging of the convective fluctuations at the instant t_0 in form of a quadratic distribution function, because mixing-length theory only provides information about the turbulent spectrum at one particular scale. Thus those terms in the equations (2.88) and (2.89), which include these expressions significantly influence the phases between the convective fluctuations and the pulsating environment of the background fluid and hence, the pulsational stability of a star.

The local nature inherent in this time-dependent theory leads to another serious failure when applied to the problem of solving the linearized pulsation equations. It fails to treat properly the convective dynamics across extensive eddies. In deeper parts of the convection zone, where the stratification is almost adiabatic, convective heat transport is very efficient, thus radiative diffusion becomes unimportant and the perturbation of the

heat flux is dominated by the advection of the temperature fluctuations. Moreover, in this limit the convective elements grow very slowly compared to the pulsationally induced changes of the local stratification, *i.e.* $\omega/\sigma \gg 1$, and local theory predicts

$$\frac{\delta F_c}{F_{c,0}} \sim \frac{\delta\Theta}{\Theta_0} \sim -i\frac{\sigma}{\omega}\frac{\delta\beta}{\beta_0}\,, \tag{2.91}$$

hence, the perturbation of the heat flux is described by means of a diffusion equation with an imaginary diffusivity (Baker & Gough 1979). This gives rise to rapid spatial oscillations of the eigenfunctions, introducing a resolution problem which is particularly severe in layers where the stratification is very close to being adiabatic. This and the other drawbacks of a local theory, discussed before, may be obliterated by using the more advanced and superior non-local theory that we shall discuss next.

2.4. Non-local mixing-length theory

One of the major assumptions in the above described local mixing-length theory is, that the characteristic length scale ℓ must be shorter than any scale length associated with the structure of the star. This condition is violated, however, for solar-like stars and red giants where evolution calculations reveal a typical value for the mixing-length parameter

$$\alpha = \ell/H_p\,, \tag{2.92}$$

of the order of unity, where H_p is the pressure scale height. This implies that fluid properties vary over the extent of a convective element and the super-adiabatic gradient can vary on a scale much shorter than ℓ.

The non-local theory takes some account of the finite size of a convective element and averages the representative value of a variable throughout the eddy. Spiegel (1963) proposed a non-local description based on the concept of an eddy phase space and derived an equation for the convective flux which is familiar in radiative transfer theory. The solution of this transfer equation yields an integral expression which would convert the usual ordinary differential equations of stellar model calculations into integro-differential equations. An approximate solution can be found by taking the moments of the transfer equation and using the Eddington approximation to close the system of moment equations at second order (Gough 1976). The next paragraphs shall give a short discussion about the derivation of the non-local convective fluxes.

2.4.1. Non-local theory in a stationary atmosphere

In the generalized mixing-length theory proposed by Spiegel (1963), the turbulent convective elements are described by a distribution function $\psi(x_i, u_i, t)$ representing the number density of elements within an ensemble in the six-dimensional phase space (x_i, u_i), where u_i is the velocity vector of an eddy at the position x_i. The conservation of the eddies within the ensemble gives rise to an equation for the evolution of ψ

$$\frac{\partial \psi}{\partial t} + \frac{\partial}{\partial x_i}\left(u_i \psi\right) + \frac{\partial}{\partial u_i}\left(\dot{u}_i \psi\right) \;=\; q - \frac{u\psi}{\ell}\,, \tag{2.93}$$

where the dot denotes the derivative with respect to time. The source term q describes the local creation of convective elements, whereas the last term on the right hand side accounts for their annihilation after having travelled a distance of one mixing-length.

In the static mean atmosphere the eddy-ensemble is described by a statistically steady-state distribution function with vanishing time-derivative and the conservation equation in a plane parallel geometry becomes

$$\mu \frac{d\Psi}{dz} + \frac{\Psi}{\ell} \;=\; \frac{\mathscr{Q}}{\ell}\,, \tag{2.94}$$

where $\Psi = u\psi$ and $\mu = \cos\theta$, with θ being the angle between the vertical co-ordinate z and the direction of line along fluid element trajectories. The non-linear term $\partial(\dot{u}_i\psi)/\partial u_i$ in equation (2.93) describes the driving of the elements through buoyancy and pressure forces, and has been absorbed into the source function $\mathscr{Q}$, which changes equation (2.94) into a form like the radiative transfer equation in a gray atmosphere. Thus the equation can be formally solved for Ψ as function of $\mathscr{Q}$ (e.g. Chandrasekhar 1950), where the first moment, obtained by multiplying Eq. (2.94) by $h'\ell$ and integrating with respect to μ, can be interpreted as the convective heat flux written as

$$\mathscr{F}_c \;=\; \int_{-1}^{1} |h'| \Psi \mu \, d\mu \;=\; \int_{0}^{\infty} |h'| \mathscr{Q}\left(\xi_0\right) E_2\left(|\xi_0 - \xi|\right) \, d\xi_0\,, \tag{2.95}$$

where E_2 denotes the second exponential integral and we assumed symmetry for upward and downward moving elements (according to Boussinesq approximation) each having a specific enthalpy fluctuation of h'. The vertical displacement of an element from its initial position has been redefined by the more natural variable

$$d\xi \;=\; -\frac{dz}{\ell}\,. \tag{2.96}$$

There is still to define the source function $|h'|\mathscr{Q}(\xi_0)$ for which Spiegel chooses in the limit for small mixing-lengths to set it equal to the convective heat flux $F_c(\xi_0)$, as it would be computed in a purely local way, i.e. as given in equation (2.78). Thus we still have in this formulation inherent the approximation that the mixing length have to be small compared to any scale length in the star. The convective heat flux is proportional to the cube of the eddy growth rate σ, and σ is proportional to the superadiabatic lapserate β [cf. Eq. (2.70)]. In order to account for the case where the trajectories of the eddies are in the order or larger than the local scale height of the envelope, Spiegel used variational calculations to suggest that β in equation Eq. (2.70) should be replaced by its average value

$$\mathscr{B}(z) = \frac{2}{\ell}\int_{z-\ell/2}^{z+\ell/2} \beta(z_0)\cos^2\left[\frac{\pi}{\ell}(z_0 - z)\right] dz_0\,, \tag{2.97}$$

We are now faced with integral expressions, which would convert the ordinary differential equations of stellar structure into integro-differential equations, increasing considerably the numerical treatment. Fortunately an approximate solution of equation (2.94) for Ψ and thus for the convective fluxes may be obtained by taking moments of the transfer equation and using the Eddington approximation to close the system of equations at second order (Gough 1976). This yields the solution

$$\frac{1}{a^2}\frac{d^2\mathscr{F}_c}{d\xi^2} = \mathscr{F}_c - F_c\,, \tag{2.98}$$

when using for the source function $|h'|\mathscr{Q} = F_c$ and for the additional parameter $a = \sqrt{3}$. The exact solution of this equation is

$$\mathscr{F}_c(\xi) = \int_{-\infty}^{\infty} F_c(\xi_0)\,\mathscr{K}(\xi,\xi_0)\,d\xi_0\,, \tag{2.99}$$

where the kernel $\mathscr{K}$ is given by

$$\mathscr{K}(\xi,\xi_0) = \frac{1}{2}a\exp(a|\xi - \xi_0|)\,. \tag{2.100}$$

Thus the approximation Eq. (2.98) is equivalent to replacing the kernel $E_2(|\xi_0 - \xi|)$ in Eq. (2.95) by the simpler form of equation (2.100). This suggests, however, a different value for the coefficient a, which can be determined by demanding that terms in the Taylor expansions about ξ of $\mathscr{K}$ and E_2 differ only at fourth order, which yields $a = \sqrt{2}$.

The expression for the averaged superadiabatic lapsrate $\mathscr{B}$, Eq. (2.97), may be obtained in a similar way. The integration limits can be formally set to $\pm\infty$, if contributions to $\mathscr{B}$ from beyond the trajectory of the eddy are assumed to vanish. By approximating the kernel, which may be written as $2\cos^2[\pi(\xi_0 - \xi)]$, by $\mathscr{K}$, one obtains

$$\frac{1}{b^2}\frac{d^2\mathscr{B}}{d\xi^2} = \mathscr{B} - \beta\,, \tag{2.101}$$

where $b \simeq \sqrt{61}$ using the Taylor-expansion technique described above.

The momentum flux of the eddies within the ensemble can be treated using exactly the same approach as for the convective heat flux, where one obtains a similar expression for the turbulent pressure written as

$$\frac{1}{a^2}\frac{d^2\mathscr{P}_\mathrm{t}}{d\xi^2} = \mathscr{P}_\mathrm{t} - p_\mathrm{t}\,. \tag{2.102}$$

The non-local equations discussed above were derived in the physical picture in which the convective elements are accelerated from rest and whose evolutions along their trajectories are described by linear growth rates, as already discussed in the local theory. Obviously the non-local equations may also be discussed in the view of the second picture, where the eddies are regarded as cells with the size of one mixing-length and centered at some fixed height, again, similar as in the local treatment of mixing length theory. This is the picture in which Gough (1976) discussed the derivation of the non-local equations, which corresponds to treating the finite extent of the eddy and the non-local transfer of heat and momentum across it by using the averaging idea which had led to the equation for $\mathscr{B}$ described above. The integral expression Eq. (2.97) may then be interpreted such that an eddy centered at z_0 samples $\mathscr{B}$ over the range determined by the extend of the eddy, *i.e.* $(z_0 - \ell/2, z_0 + \ell/2)$. Moreover, the averaged convective fluxes $\mathscr{F}_c$ and $\mathscr{P}_t$ are constructed not only by eddies located at $z_0 = z$, but by all the eddies centered between $z_0 - \ell/2$ and $z_0 + \ell/2$. Hence the two additionally parameters a and b (three, if the kernels for the convective heat flux and turbulent pressure are treated differently) control the spatial coherence of the ensemble of eddies contributing to the total heat and momentum flux (a), and the degree to which the turbulent fluxes are coupled to the local stratification (b). Theory suggests values for these parameters, but the quoted values are approximate and to some extent these parameters are free. These parameters control the degree of "nonlocality" of convection, where low values imply highly non-local solutions and in the limit $a, b \to \infty$, the system of equations reduces to the local theory. Balmforth (1992a) explored the effect of a and b on the turbulent fluxes in the solar case very thoroughly and Tooth and Gough (1989) have looked at laboratory convection and attempted to calibrate a and b.

In Fig. 2.1 the temperature gradient $\nabla = d \ln T / d \ln p$ for an equilibrium model of a 1.3 $M_\odot$ ZAMS star is depicted. The envelope was computed according to the procedure discussed in Section 3.4.4, using the values $a^2 = b^2 = 300$ for the non-local solution (solid line). In order to compare two envelope models, constructed by using different prescription for convection, the equilibria must be defined exactly on the same adiabat below the upper superadiabatic boundary layers, upon the bulk of the convection zone is described on. Once the equilibrium model is constructed according to the non-local formulation the local model is found by a proper matching procedure. Specifying the same surface boundary conditions in both models the local model is iterated to the non-local solution at a particular radius defined just above the superadiabatic layers at the bottom of the convection zone, where the temperature gradient becomes almost identical to the adiabatic one (see right panel of Fig. 2.1). At this radius the pressure and temperature have to be continuous and therefore we need to vary two parameters in the iteration process of the local model, such as the local mixing-length parameters α_c and hydrogen mass fraction X. This procedure enables us to compare models, constructed with the local and non-local formulation of convection, which differ most in the upper layers.

The non-local theory predicts a smaller temperature gradient in the upper superadiabatic regions than the local theory does. A smaller value of the non-local parameter a enhances the contribution from eddies located at different layers to the turbulent heat flux, thus reducing the temperature gradient. Moreover, the non-local gradient is slightly pushed inwards and depicts a pronounced temperature inversion at $\log p = 4.93$. Such an

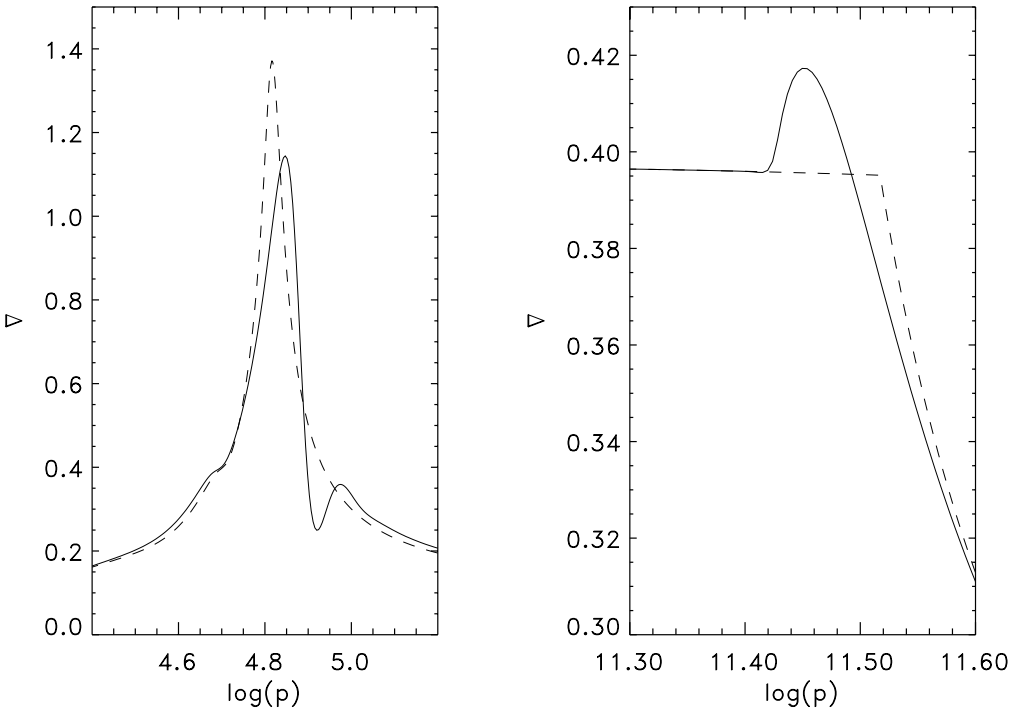

Figure 2.1: Temperature gradient $\nabla = d\ln T/d\ln p$ for a 1.3 $M_\odot$ ZAMS equilibrium model envelope, depicted at the upper (left) and lower (right) boundary of the convection zone. The solid line gives the solution according to the non-local mixing-length theory assuming the convection parameters $\alpha_c = 2.0, a^2 = b^2 = 300$; the dotted line depicts the results for the local theory, which has been matched to the same adiabat of the non-local solution at the bottom of the convection zone by varying the mixing-length parameter α_c and abundance of hydrogen X of the local solution from $\alpha_c = 2.0$ and $X = 0.7$ to the new values $\alpha_c = 1.964$ and $X = 0.7033$, respectively.

inversion results from the decoupling of the turbulent fluxes from the local stratification, controlled by the non-local parameter b. With decreasing value of b, sudden changes in the local structure, e.g. in the ionization zones, are no longer diminished by the response of the turbulent heat flux. This may result in an increase of the steepness of the temperature gradient and thus the temperature inversion amplifies.

In Fig. 2.2 the temperature gradients are portrayed for a non-local model envelope, computed with the parameters $a^2 = 900, b^2 = 2000$, and the corresponding local model, which again, has been fitted to the non-local solution. Clearly, one can see, that for larger values of a and b the non-local temperature gradient becomes more similar to the local solution. Furthermore, an increase of the non-local parameters a and b reduces the extent of the convection zone, which is similar to a decrease of the mixing-length parameter α_c. This comes about because reducing α_c means a smaller size of the convective eddies and thus convection becomes less efficient.

2.4.2. Time-dependent, non-local theory

In order to derive expressions for the pulsationally induced perturbations of the non-local turbulent fluxes, the time derivative in equation (2.93) has to be taken into account. One

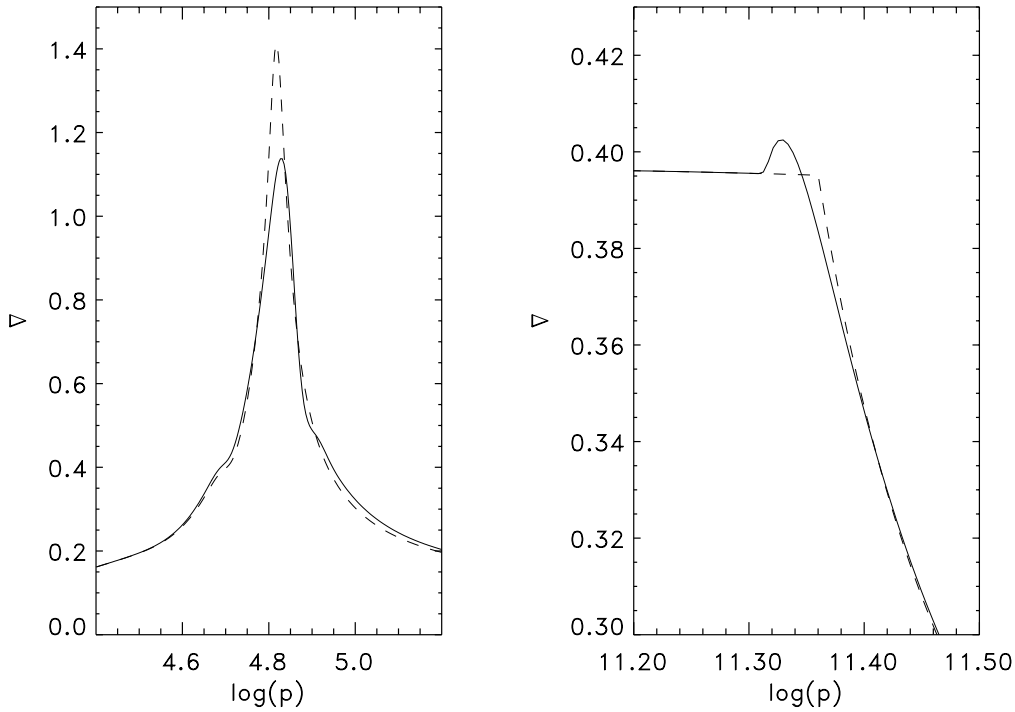

Figure 2.2: Temperature gradient ∇ for the same model as in Fig. 2.1, but using $a^2 = 900, b^2 = 2000$ for the non-local solution (solid line). The matching of the model envelope constructed with the local mixing-length theory (dashed line) was obtained with the new parameters $\alpha_c = 1.895$ and $X = 0.7038$.

can then proceed as in the static atmosphere and take moments of this equation to derive an expression for the convective flux. This expression may be linearized which provides a differential form for the perturbations to the turbulent fluxes including the term of the time-dependent source function $\mathscr{Q}$. The time-dependence of $\mathscr{Q}$, as introduced in the static discussion, can be described as the instantaneous creation of elements, whereas the term $\partial\psi/\partial t$ in equation (2.93) accounts for the phase delay between the source function and the response of the distribution function ψ. In the local prescription of Gough, the distortion of the mean eddy size between creation and annihilation with the mean environment is accounted for appropriately and thus also the phase lag between the deformation of the mean environment and the response of the turbulent fluxes. Hence, the phase lag due to the $\partial\psi/\partial t$ term is already taken into account by the source function $\mathscr{Q}$, when it is set to Gough's locally computed turbulent fluxes. Thus equation (2.93) becomes essentially the form of Eq. (2.94) and the perturbations to the turbulent fluxes are obtained by perturbing the equations (2.98), (2.101) and (2.102) to first order which gives

$$\frac{1}{\varepsilon^2}\frac{\partial}{\partial\xi}\left[\frac{\partial}{\partial\xi}\left(\delta\mathscr{T}\right) - \frac{\partial}{\partial\ln p_0}\left(\frac{\delta p}{p_0}\right)\frac{\partial\mathscr{T}}{\partial\xi}\right] = \delta\mathscr{T} - \delta T + \left(\mathscr{T} - T\right)\frac{\partial}{\partial\ln p_0}\left(\frac{\delta p}{p_0}\right), \qquad (2.103)$$

where $\mathscr{T}$ is either of $\mathscr{F}_c$, $\mathscr{P}_t$ or $\mathscr{B}$, and T is the corresponding source function or β. The Lagrangian perturbations to the pressure and the quantity $\mathscr{T}$ are represented by δp and $\delta\mathscr{T}$, respectively, and the parameter ε is either a or b. The corresponding perturbation to the local quantities T are taken according to Gough's local, time-dependent formulation of convection, as discussed above.

2.5. Other formulations of convection

The previous chapters revealed us some of the complexity of the stochastic nature of turbulent flow. It constrains one to find appropriate models for the generation of turbulence through the Reynolds stresses, which extract energy from the mean flow in the case of shear flow or from the work done by buoyancy in the case of thermal convection, as well as for the transfer of energy by turbulence itself and for the dissipation of energy into heat by molecular processes. Inherent in all these models is the need of information, how energy is distributed amongst the different scales of turbulence, *viz.* the turbulent energy spectrum. The width of the turbulent spectrum depends on the molecular viscosity; in particular the ratio between the largest and smallest size of the eddies which constitute the spectrum is $\sim \mathrm{Re}^{3/4}$, hence, for the solar case with a Reynolds number $\mathrm{Re} \approx 10^{10}$, this ratio is about 10^7. The mixing-length idea accounts only for one particular scale described by the length ℓ, which represents the vertical extend or the travel distance of the most energy-bearing eddies. Thus, it is the mixing-length theory which describes the beginning of the turbulent cascade and thus neglecting the influence of the dynamics by the small scale turbulence. One possibility to account for the momentum and heat exchange by the small scale turbulence is by introducing an additional (enhanced) scalar eddy diffusivity ν_e, assuming that the small scale dynamics is isotropic. Such an eddy diffusivity can be described by an one-equation model suggested by Prandtl and Kolmogorov in the 1940s, where ν_e is proportional to the square root of the turbulent energy $\overline{u_i' u_i'}/2$ and may be related to the velocity and length scales of the large eddies (Gough 1976) by

$$\nu_e \;=\; \frac{1}{2}\left(\overline{u_i' u_i'}\right)^{1/2} / k' \;=\; \epsilon\,(\overline{u_i u_i})^{1/2}\,k^{-1} \;=\; \frac{\epsilon \ell}{\pi}\,(\Phi-1)^{1/2}\left(\overline{w^2}\right)^{1/2}\;, \tag{2.104}$$

where k' denotes for the local wave number of small scale turbulence and ϵ is of order unity and depends on the turbulent spectrum. In accordance to the way we constructed the turbulent fluxes, Eq. (2.78) and Eq. (2.79), we may write $(\overline{w^2})^{1/2} = \sigma\ell/2$. Taking the diffusivity to be the same for both momentum and heat (*i.e.* $P_{\mathrm{r_t}} = 1$ in equation (2.37)), the convective linear growth rate may be expressed as

$$2\sigma \;=\; -\,(\tilde{\kappa}+\tilde{\nu})\,k^2 + \left[(\tilde{\kappa}+\tilde{\nu})^2\,k^4 + 4\frac{g\delta\beta}{\Phi T}\right]^{1/2}\;, \tag{2.105}$$

where $\tilde{\kappa} = \kappa + \nu_e$ and $\tilde{\nu} = \nu_e$, which is essentially equation (2.70) multiplied by the factor $[1 + \epsilon\pi\Phi(\Phi-1)^{-1/2}/2]$ and may be used to construct the turbulent fluxes according to Eq. (2.78) and Eq. (2.79). Including the enhanced diffusivity in Eq. (2.105) increases σ, and thus the turbulent fluxes become larger compared to the case, without the inclusion of ν_e. However, the modelling of the turbulent energy spectrum by means of an enhanced diffusivity as given by equation (2.104) reflects only a crude approximation, where models based on two-point closer theories may be more promising.

2.5.1. The Canuto-Mazzitelli prescription of convection

Recently, Canuto and Mazzitelli (1991, hereafter CM) proposed a model for convection which takes account for the full turbulent spectrum computed according to the Eddy Damped Quasi-Normal Markovian (EDQNM) model (Orszag 1977). This model is based on a statistical description of turbulence by means of an improved theory of the Quasi-Normal approximation by Millionschikov (1941). In this approximation the higher moments n ($n > 2$) of a non-gaussian random function (like the turbulent velocity field) with known second-order moments can be computed under the assumption that this function would be a gaussian one. The difference between the actual $n-th$ order moment of the function and the corresponding gaussian value is called the $n-th$ order *cumulant*. In the EDQNM model the fourth-order cumulants are approximated by a linear damping term, in order to achieve positiveness of the resulting energy spectrum for homogeneous turbulence.

The convective heat flux may be expressed in terms of the turbulent kinetic energy per unit mass, $E(k)$, as (e.g. Yamaguchi 1963)

$$F_c \;=\; \phi K\beta\Delta\left(\eta^2 S\right)\,, \qquad\qquad \Delta\left(\eta^2 S\right) \;=\; \frac{\rho c_p T}{g\delta K\beta}\int_0^\infty 2\sigma\left(k\right)E\left(k\right)\,dk\,, \tag{2.106}$$

where we neglected terms including the molecular viscosity in the integrand. In the CM model the function Δ, describing the energy spectrum as function of the convective efficacy $\eta^2 S$, is provided as an analytical fit to the corresponding results, obtained by computing the spectrum according to the EDQNM approximation.

In the local mixing-length theory σ describes the convective evolution only for those eddies which are characterized by the wavenumber $k_\ell = \pi/\ell$. Moreover, the spectrum of the kinetic energy is only described at this particular scale and may be approximated by the delta function $\bar{\delta}(k-k_\ell)$. Thus the function Δ can be displayed in Gough's formulation of the local mixing-length theory as

$$\Delta_\ell\left(\eta^2 S\right) \;=\; \frac{\rho c_p T}{g\delta K\beta}\int_0^\infty 2\sigma\left(k_\ell\right)E_\ell\bar{\delta}\left(1-k/k_\ell\right)\,dk \;=\; \frac{1}{4}\Phi^{1/2}\eta^{-3}S^{-1}\left[\left(1+\eta^2 S\right)^{1/2}-1\right]^3, \tag{2.107}$$

using the equations (2.70) and (2.78).

We are now in the situation to compare the convective heat flux, obtained according to the mixing-length approach, with the true flux as given by Eq. (2.106). The linear growth $\sigma(k_\ell)$ can be written in terms of characteristic time scales [cf. Eq. (2.105) with $\nu_e = 0$] as

$$2\sigma_\ell = -\frac{1}{\tau_\kappa}\left\{\left[1+\left(\frac{\tau_\kappa}{\tau_N}\right)^2\right]^{1/2}-1\right\}, \tag{2.108}$$

where

$$\tau_\kappa = \frac{1}{\phi\kappa k_\ell^2}\,, \qquad \text{and} \qquad \tau_{_N} = \left(\frac{g\delta\beta}{\Phi T}\right)^{-1/2}\,, \tag{2.109}$$

represent the characteristic time scales for radiative cooling and buoyancy [cf. Eq. (2.46)], respectively.

In the limit of efficient convection $\tau_{_N} \ll \tau_\kappa$, and $\sigma(k_\ell) \approx \tau_{_N}$, thus it becomes independent of k_ℓ. The differences between the integral expressions for Δ and Δ_ℓ are therefore solely governed by the kinetic energy spectrum. The reduced energy spectrum in the mixing-length approach, i.e. neglecting the contribution from small-scale eddies to the expression of Δ_ℓ, leads to the result that

$$F_c^\ell \ll F_c \qquad \text{if} \quad \eta^2 S \gg 1\,, \tag{2.110}$$

where $F_c^\ell = K\beta\Delta_\ell$ is the convective flux predicted by the mixing-length theory. If however, convection becomes inefficient, $\tau_{_N} \gg \tau_\kappa$, and $\sigma(k_\ell) \simeq \tau_\kappa^{-1}(\tau_\kappa/\tau_{_N})^2 \sim k_\ell^{-2}$. Thus in the wavelength-domain, where the growth rate $\sigma(k)$ decreases with k^2, the corresponding value of $\sigma(k_\ell)$ remains larger. The value for Δ_ℓ therefore dominates over Δ when calculated according to equation (2.106) providing the relation

$$F_c^\ell \gg F_c \qquad \text{if} \quad \eta^2 S \ll 1\,. \tag{2.111}$$

In the above comparison the CM-model predicts a considerably larger temperature gradient in the superadiabatic layers than the mixing-length approach does (Monteiro, Christensen-Dalsgaard & Thompson 1994, 1996).

The expressions (2.110) and (2.111) can be interpreted as a clockwise rotation of $F_c^\ell(S)$ in the 'efficiency space' $S-F_c$, with respect to the solution of F_c when calculated according to equation (2.106). In mixing-length theory the parameter $\alpha_{\rm c}$ [cf. equation (2.92)] selects the proper adiabat on which the bulk of the convection zone is defined on, in order to obtain the correct radius of a star in stellar evolution calculations. Thus the parameter $\alpha_{\rm c}$ acts only as a translation parameter and has therefore no influence on the necessarily rotational adjustment of the heat flux in the $S - F_c$ space.

In the CM model the authors define the mixing-length ℓ at each layer equal to the distance from the top of the convection zone and therefore removing any free parameter from the expressions for the convective heat flux. However, evolution calculations for a $1M_\odot$ star with the CM model reveal a too large radius for the Sun (e.g. Christensen-Dalsgaard, Monteiro & Thompson 1995) and moreover, hydrodynamical simulations of turbulent compressible convection (e.g. Chan & Sofia 1987) provide some support that ℓ is proportional to the local pressure scale height at all depths. It is therefore still an open question how the characteristic scale lengths should be taken into account and further investigations seem to be necessary.

2.5.2. Reynolds stress models

The convection models discussed so far are only applicable to the case when turbulence is homogeneous. There have been made some attempts to extend the EDQNM model for moderately inhomogeneous turbulence (e.g. Burden 1991), however, the Reynolds stress approach allow a reasonable degree of flexibility and can, in principle, account for effects such as buoyancy, curvature and rotation in inhomogeneous turbulence without ad hoc adjustments.

In the context of stellar convection, inhomogeneous turbulence becomes important when effects such as overshooting should be taken into account. Canuto (1992) introduced a turbulent convection model by means of the Reynolds stress approach using the Boussinesq approximation and extended this model for the general non-Boussinesq case very recently (Canuto 1993). Here I just give a brief review about the basic method of Reynolds stress models and about the closure procedures as Canuto has applied them in his prescription.

As proposed first by Keller & Friedmann (1924) the Reynolds stresses can be determined from a transport equation. In the Boussinesq approximation this transport equation is obtained by first multiplying equation (2.22) by u'_j to obtain Eq. (2.22a), interchanging the indices i and j in Eq. (2.22a) to obtain Eq. (2.22b), followed by a summation of Eq. (2.22a) and Eq. (2.22b). By taking the average of this result the transport equation becomes

$$\frac{\partial R_{ij}}{\partial t} + \frac{\partial \overline{u'_i u'_j u'_k}}{\partial x_k} = -\left(g_i \frac{\overline{\delta}}{\overline{T}} \overline{u'_j T'} + g_j \frac{\overline{\delta}}{\overline{T}} \overline{u'_i T'} \right) - \frac{1}{\overline{\rho}} \left(\overline{u'_i \frac{\partial p'}{\partial x_j}} + \overline{u'_j \frac{\partial p'}{\partial x_i}} \right) + \nu \frac{\partial^2 R_{ij}}{\partial x_k^2} - \epsilon_{ij} \,, \tag{2.112}$$

where $R_{ij} = \overline{u'_i u'_j}$ denotes the Reynolds stress tensor and we neglected terms including the mean flow $\overline{u_i}$. The third term on the *r.h.s* represents diffusion of turbulence by molecular viscosity and is usually neglected, whereas ϵ_{ij} [cf. Eq. (2.14)] must be taken into account, as already discussed before, and has to be modelled by another transport equation. The second term on the *l.h.s*, a triple-correlation tensor, is usually interpreted as a diffusive flux of the Reynolds stress generated by the action of the stress itself (sometimes called the turbulence self-diffusion term). It is this term which gives rise to the well known closure problem in the statistical description of turbulence. An additional equation may be established to describe this triple-correlation tensor, which will contain fourth-order moments and so on. To describe the whole problem similar transport equations have to be established for the remaining second-order moments, appearing in the fluctuating equations (2.22) and (2.24) (i.e. $\overline{u'_i T'}, \overline{T'^2}$ and $\overline{u'_i u'_i}$).

It was common to approximate the third order moments in a similar way as in the second-order closure, i.e. by means of a turbulent viscosity multiplied by the gradient of the characteristic second-order moment (down-gradient- or diffusion approximation). However, such down-gradient approximations imply many shortcomings and one should instead consider the full expressions for the third-order moments (Finger & Schmidt 1986) applying proper approximations for the fourth-order correlations. Assuming the fourth-order moments to be gaussian random variables and replacing the correlations for the

pressure by third-order damping terms, one can express the third-order correlations by the second-order moments (Hanjalic & Launder 1976). This approximation is physically equivalent to the EDQNM model discussed before. Thus one obtains a set of linear algebraic equations for the third-order moments which can be solved analytically and the whole turbulent convection problem is described by five coupled differential equations for the second-order moments which are solved numerically (Canuto 1992, 1993).

3. Damping and excitation of solar-type p modes

3.1. Introduction

The stability of solar-like p modes depends mainly on the interaction of acoustic modes with radiation and convection in the atmosphere. So far, two theories, thermal overstability and stochastic excitation by turbulent convection seem to be the most plausible explanations for solar-type p mode pulsation. In both mechanisms the energy flow from radiation and convection into and out of the p modes is taking place very near the surface.

The mechanism of thermal overstability can arise from the disturbance of the local equilibrium due to pulsation, by exchanging heat between stellar matter, the turbulent energy and the radiation field. If the pulsation is supported by the energy arising from the perturbation of the divergence of the radiation flux, we know from the more well-known theory of variable stars (e.g. Cepheids), that this kind of driving, the κ -mechanism, takes place predominantly in the ionization zones just below the photosphere. Solar-like stars, however, exhibit distinctive surface convection zones and the ionization layers lie well within these convectively unstable domains where the total energy flux is carried predominantly by the turbulent heat flux. The energy exchange with turbulent convection depends strongly on the convective Mach number which becomes largest in the superficial boundary layers, where there is the transition from convective to radiative energy transport. Thus the stability is governed by the perturbations in the radiative and turbulent fluxes (heat and momentum), demanding for a proper theory for convection, which includes non-adiabatic effects arising from the interaction of the turbulent velocity field with the pulsation. These non-adiabatic effects can lead to overstability and may therefore constitute one conceivable explanation of the excitation of solar-like oscillation (Ulrich 1970a; Antia, Chitre & Gough 1988). By solving the non-adiabatic equations for non-radial oscillations of a solar envelope, Ando & Osaki (1975) found that many of the solar p modes were overstable and that the highest growth-rates occurred for those modes having frequencies of about 5 minutes. Their results looked encouraging for the thermal overstability mechanism. However, they completely neglected the perturbations in the turbulent fluxes and therefore underestimated the damping rates severely. Moreover, if solar-like p modes were really overstable, some non-linear mechanisms must limit the amplitudes to the low values that are observed in the solar case. The only mechanism proposed to far which could perhaps limit the growth of overstable modes is non-linear mode coupling, as considered by Kumar & Goldreich (1989). For oscillations with such small amplitudes ($\delta R/R \simeq 10^{-8}$ for solar-like oscillations, R being the radius of the star, whereas the corresponding value of a Cepheid variable star is $\delta R/R \simeq 10^{-1}$), it is likely that only the lowest order coupling is of importance, *viz.* three-mode coupling, which has been studied in an analytical way by Kumar and Goldreich. Their results however, suggest, if all modes were overstable, their growth cannot be limited within the observed amplitudes through the mechanism of non-linear coupling. Thus the theory of stochastic excitation may be more favorable than the model of thermal overstability.

Stochastic excitation by turbulent convection results when intrinsically stable modes are forced by the emission of acoustical radiation generated by turbulent multipole sources

(e.g. Unno 1964). The acoustic noise generated by convection in the star's resonant cavity may result in the excitation of p modes (Goldreich & Keeley 1977b), and emits radiation in a broad-band in frequency. The radiation which is trapped inside the star's cavity, can also be re-absorbed by the turbulence which will tend to limit the amplitudes of p modes. The amplitudes are then determined by the balance between the excitation rate and the damping rate and are expected to be rather low. Thus the turbulent excitation model predicts not only the right order of magnitude for the p mode amplitudes, but it also explains the observation that millions of modes are excited simultaneously.

Beside the demand of a time-dependent theory for convection to treat properly the linear stability problem of solar-type pulsation, the theoretical calculations are complicated still further by the fact that the acoustic modes depend crucially upon the treatment of radiative transfer. This is particular true for high-order modes, since the point at which waves are reflected back towards the interior gradually moves outwards with increasing frequencies and the thermal perturbation to the modes becomes progressively more influenced by the radiative relaxation of the atmosphere. Moreover, radiative equilibrium in no longer maintained in the transition region between radiative and convective energy transport. Thus approximating the radiative transfer equation by the diffusion equation will be inappropriate and would lead to an underestimation of the atmospheric damping due to radiative losses (Ando & Osaki 1975, Christensen-Dalsgaard & Frandsen 1983a).

Balmforth (1992a) introduced improved routines using Gough's (1976, 1977) non-local, time-dependent mixing-length theory for convection (cf. Section 2.4) and the Eddington approximation to radiative transfer (Unno & Spiegel 1966) in both, the equilibrium and pulsation model. He calculated damping rates for the solar envelope and found all modes stable. The results presented here have been obtained with Balmforth's programme, for which the implementation details are discussed in Section 3.4.1.

3.2. Damping rates

3.2.1. Observations of line widths in the Sun

Assuming that solar p modes were stable, the intrinsic damping rate of the modes can be obtained from measurements of the pulsation line widths. The line widths are obtained by fitting Lorentzian profile functions (see below) to the spectral peaks of the observed power spectrum. Recent observations (Toutin & Fröhlich 1992; Elsworth 1995a,b; Goode & Strous 1996) support the hypothesis that solar acoustic modes are intrinsically damped, but excited stochastically by convection. These measurements, however, usually suffer from a rather poor signal-to-noise ratio and the demand of continuous observations over very long periods, in particular for modes of low frequencies. Further complications in the observed power spectrum of solar pulsations still arise from non-linear effects (Dziembowski 1988), mode beating of closely spaced modes (e.g. Christensen-Dalsgaard & Gough 1982) and from effects caused by deformation of the Sun (e.g. Kuhn 1996). Thus the measurements of line widths are of complicated nature and depend on the observing details, the mode re-excitation (e.g. Jefferies *et al.* 1988) and the basic mode lifetime.

The power spectrum for which all modes are stable, can be described by an ensemble of intrinsically damped, stochastically driven, simple harmonic oscillators. The power spectrum of a damped harmonic oscillator excited by random forces $f(t)$ is approximately Lorentzian and its amplitude $a(t)$ is proportional to the ratio between the power put into the mode and its damping rate (e.g. Batchelor 1956). If the random function $f(t)$ is independent from $a(t)$ (*viz.* harmonic), the oscillator satisfies the equation

$$\frac{d^2a}{dt^2} + 2\eta\frac{da}{dt} + \omega^2 a = f\,(t)\ , \tag{3.1}$$

where η is the damping rate, ω is the natural frequency of the mode and the spectrum of the forcing function $f(t)$ is assumed to be nearly white (or Gaussian). Since one particular p mode is excited by many convectively unstable elements, the latter assumption can be justified by the Central Limit Theorem (e.g. Reif 1985). It implies that $f(t)$ approaches a gaussian forcing in the limit of infinite convectively unstable elements, independent of their individual stochastic forcing function. By taking the Fourier transform of equation (3.1) and neglecting transients arising from the initial conditions on the amplitude a, we obtain

$$A\,(\Omega) \;=\; \frac{F\,(\Omega)}{\omega^2 - \Omega^2 + i2\eta\Omega}\,, \tag{3.2}$$

where $A(\Omega)$ and $F(\Omega)$ are the transforms of $a(t)$ and $f(t)$. The limited observation time from a single site additionally blurs the required frequency resolution and should be taken into account in this analysis. Thus the mean power spectrum $P_a(\Omega) = <|A|^2>$ of a time series lasting from $t = 0$ to $t = T$ is given by

$$\begin{aligned} P_a\,(\Omega) \;=\; & \frac{2P_f\,(\Omega)}{\left(\omega^2 - \Omega^2\right)^2 + 4\eta^2\Omega^2} \\ & \times \left\{\eta T + \frac{\Delta\Omega^2 - \eta^2}{\Delta\Omega^2 + \eta^2} + \frac{e^{-\eta T}}{\Delta\Omega^2 + \eta^2}\left[\left(\eta^2 - \Delta\Omega^2\right)\cos\Delta\Omega T - 2\eta\Delta\Omega\sin\Delta\Omega T\right]\right\} \end{aligned} \tag{3.3}$$

where $P_f(\Omega) = <|F(\Omega)|^2>$ represents the average power spectrum of the forcing and $\Delta\Omega = \omega - \Omega$. The expression for the power spectrum may be simplified if the harmonic oscillator is excited only once (Christensen-Dalsgaard 1989), yielding

$$P\,(\Omega) \;=\; \frac{e^{\eta T}\sin^2\left[(\Omega - \omega)\,T/2\right] + 1/4\left(e^{\eta T} - 1\right)^2}{(\Omega - \omega)^2 + \eta^2}\,a^2\,. \tag{3.4}$$

Assuming a damped oscillation with $\eta < 0$, in the limit $|\eta T| \ll 1$ the power spectrum reduces to

$$P\,(\Omega) \;=\; 1/4a^2T^2\mathrm{sinc}^2\left[(\Omega - \omega)\,T/2\right]\ , \tag{3.5}$$

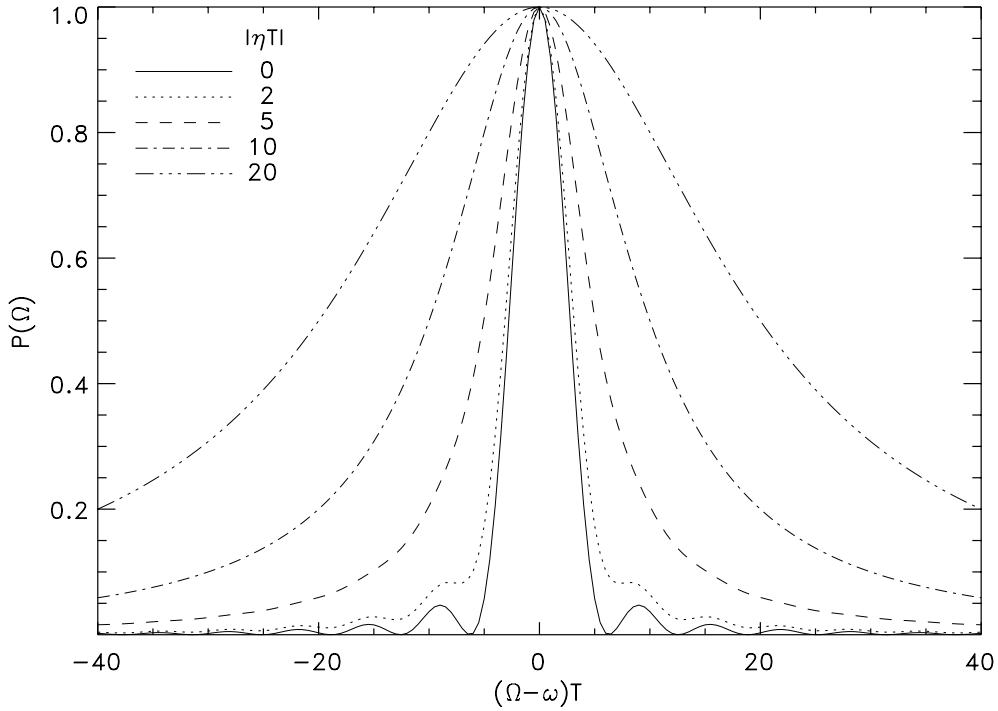

Figure 3.1: Mean power spectrum of a once excited damped harmonic oscillator [see equation (3.4)] illustrating the combined effects of damping η and finite observing time T. The abscissa is the frequency separation between frequency and the natural frequency of the oscillator, in units of $1/T$. The ordinate represents the normalized power and the curves are depicted for different values of $|\eta T|$. With increasing $|\eta T|$, the curves transform smoothly from sinc^2-profiles to Lorentz-profiles.

where sinc $x = (\sin\ x)/x$, thus we do get a sinc^2-profile. In this limit the *half width at half maximum* (HWHM) in ω of the observed peak is given by 2.89 T^{-1}.

In the other limit with $|\eta T| \gg 1$, the first term in the numerator of equation (3.4) can be neglected and we obtain

$$P\left(\Omega\right) \;=\; \frac{1}{4}\,\frac{a^2}{\left(\Omega-\omega\right)^2+\eta^2}\,, \tag{3.6}$$

which represents a Lorentz-profile with a HWHM of η. The transition between these two limits is displayed in Fig. 3.1 for which the HWHM$\approx \eta + T^{-1}$. Thus for $|\eta T| \gg 5$ the line profile is essentially purely Lorentzian.

The average power spectrum for a stochastically excited damped harmonic oscillator [see equation (3.3)] becomes in the limit $|\eta T| \gg 1$

$$P_a\left(\Omega\right) \;=\; \frac{P_f\left(\Omega\right)}{\left(\omega^2-\Omega^2\right)^2+4\eta^2\Omega^2} \approx \frac{1}{4\omega^2}\,\frac{P_f\left(\Omega\right)}{\left(\omega-\Omega\right)^2+\eta^2} \propto P_L\left(\Omega\right) P_f\left(\Omega\right)\,, \tag{3.7}$$

provided $|\eta| \ll \omega$ and the average power spectrum $P_f(\Omega)$ of the forcing varies slowly with ω. $P_L = 1/[(\omega-\Omega)^2+\eta^2]$ represents a Lorentzian profile with a HWHM$=\eta$. An example

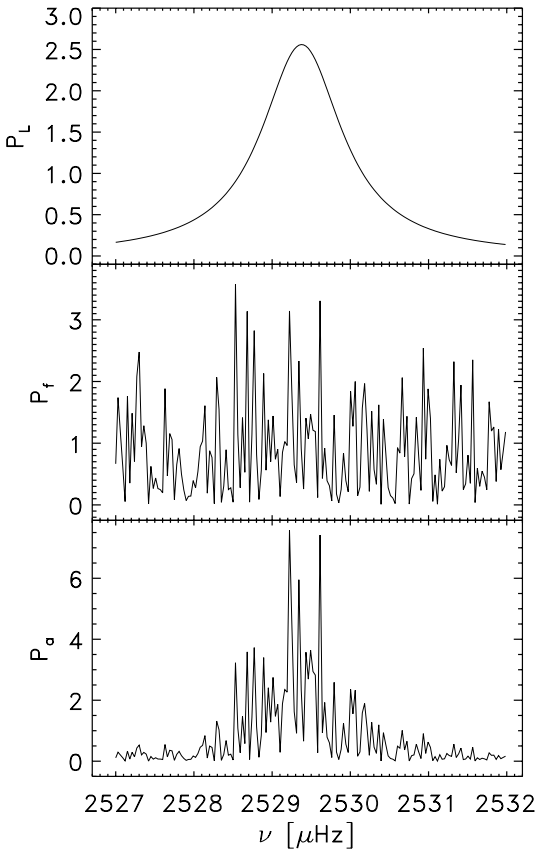

Figure 3.2: Power spectra of a randomly excited spectral line. P_L depicts a pure Lorentzian profile for the solar p mode with degree $l = 20$ and radial order $n = 11$ ($\nu = 2529.378$ μHz, $\eta = 1.25$ μHz). P_f represents a stochastic source spectrum and P_a is the product of the Lorentzian and the source spectrum [see equation (3.7)]. The sampling rate is 0.03 μHz (adopted from Kosovichev 1995).

of the power spectra of P_L, P_f and P_a for a particular oscillation mode are depicted in Fig. 3.2. Taking the integral of equation (3.7) one obtains the result

$$\int_0^\infty P_a\left(\Omega\right)\, d\Omega \approx \frac{1}{|\eta|}\,\frac{\pi}{4}\,\frac{P_f\left(\omega\right)}{\omega^2}\,. \tag{3.8}$$

Thus, as already stated before, the power in a particular oscillation mode is proportional to the power of the forcing at the oscillation frequency and inversely proportional to the linear damping rate. Moreover, the lower the damping rates η become, the longer have to be the observing time T, in order to obtain accurate line width measurements by means of fitting Lorentzian profiles to the spectral peaks in the observed power spectrum.

3.2.2. Physical effects contributing to line widths

Various physical processes are responsible for stabilizing the p modes. Beside the non-adiabatic effects, such as radiative damping, contributions arising from dynamical effects may be of similar importance. Basically the damping rates of oscillation can be divided into two parts: contributions that are caused through processes governed by the momentum equation and effects described by the energy (thermal) equation. Moreover, each of them can be still further divided according to their physical meaning as it is illustrated in

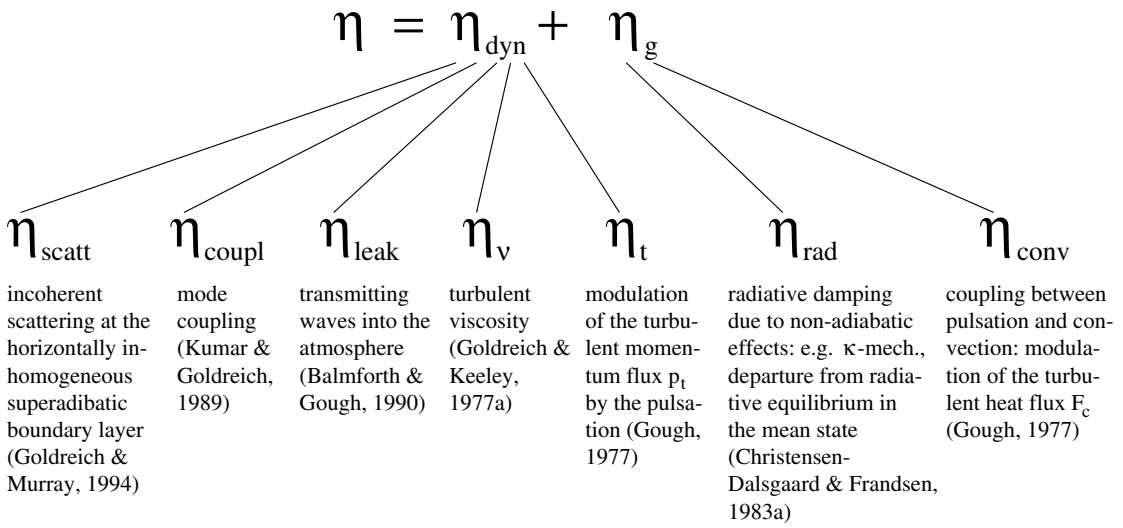

Figure 3.3: Physical processes contributing to the damping rate η.

Fig. 3.3. In particular, the dynamical damping rate consists of those due to scattering, due to turbulent viscous dissipation, due to leakage of waves into the upper atmosphere, as well as redistribution of pulsation energy between modes by non-linear interaction (coupling). On the other hand, the thermal damping is due to the non-adiabatic effects and can be divided into contributions associated to radiative damping and to the interaction between acoustic modes with convection through the modulation of the turbulent heat flux by the oscillations.

Turbulent convection as it is modelled by means of a mixing-length theory is treated as though it were horizontally homogeneous. However the superficial layers exhibit a reasonable inhomogeneous structure on a scale comparable to the vertical length-scale of high-order p modes (e.g. Bogdan 1989). Such modes therefore experience a substantial amount of incoherent scattering at these layers and hence their line widths become increased. Murray (1993) and Goldreich & Murray (1994) analyzed the effects of scattering of a linear acoustic wave by a turbulent velocity field. They obtained the expression

$$\eta_{\rm scatt} \propto \frac{\omega}{\pi\,(n+1)}\,{\rm M_t}^2\,, \tag{3.9}$$

where $\mathrm{M_t} = u/c$ represents the Mach number of the turbulence at the top of the acoustic cavity. The authors assumed that the bulk of the scattering comes from this depth of the convection zone, where the product of the p mode wave-vector and the characteristic scale of the energy-bearing eddies is in the order of unity. In order to get an estimate of the total scattering line width, contributions from all modes, between phonons are exchanged by scattering, have to be taken into account. Thus one has to take the sum over all modes including the f mode[8], which contribute to the total scattering line width of a particular

[8] The f mode (fundamental mode) appears to be a surface gravity mode with $n = 0$ (like surface waves on a pond) whose restoring force is buoyancy and its frequency increases slowly with increasing degree l.

radial or non-radial p mode. They concluded, that scattering acts as a source of damping for low degree p modes, and a source of excitation for high degree p modes and the f mode.

Non-linear mode coupling is one mechanism which could perhaps halt the growth of overstable modes. Kumar & Goldreich (1989) investigated what sort of non-linear mechanism might arrest the growth of linearly overstable modes. Since the mode amplitudes are very small, it is very likely that only the lowest order coupling, namely the three-mode coupling, is important for solar-like pulsation. Their calculations reveal that strongest coupling of p modes occur with the f modes, although there is some much weaker coupling between p modes alone. The energy equation for a p mode can be written approximately as (Kumar & Goldreich 1989)

$$\frac{d\,E_{\rm p}}{d\,t} \;=\; \alpha E_{\rm p} - \beta E_{\rm p} E_{\rm f}\,, \tag{3.10}$$

where $E_{\rm p}$ and $E_{\rm f}$ represent the kinetic energy of a p mode and f mode respectively, and $\alpha > 0$ and $\beta > 0$. The equation for a f mode is approximately

$$\frac{d\,E_{\rm f}}{d\,t} \;=\; \alpha_{\rm f} E_{\rm f} - \beta_{\rm f} E_{\rm f} E_{\rm f}\,, \tag{3.11}$$

indicating that f modes are independent of the energy of p modes and couple most strongly to other f modes. Thus, three-mode coupling drain energy from p modes that is linear in $E_{\rm p}$ and the calculations of Kumar and Goldreich reveal that it occurs at a rate that is less then the energy gained from the assumed overstability. Although mode coupling do provide a contribution to the line widths, it is unimportant compared to other effects discussed here.

Discontinuities in the density and its gradient, such as that encountered in the transition between a chromosphere and a corona as well as near the photosphere and the ionization zones of the abundant elements give rise to reflection of acoustic waves. However part of the wave energy tunnel through the potential energy barrier at those outer turning points and such leakage provides a contribution to the total damping rates. Balmforth & Gough (1990b) investigated this leakage using a complete description of the outer boundary condition derived by matching the pulsation to an outwardly propagating, adiabatic wave in an isothermal atmosphere which was applied at the temperature minimum (e.g. Baker & Kippenhahn 1965). The authors concluded that the enhancement to the damping rate due to leakage of wave energy is insignificant in comparison to the observed line widths.

Vibrational stability is influenced further by the exchange of energy between pulsation and the turbulent velocity field. In the time-dependent mixing-length theory the driving and damping of pulsation due to its coupling with convection can be associated to thermal effects arising from the pulsationally perturbed convective heat flux and due to dynamical effects generated by the fluctuating Reynolds stresses (see below). Mixing-length theory, however, accounts only for the large-scale eddies of the turbulent cascade, thus neglecting momentum and heat exchange by the eddies lying farther down the turbulent spectrum. As discussed in Section 2.5, dissipative effects associated to the small-scale turbulence

can by modelled by means of an enhanced turbulent viscosity. One possible form of the enhanced turbulent viscosity ν_e was given by equation (2.104) and according to Ledoux & Walraven (1958) the associated damping contribution can be written in the form

$$\eta_\nu = \frac{\omega^2}{3E_k}\int_{M_\star}\nu_{\rm e}\left|r\frac{\partial}{\partial r}\left(\frac{\delta r}{r}\right)\right|^2 dm\,, \tag{3.12}$$

where $\delta r/r$ represents the relative radius displacement in a Lagrangian frame of reference and the kinetic energy E_k is given by equation (3.51). Balmforth (1992a) computed the damping contributions of small-scale turbulence according to equation (2.104) for the solar case and concluded that η_ν is negligible compared to the total damping rate. A different form of ν_e was introduced by Goldreich & Keeley (1977a), who derived an expression in which eddies with turnover times close to the pulsation period contribute most to the viscous damping. However, their expression for ν_e provide similar results as equation (2.104) and thus one substantially underestimates the stabilizing influence of the dynamical effects of convection when modelled only by a turbulent viscosity.

Non-adiabatic processes like the conventional $\varkappa$-mechanism or radiative damping are responsible for both the driving and damping of pulsation. The $\varkappa$-effect works upon the principle of the modulation of the radiative energy flux. If the stellar matter is in a particular state of ionization the opacity becomes increased during a local compressive perturbation. Usually an increase of the temperature decreases the abundance of absorbing material like partially ionized atoms, and the opacity, $\varkappa$, decreases. However, in the hydrogen and helium ionization zones there is a temperature range where an increase in the temperature produces an opacity increase. This is mostly caused by the energy increase of the photons with increasing temperature, moving into the photon energy range that hydrogen and helium can absorb effectively. This increase of the opacity with compression and the natural temperature increase that goes with the compression, causes the stellar matter to absorb a greater amount of heat from the incident energy flux than would be the case if the star were undisturbed. In the subsequent expansion, the extra heat stored in these layers is converted into mechanical work, which drives the pulsation.
On the other hand temperature variations in different layers of the star cause an additional heat exchange between these regions. Thus rapid radiative relaxation, which becomes important for high-order modes, contribute significantly to the damping (radiative damping). One property of modes with increasing order is that the point of reflection where their component wave is headed back into the interior gradually moves further out into the atmosphere. Thus the mode amplitude is quite large there, making radiative effects more important. The rate at which radiative damping in the atmosphere takes place, can be described by the expression (e.g. Unno & Spiegel 1966)

$$\omega_{\rm R} = \frac{a_r\, c\, \varkappa T^4}{p\,\delta}\rho\,, \tag{3.13}$$

where a_r denotes the radiation density constant. The radiative relaxation rate $\omega_{\rm R}$ decreases with height in the atmosphere, due to the rapid decrease of the temperature and density. Although the detailed structure of the temperature stratification in a static atmosphere has no significant influence on the resulting damping rates (Balmforth 1992a)

it determines the photospheric conditions and thus the details of the stellar interior of the equilibrium model (Ando & Osaki 1975). Such a fundamental change in the model however, substantially affects the stability properties. Moreover, this demands a more accurate treatment of the radiative transport then just employing the diffusion approximation. Christensen-Dalsgaard & Frandsen (1983a) have shown that the use of the grey Eddington approximation to radiative transfer, when applied correctly, does not introduce a too large error in the calculation of the damping rates. Moreover, these authors have demonstrated that in a pulsating atmosphere the departures from radiative equilibrium in the mean state must not be neglected in the stability calculations. In the upper part of the convection zone, where there is a transition from convective to radiative energy transport, the radiative equilibrium is no longer maintained, thus the mean intensity J is no longer equal to the Planck function B. In particular, by perturbing the equations describing the radiation field in the Eddington approximation [cf. equation $(A.14)$] one obtains

$$\delta\left(\frac{1}{\rho}\boldsymbol{\nabla}\cdot\mathbf{F_r}\right) = 4\pi\varkappa\left[\delta B-\delta J+\frac{\delta\varkappa}{\varkappa}\left(B_0-J_0\right)\right], \tag{3.14}$$

where δX represents the perturbation of the quantity X in a Lagrangian frame of reference and the subscript "0" denotes the equilibrium quantities. The last term in (3.14) describes the departure from the mean state and was neglected in many stability calculations, such as the one by Ando and Osaki (1975, 1977).

The above discussed $\varkappa$-effect is believed to be the major excitation mechanism in classical pulsating stars which exhibit surface temperatures in a very narrow temperature-band, the so called instability strip (cf. Section 4.3.2). In these stars, such as the Cepheids, the ionization zones of hydrogen and helium do lie predominantly in radiative region. However, in solar-type stars the zones of ionization lie well inside the convection zone. Thus the $\varkappa$-mechanism provides only a small contribution to the driving, whereas the modulation of the turbulent fluxes by the pulsations seems to be the responsible mechanism for the detailed driving and damping of solar-type acoustic modes. This demands for a time-dependent theory of convection, such as the one we have discussed in Section 2.3.2. The coupling between the oscillations and convection takes two principal forms: first, thermal (non-adiabatic) effects due to modulation of the convective heat flux by the pulsation [cf. equation (2.88)], which contribute to the total damping rates by an amount of $\eta_{\rm conv}$, and second, dynamical effects of convection attributed to the turbulent pressure fluctuations [cf. equation (2.89)], causing additional damping by the value $\eta_{\rm t}$. Inherent in equation (2.88) are terms describing the opacity fluctuation $\delta\varkappa$ [see equations $(B.1)$-$(B.3)$ and $(B.14)$-$(B.16)$ in the Appendix B]. Mathematically, the appearance of the opacity perturbation, as it is found in the radiative diffusion equation (3.14), describes the conventional $\varkappa$-mechanism. However, in the perturbed convective heat flux, $\delta\varkappa$ is related to the way that radiative diffusion damps convective temperature fluctuations, and this can also influence pulsational stability. The latter effect together with the conventional $\varkappa$-mechanism constitute the generalized $\varkappa$-effect which was discussed in more detail by Balmforth (1992a).

It was first reported by Baker and Gough (1979) that the dynamical effects arising from the turbulent momentum flux perturbations contribute significantly to the damping. Moreover, Balmforth & Gough (1990a) and Balmforth (1992a) showed that solar acoustic

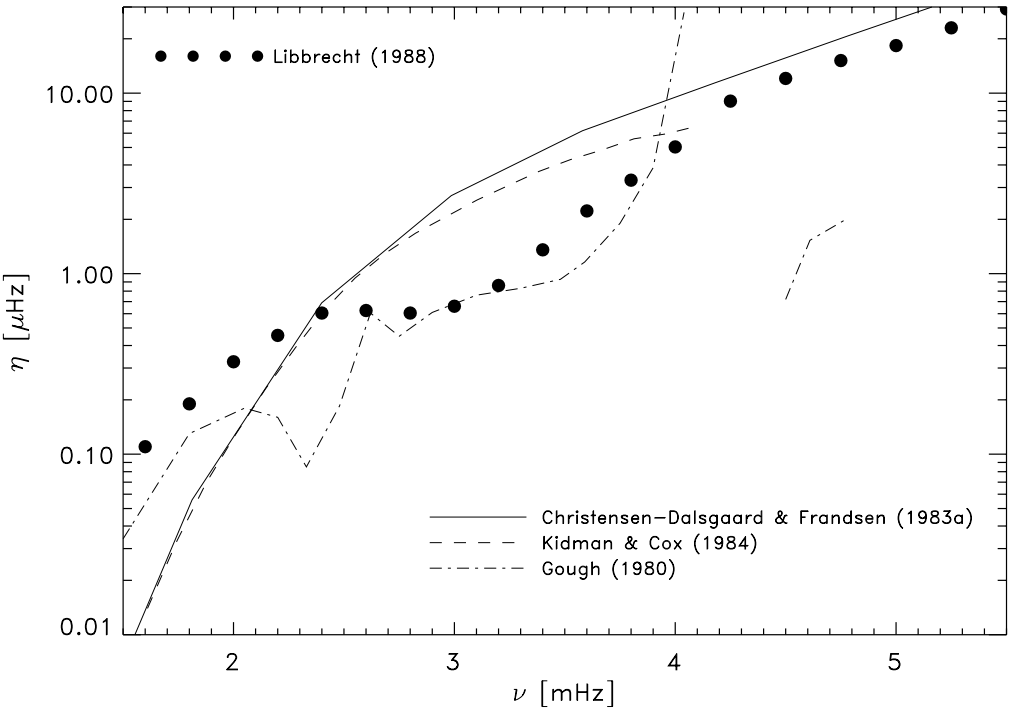

Figure 3.4: Theoretical damping rates for the Sun, using different physical prescriptions in the calculations for η (details are discussed in the text). The filled dots represent the measured line widths by Libbrecht (1988).

p modes become overstable without the inclusion of the physics describing $\eta_{\rm t}$. Detailed analyses reveal (cf. Section 3.4.5) that damping is much enhanced by the phase difference between the turbulent pressure perturbation $\delta p_{\rm t}$ and the density perturbation $\delta\rho$; it is only at the highest frequencies that the contribution to damping of solar p modes from gas pressure exceeds that from the turbulent pressure.

The vibrational stability of the Sun has already been investigated by many authors: Ulrich (1970b); Ando & Osaki (1975, 1977); Goldreich & Keeley (1977a); Gough (1980); Christensen-Dalsgaard & Frandsen (1983a); Antia, Chitre & Narasimha (1982); Kidman & Cox(1984); Antia, Chitre & Gough (1988); Christensen-Dalsgaard, Gough & Libbrecht (1989); Balmforth & Gough (1990a); Balmforth (1992a) as well as Goldreich & Murray (1994). Results of computed damping rates of some of the above mentioned authors are depicted in Fig. 3.4 together with observational line widths by Libbrecht (1988). Goldreich & Keeley (1977a) treated the modal growth rates by a turbulent viscosity η_ν, whereas Gough (1980) used the diffusion approximation for radiation, but described the effects of convection according to his local, time-dependent mixing-length theory (cf. Section 2.3.2), thus considering contributions from $\eta_{\rm t}$ and $\eta_{\rm conv}$ to the total growth rate η. Christensen-Dalsgaard & Frandsen (1983a) used the grey Eddington approximation for radiative transfer including the term $B_0 - J_0$, however they neglected the perturbation of the divergence of the convective heat flux. Kidman and Cox (1984) used the diffusion approximation for radiation and also neglected the perturbation in the convective heat flux. They found damping rates quite close to those obtained by Christensen-Dalsgaard & Frandsen (1983a). Goldreich & Murray (1994) calculated scattering line widths for modes with degree $l = 0$ including the contributions from the first 30 p modes and the f mode.

3.3. Stochastic Excitation

The results of the previous chapter supports the assumption that solar-type acoustic pulsations are intrinsically damped in the linear stability analysis. In that case external sources must be sought for their excitation and the emission of acoustical radiation by turbulent convective flows is perhaps the correct driving mechanism for solar-type p modes. Acoustical radiation by turbulent multipole sources in the context of stellar aerodynamics were considered by Unno & Kato (1962), Moore & Spiegel (1964), Unno (1964), Stein (1967), Goldreich & Keeley (1977b), Osaki (1990), Balmforth (1992c), Musielak *et al.* (1994) and Goldreich, Murray & Kumar (1994). In the following I shall review the basic physics of sound generation by means of the so-called Lighthill mechanism and its application in the theory of stochastic excitation of solar-type p modes which will enable us to estimate the energy injection into a particular mode as function of depth in the model envelope.

3.3.1. Lighthill mechanism and lower order acoustical sources

Lighthill (1952, 1954) considered in his pioneering work on aerodynamic sound generation an unbounded region of space in which there is a fluctuating fluid flow. He proposed the acoustic sources of sound to be the difference between the exact laws of fluid motion and the linearized acoustical approximations, thus it is the nonlinearities that generate the sound. In Section 2 we introduced the basic fluid-dynamic equations for studying convective motion. We take the divergence of the momentum equation (2.2) and subtract it from the time derivative of the continuity equation as expressed in Eq. (2.1). Then we subtract $c_0^2\nabla^2\rho$ from both sides to yield the result

$$\frac{\partial^2\rho'}{\partial t^2} - c_0^2\nabla^2\rho' \;=\; \frac{\partial^2 T_{ij}}{\partial x_i \partial x_j} - \frac{\partial F_i}{\partial x_i}\,, \tag{3.15}$$

since $\rho' = \rho - \overline{\rho}$, and $\overline{\rho}$ is time invariant, denoting the mean density in the distant acoustic field, with

$$T_{ij} \;=\; \rho u_i u_j + \left(p' - c_0^2\rho'\right)\delta_{ij} - \tau_{ij}\,, \tag{3.16}$$

and

$$F_i \;=\; \rho' g_i\,. \tag{3.17}$$

Equation (3.15) represents the inhomogeneous wave equation in a static atmosphere. The quantity c_0 denotes the speed of sound in the radiation field and may be quite different from that in the turbulence. The turbulent field is described by convective eddies which advect heat from the deeper layers in the envelope and thus the eddy region exhibit a larger speed of sound than the background fluid. Lighthill considered a fluid with uniform mean density and a speed of sound to be constant at c_0, for which the source term in equation (3.15) reduces to the simple expression $\rho u_i u_j$. In this case, it is the fluctuating Reynolds

stress that generate sound in exactly the same way as would a distribution of quadrupoles, as demonstrated next. A linear non-homogeneous equation, such as the wave equation (3.15), can be solved in terms of the Green function of the problem. This function is the solution of the equation with the inhomogeneity concentrated at a point, in both space and time. Thus it is defined by

$$\left(\frac{\partial^2}{\partial t^2} - c_0^2 \nabla^2\right) G\left(\mathbf{x}, t\right) \;=\; \delta\left(\mathbf{x}\right) \delta\left(t\right) \;, \tag{3.18}$$

with

$$G\left(\mathbf{x}, t\right) \;=\; \frac{1}{4\pi c_0^2} \, \frac{\delta\left(\mathbf{x} - c_0 t\right)}{|\mathbf{x}|} \,, \tag{3.19}$$

in the three space dimensions $\mathbf{x}$. For low turbulent Mach numbers $\mathrm{M_t} = u/c_0$ the acoustic source field, which is typical of the eddy size ℓ, is called *compact* relative to the emitted wavelength $\ell/\mathrm{M_t}$, and the retarded time differences ℓ/c_0 over the eddy length ℓ are negligible on the eddy time scale ℓ/u. In this limit of $\mathrm{M_t} \ll 1$ the solution of the wave equation with the inhomogeneous source term $\partial^2 T_{ij}/\partial x_i \partial x_j$ is obtained by integrating the convolution product of the Green function (3.19) with the source term which yields (e.g. Crighton *et al.* 1992)

$$\rho'\left(\mathbf{x}, t\right) \;=\; \frac{1}{4\pi c_0^4 x} \left(\frac{x_i x_j}{x^2}\right) \frac{\partial^2}{\partial t^2} \int T_{ij} \left(\mathbf{y}, t - \frac{x}{c_0}\right) d\mathbf{y} \,. \tag{3.20}$$

With the following assumptions

$$T_{ij} \approx \overline{\rho} u_i u_j \,, \quad \frac{\partial}{\partial t} \approx \frac{u}{\ell} \,, \quad \text{and} \int dy \approx \ell^3 \tag{3.21}$$

we obtain an estimated solution of Eq. (3.20) in the form

$$\rho'\left(\mathbf{x}, t\right) \approx \frac{1}{c_0^4 x} \left(\frac{u}{l}\right)^2 \overline{\rho} u^2 \ell^3 \;=\; \overline{\rho} \left(\frac{\ell}{x}\right) \mathrm{M_t}^4 \,, \tag{3.22}$$

which represents the central result of Lighthill's basic theory. A convenient statistical measure of the radiation is the magnitude of the intensity vector $\mathbf{I}$, which is proportional to the mean square density fluctuation

$$I \;=\; \frac{c_0^3}{\overline{\rho}} < \rho'^2 > \,, \tag{3.23}$$

and thus the total acoustic power, P_{Q}, radiated from the flow, which is the integral of the intensity over a large spherical surface, becomes for a quadrupole source

$$P_{\mathrm{Q}} \propto x^2 I \propto \overline{\rho} u^3 \ell^2 {\mathrm{M_t}}^5 \,. \tag{3.24}$$

The term $\overline{\rho} u^3 \ell^2 = \overline{\rho} u^2 \ell^3 / (\ell/u)$ represents a measure of the rate of kinetic energy decay of the eddy through viscous action, this being equal to the energy supply rate in a steadily maintained flow. Thus we may define an acoustic efficiency as the ratio of sound power to sound supply which varies in the case of quadrupole radiation as ${\mathrm{M_t}}^5$. Moreover, equation (3.24) tells us, that the radiated power of a quadrupole source is proportional to the eight power of the eddy's convective velocity u.

The above discussed quadrupole emission due to the fluctuations of the Reynolds stresses represents the main acoustic source for homogeneous isotropic turbulence. In a star's atmosphere however, the turbulence is a function of depth, and therefore inhomogeneous. Furthermore, detailed numerical hydrodynamical simulations of convective turbulence (e.g. Stein & Nordlund 1991; Trampedach 1996) suggest an asymmetrical behaviour of the convective velocities in the up- and down-stream flow. The upward slower moving and spatially larger streams are surrounded by the much faster moving and colder down-streams. Thus the turbulent flow exhibits regions of quite different temperatures which can have a significant effect on both sound speed and density. Consequently we may expect these differences to affect the results obtained so far through making the second term of Lighthill's stress tensor T_{ij}, Eq. (3.16), dominant. For a perfect gas the equation of state may be written in the form

$$\frac{\partial \rho'}{\partial t} = \frac{1}{c_l^2} \frac{\partial p'}{\partial t} - \frac{\rho}{c_p} \frac{\partial s'}{\partial t} \,, \tag{3.25}$$

where $c_l = (\Gamma_1 p/\rho)^{1/2}$ represents the local sound speed, c_p is the specific heat at constant pressure and s' denotes the fluctuations of the entropy. The second term in equation (3.16) therefore becomes

$$\frac{\partial}{\partial t} \left(p' - c_0^2 \rho' \right) = \left(1 - \frac{c_0^2}{c_l^2} \right) \frac{\partial p'}{\partial t} + \frac{\rho c_0^2}{c_p} \frac{\partial s'}{\partial t} \,. \tag{3.26}$$

The first term on the right hand side of equation (3.26) was considered by Lighthill (1954) in a homogeneous flow, who showed that it was unlikely to dominate the Reynolds stress term. However under the conditions which are prevalent in a star's atmosphere, it might become important due to the local changes in the density and sound speed. In particular it can be shown (e.g. Crighton *et al.* 1992) that this term contributes to the acoustical source term by

$$\rho' = \frac{1}{4\pi c_0^4 x} \frac{\partial^2}{\partial t^2} \int \left(1 - \frac{c_0^2}{c_l^2} \right) p \left(\mathbf{y}, t - \frac{x}{c_0} \right) d\mathbf{y} \,, \tag{3.27}$$

which can be estimated with $dp = c_l^2 \, d\rho$, $\rho \sim \overline{\rho} u^2$ and with equation (3.21) as

$$\rho' \sim \overline{\rho} \left(\frac{l}{x}\right) \left(1 - \frac{c_0^2}{c_l^2}\right)^2 \mathrm{M_t}^4 . \tag{3.28}$$

Thus it represents a quadrupole field whose strength is a function of the inhomogeneities of the sound speed. Recently, Kosovichev (1996) demonstrated a new technique for observing such horizontal inhomogeneities in the speed of sound.

The last term in equation (3.26) accounts for the gain and loss of specific entropy in the turbulent flow. These entropy fluctuations contribute to the acoustical sources by an amount of

$$\rho' = \frac{1}{4\pi c_0^2 x} \frac{\rho_l}{c_p} \int \frac{\partial^2 s'}{\partial t^2} \left(\mathbf{y}, t - \frac{x}{c_0}\right) d\mathbf{y} , \tag{3.29}$$

whose estimated value yields

$$\rho' \sim \rho_l \left(\frac{l}{x}\right) \left(\frac{s'}{c_p}\right) \mathrm{M_t}^2 , \tag{3.30}$$

where ρ_l denotes the arithmetic mean of the density mixture in the turbulent flow. The acoustic density field is proportional to the square of the turbulent Mach number and hence represents a monopole field.

The entropy changes give rise to an additional source in a stratified atmosphere, expressed by the last term in the wave equation (3.15). This term can be written for an atmosphere under constant gravity as

$$\frac{\partial F_i}{\partial x_i} = g_i \frac{\partial}{\partial x_i} \left(\frac{p'}{c_l^2} - \frac{\rho' s'}{c_p}\right) , \tag{3.31}$$

where we used the adiabatic equation of state in the form [cf. Eq. (3.25)]

$$\frac{p'}{p} - \frac{\Gamma_1 \rho'}{\rho} = \frac{s'}{c_v} . \tag{3.32}$$

The first term on the right hand side of equation (3.31) represents a linear term and thus has to be put on the left side of the wave equation, which describes the wave propagation term. For the sake of simplicity we neglect this linear term in order to use the Green function as expressed in equation (3.19) for an estimate of the contribution arising from the remaining non-linear term of equation (3.31). This term, which is similar to the expression in Goldreich & Kumar's (1990) discussion, may then be written as

$$\rho' \approx -\frac{1}{4\pi c_0^2 x} \frac{\rho_l}{c_p} \frac{\partial}{\partial x_i} \int \frac{\partial}{\partial t} \left(u_i s'\right) \left(\mathbf{y}, t - \frac{x}{c_0}\right) d\mathbf{y} \approx \rho_l \left(\frac{l}{x}\right) \left(\frac{s'}{c_p}\right) \mathrm{M_t}^3 . \tag{3.33}$$

The acoustic source field varies with the third power of the turbulent Mach number and represents therefore a dipole field.

We conclude that quadrupole emission due to the Reynolds stresses and inhomogeneities in the temperature produce equal and opposite forces on opposite sides of a fluid element leading to the distortion of its surface without changing the volume or, in other words, that kinetic energy is converted into acoustic energy by forcing the rates of momentum flux across fixed surfaces to vary. The monopole and dipole sources, arising from the entropy fluctuations, describe the conversion of kinetic energy into acoustic energy resulting from forcing the volume and the momentum in a fixed region of space to fluctuate, respectively, where the latter is produced by variations of the buoyancy (gravitational force).

3.3.2. Acoustical emission in a pulsating atmosphere

The discussion so far was carried out in a static atmosphere. In a pulsating atmosphere the full pulsation-convection gas dynamic equations have to be derived from the fluid-dynamic equations where the fluid velocity includes both turbulent and pulsating motion. This demands the use of a time-dependent theory for convection and in a complete theory the non-linear acoustical source terms, exciting the pulsation, would naturally follow from these equations. However, time-dependent convection theories available to date, as the one we introduced in Section 2.3.2, impose the anelastic approximation (cf. Section 2.2) which neglect non-linear terms including the density fluctuations and therefore filter out any generation of sound waves. Thus one is left with a procedure in which the dynamical convective effects are inserted solely in the pulsation equations which however is only consistent in an isothermal atmosphere. Moreover, if the turbulent stresses (turbulent pressure) are regarded as second order effects, a conventional theory for convection, like the mixing-length theory, may be used to describe the dynamical convective effects, and the estimation of the turbulent velocity. Moreover, the velocity field can be mathematically strictly decomposed into a large-scale pulsation and the turbulent velocity field only for radial pulsation and only in the Boussinesq approximation (Gough 1977).

Balmforth (1992c) reviewed the theory of acoustical excitation in a pulsating atmosphere according to the procedure outlined above. In the derivation of the inhomogeneous wave equation, additional linear components emerge describing the dynamical and thermal coupling of convective and pulsating motions. The dynamical term can be regarded, analogous to the fluctuation of the momentum flux of the time-dependent convection theory, as an additional viscous stress term [cf. equation (2.104)]. Thus it can be considered as a damping term arising from dissipation through 'eddy viscosity', modelling the eddy dynamics of the whole turbulent energy spectrum. The thermal term can be related to the work integral arising from non-adiabatic effects and is to be thought of as linear in the pulsation eigenfunction. Such an interpretation of these terms enables us to replace them by an expression proportional to the modal damping rate η (Balmforth 1992c). The remaining non-linear source terms are then composed of expressions arising from the action of the Reynolds stresses and the turbulent entropy fluctuations, respectively. The wave equation may then be solved by rewriting it in terms of the pulsational displacement $\delta r(r,t)$, and expanding $\delta r(r,t)$ in terms of the normal, adiabatic eigenfunctions, $\xi(r)\exp(-\omega_r t)$, satisfying the relation

$$\delta r\,(r,t) \;=\; A_\omega\,(t)\,\xi\,(r)\,e^{-\omega_r t}\,. \tag{3.34}$$

The quantity $A_\omega(t)$ describes the instantaneous, finite, mode amplitude, determined by the balance between damping and driving, and is assumed to vary slowly compared to the cyclic frequency ω_r. As a result we obtain an expression for the time evolution of the mode amplitude, which can be integrated in time in order to obtain the expectation value $< |A_\omega| >$. In this derivation, however, one has to solve a fourth-order correlation function of the convective velocity and entropy fluctuations, representing the well known closure problem in the statistical description of turbulence (cf. Section 2.5.2). Approximate solutions of this correlation function were discussed by Stein (1967) and Musielak *et al.* (1994) assuming an incompressible, isotropic, and homogeneous turbulence spectrum and that this energy spectrum may be separated into a wavenumber and a frequency dependent part. An even more simpler form of this correlation function was obtained by Goldreich & Keeley (1977b) which was also employed by Balmforth. The energy in a particular mode, $\mathcal{E}_\omega$, is related to the instantaneous mode amplitude A_ω by

$$\mathcal{E}_\omega \;=\; \frac{P}{2\eta} \;=\; \frac{1}{2} < |A_\omega|^2 > \omega_{\rm r}^2 I\,, \tag{3.35}$$

where P denotes the noise generation rate due to the acoustical multipole sources, and the mode inertia

$$I \;=\; \int\limits_{M_\odot} \xi^2\,(m,\omega_r)\;dm\,. \tag{3.36}$$

The treatment of the lower order multipole sources due to the entropy fluctuations needs a more detailed consideration. First, it is assumed that the background state can be regarded approximately as homentropic and thus the entropy fluctuations are described entirely by the mixing-length estimate for the entropy perturbation

$$s' \approx \delta s \;=\; -\frac{\ell}{2}\,\frac{ds}{dr}\,, \tag{3.37}$$

associated with an energy-bearing eddy. Here s denotes the background entropy, whose gradient is a function of the mixing-length parameter $\alpha_{\rm c}$ (cf. Section 2.5.1). With this assumption the correlation $< s's' >$ may then approximated by the method of Goldreich & Keeley (1977b). The evaluation of this correlation function becomes unclear when the homentropic assumption were not taken into account. Several more terms would emerge describing both the convective velocity and pulsational displacement, where the latter term should then be placed in the wave propagation term and the correlation $< us' >$ would require further assumptions. Secondly, the explicit form of the non-linear source functions depends upon the field variable. It was shown by Balmforth (1992c) that the source terms are quite different when employing different expression for the dependent

variable in the inhomogeneous wave equation and that the decompositions of all terms into linear, dynamical coupling terms and non-linear excitation terms can become quite ambiguous. This ambiguity results from the lack of a complete description of the turbulent eddy dynamics, in which the time-dependent turbulent flow and its acoustical emission is evaluated simultaneously.

The anisotropy of a stratified atmosphere gives rise to destructive interference between the monopole and dipole source function (Goldreich & Kumar 1990; Osaki 1990). This cancellation effect depends on the symmetry between the rising and falling eddies, where two dipoles sit side by side and the entropy perturbation of these two dipoles cancel each other, resulting in a quadrupole radiation. However at the top of the convection zone this symmetry may break down and the emitted radiation by the dipoles may become effectively at these layers. Moreover, the typical frequency of quadrupole radiation is twice as high than the acoustical emission through the dipoles and may therefore occur in the propagating zone radiating more effectively than the dipole emission (Osaki 1990). The symmetry between the rising and falling eddies, however, is an artifact of the mixing-length theory due to the inclusion of the Boussinesq approximation. As already mentioned above, detailed hydrodynamical simulations in the Sun suggest up to three times larger convective velocities of the down-stream flow compared to the velocities of the up-flow. Indeed, Stein & Nordlund (1991) have found that excitation due to the entropy fluctuation may exceed the amplitudes emitted through the fluctuations of the Reynolds stresses by an order of magnitude, which was also found by an analytical approach by Goldreich, Murray & Kumar (1994).

The ambiguity in the derivation of the lower order multipole sources due to the entropy fluctuations and the incomplete theory of the mixing-length prescription for convection have led Balmforth (1992c) to neglect these terms from the acoustical source functions. He derived an expression for the quadrupole emission through the action of the Reynolds stresses of the form

$$P_{\rm Q} = \frac{\pi^{1/2}}{8I} \int\limits_{M_*} \left(\frac{d\xi\,(m,\omega_r)}{dr} \right)^2 \rho \ell_0^3 u_0^4 \tau_0 \mathcal{S}\,(m,\omega_r)\, dm\,, \tag{3.38}$$

where ℓ_0,u_0,τ_0 are the length, velocity and correlation time-scale respectively of the most energetic eddies, determined by the mixing-length theory. The function $\mathcal{S}(m,\omega)$ accounts for the turbulent spectrum, which approximately describes the contribution from eddies with different sizes to the noise generation rate $P_{\rm Q}$ (i.e. how the energy is distributed throughout the turbulent cascade). We have chosen a spectrum based on Spiegel (1962), since this choice leads to a theoretical oscillation power spectrum similar to the envelope of solar oscillations (cf. Section 4.2).

Examples for the differential quadrupole emission, as given by the integrand of equation (3.38), are depicted in Fig. 3.5 and Fig. 3.6 for the Sun and a $1.45\,M_\odot$ ZAMS star, respectively. With increasing frequency the maximum value of the 'differential emission' becomes manifested in the superadiabatic layers. For higher mass stars the amplitude of the 'differential emission' increases quite severely due to its strong dependence on the turbulent Mach number $\mathrm{M_t}$ [cf. Eq. (3.24)], which becomes larger with mass and may exhibit values up to ~ 0.6 for an $1.6\,M_\odot$ star (see Fig. 4.8).

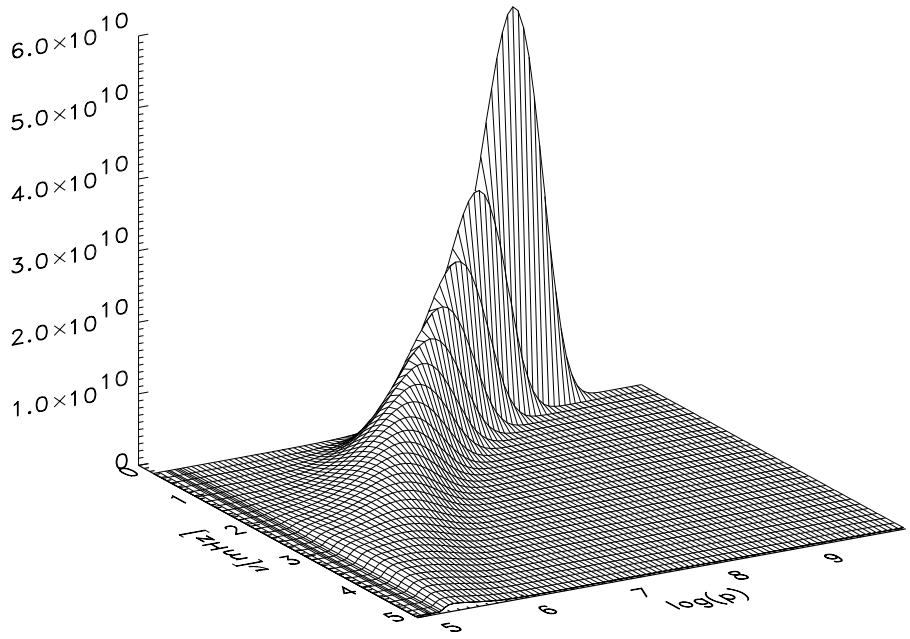

Figure 3.5: Acoustical emission due to the Reynolds stresses as function of depth and frequency for the Sun. The plot depicts the quantity $|\rho\ell_0^3 u_0^4 (d\xi/dr)^2 \mathcal{S}\,(dm/d\ln p)|$ [cf. Eq. (3.38)], assuming the turbulent energy spectrum according to Spiegel (1962). For the mixing-length parameters the values $\alpha_c = 2.0, a^2 = 900, b^2 = 2000$ have been used.

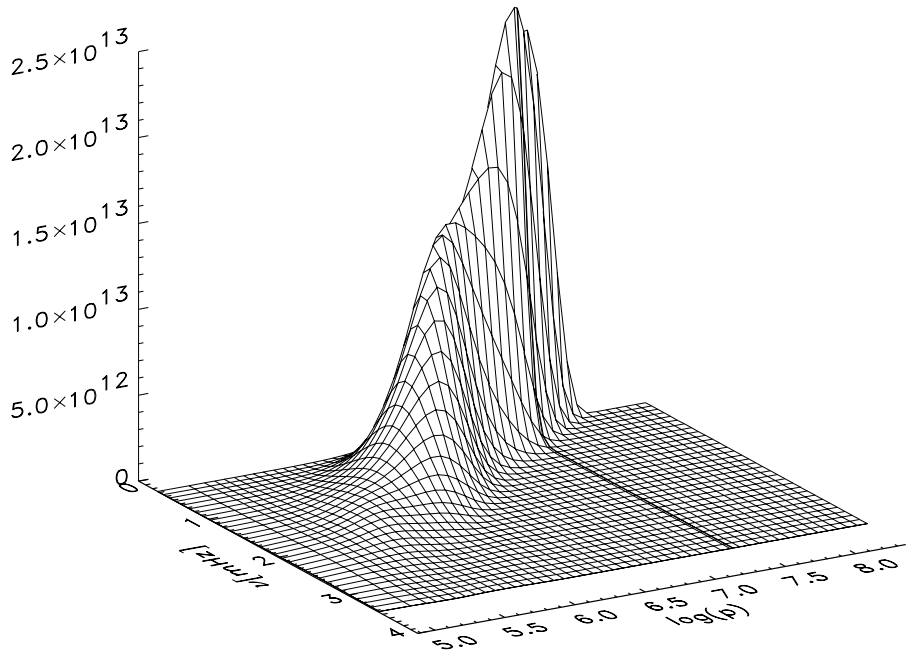

Figure 3.6: Differential emission for a $1.45\,M_\odot$ ZAMS star as given by the quantity in Fig. 3.5 using the same turbulent energy spectrum and convection parameters.

3.4. Results

3.4.1. Computation Details

The basic model calculations are as described by Balmforth (1992a), and consider turbulent pressure in the equilibrium model envelope assuming a mesh of 800 points. The integration is carried out inwards, starting at an optical depth of $\tau = 10^{-4}$ and ending at a radius fraction of 0.2, using initially the local mixing-length theory and the diffusion approximation to radiative transfer to complete a trial solution. The entire envelope is then re-integrated using the equations appropriate to the non-local mixing-length theory and the Eddington approximation to radiative transfer (cf. Appendix A.1). For the eddy shape parameter Φ a constant value of 5/3 has been employed. In the non-local theory the meaning of this parameter becomes somewhat clouded, since we have assumed that the source function $\mathscr{Q}$ for the turbulent fluxes [cf. equation (2.94)] is isotropic. However, in order to be consistent with this assumption, we should have set $\Phi = 3$ instead. Nevertheless, the shape of the eddies and the isotropy of the evolution of buoyancy force are different effects, and so it appears that the least ambiguous step one can do is to set Φ to a constant. The atmosphere is treated with grey radiation and is assumed to be plane parallel. The temperature gradient is corrected by using a spatially varying Eddington factor (Auer & Mihalas 1970) derived from a model C of Vernazza, Avrett & Loeser (1981). For the opacities the OPAL tables (Iglesias, Rogers & Wilson 1992) and the Kurucz tables (Kurucz 1991) for low temperatures have been used assuming the abundances to be $X = 0.7, Z = 0.02$. Interpolation in these tables is carried out using the minimum-norm method as described in the Appendix C.2.3. The equation of state included a detailed treatment of the ionization of C, N, and O, and a treatment of the first ionization of the next seven most abundant elements (Christensen-Dalsgaard 1982), as well as pressure ionization by the method of Eggleton, Faulkner & Flannery (1973).

In the pulsation model the boundary conditions used are essentially those of Baker & Kippenhahn (1965), but supplemented by the conditions on the variables of the non-local mixing-length theory. The outer boundary conditions are applied at the temperature minimum; at the base of the model envelopes the conditions of adiabaticity and vanishing displacement were imposed (cf. Appendix A.2). According to Libbrecht *et al.* (1986) the oscillation properties of low-degree modes depend little on degree l. Thus the calculations are based on the analysis of radial pulsations.

The equations, as given in the Appendix A, are solved with a second-order Newton-Raphson-Kantorovich algorithm (Baker, Moore & Spiegel 1971; Cash & Moore 1980). With this algorithm the eigenfunctions and eigenvalues can be computed simultaneously which, however, increases the order of the system by one. Furthermore, one has to provide a proper trial solution, which can be obtained by solving first the adiabatic pulsation equations and then apply the quasi-adiabatic approximation to the non-adiabatic system.

3.4.2. Non-adiabatic effects

In Section 3.2.2 we discussed some of the physical effects responsible for the energy exchange between mass elements during oscillations. These effects are coupled to each other in a rather complicated way (such as the constituents in the generalized $\varkappa$-mechanism) and it is therefore not always a straightforward task to isolate each mechanism in order to get a measure of the degree of the energy leakage associated to each individual effect. As already discussed in Fig. 3.3 the energy flow into and out of a particular mode can be basically divided into contributions arising from the momentum equations and into effects associated with the entropy perturbation or nonadiabaticity. The nonadiabaticity of stellar oscillations is described by the perturbed energy conservation equation, derived from the first law of thermodynamics, and may be expressed for radial modes in the absence of any nuclear reactions and to first order as

$$T\frac{\partial}{\partial t}\left(\delta s\right) \;=\; -\frac{\partial}{\partial m}\left(\delta L\right) \;, \tag{3.39}$$

where δL denotes the Lagrangian perturbation of the total luminosity (radiative plus convective). Its spatial dependence describes the energy gain (loss) due to the excess (deficient) energy outflow. The detailed energy equation is derived in the Appendix A [cf. equation $(A.75)$] and provides a proper measure of the degree of nonadiabaticity of the form

$$\Upsilon \;=\; \left(\frac{\delta p_{\rm g}}{p_{\rm g0}}\nabla_{\rm ad} - \frac{\delta T}{T}\right)\left(\left|\frac{\delta p_{\rm g}}{p_{\rm g0}}\right| + \left|\frac{\delta T}{T}\right|\right)^{-1} \;, \tag{3.40}$$

where $p_{\rm g}$ denotes the gas pressure and $\nabla_{\rm ad}$ the temperature gradient of a fluid element when it experiences a purely adiabatic expansion or contraction [cf. equation (2.82)]. The non-adiabatic effects cause the temperature variations δT to fluctuate out of phase with the gas pressure variations $\delta p_{\rm g}$. In particular the Lagrangian perturbation of the temperature, as it is derived in the Appendix A [cf. equation $(A.87)$], can be written as

$$\begin{aligned}\frac{\delta T}{T_0} \;=\; & \left[4 + i\frac{\omega}{\omega_{\rm R}} + \left(1 - J_0/B_0\right)\varkappa_{\rm T}\right]^{-1} \\ & \times \left\{\frac{\delta J}{B_0} + \frac{1}{4\pi\varkappa_0 B_0}\frac{\partial}{\partial m}\left(\delta L_{\rm c}\right) + \left[i\frac{\omega}{\omega_{\rm R}}\,\nabla_{\rm ad} - \left(1 - J_0/B_0\right)\varkappa_{\rm p}\right]\frac{\delta p_{\rm g}}{p_{\rm g0}}\right\} ,\end{aligned} \tag{3.41}$$

where the $\omega/\omega_{\rm R}$ terms account for the radiative damping contribution, terms with $(1 - J_0/B_0)$ arise from the mean departure from the radiative equilibrium ($\varkappa_{\rm T}$ and $\varkappa_{\rm p}$ are the partial logarithmic derivatives of the opacity with respect to temperature and gas pressure), and the term with $\partial/\partial m(\delta L_c)$ together with $\delta J/B_0$ account for the generalized $\varkappa$-mechanism (L_c being the convective luminosity).

The departure from adiabaticity, as defined in equation (3.40) is depicted as function of radius and frequency for the Sun and for a $1.4\,M_\odot$ ZAMS star in Fig. 3.7 and Fig. 3.8, respectively. Also illustrated is the locus of the function Υ in the complex plane as the depth varies throughout the envelope. The non-adiabatic eigenfunctions were solved with

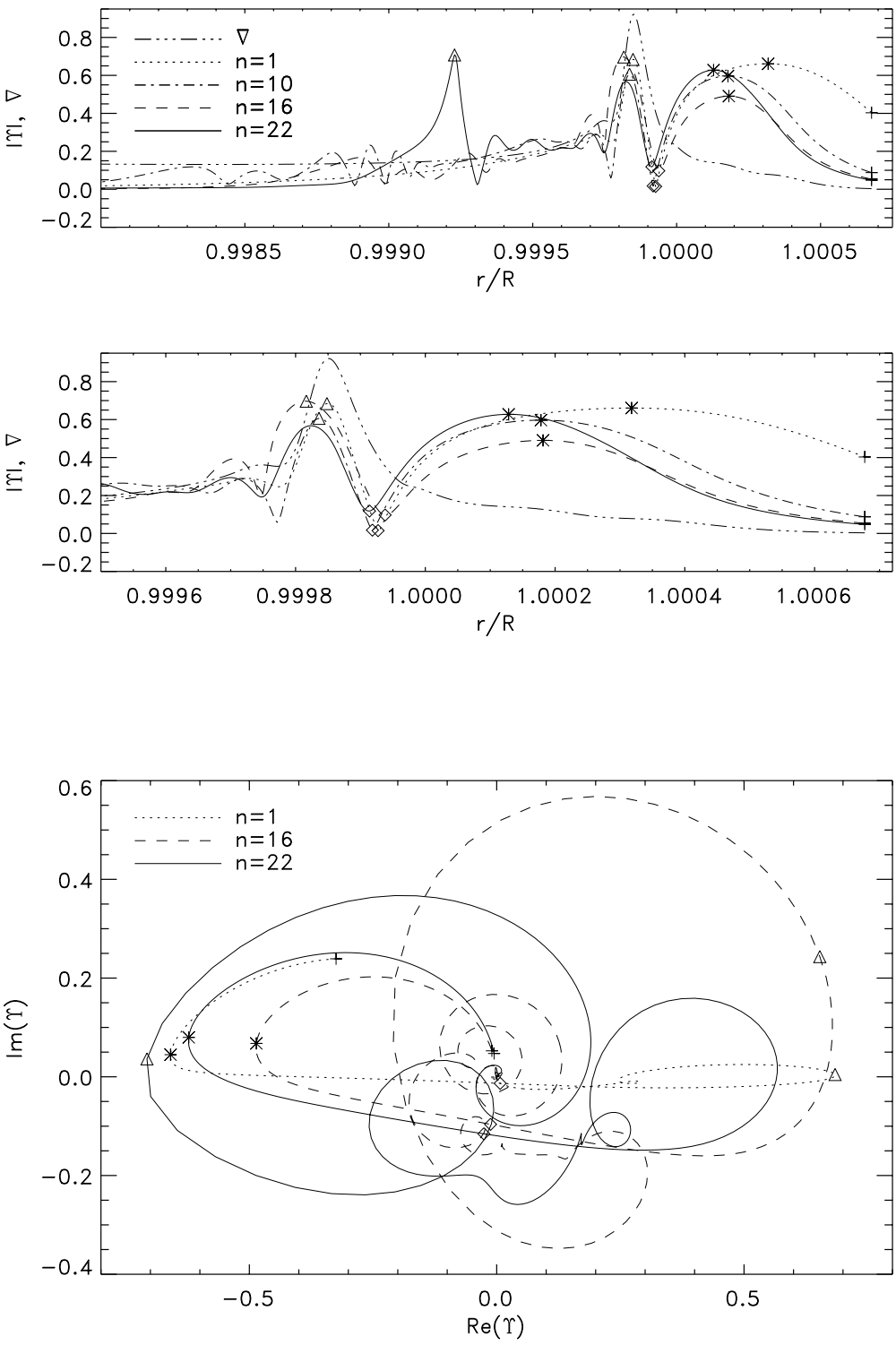

Figure 3.7: Degree of nonadiabaticity Υ, as defined by equation (3.40), versus radius and function of frequency for the Sun. The locus of the function Υ (bottom) is plotted in the complex plane as the depth varies throughout the envelope. The non-local model computations assumed the convection parameters $a^2 = b^2 = 300$ and $\alpha_c = 2.0$. The symbols mark for each individual mode similar depths in the star's envelope.

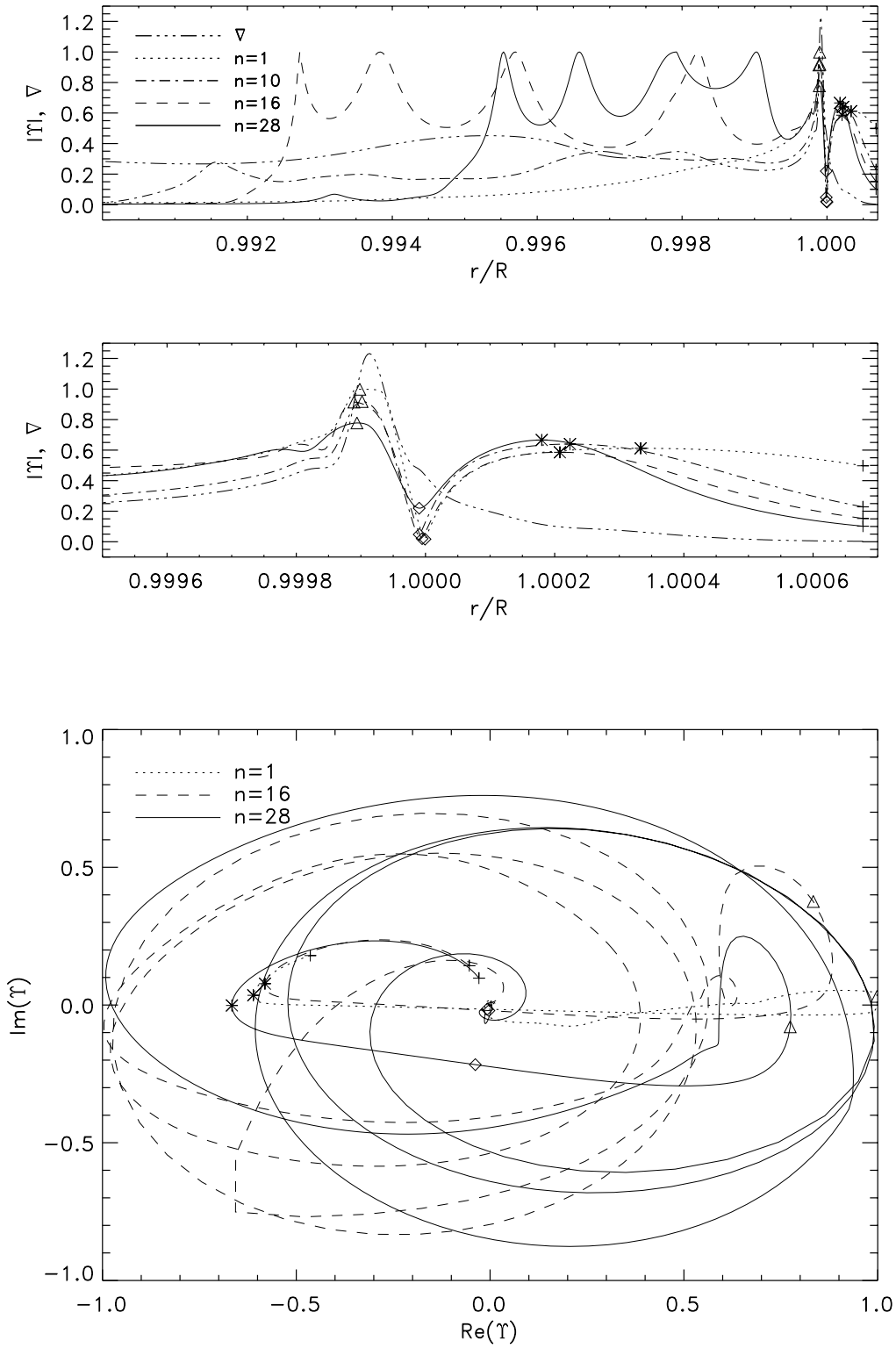

Figure 3.8: Degree of nonadiabaticity, Υ, as defined by equation (3.40), of function of radius and frequency for a 1.4 $M_\odot$ ZAMS star. The locus of the function Υ is plotted in the complex plane as the depth varies throughout the envelope (bottom). The non-local model computations assumed the convection parameters $a^2 = 900$, $b^2 = 2000$ and $\alpha_c = 2.0$. The symbols mark for each individual mode similar depths in the star's envelope.

the inclusion of the perturbations in the turbulent pressure $\delta p_{\rm t}$. This has some effect on the non-adiabatic processes due to the change of the shape of the modal eigenfunctions (see also Section 4.3.2). The largest deviation from adiabaticity is predicted predominantly in the superadiabatic boundary layers, indicated by the temperature gradient $\nabla = d\ln p/d\ln T$, and in the lower parts of the atmosphere. With increasing height in the atmosphere the density declines very rapidly and heat diffusion becomes very inefficient. The degree of nonadiabaticity is still further depressed by the rapid decrease of the opacity in these atmospheric layers. Moreover, the increase of the radiative relaxation-time [cf. equation (3.13)] promotes high-order modes to become progressively adiabatic again. In the superadiabatic boundary layer coupling between oscillation and convection becomes strongest and non-adiabatic effects, such as the generalized $\varkappa$-mechanism, are enforced. Thus the convective temperature fluctuation oscillates out of phase with the density perturbation and consequently the heat flux feeds back into driving the pulsation. This forced oscillation in the superadiabatic layer is responsible for driving the perturbations of the thermodynamic quantities into the lower parts of the convection zone, which can be seen quite obviously for the $1.4\,M_\odot$ star. At a particular pulsation frequency, which is close to the natural rate of thermal adjustment of the superadiabatic layer, the coupling and thus the forced oscillation becomes promoted even further leading to an increase of the nonadiabaticity. This effect is demonstrated in the plot of the locus of the function Υ for the mode with radial order $n = 16$, for both the Sun and the $1.4\,M_\odot$ ZAMS star (the location of the superadiabatic layers are indicated by the triangle symbol).

3.4.3. The influence of non-adiabatic effects and turbulent pressure upon solar oscillation frequencies

One method to test the various theories for convection is the comparison of theoretical pulsations frequencies with observations. Todays observation techniques of solar acoustic frequencies have reached an accuracy which allows one to interpret the differences between observed and computed eigenfrequencies to stem solely from the incomplete physics describing the equilibrium and pulsation models. Effects due to opacity and the equation of state in the equilibrium model upon adiabatic and non-adiabatic eigenfrequencies have been investigated by several authors (Guzik & Cox 1993; Guenther 1994; Tripathy & Christensen-Dalsgaard 1996; Antia & Basu 1996). In particular the increase of low-temperature opacities and the use of more sophisticated thermodynamics have reduced the discrepancy between computed and observed frequency values (e.g. Christensen-Dalsgaard & Däppen 1992; Guzik *et al.* 1996). However for modes having frequencies larger than $\sim$ 2 mHz, computed adiabatic eigenfrequencies of a 'standard' solar model (e.g. Christensen-Dalsgaard *et al.* 1996) using the Böhm-Vitense (1954) local mixing-length theory for convection still exhibit values with up to $\sim$ 20 μHz too large relative to the observations. In Fig. 3.9a such a comparison between computed adiabatic frequencies of the 'standard' solar model and results from the BISON[9] (Elsworth *et al.* 1994) and BBSO[10] (Libbrecht *et al.* 1990) observations is shown. For frequencies with a degree

[9] Birmingham Solar Oscillation Network

[10] Big Bear Solar Observatory

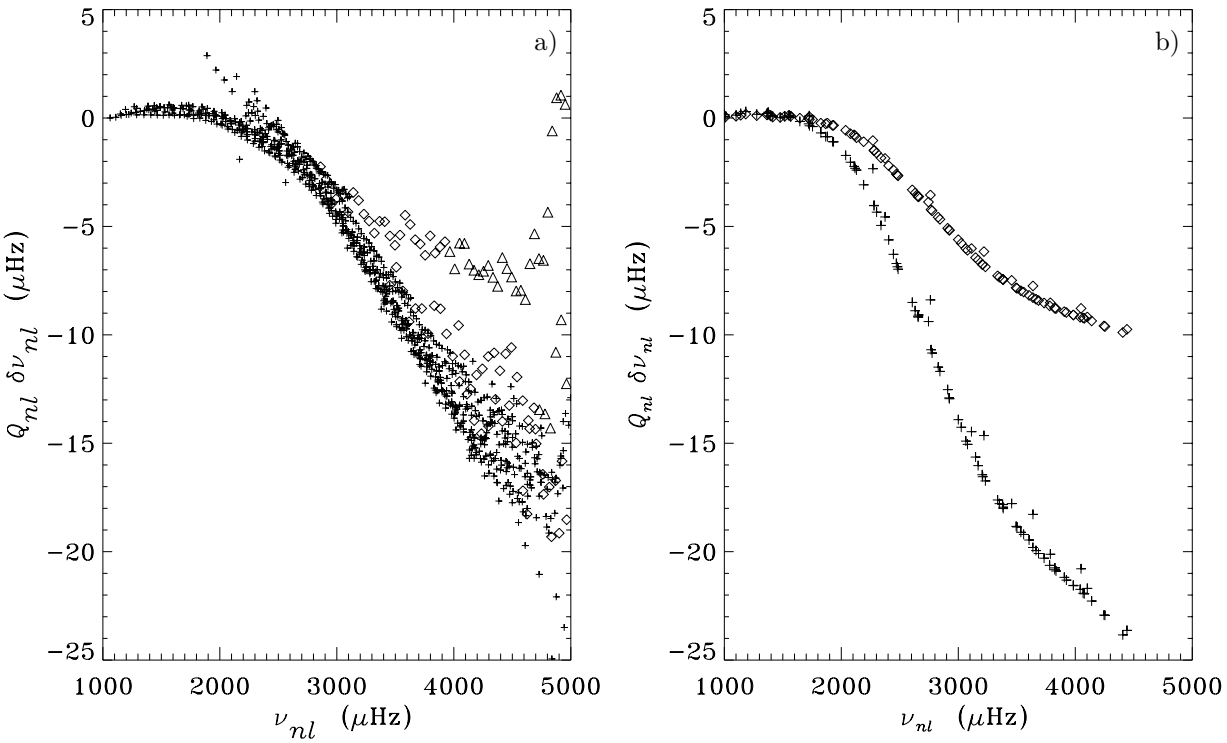

Figure 3.9: Panel a) Frequency residuals between observed and computed adiabatic frequencies of the 'standard' solar model, scaled by $Q_{nl} = I_{nl}/I_0(\nu_{nl})$, where $I_0(\nu_{nl})$ is the inertia of the radial modes, interpolated to the frequency ν. The symbols denote different mode degree: + for $0 \leq l \leq 500$, $\diamondsuit$ for $500 \leq l \leq 1000$, and $\triangle$ for $l > 1000$.
Panel b) Adiabatic frequency residuals between 'standard' Solar model using the local mixing-length theory and the CM-theory for convection (diamonds) and an averaged hydrodynamical simulation (pluses) (adopted from Rosenthal *et al.* 1995).

$l \lesssim 500$, the exhibited differences are to be assumed arising essentially from uncertainties in the model physics describing the superficial layers in the solar atmosphere (Rosenthal *et al.* 1995; Rosenthal 1996; Christensen-Dalsgaard & Thompson 1996). These upper layers however are dominated by the physics describing the interaction of convection and radiation and thus the shape of the eigenfunctions for high-order modes become crucially dependent upon the treatment of these effects.

As discussed in Section 2.5.1 the CM-theory for convection predicts a much steeper superadiabatic temperature gradient relative to the standard mixing-length theory. The first adiabatic exponent

$$\Gamma_1 = \left(\frac{\partial \ln p_{\rm g}}{\partial \ln \rho}\right)_s , \tag{3.42}$$

where $p_{\rm g}$ denotes the gas pressure and s the entropy, exhibits therefore a much steeper depression in the hydrogen ionization zone, which results in a decrease of the adiabatic frequencies for high-order modes. Calculations of adiabatic frequency differences between the 'standard' solar model and a model constructed with the Canuto & Mazzitelli convection theory were performed by Rosenthal *et al.* (1995) and are depicted in Fig. 3.9b. In

these calculations however, turbulent pressure was not considered in the equilibrium and pulsation model.

The influence of the turbulent pressure and its pulsationally induced perturbation upon adiabatic and non-adiabatic pulsation frequencies were first investigated by Gough (1984), using the local time-dependent mixing-length prescription for convection (cf. Section 2.3.2), however using a simplified analytical approximation of the eigenfunctions in the atmosphere. Balmforth (1992b) studied these effects in a more consistent way and by means of the more sophisticated non-local time-dependent mixing-length theory (cf. Section 2.4.2). Both authors concluded that the correction of the stratification of the superadiabatic boundary layers due to the inclusion of the mean turbulent pressure substantially decreases the adiabatic frequency residuals. The effects of the turbulent pressure fluctuations as well as nonadiabaticity, however, tend to increase the pulsation frequencies, although by a much smaller value. Similar results of the influence of the mean turbulent pressure on the adiabatic eigenfrequencies have been obtained by Rosenthal *et al.* (1995) based on a hydrodynamical simulation of the outer 2% of the solar radius (Stein & Nordlund 1991), matched continuously in the sound speed to a model envelope calculated in the usual fashion as is the 'standard' solar model. These frequency residuals are represented in Fig. 3.9b.

If turbulent pressure is considered in the model calculations, additional care must be given in solving the adiabatic pulsation equations. The first adiabatic exponent Γ_1, as defined

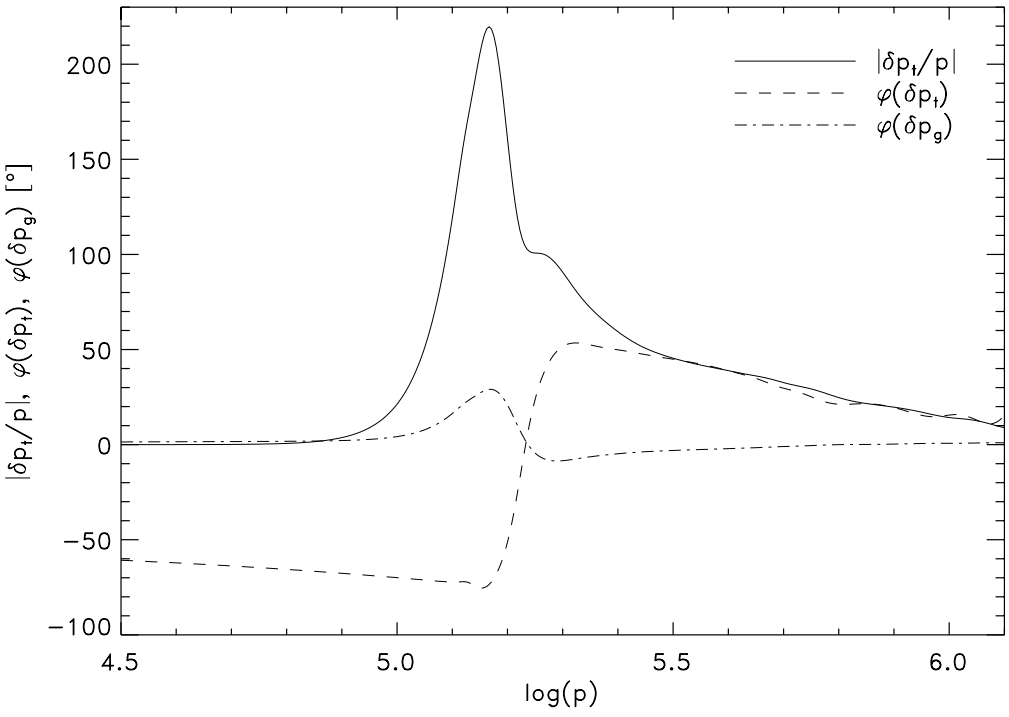

Figure 3.10: Phases of the turbulent, $\varphi(\delta p_{\rm t})$, and gas pressure, $\varphi(\delta p_{\rm g})$, fluctuations relative to the phases of the displacement versus the total pressure in the solar atmosphere for the acoustical radial mode of order $n = 16$. The solid line displays the norm of the turbulent pressure eigenfunction. Calculations were carried out solving the pulsation equations describing the time-dependent non-local mixing-length theory and using the parameters $\alpha_{\rm c} = 1.99$ and $a^2 = b^2 = 300$ in the mean envelope.

by equation (3.42), is expressed by means of the thermo-dynamical gas pressure $p_{\rm g}$. Thus in the presence of turbulent pressure $p_{\rm t}$, such that the total pressure $p = p_{\rm g} + p_{\rm t}$ satisfies the hydrostatic equilibrium, Γ_1 would experience a modification of the form

$$\tilde{\Gamma}_1 = \left(\frac{\partial \ln p}{\partial \ln \rho}\right)_s = \frac{1}{p}\left[\left(\frac{\partial p_{\rm g}}{\partial \ln \rho}\right)_s + \left(\frac{\partial p_{\rm t}}{\partial \ln \rho}\right)_s\right], \tag{3.43}$$

and the Lagrangian perturbation in the total pressure has to satisfy the equation

$$\frac{\delta p}{p_0} = \frac{\delta p_{\rm g}}{p_0} + \frac{\delta p_{\rm t}}{p_0} = \tilde{\Gamma}_1 \frac{\delta \rho}{\rho_0}, \tag{3.44}$$

where the zero subscripts denote the equilibrium values. However calculations solving the fully non-adiabatic pulsation equations with the inclusion of the turbulent pressure fluctuations $\delta p_{\rm t}$ reveal, that the phase of $\delta p_{\rm t}$ is approximately 90° out of phase with the other terms in the momentum equation [cf. equation $(A.57)$], as portrayed in Fig. 3.10. The phase of $\delta p_{\rm g}$, however, is rather small which may allow us to consider $p_{\rm g}$ to respond adiabatically. Thus we may conclude, that $\delta p_{\rm t}$ in equation (3.44) contributes predominantly to the imaginary part of the eigenfrequency, *viz.* the damping rates, as discussed in more detail in Section 3.2.2, and may therefore be neglected in the calculation of the real adiabatic eigenfrequencies. These results were also confirmed through hydrodynamical simulations by Rosenthal *et al.* (1995). The modified Γ_1, as defined by equation (3.43), may then be rewritten as

$$\tilde{\Gamma}_1 = \frac{p_{\rm g}}{p}\Gamma_1, \tag{3.45}$$

and the only change in the adiabatic momentum equation is the replacement of Γ_1 by $\tilde{\Gamma}_1$.

The comparison between models computed with different convection theories requires a more involved consideration. In order to isolate the effects in the superadiabatic layers arising from the different prescription of convection, all the models should exhibit the same structure in their deeper layers and thus have to match in their cores. The same structure in the core is obtained by requiring the models to lie on the same adiabat near the bottom of the convection zone (CZ) as well as to exhibit the same depth of the CZ. In the model calculations performed here with the local and non-local mixing-length theory the matching procedure was carried out by specifying the same surface boundary conditions in both models and iterating the local solution to the non-local one by varying the mixing length parameter $\alpha_{\rm c}$ and chemical composition X such, that temperature and pressure match exactly near the bottom of, but still inside, the CZ. At this fitting point, the non-local model is then extended by the local solution down to a radius fraction of 0.2 $R_\odot$, where $R_\odot$ denotes the Sun's radius defined at the point where the temperature is equal to the effective temperature $T_{\rm eff}$. By doing so, we avoid the unphysical superadiabaticity of the non-local solution at the bottom of the CZ (see for instance Fig. 2.1). Moreover the depth of the CZ in both equilibrium models is ensured to be the same and exhibits a value of $0.287R_\odot$ (according to the value measured accurately by helioseismology, Christensen-Dalsgaard, Gough & Thompson 1991) relative to $R_\odot$ when the mixing-length parameters

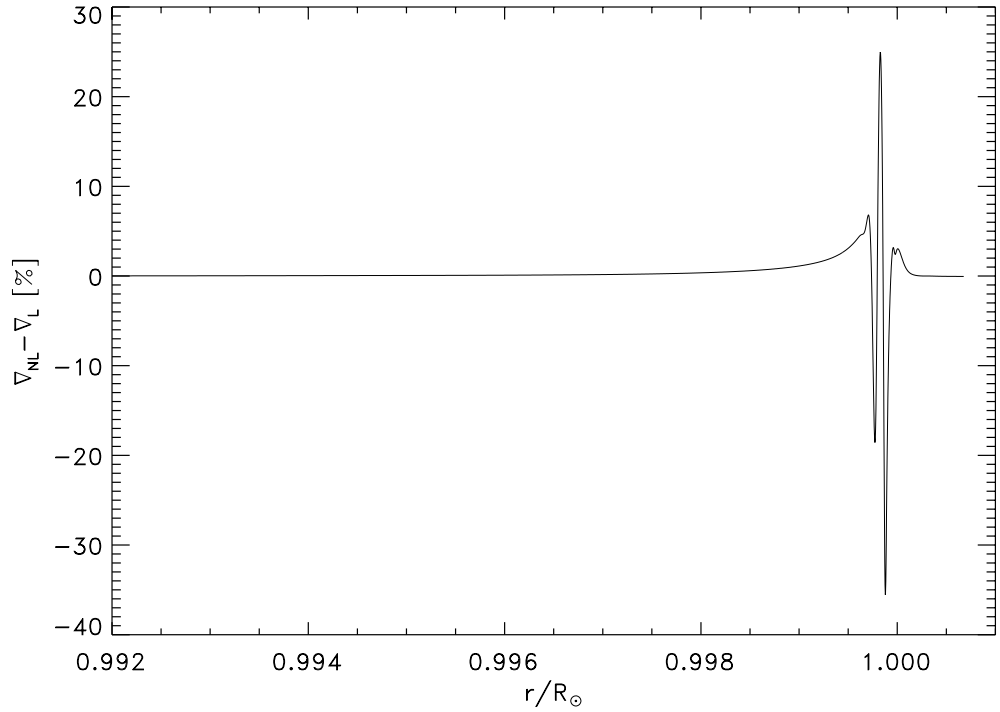

Figure 3.11: Relative differences of the temperature gradient as function of depth between the model computed with the non-local mixing-length theory ($\nabla_{\rm NL}$) using $\alpha_{\rm c} = 1.99$, $a^2 = b^2 = 300$ and the corresponding matched model calculated with the local prescription for convection ($\nabla_{\rm L}$) found by the fitting process discussed in the text.

$\alpha_{\rm c} = 1.99$ and $a^2 = b^2 = 300$ are employed in the non-local model computation. The relative differences of the temperature gradient between the local and non-local model are displayed in Fig. 3.11.

The radial oscillation frequencies were computed for the following models:

L.a Using the local mixing-length theory as discussed in Section 2.3 without turbulent pressure in the mean envelope. Frequencies were computed in the adiabatic approximation.

NL.a Using the non-local theory for convection (cf. Section 2.4) including turbulent pressure in the mean model. Frequencies were calculated in the adiabatic approximation neglecting the turbulent pressure fluctuations.

NL.na Using the time-dependent non-local convection theory (cf. Section 2.4.2) including turbulent pressure in the mean model. Frequencies were computed by solving the fully non-adiabatic pulsation equations with the inclusion of the Lagrangian turbulent pressure perturbation.

The model envelopes were integrated on a grid with 3200 mesh-points starting at an optical depth of $\tau = 10^{-4}$ and solving the equations appropriate to the local and non-local mixing-length theories, as outlined in the Sections 2.3 and 2.4, respectively. The non-local model is constructed using the Eddington approximation to radiative transfer, whereas the local model assumes diffusion approximation. This particular difference however generates

only a small fraction of the frequency residuals (Balmforth 1992b). Further details on the computations will be given in Section 3.4.1.

The results are portrayed in Fig. 3.12. The adiabatic frequencies are depressed for values larger than about 2 mHz if turbulent pressure is taken into account in the mean envelope. Compared to the results obtained by Balmforth (1992b) however, our calculations for NL.a-L.a predict a larger maximum deficit of ~ 15 μHz, whereas Balmforth found a value of about 10 μHz. This discrepancy may be explained through the different implementation of the adiabatic momentum equation, for which Balmforth used the unmodified value for Γ_1, as defined by equation (3.42). Turbulent pressure however approximately modifies Γ_1 such, as expressed by $\tilde{\Gamma}_1$ in equation (3.45), that it becomes more depressed in the ionization zones, which results in a further decrease of the adiabatic frequencies. It is perhaps interestingly to notice, that the effect of turbulent pressure on $\tilde{\Gamma}_1$ has a superficial similarity to the change of Γ_1 in the CM-theory, caused by the substantially steeper predicted superadiabatic gradient, relative to the local mixing-length theory. The dashed line in Fig. 3.12 displays the residuals of the radial pulsation frequencies arising from nonadiabaticity and the Lagrangian perturbation of the turbulent pressure (NL.na-NL.a) , predicting frequency shifts of the opposite sense to the observed discrepancy with a maximum value of about 9 μHz. Balmforth obtained values with the same sign however with a maximum of ~ 2 μHz in the frequency shifts affected by these processes. This is probably due to the fact, that Balmforth considered a different approach in the matching

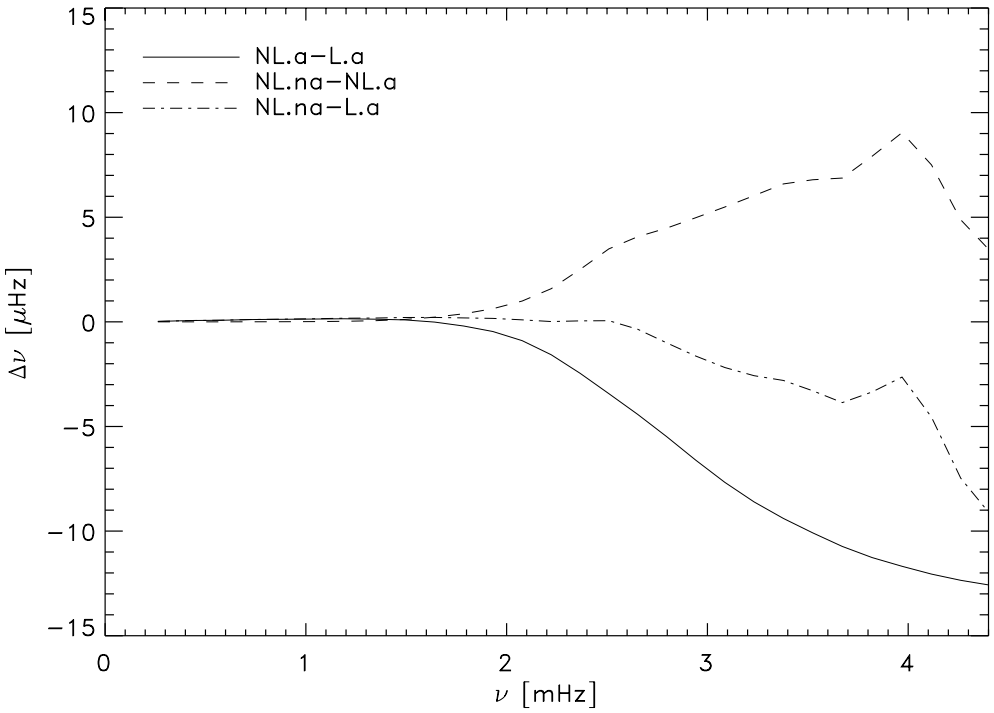

Figure 3.12: Frequency differences calculated from non-local mixing-length theory relative to the local mixing-length theory. The solid line displays the adiabatic frequency residuals if turbulent pressure is considered in the mean model. The dashed line demonstrates the effects due to nonadiabaticity and $\delta p_{\rm t}$, and the dash-dotted line portrays the residuals if all the effects are taken into account.

procedure between the local and non-local model. In particular he iterated the local solution to the non-local model by varying the luminosity and effective temperature, which results in different surface boundary conditions, and presumedly does no longer reflect a consistent acoustical comparison between the models. From our results the overall change in the frequencies (NL.na-L.a) imply a moderate downshift in the order of 5 μHz, represented by the dash-dotted curve in Fig. 3.12, suggesting that the inclusion of non-adiabatic effects and turbulent pressure fluctuations nearly cancel the effects of the modification of the superadiabatic layers in the equilibrium envelope due to the mean turbulent pressure.

With our calculations we could confirm the results obtained by the other authors discussed before when turbulent pressure is taken into account. The introduction of turbulent pressure in the mean model means that there is an additional dynamical pressure gradient that can oppose the acceleration of convective elements. This lowers the effectiveness of convective heat transfer in the superadiabatic boundary layers and results in a steeper temperature gradient. Similar to the results predicted by the CM-model, this causes a more pronounced depression of $\tilde{\Gamma}_1$ in the superficial layers reducing the discrepancy to the observed frequencies. Effects due to processes damping the oscillations suggest to increase the pulsation frequencies over the value it would have if these effects were absent, obliterating almost the frequency shifts arising from the mean turbulent pressure. However, the non-local mixing-length formulation represents an incomplete theory of turbulent convection and underestimates the damping rates compared to the measured line widths at high frequencies (cf. Section 3.4.4). Thus nonadiabaticity and effects through the turbulent pressure fluctuations are modelled only approximately and the predicted frequency shifts due to these processes should therefore be regarded as a preliminary assessment. Moreover, hydrodynamical convection model results suggest that our non-local calculations underestimate the change in the equilibrium structure (cf. Fig. 3.9b). Thus if we were to combine the frequency shifts predicted by the hydrodynamical simulations with the non-adiabatic corrections to the pulsation frequencies from the non-local calculations, then the resulting mode frequencies will be close to the observational data. Such an interpretation however, must be considered with great care, since it involves combining the results of two completely different theories of convection.

3.4.4. Theoretical damping rates in solar-type stars

The imaginary part of the complex eigenfrequency $\omega = \omega_r + i\,\omega_i$, as obtained from solving the fully non-adiabatic pulsation equations, represents the damping rate and which we define as $\eta = -\omega_i$. We first computed damping rates for the solar case, similar to Balmforth (1992a), using however, the OPAL tables for the opacities, and depicted the results for different values of α_c and non-local parameters a and b in Fig. 3.13 together with the observed line widths by Libbrecht (1988). As Balmforth (1992a) already reported, all modes are found to be stable and agree tolerable with the observation for frequencies between 2 mHz and 4 mHz. Below and above this frequency domain, the theoretical damping rates predict less stable modes than observations would suggest. Contributions to the damping rates arising from incoherent scattering, as discussed above, may increase the theoretical damping rates considerable at low and high frequencies, which are not modelled yet in our calculations.

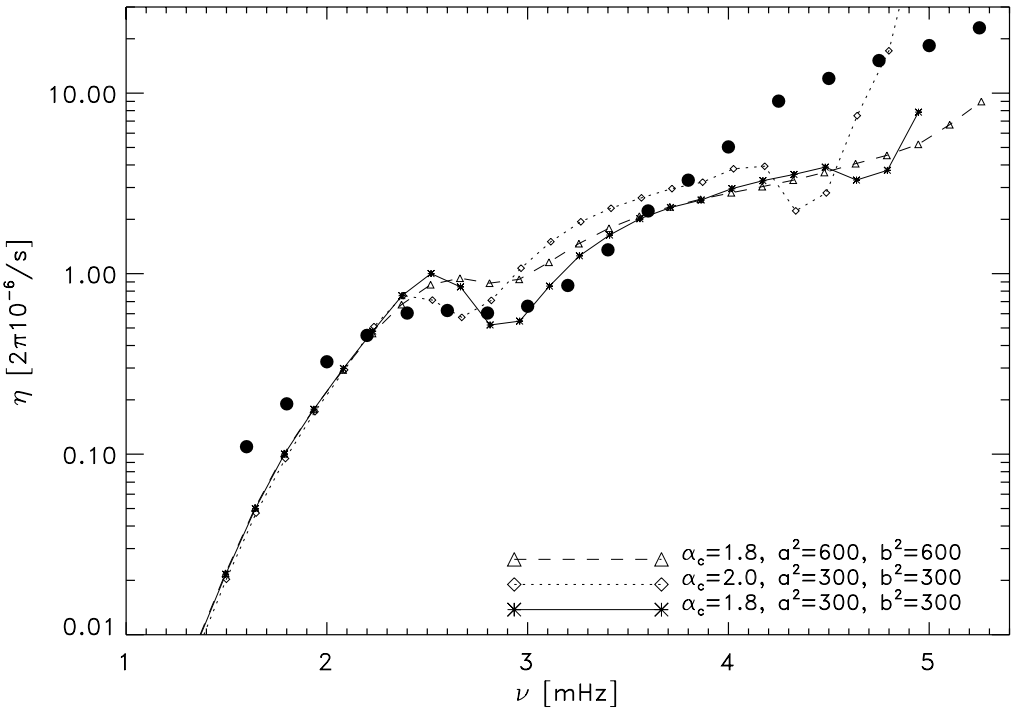

Figure 3.13: Damping rates η for the Sun as function of frequency and different mixing-length parameters. The filled dots represent the measured line widths of Libbrecht (1988).

The theoretical damping rates are most sensitive to the mixing-length parameter α_c near the plateau (or depression) at $\sim$ 2.6 mHz. At low frequencies the modes are less sensitive to the structure of the upper superadiabatic boundary layers, sampling these layers with less detail than high-order modes, and thus become almost independent of α_c. At high frequency the damping rates are mainly determined by radiative damping which occurs preferentially in the atmospheric layers and thus again become less sensitive to α_c. For the intermediate frequency range, the explanation is slightly more involved. Mixing-length theory provides for the convective growth rate of an eddy characterized by ℓ the expression [cf. equation (2.48)]

$$\sigma = 2\left(\overline{w^2}\right)^{1/2}/\ell\,, \tag{3.46}$$

which enables us to define a characteristic frequency $\nu_\ell = \sigma/2\pi = (\overline{w^2})^{1/2}/\pi\ell$ for the convective element. This frequency peaks in the superadiabatic boundary layer with a typical value of $\sim$ 2.5 mHz. Therefore one may expect a resonant interaction between pulsation and the convective turn-over time of the eddies in the superadiabatic boundary layers at this characteristic frequency, which is close to the region where the damping rates display the depression. Moreover, the superadiabatic boundary layer is relatively thin and exhibits a clearly defined thermal adjustment time, whose value depends critically upon the details of convection and is in the order of 2.8 mHz (Balmforth 1992a). Thus there occurs a thermodynamic resonance between pulsation and the disturbance of the stratification that it generates. At this frequency non-adiabatic effects are largest and result in a destabilization of the modes provided by the gas pressure perturbation in the

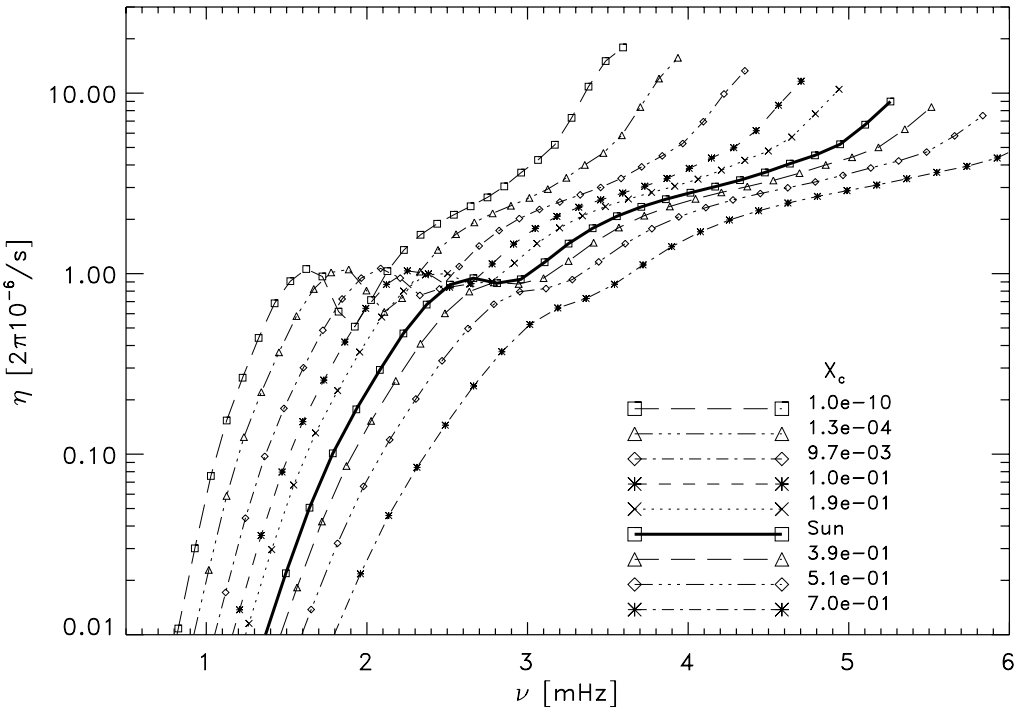

Figure 3.14: Damping rates for an evolving $1\,M_\odot$ star as function of frequency. The evolution steps are indicated by the hydrogen mass fraction in the core (X_c) For the mixing-length parameters the values $\alpha_c = 1.8, a^2 = b^2 = 600$ have been used.

superadiabatic layers. Reducing α_c increases ν_ℓ and shortens the thermal adjustment time of the superadiabatic layer shifting the depression in η to higher frequencies. Furthermore, the turbulent eddies become less efficient to reduce local temperature gradients which leads to an increase of the superadiabaticity. Non-local motion is therefore amplified which deepens the depression in the damping rates.

In Fig. 3.14 damping rates are depicted for an evolving $1\,M_\odot$ star. The models were generated by specifying the mass, luminosity and effective temperature. These parameters were taken from full evolution sequences by Christensen-Dalsgaard (1993). The individual evolution steps are displayed by the hydrogen mass fraction in the core (X_c). With increasing age the damping rates become larger particular for low and high-order modes. For intermediate modes the depression in the damping rate increases as the star evolves, due to the decreasing density in the atmospheric layers. The surface density ρ_s may be written as function of the surface gravity $g_{\rm eff}$ and effective temperature $T_{\rm eff}$ in the form (Christensen-Dalsgaard 1995)

$$\rho_s \propto \left[(r+1)\, g_{\rm eff}\right]^{1/(r+1)} T_{\rm eff}^{-(s+1)/(r+1)}\,, \tag{3.47}$$

where the parameters r and s describe the exponential dependence of the opacity on density and temperature according to the approximation

$$\varkappa = \varkappa_0 \rho^r T^s\,. \tag{3.48}$$

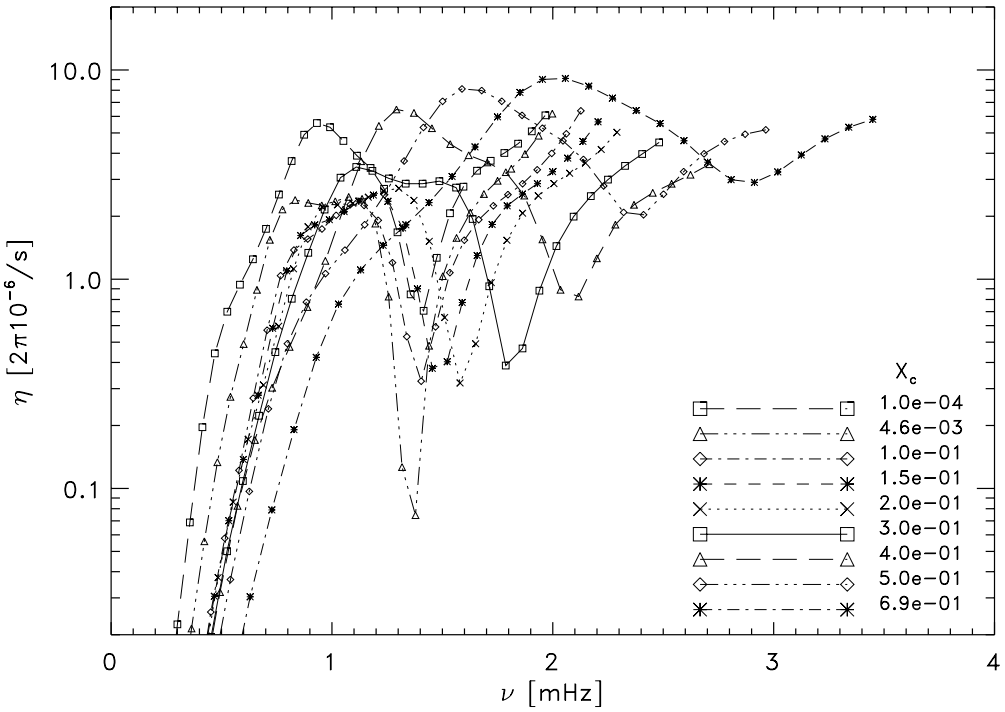

Figure 3.15: Damping rates for an evolving $1.45\,M_\odot$ star as function of frequency. The evolution steps are indicated by the hydrogen mass fraction in the core (X_c) For the mixing-length parameters the values $\alpha_c = 2.0, a^2 = 900, b^2 = 2000$ have been used.

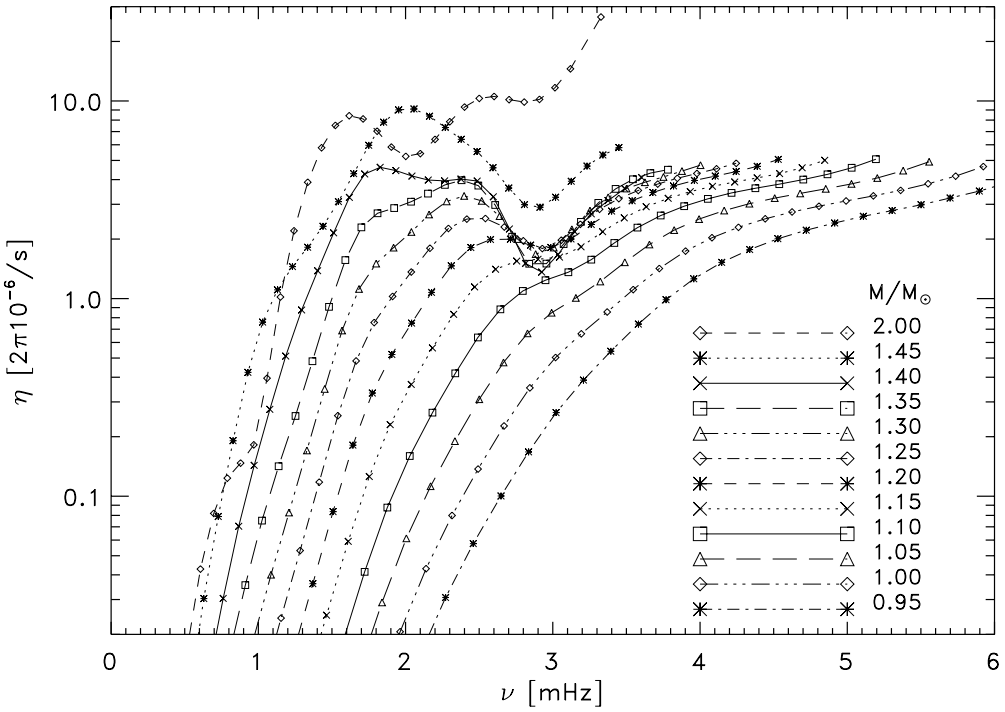

Figure 3.16: Damping rates as function of frequency for ZAMS models. For the mixing-length parameters the values $\alpha_c = 2.0, a^2 = 900, b^2 = 2000$ have been used.

The superadiabatic boundary layer becomes manifested in the hydrogen ionization zone, where the opacity is described mainly by the contribution of the negative hydrogen ions (H^-). Hence the opacity increases with temperature and the parameter s is therefore positive. In particular for sun-like stars one obtains for the parameters r and s in the hydrogen ionization zone the values ~ 0.4 and ~ 10, respectively. As the star evolves its radius becomes larger and thus the surface gravity decreases. Moreover, for young stars with a mass of $\sim 1\,M_\odot$ the surface temperature $T_{\rm eff}$ increases with age and the density in the atmosphere declines. The superadiabatic gradient increases by approximately 24% along the main-sequence of a $1\,M_\odot$ star promoting the depression in the damping rates.

A similar behaviour of the damping rates is obtained for more massive stars as indicated for an evolving $1.45\,M_\odot$ star depicted in Fig. 3.15. The depression in the damping rates is already pronounced at the ZAMS, since the surface gravity and thus the surface density decline rapidly with increasing mass. This may be seen even more obviously in Fig. 3.16, where damping rates are depicted for stars along the ZAMS.

Goldreich & Kumar (1991) derived a simplified equation for the damping rates accounting for the effects of radiative damping and convective dynamics. They treated radial modes in the quasi-adiabatic approximation (cf. Section A.2.2) assuming the standard mixing-length theory for convection (e.g. Böhm-Vitense 1958) and obtained the expression

$$\eta \;=\; \frac{L}{c_{\rm t}^2 M_\omega}\left(\frac{\omega_r}{\omega_{\rm co}}\right)^2 , \tag{3.49}$$

where $c_{\rm t}$ denotes the sound speed at the top of the convection zone, $\omega_{\rm co}$ is the acoustical cut-off frequency in an isothermal atmosphere [cf. equation $(A.65)$] and M_ω is the mode mass of the radial mode with the pulsation frequency ω_r. The mode mass is defined such, that it represents the coefficient of proportionality between the mode's kinetic energy and the root mean square value of its surface velocity $V_{\rm rms}$. Thus the mode mass may be expressed by the kinetic mode energy E_k as

$$M_\omega \;=\; \frac{2E_k}{\omega_r^2 R_\star^2}\,, \tag{3.50}$$

with

$$E_k \;=\; \frac{1}{2}\omega_r^2 \int_{m_b}^{M_\star} |\delta r\,(m,\omega)\,|^2\, dm\,, \tag{3.51}$$

and where $R_\star$ and $M_\star$ represent radius and mass of the star and m_b denotes the mass at the bottom boundary of the envelope. The mode energy, as defined by equation (3.51) is displayed as function of frequency in Fig. 3.17 for model envelopes of the Sun, a $1.25\,M_\odot$ and a $1.45\,M_\odot$ ZAMS star, using the adiabatic and non-adiabatic eigenfunctions for the displacement δr, respectively. The non-adiabatic solutions were obtained from using the equations appropriate to the non-local, time-dependent theory assuming the convection parameters $a^2 = b^2 = 300$ for the solar model and $a^2 = 900$, $b^2 = 2000$ for the ZAMS

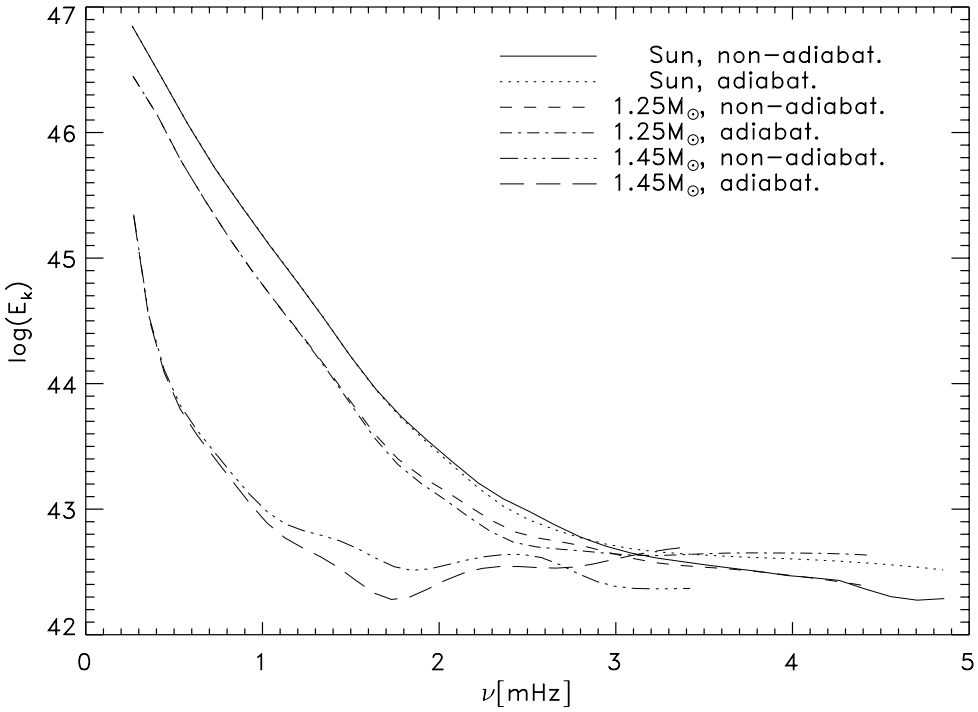

Figure 3.17: Mode energy, as defined by equation (3.51), versus frequency for the Sun, a $1.25\,M_\odot$ and a $1.45\,M_\odot$ ZAMS star. The results are obtained from computations assuming adiabatic and non-adiabatic eigenfunctions using the equations appropriate to the non-local mixing-length theory in the latter case. The solutions are indicated by different line styles.

models. The mixing-length parameter was chosen to be $\alpha_c = 2.0$ for all model computations. For modes with cyclic frequencies $\nu \gtrsim 1.5\,\mathrm{mHz}$ the adiabatic solutions suggest different values for E_k relative to the non-adiabatic results, demonstrating the fact, that non-adiabatic effects become relevant at these frequencies. Moreover, at low frequencies the mode energy declines with increasing mass of the star, leading to an increase of the damping rates as expressed by equation (3.49).

With the help of equations (3.50), ($A.65$) and the continuity equation ($A.2$) the expression (3.49) can be rewritten as

$$\eta = \frac{1}{4\pi} \frac{(2H_{\mathrm{pt}}R_\star)^2\, L}{2E_k} \left(\frac{\omega_r^2}{c_{\mathrm{t}}^2}\right)^2 , \tag{3.52}$$

where H_{pt} represents the pressure scale height at the top of the convection zone. In Fig. 3.18 the damping rates according to the analytical expression (3.52), assuming adiabatically and non-adiabatically computed displacement eigenfunctions, are displayed together with the results obtained from solving the fully non-adiabatic pulsation equations appropriate to the non-local mixing-length theory (indicated by the symbols). For frequencies less than half the acoustical cut-off frequency ω_{co}, the results suggest a fair agreement between the analytical and modelled damping rates. An interesting feature is the bend in the analytical solution for the $1.45\,M_\odot$ star near the frequency $\nu \approx 1.85$ mHz. Since this property appears

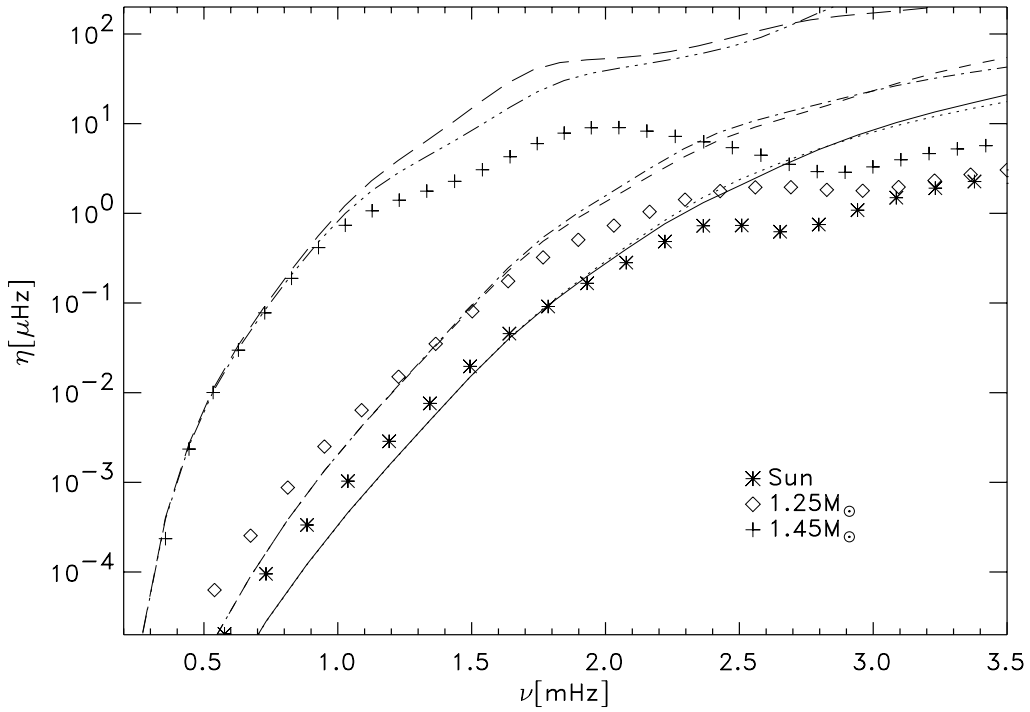

Figure 3.18: Theoretical damping rates as function of frequency for the Sun, a $1.25\,M_\odot$ and a $1.45\,M_\odot$ ZAMS star. The curves display the solutions according to the analytical expression (3.52), assuming the adiabatically and non-adiabatically computed kinetic mode energy. The line styles are similar to those used in Fig. 3.17. The symbols show the results of the corresponding models, obtained from solving the fully non-adiabatic pulsation equations using the non-local, time-dependent mixing-length theory.

to be present also in the solution obtained with the adiabatically computed displacement eigenfunction, it may be associated with the stratification of the equilibrium structure (e.g. mean turbulent pressure). The analytical expression (3.49), as obtained from Goldreich & Kumar (1991), may therefore be used for estimating damping rates of low-order modes by means of adiabatic eigenfunctions.

3.4.5. Work Integrals

In Section 3.4.2 we discussed the degree of nonadiabaticity as function of depth in the star's envelope. In particular we measured the amplitude of the local entropy perturbation as defined by

$$\frac{\delta s}{c_\mathrm{p}} = \frac{\delta T}{T_0} - \nabla_\mathrm{ad}\,\frac{\delta p_\mathrm{g}}{p_\mathrm{g0}}\,. \tag{3.53}$$

The information of the local entropy perturbation alone, however, provides yet no information about the damping or excitation of the mode. Instead one has to study the net rate of gain of heat in order to obtain the growth or decay of the pulsation amplitudes in time. Since vibrational instability is characterized by the existence of a periodicity in the temporal behaviour of the perturbations, a reasonably useful criteria for this kind of

instability will be the sign of the total energy change over one pulsation period assuming that the system returns precisely to its original state at the end of the period. This is the definition of the so-called work integral W, which is obtained by integrating the energy equation (3.39) over one period of oscillation. This integral, however, will vanish in the linear approximation and thus has to be solved to second order. It was demonstrated first by Eddington (1926), that the second order quantity W can still be solved in terms of first order solutions of the pulsation equations. In particular, it is the assumption of exact periodicity, or more precisely quasi-periodicity[11], which provides the relations

$$\oint\limits_{1\ \mathrm{period}} \delta s\, dt \approx 0\,, \qquad \text{and} \qquad \oint\limits_{1\ \mathrm{period}} \delta T\, dt \approx 0\,, \tag{3.54}$$

and the differential work integral becomes to second order

$$dW \;=\; dm \oint\limits_{1\ \mathrm{period}} \delta T \frac{\partial}{\partial t}\left(\delta s\right)\, dt\,, \tag{3.55}$$

for a star with zero pressure at its surface. Basically, equation (3.55) resembles the energy production of a Carnot-type heat engine and the mass shell dm drives (damps) the pulsation if $dW > 0$ ($dW < 0$). The work integral represents a very useful diagnostic tool for investigating the location of the layers in which damping and driving take place. So far only contributions arising from the non-adiabatic effects have been considered. Baker & Gough (1979) derived the appropriate work integrals for non-adiabatic pulsation when also turbulent pressure is taken into account. Basically the contribution to the total integral can be divided into two terms: the first accounts for the effects of the gas pressure fluctuation (W_g), and the second considers the contribution arising from the fluctuating momentum flux (W_t). These integral expressions may be derived from the equations of motion and the thermal energy conservation equation and may be written as

$$W_\mathrm{g}\left(m\right) \;=\; \pi \int_{m_b}^{M_\star} \mathrm{Im}\left(\delta p_\mathrm{g}{}^{*}\, \delta\rho\right) \frac{dm}{\rho^2}\,, \tag{3.56}$$

$$\begin{aligned} W_\mathrm{t}\left(m\right) \;=\; & \pi \int_{m_b}^{M_\star} \mathrm{Im}\left(\delta p_\mathrm{t}{}^{*}\, \delta\rho\right) \frac{dm}{\rho^2} \\ & + \pi \int_{m_b}^{M_\star} \left\{ \left(3-\Phi\right) \left[\mathrm{Im}\left(\delta r^{*}\, \delta p_\mathrm{t}\right) - \frac{p_\mathrm{t}}{\rho}\, \mathrm{Im}\left(\delta r^{*}\, \delta\rho\right) \right] - p_\mathrm{t}\, \mathrm{Im}\left(\delta r^{*}\, \delta\Phi\right) \right\} \frac{dm}{\rho r}\,, \end{aligned} \tag{3.57}$$

obeying the equality (Baker & Gough 1979)

$$\frac{4\pi E_k}{\omega_r} \;=\; W_\mathrm{g}\left(M_\star\right) + W_\mathrm{t}\left(M_\star\right) + F\,, \tag{3.58}$$

[11] *viz.* the quasi-adiabatic approximation, which assumes the adiabatic eigenfunctions for the evaluation of the mode stability.

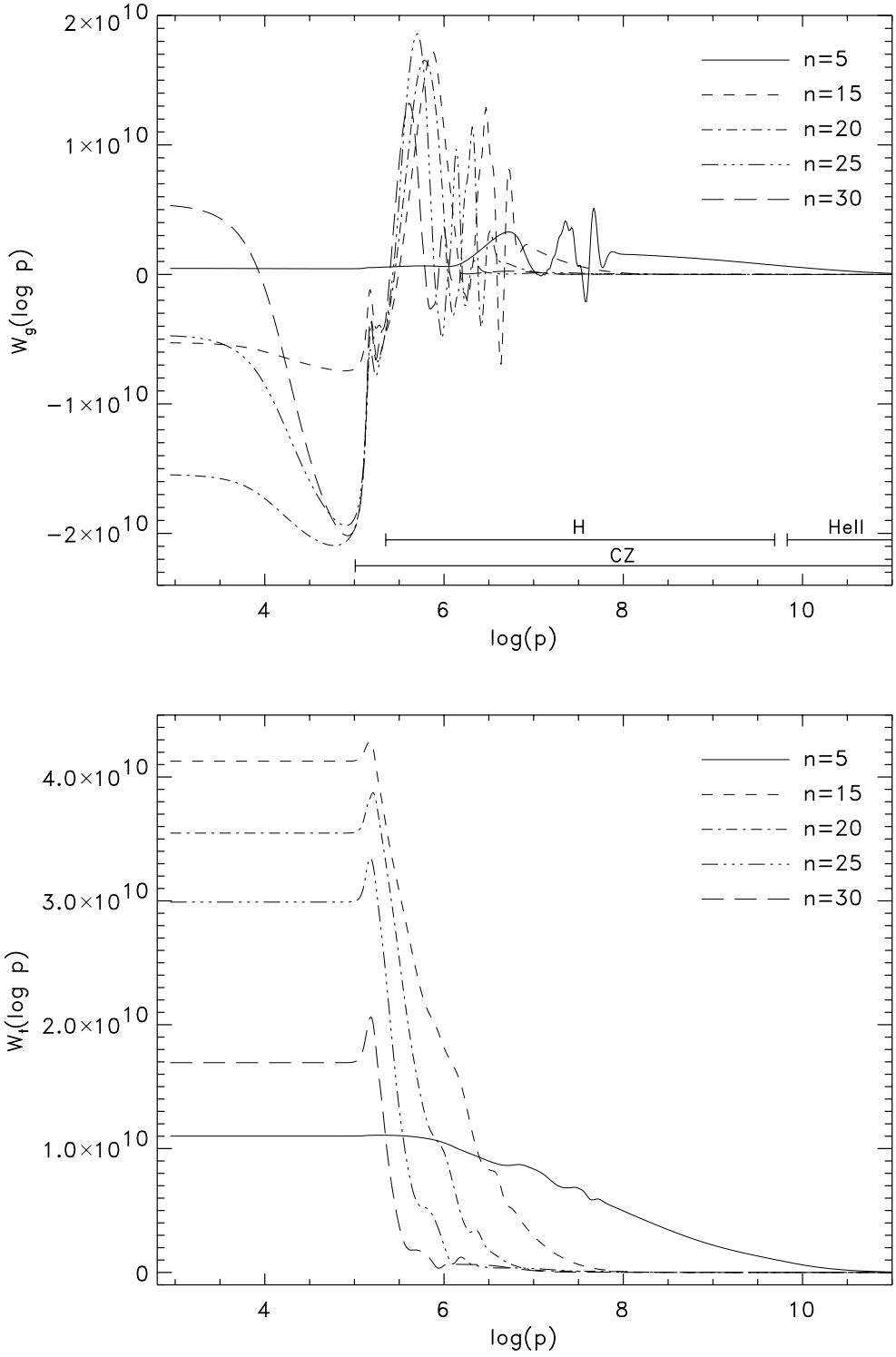

Figure 3.19: Accumulated work integrals (in units of 10^{30} erg) for the Sun and for selected modes in the relevant frequency spectrum. The upper panel portrays the contribution arising from the gas pressure perturbation, the lower from the perturbation of the Reynolds stresses $\delta p_{\rm t}$. The extents of the zones of convection (CZ) and of ionization of H and He, from 5% to 95% ionization, are similarly indicated. For the mixing-length parameters the values $\alpha_{\rm c} = 1.8, a^2 = 600, b^2 = 600$ have been used.

and where the term F is given by

$$F = \left[4\pi^2 r^2 \,\mathrm{Im}\,(\delta p * \delta r)\right]_{m_b}^{M_\star} . \tag{3.59}$$

The second term in W_t results from the anisotropy of the Reynolds stresses and can be neglected compared to the isotropic component. The spatial dependence of integrated work integrals for the Sun and a $1.45\,M_\odot$ ZAMS star are illustrated in Fig. 3.19 and Fig. 3.20 for modes spanning the relevant frequency spectrum. In regions where the accumulated work increases with radius, the modes are damped, and where it declines pulsation is locally excited.

At low-order the contribution to both terms of the work integral stems from nearly all depths of the convection zone and becomes concentrated towards the upper layers as frequency increases. In these upper layers, W_g exhibits strong spatial oscillations arising from the thermodynamic resonance between pulsation and the modulation of the convective heat flux which extracts energy from the mechanical motion. In the superficial layers of the convection zone, where there is the peak in the superadiabatic gradient, the accumulated work arising from the gas pressure perturbation experiences a severe destabilization. This negative contribution to W_g becomes substantial for moderate and higher-order modes and is the solely reason for the dip in the damping rates discussed before. In the outer layers of the atmosphere radiative damping contributes positive to W_g. Interestingly, although the degree of nonadiabaticity declines with increasing frequency in these superficial atmospheric layers [cf. Fig. 3.7], the W_g component of the total work integral becomes larger. This comes about because the phase between the temperature and entropy perturbation, or between density and gas pressure fluctuations, increases with height in the atmosphere. Moreover, the point at which waves are reflected back towards the interior gradually moves further out for modes with increasing frequency and thus radiative damping is further amplified for these oscillations. With increasing mass radiative damping in the upper layers becomes less dominant due to the decreasing surface density, as we already noticed in Section 3.4.4. Thus W_g becomes almost constant in the upper layers as portrayed for the $1.45\,M_\odot$ ZAMS model.

The contribution from the turbulent pressure fluctuation appears to stabilize the pulsation substantially which results from the phase difference between the fluctuating momentum flux and the density perturbation. The locations of the damping zones are found to be in the adjacent turbulent layers below the superadiabatic region.

In Fig. 3.21 the accumulated work for the four lowest-order modes of a $1.5\,M_\odot$ ZAMS star are depicted. The calculations suggest the first three modes to be overstable. The contribution from the turbulent pressure fluctuation promotes the destabilization of the first two modes. The negative contributions arising from the gas pressure perturbation stem predominantly from the HeII ionization zones as one would expect for a δ Scuti star (see also Section 4.3.2). When the radial order increases through 4, the perturbations in the Reynolds stresses stabilize the modes in the HeI ionization zone and pulsation becomes damped.

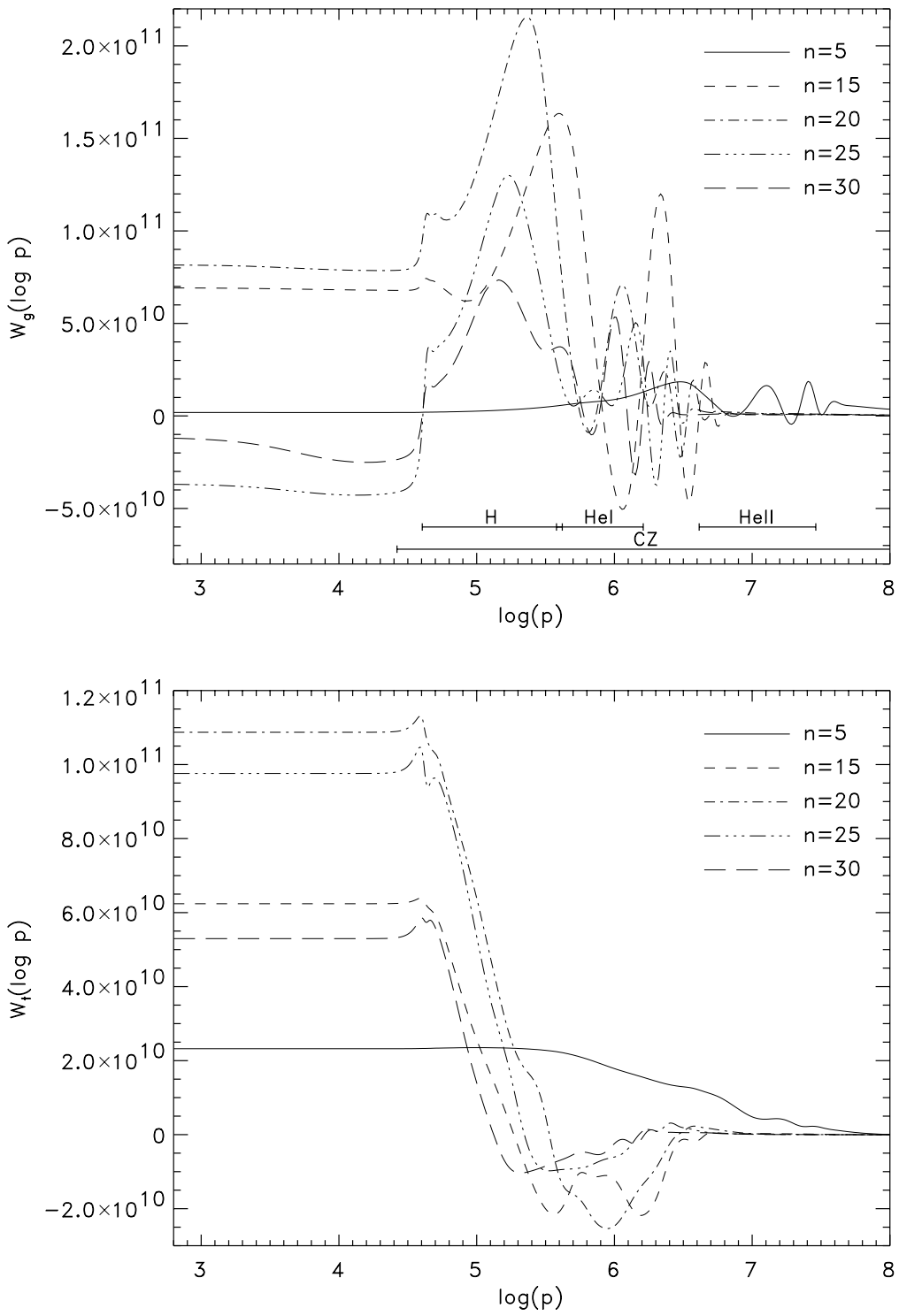

Figure 3.20: Accumulated work integrals (in units of 10^{30} erg) for a $1.45\,M_\odot$ ZAMS star for selected modes in the relevant frequency spectrum. The upper panel portrays the contribution arising from the gas pressure perturbation, the lower from the perturbation of the Reynolds stresses $\delta p_{\rm t}$. The extents of the zones of convection (CZ) and of ionization of H and He, from 5% to 95% ionization, are similarly indicated. For the mixing-length parameters the values $\alpha_{\rm c} = 2.0, a^2 = 900, b^2 = 2000$ have been used.

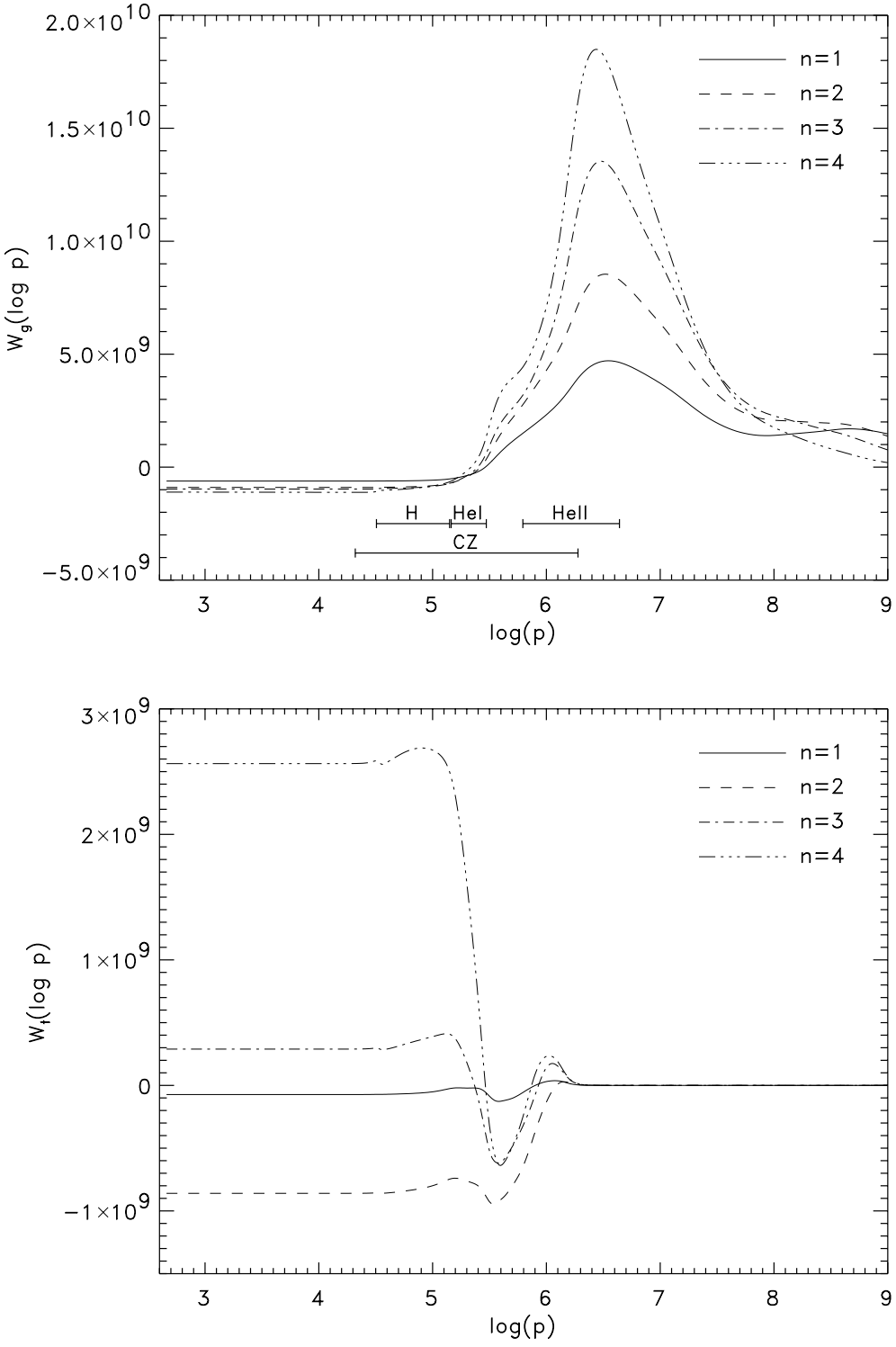

Figure 3.21: Accumulated work (in units of 10^{30} erg) for a $1.5\,M_\odot$ ZAMS star for the first four modes. The upper panel portrays the contribution arising from the gas pressure perturbation, the lower from the perturbation of the Reynolds stresses δp_{t}. The extents of the zones of convection (CZ) and of ionization of H and He, from 5% to 95% ionization, are similarly indicated. For the mixing-length parameters the values $\alpha_{\mathrm{c}} = 2.0, a^2 = 900, b^2 = 2000$ have been used.

4. Amplitudes and overstable modes in other stars

4.1. Introduction

Observational data of oscillation properties in stars other than the Sun provide important informations for testing evolution theory for distant stars and constitute the foundation for the research in the field of asteroseismology. A comprehensive definition of asteroseismology was given by Däppen *et al.* (1988) and recent reviews on this topic were represented by Brown & Gilliland (1994) and Brown (1996). For instance, the mean value of the differences between frequencies of modes of like angular degree l and varying radial order n (e.g. Gough & Novotny 1991), i.e. the large separation Δ, carry information on the gross structure of the star and principally depend on M/R^3 and thus provide information about the mean density. The mean value of frequency splitting between modes with like order and varying degree, i.e. the small separation δ, depends strongly on the variation of the sound speed in the core and thus to the amount of helium that has been produced by the nuclear reactions. It is therefore a measure of the age of the star (e.g. Christensen-Dalsgaard 1988). These seismic parameters therefore represent an important tool in asteroseismic calibrations and were discussed in detail by Gough (1995), for example. Additional, mode lifetimes (damping rates) and the variation of the oscillation amplitude with stellar parameters would be of intrinsic interest in connection with the determination of the excitation mechanism for solar-like oscillations. Moreover, they would provide statistical properties of convection in the region where pulsations are excited, most probably in the superficial layers of the convection zone.

A crucial problem with the detection of oscillations in solar-type stars, however, is their very small amplitudes in the order of 1 m/s. Observed in disk-integrated light, velocity variations in the surface of the Sun are predicted to have values $\lesssim 25$ cm/s (Grec *et al.* 1983; Isaak *et al.* 1989; Libbrecht & Woodard 1991). To detect similar variations in distant stars is therefore an extremely challenging task, requiring that observations be made with the utmost precision. So far three observing methods have been developed to detect such oscillations. Velocity amplitudes can be found from periodic Doppler shifts of spectral lines (e.g. Kennelley 1995). By means of this method the mostly successful results were the prediction of the upper limit to the oscillation amplitudes in some of the brightest stars (e.g. Brown & Gilliland 1990; Brown *et al.* 1991). The second method is to look for periodic brightness fluctuations using photometry to deliver information about the luminosity amplitudes. The latter method, when used with area detectors such as CCDs, does have a clear advantage over spectroscopic techniques allowing more easily to observe large ensembles of stars simultaneously and thus improving the precision of ground-based observations (e.g. Gilliland 1995). Christensen-Dalsgaard (1986, 1988) has demonstrated, that the mass and age of late-type main-sequence stars could be determined from Δ and δ, if only the composition and mixing-length parameter α_c were known; thus a relative comparison of an ensemble of cluster stars having the same age and chemical composition, and for which CCD-photometry is perhaps the most appropriate ground-based method, may therefore provide additional constraints on the control parameters of stellar evolution theory (e.g. Brown *et al.* 1994). Using differential CCD photometry with seven 4m-class

telescopes, Gilliland *et al.* (1993) predicted the upper limits of luminosity amplitudes of possible oscillations in twelve stars in M67. Recently Kjeldsen *et al.* (1995) introduced a new observing technique for measuring stellar oscillations and reported the possible detection of solar-like oscillation in the sub-giant η Boo (see Section 4.2.3). This new method measures the temperature fluctuations induced by the stellar oscillations via their effects on the equivalent-width of the Balmer lines (a detailed discussion was given by Bedding *et al.* 1996). Differential CCD photometry, on the other hand, measures these temperature fluctuations via changes in the stellar luminosity. The equivalent-width method, although constrained for observing only isolated stars, is insensitive to atmospheric scintillation, yielding a substantial improvement in signal to noise relative to the other methods discussed above.

The limitations of ground-based observation techniques in asteroseismology were addressed by Frandsen (1992) and recently by Gilliland (1995), who suggested that seismology as used to explore the Sun can only be applied to distant stars by observing them from space. The elimination of atmospheric noise and the possibility of obtaining continuous data sequences during long observing periods will provide information of much higher quality than any ground-based method will do. To date, one asteroseismological space project is in preparation. Supported by the French space agency, CNES, the COROT[12] project shall provide frequency measurements of stellar oscillations with a precision better than 0.1% as well as mode amplitudes and lifetimes of these oscillations for up to 7 solar-type and F-type stars (Catala *et al.* 1995). Recently COROT has been selected, and is planned to get launched in 2003.

When preparing an observing campaign, a helpful fact in the choosing process for target stars is to have a good prediction for the amplitude of the signal one is trying to observe. To date, the only predictions of amplitudes of solar-like oscillations in other stars using theoretical model calculations have been made by Christensen-Dalsgaard & Frandsen (1983b). They obtained velocity and luminosity amplitudes by means of the equipartition between the energy of an oscillation mode and the kinetic energy in one convective eddy having the same turnover-time as the period of the oscillation. This simplified excitation mechanism was first proposed by Goldreich & Keeley (1977b) who used this method to estimate amplitudes for the solar case. In the calculations of Christensen-Dalsgaard & Frandsen (1983b), radial eigenfunctions of model envelopes were found by solving the equations of linear non-adiabatic oscillation, neglecting turbulent pressure and the Lagrangian perturbation to the convective heat flux. They found velocity and luminosity amplitudes to increase with age of the model and with increasing mass along the main-sequence. For an 1.5 $M_\odot$ ZAMS star of spectral type F0, the predicted velocity amplitude was ten times larger than those found in the Sun. Here we investigate the oscillation properties of main-sequence stars by means of the non-local, time-dependent mixing-length theory (cf. Section 2.4), delimiting the region in the HR diagram for stars with stable modes. The estimation of the velocity and luminosity amplitudes are determined by the balance of damping and driving in stable stars, as discussed in the Section 3.2 and 3.3, respectively.

In a subsequent section we shall discuss the selection of overstable modes and their dependence on stellar parameters for stars being in their main-sequence phase and having

[12] COnvection and ROTation

a mass up to 2 $M_\odot$. Due to the inclusion of the turbulent pressure and its pulsationally induced fluctuation in the model calculations, the red edge of the instability strip could be well reproduced, as it was first shown by Baker & Gough (1979) for RR-Lyrae stars. Moreover, the dependence of the instability-strip of classical variables upon the chemical composition and the mixing-length parameter α_c shall be demonstrated for an evolving 1.7 $M_\odot$ δ Scuti star.

4.2. Amplitudes

With the computation of the damping rate η as discussed in Section 3.4.4, and with the estimation of the noise generation rate P_Q according to equation (3.38), we are able to obtain an expression for the velocity amplitudes. Using equation (3.35), the root-mean-square velocity at a particular level in the atmosphere may then be written as

$$V_s = \xi_s \sqrt{\frac{\mathcal{E}}{I}} = \xi_s \sqrt{\frac{1}{2}\frac{P_Q}{\eta I}}\,, \tag{4.1}$$

where $\xi_s = \xi(R_s)$ denotes the displacement at the radius $r = R_s$. The velocity amplitudes are computed using the adiabatic displacement eigenfunctions ξ, which allowed us to expand the velocity field in terms of ξ [cf. equation (3.34)]. The amplitude of the displacement ξ increases quite substantially in the outer region of the atmosphere, where the density declines very rapidly. Thus care has to be taken at which atmospheric level the velocity amplitudes are computed. Observations are mainly performed in the neutral potassium line, which is formed at a height of h=200 km relative to the point where the temperature is equal the effective temperature [cf. Section 5.2].

Although Musielak *et al.* (1994) concluded that there is little effect upon the emerging acoustic energy spectrum if assuming various forms for the turbulent spectrum, we found noticeable effect upon the resulting oscillation power spectrum. Following Balmforth (1992c) we employed in equation (3.38) for the function

$$\mathcal{S}(m,\omega) = \int_0^\infty \left(\frac{u(k)}{u_0}\right)^3 \left(\frac{k}{k_0}\right)^{-5} \exp\left[-\omega\tau_0 / \left(2\frac{k u(k)}{k_0 u_0}\right)\right]^2 d(k/k_0)\,, \tag{4.2}$$

two different turbulent spectra $E(k)$ according to Kolmogorov (e.g. Stein 1968) and Spiegel (1962), where k represents the wavenumber describing the eddy with velocity

$$u(k)^2 = \int_k^{2k} E(k)\, dk\,, \tag{4.3}$$

and where k_0 is the wavenumber at the peak of the spectrum.

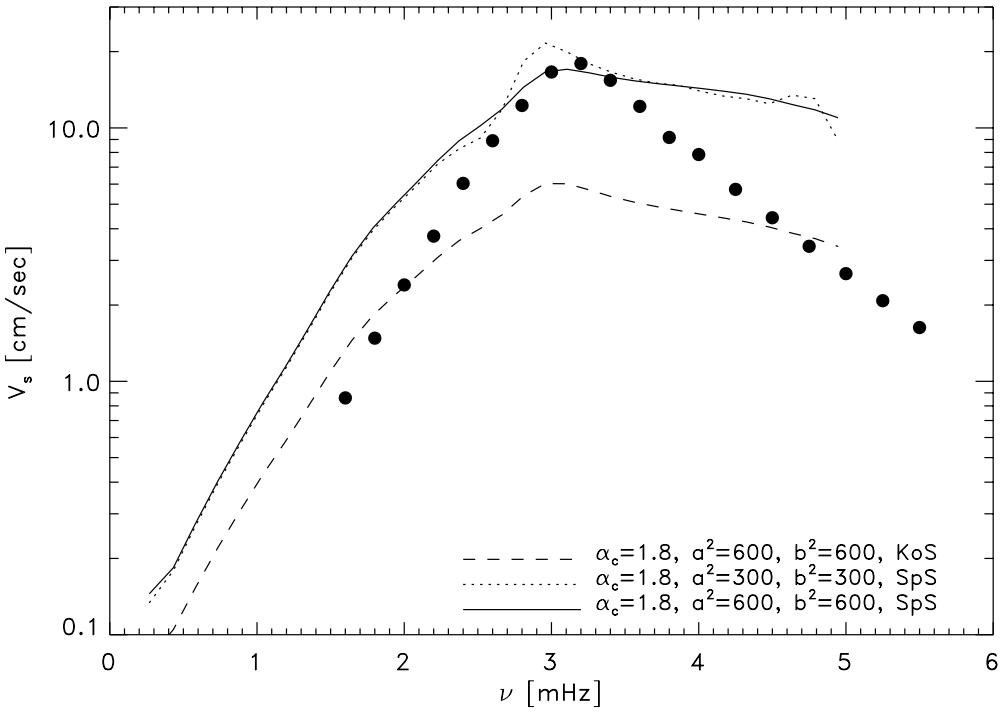

Figure 4.1: Mean velocity amplitudes for the Sun using various convection parameters and turbulent spectra. The curves labeled with 'KoS' are computed assuming the Kolmogorov spectrum, as given by equation (4.4). The plots indicated by the label 'SpS' were obtained using the turbulent spectrum according to Spiegel (1962), given by equation (4.5). The filled dots indicate the measured amplitudes by Libbrecht (1988).

The Kolmogorov spectrum was implemented as

$$E(k) = \frac{u_0^2}{k_0}\left(\frac{k}{k_0}\right)^{-5/3} \qquad \text{for} \qquad k \geq k_0 = \frac{2\pi}{\ell_0}, \tag{4.4}$$

and the spectrum according to Spiegel in the form

$$E(k) = \frac{9u_0^2}{k_0}\left(\frac{k}{k_0}\right)^{-5/3}\left\{1-\left(\frac{k}{k_0}\right)^{-8/3}-\frac{4\pi}{7k_0\ell_0}\left[1-\left(\frac{k}{k_0}\right)^{-14/3}\right]\right\}^2, \tag{4.5}$$

where the value for $k_0 = \pi/\ell_0$ was chosen.

4.2.1. Amplitudes of the Sun

In Fig. 4.1 the mean velocity amplitudes for the Sun, calculated at a height h=200 km for various convection parameters and assuming the Kolmogorov and the Spiegel turbulent spectrum, respectively, are depicted together with observations by Libbrecht (1988). There is a substantial difference in the magnitude of the amplitudes between models computed with the Kolmogorov (dashed line) and Spiegel (solid line) turbulent spectrum, where the

latter agrees fairly well with Libbrecht's observations. These residuals are mainly due to the different treatment of the scaling of the energy-bearing eddies, described by the various forms of the wavenumber k_0 and hence correlation time $\tau_0 = 1/(k_0 u_0)$. The rather abrupt cut-off at $k = k_0$ in the Kolmogorov (e.g. Stein 1968) spectrum resembles only crudely the dynamic scaling of the energy-bearing eddies, since Kolmogorov scaling applies strictly only for the inertial subrange eddies. This may result in a too low prediction of the acoustic energy rate and thus oscillation amplitudes.
Decreasing the non-local mixing-length parameters a and b (cf. Section 2.4) leads to larger predicted amplitudes (dotted curve). Smaller values for a and b increase the degree of "non-locality" of convection and the velocities of the eddies become larger, increasing the acoustic generation rate. This is equivalent to an increase of the mixing-length parameter α_c, resulting in a more efficient convection due to the larger extend of the convective elements.

As stated before, the velocity amplitudes were obtained by expanding the velocity field in terms of adiabatic displacement eigenfunctions, in order to calculate the instantaneous mode amplitude. The imaginary part of the non-adiabatic displacement eigenfunctions exhibits very small values relative to the value of its real part. Thus the differences in the velocity amplitudes, when using the adiabatic instead of the non-adiabatic displacement eigenfunctions are negligible relative to the uncertainties inherent in modelling the theory of stochastic excitation. For the estimation of the luminosity amplitudes, however, non-adiabatic eigenfunctions of the relative luminosity fluctuations, $\delta L/L_0$, have to be taken into account, which appear to have substantial phase-shifts relative to the displacement (cf. Section 5.2). A simplified explanation why the phases of luminosity variations are substantially larger than the phases of the displacement may be given under the assumption for purely radiative envelopes: The no longer negligible imaginary part of $\delta L/L_0$ stems

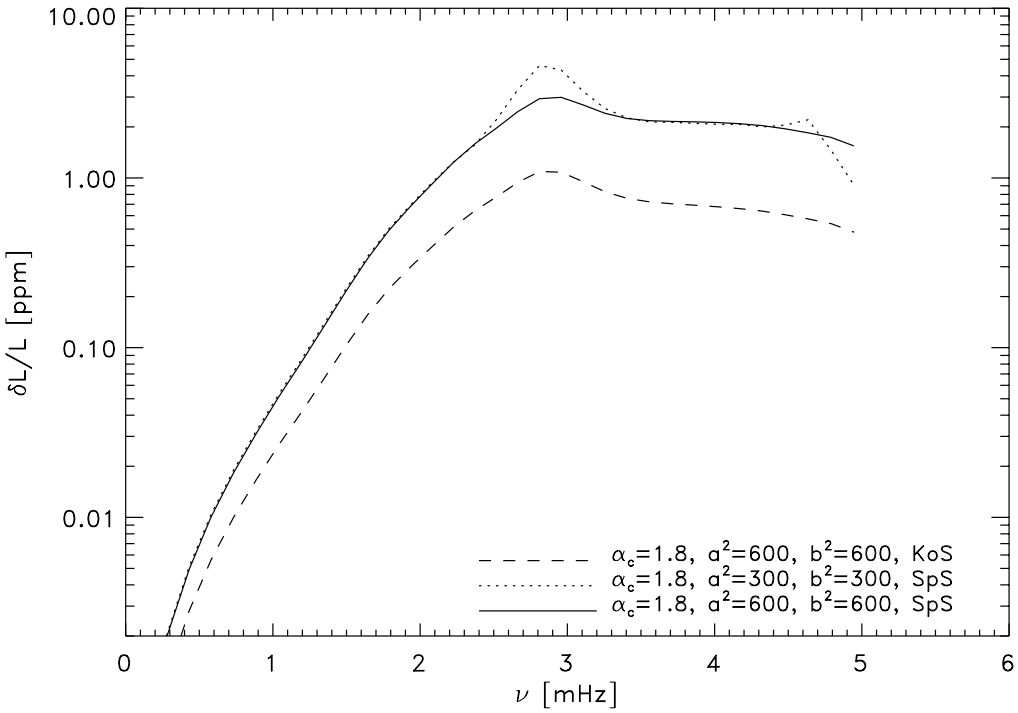

Figure 4.2: Mean luminosity amplitudes for the Sun assuming different convection parameters and energy-spectra for the turbulent cascade, similar as in Fig. 4.1.

Table 4.1: Theoretical mean velocity and luminosity amplitudes calculated at the height $h = 200\,\mathrm{km}$ as well as damping rates,η, as function of frequency for solar oscillations. The results were obtained for a model envelope assuming the convection parameter $\alpha_c = 1.8$ and $a^2 = b^2 = 600$ as well as the Spiegel spectrum for the calculations of the acoustical noise generation rate.

n	ν [mHz]	V_s [cm/s]	$\delta L/L_0$ [ppm]	η [μHz]
1	0.269	0.145	0.00185	2.88E-07
2	0.432	0.184	0.00495	4.12E-06
3	0.580	0.273	0.0100	2.54E-05
4	0.734	0.403	0.0184	0.000115
5	0.886	0.578	0.0310	0.000398
6	1.039	0.820	0.0511	0.00121
7	1.192	1.138	0.0817	0.00327
8	1.344	1.601	0.132	0.00858
9	1.495	2.266	0.214	0.0219
10	1.642	3.105	0.334	0.0505
11	1.788	4.027	0.491	0.101
12	1.934	4.967	0.679	0.177
13	2.081	6.060	0.921	0.293
14	2.227	7.425	1.237	0.466
15	2.372	8.890	1.589	0.674
16	2.517	10.196	1.963	0.869
17	2.663	11.847	2.459	0.944
18	2.810	14.472	2.931	0.886
19	2.958	16.623	2.986	0.930
20	3.106	17.039	2.695	1.156
21	3.255	16.497	2.406	1.467
22	3.405	15.843	2.242	1.784
23	3.556	15.354	2.177	2.080
24	3.708	14.976	2.155	2.345
25	3.861	14.645	2.143	2.584
26	4.014	14.316	2.123	2.806
27	4.168	13.967	2.088	3.033
28	4.323	13.581	2.035	3.295
29	4.478	13.036	1.949	3.636
30	4.633	12.372	1.847	4.067
31	4.789	11.783	1.736	4.523
32	4.946	10.968	1.545	5.206
33	5.102	9.553	1.302	6.686
34	5.260	8.093	1.168	8.986

directly from the non-adiabatic effects expressed by the energy equation ($A.75$). The temperature fluctuations are found by integrating $\delta L/L_0$ [cf. equation ($A.74$)], yielding a smaller phase of $\delta T/T_0$. Finally, in order to obtain the solution for the displacement eigenfunctions, the temperature fluctuations have to be integrated once more, resulting in the negligible phases of ξ. The relative luminosity amplitudes may be obtained from the velocity amplitudes by the linear relation

$$\frac{\delta L}{L_0} = \frac{\delta r}{R_s} \frac{\delta L/L_0}{\delta r/r_0}, \tag{4.6}$$

where

$$\frac{\delta r}{R_s} = \frac{V_s}{\omega_r R_s}, \tag{4.7}$$

represents the relative displacement derived from the estimated velocity amplitude at the surface specified by the radius R_s. Results of luminosity variations for the Sun according to equation (4.6) are displayed in Fig. 4.2 using the Spiegel (solid line) and Kolmogorov (dashed line) turbulent spectra, respectively. Similar to the velocity amplitudes, the results of the luminosity amplitudes exhibit their maximum value near 3 mHz. Assuming the Spiegel spectrum and the non-local parameters $a^2 = b^2 = 300$ (dotted line), the predicted maximum value of 4.6 ppm is close to the observation of 4.7 ppm by Woodard & Hudson (1983a,b). However, it should be stated here that no unambiguous agreement has been found so far on the observed luminosity amplitude of solar 5 min oscillations. The corrected values (Kjeldsen & Bedding 1995) of the observations by Toutin & Fröhlich (1992) predict smaller amplitudes of ~ 3.6 ppm, which would suggest larger values for the model parameters a and b, or smaller values for α_c. Although the theory gives some agreement with the observed amplitudes and line widths of solar oscillations, the calculated amplitudes appear too large at low and high frequencies, due to the underestimation of the computed damping rates at these frequencies (cf. Section 3.4.4). The computed values of both the velocity and luminosity amplitudes as well as the theoretical damping rates as function of frequency for the Sun assuming the Spiegel spectrum and mixing-length parameters $\alpha_c = 1.8$ and $a^2 = b^2 = 600$ are summarized in table Table 4.1.

4.2.2. Amplitudes of solar-type oscillations

The mean velocity and luminosity amplitudes as function of frequency for an evolving 1 $M_\odot$ star are displayed in Fig. 4.3 and Fig. 4.4, respectively, using the same model parameters as in Table 4.1. Similar to the damping rates, as demonstrated in Fig. 3.14, the oscillation amplitudes become larger with age exhibiting a maximum value of $V_s = 46$ cm/s and $\delta L/L_0 = 10$ ppm at the end of the hydrogen core-burning phase. Thus the acoustic noise generation rate P_Q increases more steeply with age than the damping rates do, which is an effect due to the strong dependence of P_Q upon the convective velocity. In Fig. 4.5 and

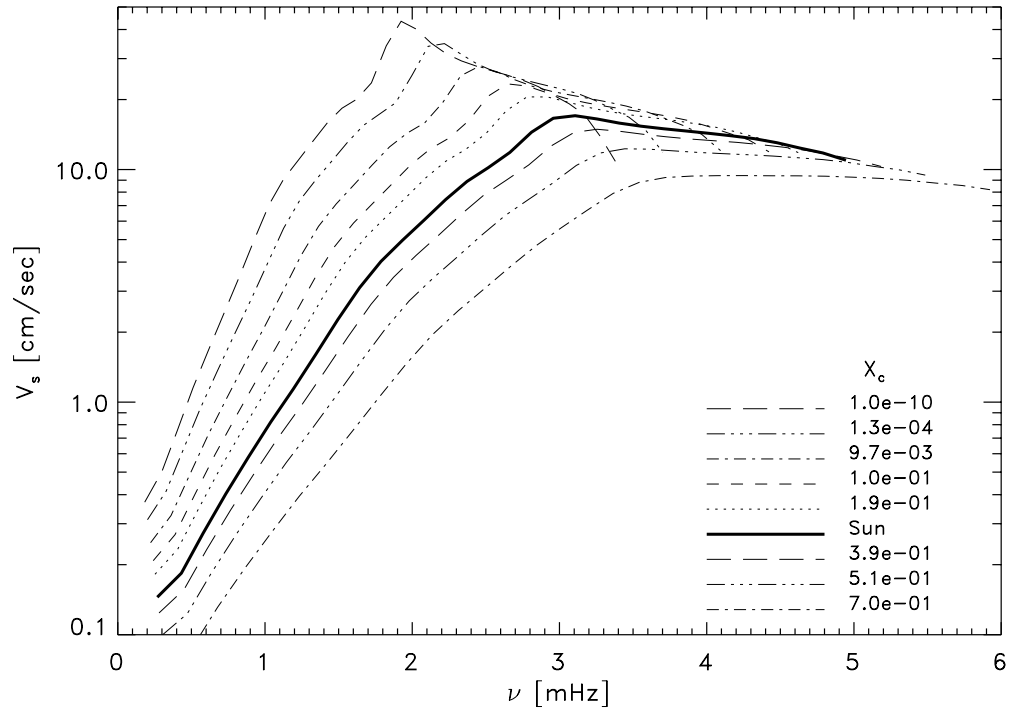

Figure 4.3: Mean velocity amplitudes as function of frequency for an evolving $1\,M_\odot$ star assuming the same model parameters as in Table 4.1. The evolution steps are indicated by the hydrogen mass fraction in the core (X_c).

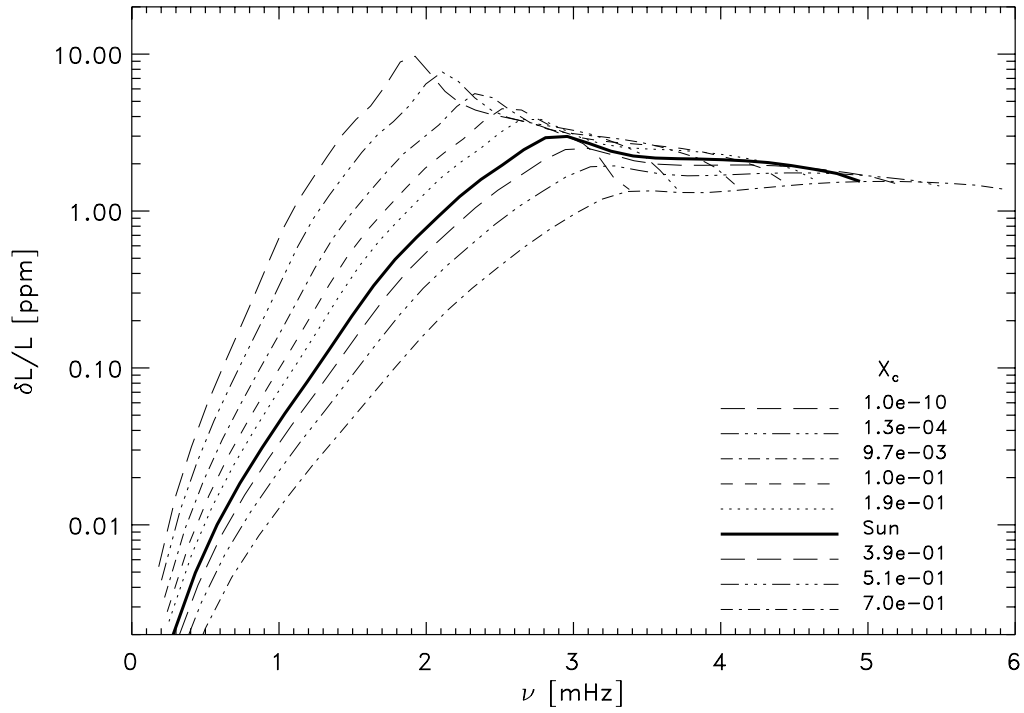

Figure 4.4: Luminosity amplitudes as function of frequency for an evolving $1\,M_\odot$ star assuming the same model parameters as in Table 4.1. The evolution steps are indicated by the hydrogen mass fraction in the core (X_c).

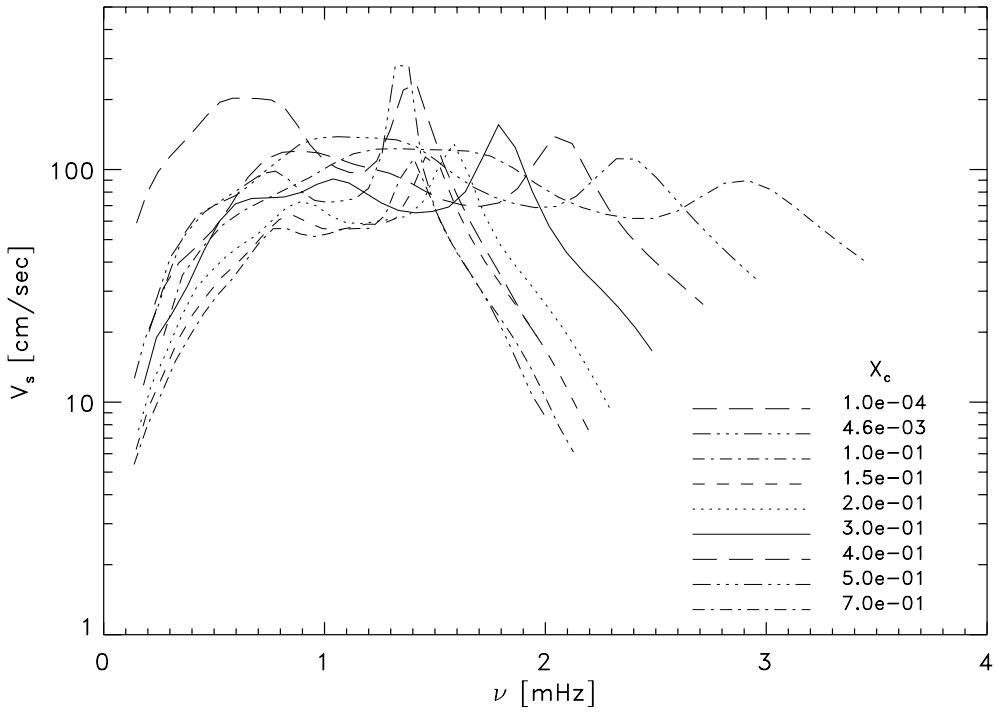

Figure 4.5: Mean velocity amplitudes as function of frequency for an evolving $1.45\,M_\odot$ star computed at a height $h = 200\,\mathrm{km}$ and assuming the convective parameters $\alpha_\mathrm{c} = 2.0$ and $a^2 = 900$, $b^2 = 2000$. The acoustic noise generation rate was obtained with Spiegel's turbulence spectrum. The evolution steps are indicated by the hydrogen mass fraction in the core (X_c).

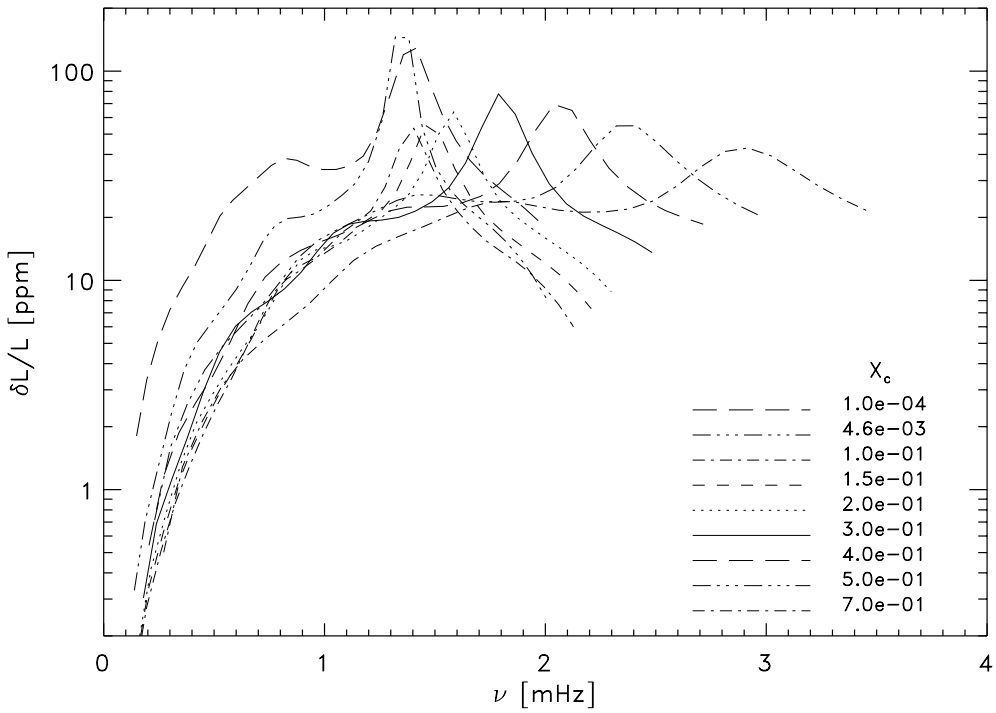

Figure 4.6: Luminosity amplitudes as function of frequency for an evolving $1.45\,M_\odot$ star assuming the same model parameters as in Fig. 4.5.

Fig. 4.6 the amplitudes are depicted for an evolving 1.45 $M_\odot$ star. The amplitudes increase less steeply with age relative to the evolving 1 $M_\odot$ star, indicating that the convective properties become less sensitive to age for more massive stars. At the end of the hydrogen core-burning phase the theory predicts maximum values of $\sim 200\,\mathrm{cm/s}$ and ~ 100 ppm for the velocity and luminosity oscillation amplitudes, respectively. These maximum values coincide with the sharp depression in the damping rates (see Fig. 3.15), where the pulsation period is close to the thermal adjustment time of the superadiabatic boundary layer (cf. Section 3.4.2). For models at the end of the main-sequence, the calculations suggest a substantially pronounced dip in the damping rates at these frequencies, which is perhaps an artifact of the incomplete theory of the time-dependent mixing-length formulation. Thus the oscillation amplitudes may exhibit values too large in their maximum which implies a need to interpret these results with some care.

For moderate mass stars along the ZAMS where all modes have been found to be stable the luminosity amplitudes are depicted in Fig. 4.7. For the calculations the same convection parameters were assumed as indicated in Fig. 4.5 and the corresponding damping rates are depicted in Fig. 3.16. Up to a maximum value of $\sim 40\,\mathrm{ppm}$ the amplitudes increase monotonously for stars with $M \leq 1.45\,M_\odot$. For models with $M \gtrsim 1.6\,M_\odot$, however, amplitudes of stochastically excited modes decrease again as shown for a $2\,M_\odot$ ZAMS star, displaying a maximum amplitude of $\sim 0.02\,\mathrm{ppm}$. The dependence of the amplitude variations upon mass or more precisely upon luminosity may be explained by the strong dependence of the acoustic noise generation rate on the convective velocity u. For quadrupole emission the radiated acoustic intensity is a function of the eight power of u,

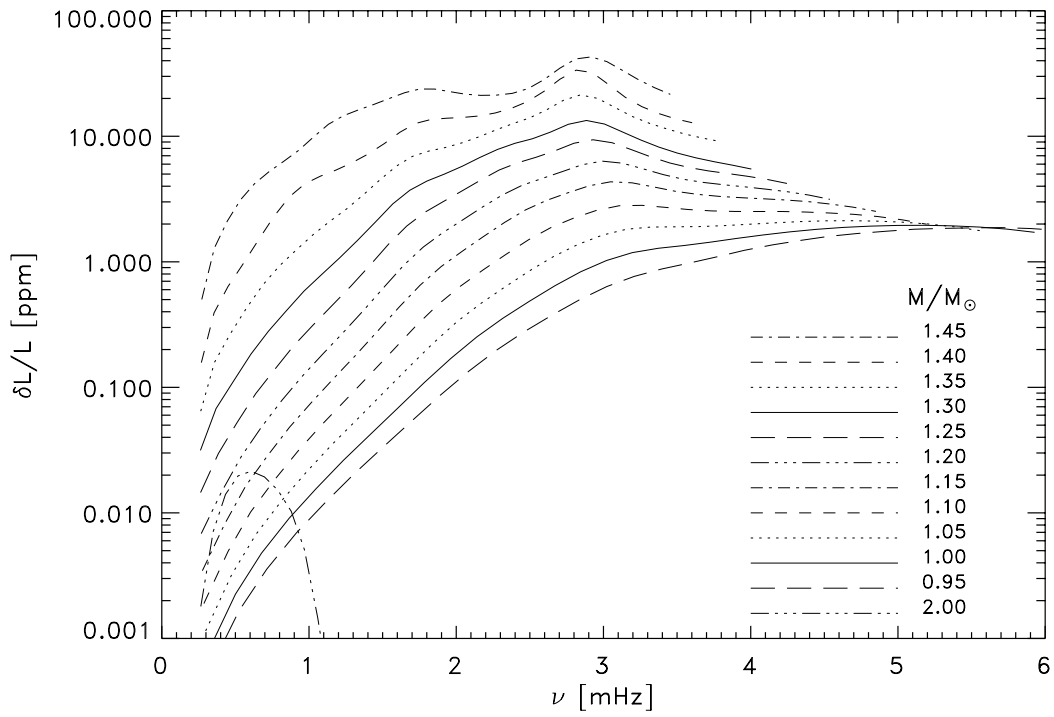

Figure 4.7: Luminosity amplitudes as function of frequency for ZAMS stars assuming the convection parameters of Fig. 4.5. The amplitudes increase with mass for $M \leq 1.45\,M_\odot$.

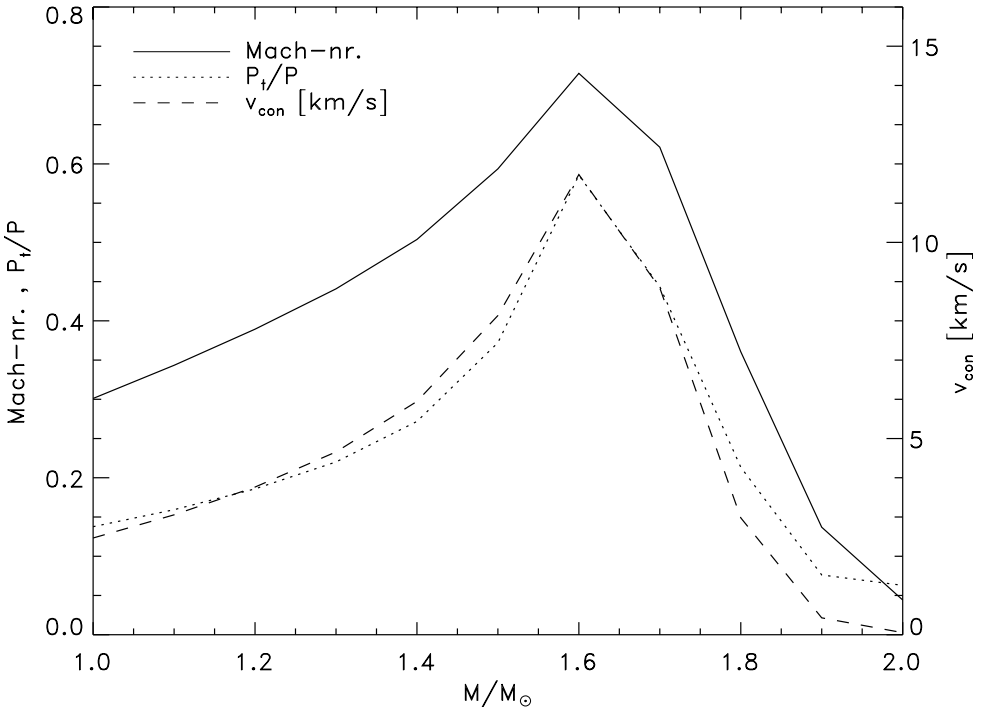

Figure 4.8: Maximimum values of Mach number, turbulent pressure fraction (P_t/P) and convective velocities (v_con) as function of model mass along the ZAMS.

as given by equation (3.24). The dependence of the maximum values of the convective velocities and turbulent Mach number upon model mass along the ZAMS is illustrated in Fig. 4.8. Using the convection parameters as given in Fig. 4.5 the calculations predict the largest convective velocities for models with a mass of $\sim 1.6\,M_\odot$. The $2\,M_\odot$ ZAMS star exhibits two very thin convection zones in the outer part of the envelope and the theory predicts a maximum turbulent Mach number $\mathrm{M_t} < 0.1$; thus the amplitudes of solar-like oscillations become very small relative to the Sun.

For models being on their main-sequence and for those where all the modes are predicted to be stable, the computed maximum velocity and luminosity amplitudes of stochastically excited modes are depicted as contour plots in Fig. 4.9 and Fig. 4.10, respectively. The 166 models (indicated by the diamond symbols) were generated by specifying the mass, luminosity and effective temperature provided from full evolution sequences, as obtained by Christensen-Dalsgaard (1993), and assuming the convective parameters from Fig. 4.5. For more massive stars the maximum amplitudes exhibit sharp peaks in their frequency spectrum due to the steep depression in their damping rates (cf. Fig. 3.15). In the contour plots we therefore applied a one-dimensional median filter on the amplitudes in order to smooth the peaks at the maximum values. The low-temperature border of the contour-lines indicates merely the point where the model's hydrogen mass fraction $X_c \lesssim 10^{-10}$ in the core and beyond no further calculations were carried out. In accordance with the discussion outlined before, the amplitudes increase quite steeply with luminosity in particular for stars with a mass $M \gtrsim 1.4\,M_\odot$. The largest amplitudes are predicted for a $1.5\,M_\odot$ model of spectral type F1, which appears to have a maximum luminosity

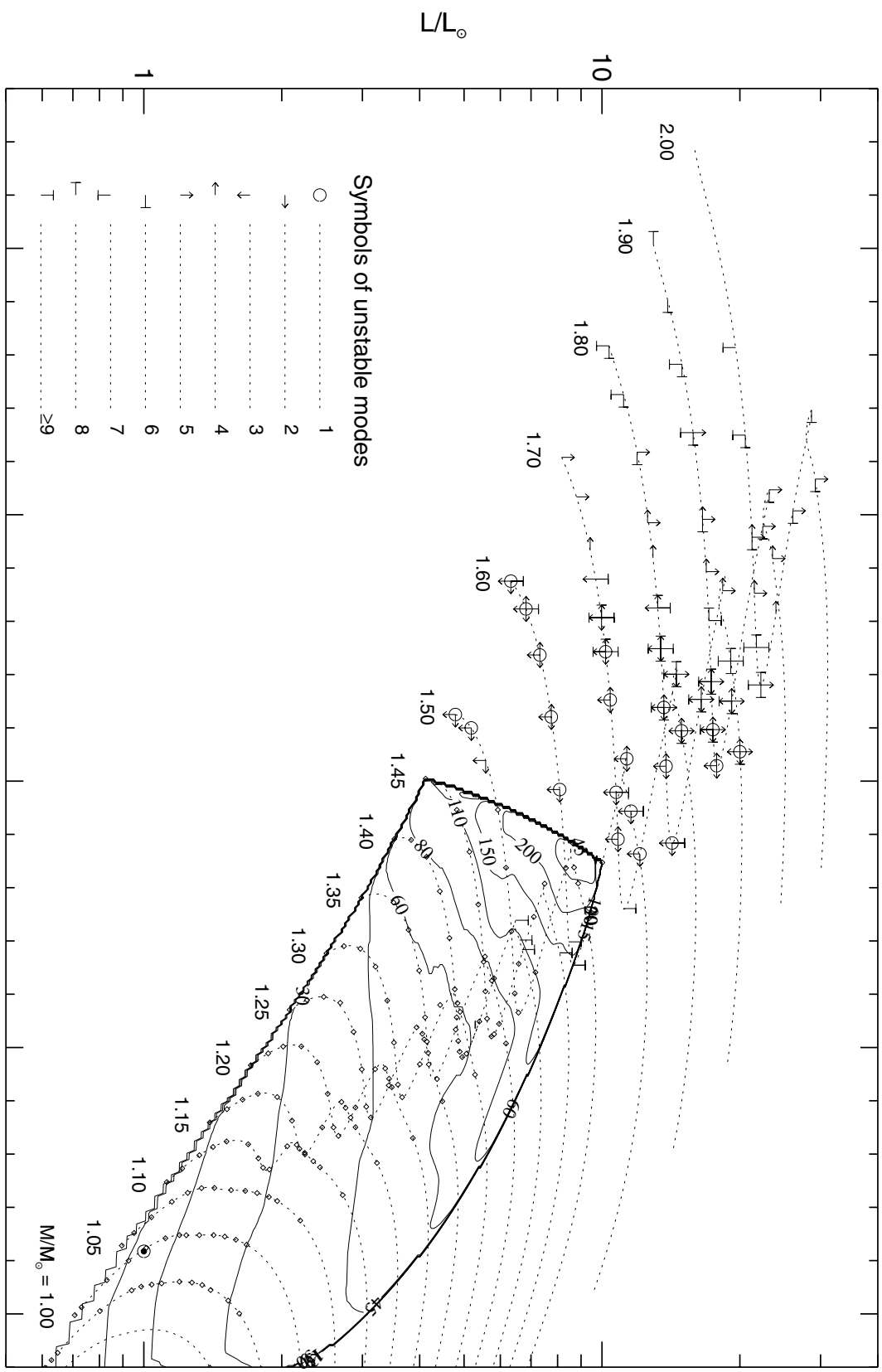

Figure 4.9: Unstable modes and mean velocity amplitudes of stochastically excited oscillations. Amplitudes are depicted as contour-plots at the contour-levels=(10, 15, 20, 30, 45, 60, 80, 110, 150, 200, 250) cm/s. The Sun, indicated by its symbol, exhibits a mean (rms) velocity of 16 cm/s. Calculations have been carried out till end of hydrogen core-burning giving the low-temperature border of the contour-lines.

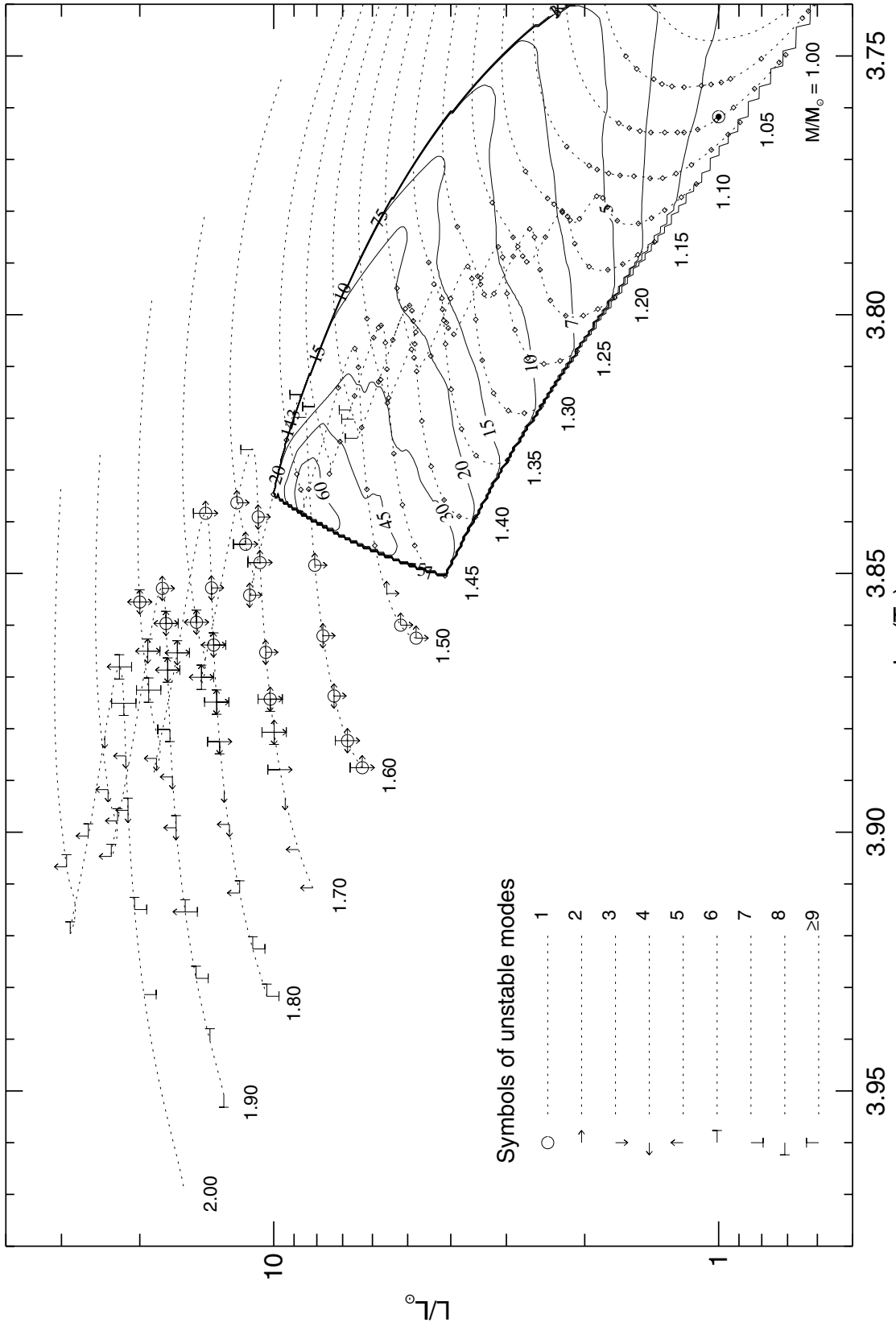

Figure 4.10: Unstable modes and mean luminosity amplitudes of stochastically excited oscillations. Amplitudes are depicted as contour-plots at the contour-levels=(1, 2, 3, 5, 7, 10, 15, 20, 30, 45, 60) ppm. The Sun, indicated by its symbol, exhibits a mean (rms) luminosity of 2.5 ppm. Calculations have been carried out till end of hydrogen core-burning giving the low-temperature border of the contour-lines.

amplitude of ~ 16 times larger than those found in the Sun. In both plots the contour-lines of the amplitudes are nearly perpendicular to the evolutionary tracks of models with $M \lesssim 1.25\,M_\odot$ and appear to become parallel with increasing mass, implying that the convective velocity field becomes less dependent on age for more massive stars. Moreover, amplitudes of stochastically excited modes depend crucially upon the models luminosity and are nearly independent of the effective temperature for stars with $L \lesssim 3\,L_\odot$. This fact is demonstrated more obviously in Fig. 4.11 for the luminosity amplitudes. However, the ratios between luminosity and velocity amplitudes, $\Delta L/\Delta V_s$, appear to be nearly insensitive to the luminosity for stars with values up to $\sim 4\,L_\odot$, and depend mainly on the model's effective temperature, as indicated in Fig. 4.12. Recently, Kjeldsen & Bedding (1995) derived an expression for $\Delta L/\Delta V_s$ as function of fundamental stellar parameters. By calibrating their result to observational data the authors obtained the following relation

$$\frac{\Delta L}{\Delta V_s} = \frac{1022.529}{T_{\rm eff}\ [K]}\,{\rm ppm/cm\,s^{-1}}\,, \tag{4.8}$$

proposing that the amplitude ratios are inverse proportional to the model's effective temperature, as depicted in Fig. 4.12 by the long-dashed line. This is in contradiction to our results, which may be explained by the various simplifications assumed in Kjeldsen & Bedding's derivation, such as considering purely radiative models in the adiabatic approximation. The amplitude ratio for the Sun, obtained according to our calculations, shows a value of $0.16\,{\rm ppm/cms^{-1}}$, as indicated by its symbol in Fig. 4.12. Compared to the calibrated value of Kjeldsen & Bedding, the theory, assuming the convection parameters of Fig. 4.5, predicts a too small value. The dependence of the amplitude ratio upon frequency and height in the atmosphere for models computed with different convection parameters will be discussed in more detail in Section 5.

Based on the model calculation results of Christensen-Dalsgaard & Frandsen (1983b), Kjeldsen & Bedding (1995) proposed a scaling relationship for solar-type velocity amplitudes as function of control parameters used in stellar evolution theory. In particular they obtained the relation

$$\frac{V}{V_\odot} \sim \frac{L/L_\odot}{M/M_\odot}\,, \tag{4.9}$$

suggesting that the velocity amplitudes scale directly with the light-to-mass ratio L/M of the star. In Fig. 4.13 the velocity amplitudes versus the light-to-mass ratio are depicted for model calculations assuming the convection parameters of Fig. 4.5. For models with values $L/M \gtrsim 3$ amplitudes start to deviate from the predicted relation (4.9), as indicated by the dashed line.

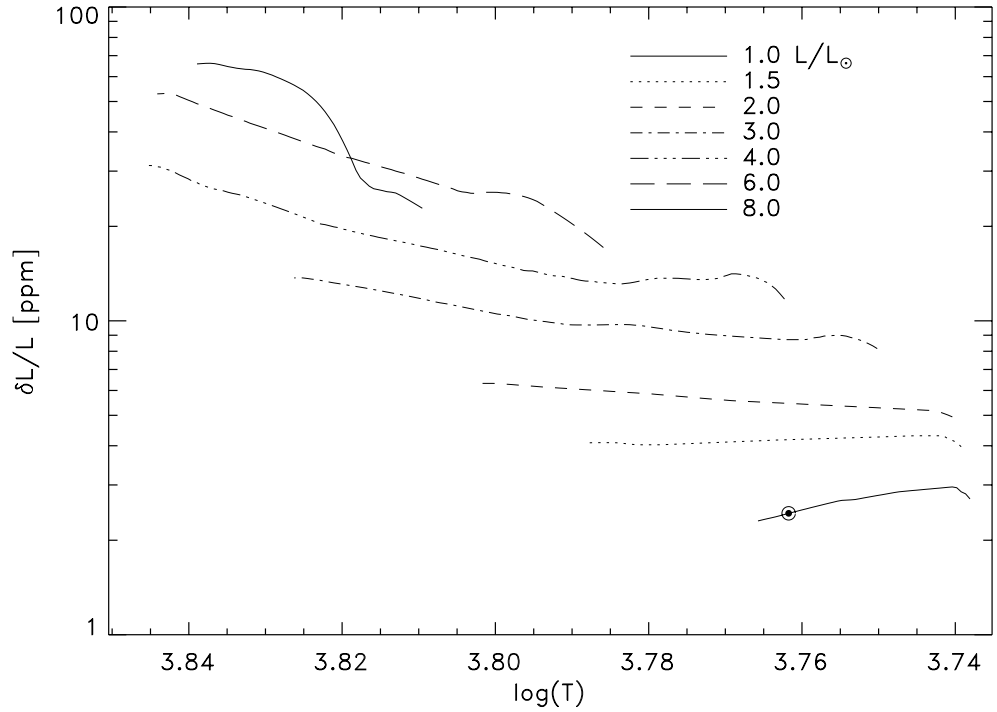

Figure 4.11: Luminosity amplitudes as function of effective temperature and model luminosity. The computations assumed model parameters as given in Fig. 4.5. The value for the Sun is indicated by its symbol.

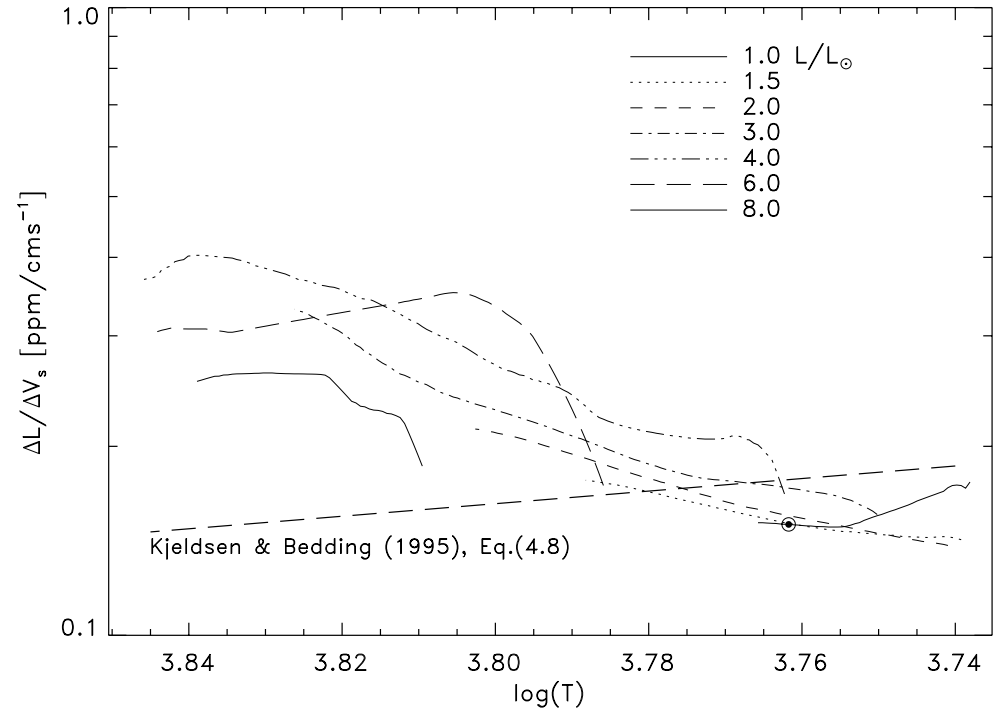

Figure 4.12: Amplitude ratios as function of effective temperature and model luminosity. The computations assumed model parameters as given in Fig. 4.5. The location of the Sun is indicated by its symbol.

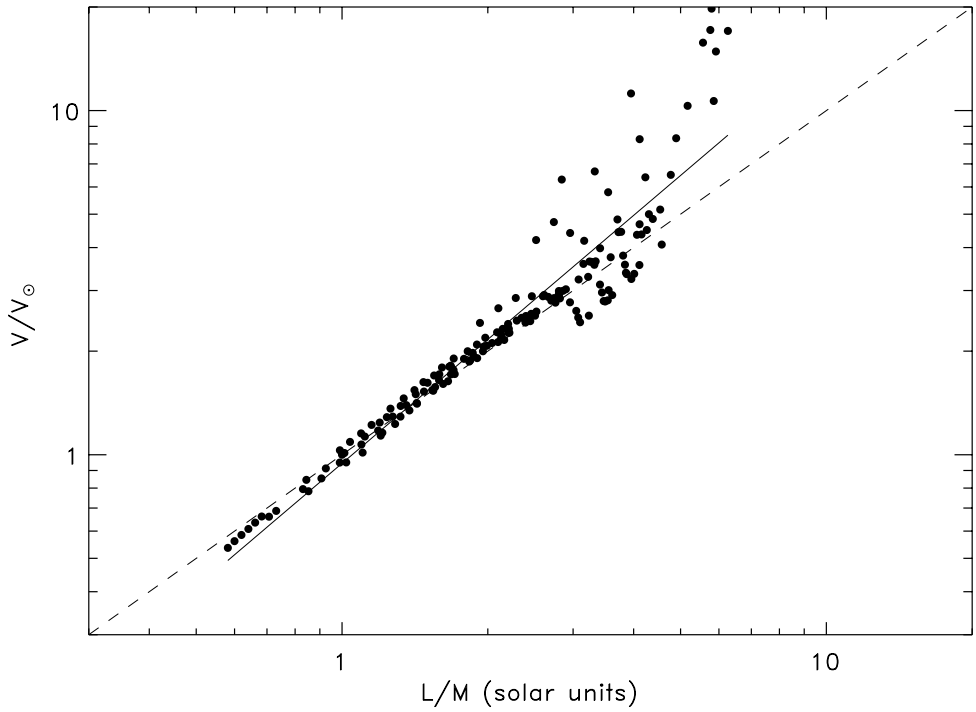

Figure 4.13: Theoretical velocity amplitudes as function of light-to-mass ratio for stochastically excited oscillations in 166 models (indicated by the filled dots) calculated with the convection parameters as given in Fig. 4.5. The solid line represents a linear polynomial fit to the amplitude results. The amplitudes are displayed relative to the value found in the Sun.

Applying a linear regression fit to the theoretical amplitude estimations, the computations suggest the relation

$$\frac{V}{V_\odot} \sim \left(\frac{L/L_\odot}{M/M_\odot}\right)^{1.2} . \tag{4.10}$$

Equation (4.10) and Fig. 4.12 may be used for tentative estimations of the velocity and luminosity amplitudes of solar-type oscillations in main-sequence stars. A complete list of the median smoothed maximum values of amplitudes in the 166 calculated models is given in Table 4.2.

Table 4.2: Estimated maximum values of median smoothed velocity and luminosity amplitudes for stochastically excited modes in solar-type stars. The models are characterized by mass, luminosity, effective temperature and hydrogen abundance in the core, as obtained from full evolution sequences (Christensen-Dalsgaard 1993). The results were obtained for model envelopes assuming the convection parameter $\alpha_c = 2.0$, $a^2 = 900, b^2 = 2000$ and the Spiegel spectrum for the calculations of the acoustical noise generation rate.

$M/M_\odot$	$L/L_\odot$	$T_{\rm eff}$ [K]	X_c	V_s [cm/s]	$\delta L/L_0$ [ppm]
0.90	1.394	5494.1	1.0E-10	28.30	4.10
0.95	0.552	5435.0	0.70	8.93	1.87
0.95	0.570	5455.0	0.66	9.34	1.90
0.95	0.589	5475.0	0.62	9.75	1.94
0.95	0.609	5493.9	0.58	10.18	1.97
0.95	0.629	5512.2	0.55	10.61	2.02
0.95	0.648	5529.5	0.51	11.02	2.06
0.95	0.802	5630.3	0.30	14.23	2.33
0.95	0.940	5680.9	0.15	17.16	2.56
0.95	0.987	5690.0	0.10	18.15	2.70
0.95	1.040	5695.1	0.050	19.21	2.84
0.95	1.093	5698.1	0.015	20.33	3.02
0.95	1.196	5702.1	0.0011	22.67	3.35
0.95	1.274	5700.0	0.00012	24.28	3.57
0.95	1.341	5694.0	1.4E-05	25.67	3.76
0.95	1.399	5681.7	1.0E-10	27.08	3.94
0.95	1.528	5655.8	1.0E-10	29.86	4.31
0.95	1.615	5624.1	1.0E-10	31.70	4.55
0.95	1.804	5491.1	1.0E-10	34.81	4.88
1.00	0.707	5620.4	0.70	11.01	1.95
1.00	0.731	5639.6	0.65	11.46	1.99
1.00	0.831	5706.0	0.51	13.33	2.17
1.00	0.926	5754.1	0.39	15.20	2.36
1.00	1.000	5777.5	0.37	16.65	2.51
1.00	1.012	5785.8	0.30	16.85	2.57
1.00	1.115	5810.3	0.19	18.81	2.90
1.00	1.196	5818.1	0.10	20.66	3.14
1.00	1.237	5817.9	0.056	21.42	3.26
1.00	1.321	5818.1	0.0097	23.08	3.54
1.00	1.420	5818.1	0.0010	24.97	3.85
1.00	1.502	5814.4	0.00013	26.95	4.17
1.00	1.588	5806.6	1.3E-05	28.52	4.42
1.00	1.676	5794.0	1.0E-10	30.21	4.78
1.00	2.202	5493.8	1.0E-10	39.95	5.47
1.05	0.895	5791.8	0.70	13.19	2.11
1.05	0.952	5823.4	0.62	14.21	2.22
1.05	1.039	5863.3	0.52	15.80	2.46
1.05	1.151	5902.6	0.40	17.84	2.81

Table 4.2 continued....

$M/M_\odot$	$L/L_\odot$	$T_{\rm eff}$ [K]	$X_{\rm c}$	$V_{\rm s}$ [cm/s]	$\delta L/L_0$ [ppm]
1.05	1.247	5925.4	0.30	19.58	3.19
1.05	1.336	5937.6	0.21	21.50	3.52
1.05	1.425	5938.0	0.10	23.21	3.82
1.05	1.550	5932.4	0.011	25.42	4.21
1.05	1.665	5930.4	0.0011	27.44	4.83
1.05	1.767	5924.9	0.00013	29.83	5.12
1.05	1.875	5914.9	1.0E-05	31.63	5.37
1.05	1.955	5904.4	1.3E-06	32.92	5.57
1.05	2.195	5855.0	1.0E-10	37.79	6.54
1.10	1.122	5953.1	0.70	15.82	2.54
1.10	1.213	5988.2	0.60	16.90	2.87
1.10	1.322	6022.6	0.50	18.92	3.30
1.10	1.416	6044.0	0.40	20.46	3.62
1.10	1.515	6058.4	0.30	22.40	4.05
1.10	1.689	6051.1	0.20	25.66	4.90
1.10	1.779	6014.5	0.15	26.74	4.88
1.10	1.821	5990.2	0.10	27.23	4.87
1.10	1.880	5985.5	0.050	28.58	5.16
1.10	2.056	6046.0	0.010	32.18	6.11
1.10	2.156	6049.4	0.0012	34.31	6.82
1.10	2.245	6028.6	0.00013	35.17	7.17
1.10	2.344	6006.9	1.0E-05	36.28	7.23
1.10	2.424	5991.2	1.1E-06	37.67	7.35
1.10	2.717	5919.6	1.1E-10	42.57	8.28
1.15	1.393	6108.4	0.70	19.30	3.54
1.15	1.518	6143.5	0.60	21.49	4.20
1.15	1.642	6169.1	0.50	23.43	4.76
1.15	1.774	6184.7	0.40	25.55	5.38
1.15	1.954	6176.0	0.30	29.35	5.99
1.15	2.106	6113.3	0.20	31.07	6.59
1.15	2.187	6039.4	0.10	31.79	6.06
1.15	2.247	6024.7	0.050	33.28	6.32
1.15	2.452	6095.4	0.011	37.09	7.55
1.15	2.701	6162.8	0.0011	41.63	9.20
1.15	2.757	6147.3	0.00019	42.13	9.21
1.15	2.827	6121.2	1.9E-05	42.75	9.53
1.15	2.898	6095.8	1.7E-06	43.40	9.84
1.15	3.227	6002.5	1.0E-10	48.82	10.09
1.20	1.712	6261.4	0.70	23.55	4.96
1.20	1.868	6293.6	0.60	26.19	5.81
1.20	2.014	6312.1	0.50	28.51	6.52
1.20	2.206	6312.4	0.40	31.27	7.41
1.20	2.389	6269.5	0.30	34.52	8.26

Table 4.2 continued....

$M/M_\odot$	$L/L_\odot$	$T_{\rm eff}$ [K]	$X_{\rm c}$	$V_{\rm s}$ [cm/s]	$\delta L/L_0$ [ppm]
1.20	2.520	6184.6	0.20	35.40	8.06
1.20	2.594	6095.3	0.10	35.90	7.72
1.20	2.659	6073.2	0.050	37.66	7.64
1.20	2.897	6148.0	0.010	41.69	9.27
1.20	3.199	6250.9	0.0025	47.88	12.08
1.20	3.365	6252.6	0.00013	49.80	13.17
1.20	3.430	6224.8	1.1E-05	49.85	12.69
1.20	3.478	6202.3	1.5E-06	50.38	12.15
1.20	3.867	6067.3	1.0E-10	54.75	12.36
1.25	2.081	6413.1	0.70	30.02	6.87
1.25	2.272	6440.5	0.60	33.29	7.90
1.25	2.470	6449.2	0.50	36.43	9.21
1.25	2.684	6432.8	0.40	38.66	10.47
1.25	2.869	6352.2	0.30	40.85	10.23
1.25	2.990	6250.3	0.20	40.31	9.62
1.25	3.059	6150.1	0.10	40.71	9.56
1.25	3.129	6121.8	0.050	42.23	9.20
1.25	3.425	6207.1	0.010	47.50	11.92
1.25	3.938	6364.7	0.0010	59.71	15.99
1.25	4.054	6347.2	0.00013	60.66	16.33
1.25	4.093	6331.9	1.8E-05	60.51	16.42
1.25	4.174	6294.8	1.1E-06	60.74	16.85
1.25	4.483	6164.5	1.0E-10	62.42	16.29
1.30	2.505	6571.6	0.70	40.23	9.56
1.30	2.734	6592.1	0.60	44.38	11.19
1.30	2.969	6584.7	0.50	47.53	12.94
1.30	3.205	6533.7	0.40	48.09	13.00
1.30	3.399	6438.8	0.30	48.52	13.35
1.30	3.515	6322.9	0.20	46.69	12.85
1.30	3.586	6209.0	0.10	46.08	11.43
1.30	3.663	6175.4	0.050	47.40	11.78
1.30	4.004	6264.2	0.010	53.79	13.85
1.30	4.433	6426.6	0.0017	66.30	19.75
1.30	4.838	6431.6	1.6E-05	73.85	22.37
1.30	4.901	6407.5	1.9E-06	73.99	21.34
1.30	5.283	6235.8	1.0E-10	72.55	19.34
1.35	2.984	6731.5	0.70	38.68	14.38
1.35	3.508	6717.8	0.50	48.09	18.72
1.35	3.784	6638.5	0.40	48.80	18.57
1.35	3.990	6522.8	0.30	46.17	17.66
1.35	4.111	6392.4	0.20	43.60	16.77
1.35	4.149	6325.4	0.15	41.70	15.82
1.35	4.187	6263.5	0.10	40.41	15.90

Table 4.2 continued....

$M/M_\odot$	$L/L_\odot$	$T_{\rm eff}$ [K]	$X_{\rm c}$	$V_{\rm s}$ [cm/s]	$\delta L/L_0$ [ppm]
1.35	4.365	6224.2	0.030	42.24	15.17
1.35	4.794	6358.6	0.0067	50.09	20.87
1.35	5.555	6562.4	0.00018	77.85	31.38
1.35	5.749	6494.5	2.9E-06	74.89	29.09
1.35	6.172	6320.5	1.0E-10	67.95	27.80
1.40	3.522	6904.5	0.70	70.04	20.44
1.40	3.832	6901.7	0.60	79.00	22.96
1.40	4.141	6851.7	0.50	73.43	26.70
1.40	4.427	6750.3	0.40	69.69	26.04
1.40	4.646	6615.2	0.30	59.35	24.23
1.40	4.772	6470.5	0.20	51.99	21.69
1.40	4.817	6392.2	0.15	49.32	18.98
1.40	4.857	6327.2	0.10	46.57	18.84
1.40	4.891	6298.3	0.075	46.43	19.21
1.40	4.952	6283.6	0.050	46.79	19.06
1.40	5.058	6292.7	0.030	48.46	19.52
1.40	5.399	6380.7	0.010	56.29	22.87
1.40	5.814	6501.1	0.0035	72.71	27.81
1.45	4.122	7086.9	0.70	104.98	39.34
1.45	4.822	6991.9	0.50	110.85	37.24
1.45	5.138	6866.5	0.40	96.44	34.37
1.45	5.371	6712.0	0.30	80.38	28.93
1.45	5.516	6547.6	0.20	63.12	25.24
1.45	5.565	6464.5	0.15	59.39	25.25
1.45	5.611	6388.7	0.10	55.77	21.52
1.45	5.737	6339.8	0.046	53.98	22.86
1.45	5.816	6346.1	0.033	55.86	23.32
1.45	5.962	6374.2	0.020	59.27	24.16
1.45	6.581	6542.0	0.0046	85.89	34.41
1.45	7.100	6676.1	0.0016	138.40	46.93
1.45	7.497	6772.6	0.00010	171.92	50.99
1.50	5.926	6992.2	0.40	251.32	55.43
1.50	6.174	6819.4	0.30	137.54	37.02
1.50	6.344	6634.6	0.20	106.57	31.06
1.50	6.452	6458.6	0.10	83.27	24.54
1.50	6.573	6405.3	0.050	80.65	25.46
1.50	7.160	6517.9	0.010	108.34	30.99
1.50	8.344	6818.8	0.0011	262.37	75.18
1.50	8.639	6891.8	0.00011	312.90	75.34
1.50	8.692	6820.2	1.4E-05	329.45	78.17
1.50	8.872	6773.3	1.3E-06	247.30	63.56
1.60	9.366	6671.6	0.010	177.57	25.41
1.60	10.018	6834.7	0.0038	307.32	37.46

4.2.3. Theoretical amplitudes in η Bootis

Recently Kjeldsen *et al.* (1995) reported the probable detection of solar-like oscillation in the G0 IV star η Bootis. They identified thirteen oscillation modes in the frequency range $750 - 950\,\mu$Hz and estimated the average amplitude of the luminosity variation to be 45 ppm. Evolutionary tracks and theoretical oscillation spectra for η Boo have been computed by Christensen-Dalsgaard, Bedding & Kjeldsen (1995) and Guenther & Demarque (1995). Solving the pulsation equations in the adiabatic approximation, Christensen-Dalsgaard *et al.* succeeded in reproducing the observed frequency separations Δ and the small separation δ_{02}. They found the frequency separations to be very sensitive upon the mixing length and almost independent on the heavy element abundance Z at fixed location in the HR diagram. Guenther & Demarque calculated non-adiabatic oscillation frequencies for models assuming different stellar parameters and versions for the equation of state. In both papers, however, the effect of turbulent pressure was not taken into account in the computations. Here, we present damping rates and amplitudes of stochastically excited radial oscillations including turbulent pressure in the equilibrium model and convection dynamics in the pulsation calculations, as well as their effects upon the pulsation frequencies.

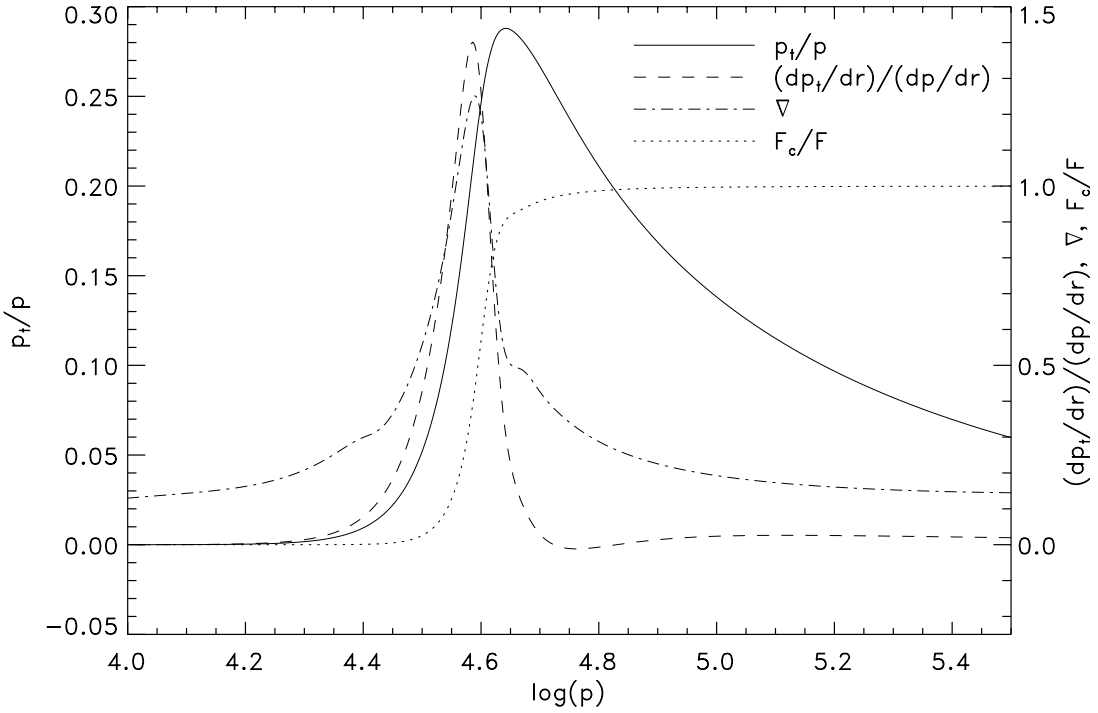

Figure 4.14: Upper layers of an equilibrium model of η Boo assuming the parameters: $M = 1.63\,M_\odot$, $L = 9.5\,L_\odot$, $T_{\rm eff} = 6050\,K$, $X = 0.7$, $Z = 0.03$. The model envelope was constructed with non-local mixing-length theory using the parameters $\alpha_{\rm c} = 2.1$, $a^2 = 900$ and $b^2 = 2000$, including turbulent pressure $p_{\rm t}$. The solid line shows the turbulent pressure fraction $p_{\rm t}/p$, the dashed line the fraction of the pressure gradient arising from the turbulent pressure gradient, $(d\,p_{\rm t}/d\,r)/(d\,p/d\,r)$. The temperature gradient $\nabla = d\log T/d\log p$ is indicated by the dot-dashed line and the upper boundary of the convection zone is marked by the ratio of the convective to the total heat flux, $F_{\rm c}/F$ (dotted line).

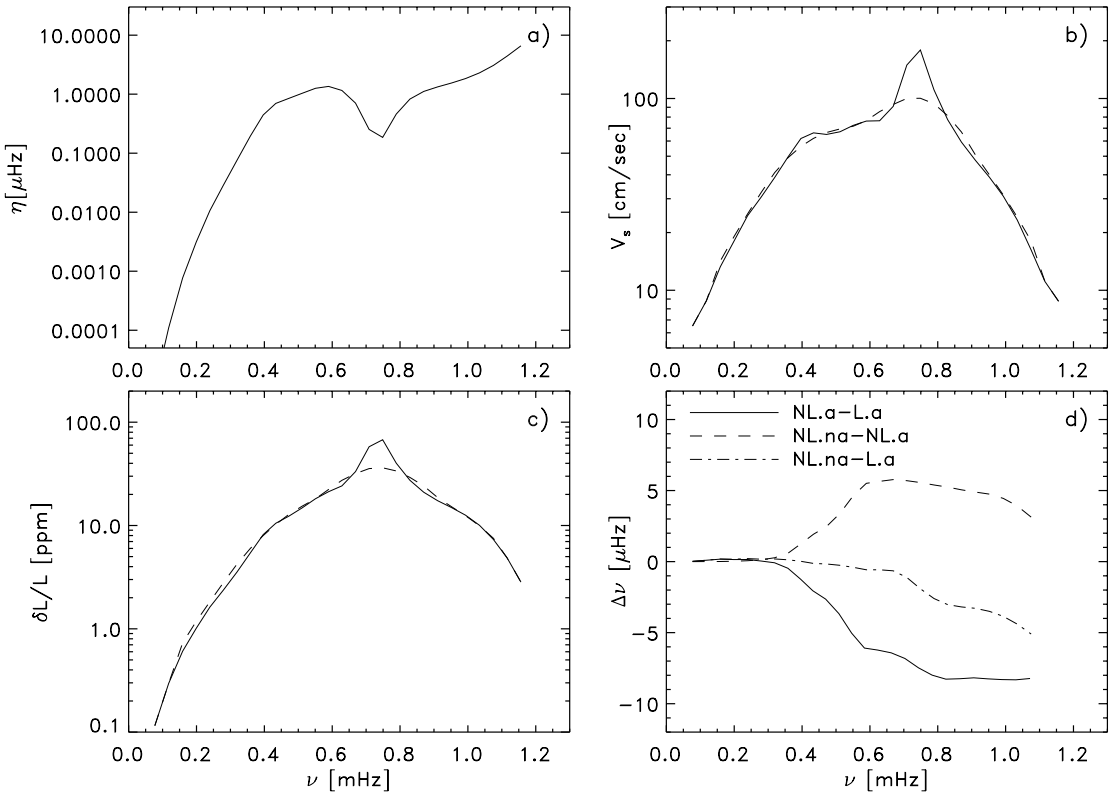

Figure 4.15: Theoretical damping rates (a), velocity (b) and luminosity (c) amplitudes versus frequency for η Boo. The model calculations were performed with the parameters of Fig. 4.14. The dashed curves in panels b) & c) represent a boxcar average of the amplitudes. Panel d) displays the frequency differences between models computed with non-local and local mixing-length theory, respectively. The individual models, labeled as L.a, NL.a and NL.na, are described in detail on page 63. The line-styles have the same meaning as in Fig. 3.12.

Fig. 4.14 illustrates the equilibrium structure of the superadiabatic boundary layers of η Boo, computed with the non-local mixing-length theory (cf. Section 2.4). For the model parameters we assumed the suggested values from Christensen-Dalsgaard, Bedding & Kjeldsen (1995), which are indicated in Fig. 4.14. In the upper layers of the convection zone the turbulent pressure p_t becomes up to $\sim 29\,\%$ of the total pressure $p = p_\mathrm{g} + p_\mathrm{t}$. Also indicated is the ratio between the turbulent pressure gradient and the total pressure gradient, $(d\,p_\mathrm{t}/d\,r)/(d\,p/d\,r)$. These results demonstrate quite obviously the significant contribution of the turbulent pressure gradient to the hydrostatic support. Moreover, in the layers of largest superadiabaticity the gradient of the gas pressure $d\,p_\mathrm{g}/d\,r$ becomes negative, which results in a value of > 1 for the fraction of the turbulent pressure gradient relative to the total pressure gradient. Similar results were also obtained from hydrodynamical convection models (Christensen-Dalsgaard *et al.* 1995, Trampedach 1996).

The linear damping rates and amplitudes of luminosity and velocity variations for η Boo are portrayed in Fig. 4.15 a-c. The peak in the amplitudes near the frequency of 0.8 mHz results from the depression in the damping rates, which may be an artifact of

the time-dependent mixing-length formalism and from an incomplete treatment of the non-adiabatic effects. Applying a smoothing process on the amplitudes by means of a boxcar average, the predicted values for the luminosity variations of ~ 36 ppm are in fair agreement with the values obtained by the observations of Kjeldsen *et al.* (1995).

Although the adiabatically computed frequency separations Δ and δ_{02}, obtained by Christensen-Dalsgaard, Bedding & Kjeldsen (1995), agreed fairly well with the observations, there remained a difference of $\sim 10\,\mu$Hz between observed and computed frequencies. These frequency differences may be reduced by using more sophisticated prescriptions for convection including turbulent pressure and convection dynamics in the calculations. Similar as for the solar case (cf. Section 3.4.3) we compared radial oscillation frequencies between models using the non-local and local mixing-length theory. Details of the individual models considered in this comparison, L.a, NL.a and NL.na, are discussed on page 63. The results for η Boo are portrayed in Fig. 4.15 d. The solid line displays the adiabatic frequency residuals if turbulent pressure is considered in the mean model (NL.a-L.a), implying a frequency shift of approximately $-8\,\mu$Hz in the region of the observed oscillations ($750 - 950\,\mu$Hz). The dashed line demonstrates the effects due to nonadiabaticity (e.g. generalized $\varkappa$-mechanism, see Section 3.2.2) and turbulent pressure fluctuations (NL.na-NL.a). The dash-dotted line portrays the frequency residuals if all effects are taken into account (NL.na-L.a), yielding an overall change in the frequencies of only $\sim 3\,\mu$Hz in the observed region. As in the solar case the effects of nonadiabaticity and turbulent pressure fluctuations almost cancel the effects of the modification of the superadiabatic layers in the equilibrium model due to the mean turbulent pressure. However, results of hydrodynamical simulations suggest that the non-local mixing-length prescription underestimates the change in the equilibrium structure (Christensen-Dalsgaard *et al.* 1995).

4.3. Overstable modes

For stars with $\log T_{\rm eff} \gtrsim 3.85$ the model calculations predict overstable modes, lying more or less in the δ Scuti instability strip. The δ Scuti stars are variables with spectral types A and F in the lower part of the classical Cepheid instability strip, which are in the very interesting evolutionary phase of the main sequence and near the end of central hydrogen burning. It was first shown by Baker & Kippenhahn (1962) that the excitation mechanism in Cepheids, which are horizontal branch pulsators with large amplitudes of low-order radial modes (n=1,2 in double-mode Cepheids), is due to the opacity mechanism acting in the HeII ionization zone. The same mechanism is believed to be responsible for the excitation in δ Scuti stars (e.g. Dziembowski 1995 and references therein). Many δ Scuti stars, however, have far more complex spectra of oscillation, involving both radial and non-radial modes with low amplitudes, lying often in a narrow frequency range, which complicates the frequency and mode identification substantially (e.g. Mangeney *et al.* 1991). In cooler δ Scuti stars the outer layers still exhibit distinct convection zones. Thus in these layers the pulsationally induced fluctuations of the turbulent fluxes may become important for the selection mechanism of modes with observable amplitudes. The dependence of the mode selection mechanism upon the heavy element abundance Z and mixing length will be discussed in greater detail in Section 4.3.1 for the δ Scuti star FG Vir.

The theoretically predicted radial order of unstable p modes in sequences of evolving stellar models of δ Scuti stars are depicted by different symbols in Fig. 4.9 (e.g. circles indicate the location of models in the HR-diagram for which the radial fundamental mode was found to be overstable). The models have only a few excited modes lying in a narrow frequency interval and some of it display radial orders in a discontinuous sequence. Moreover, with increasing effective temperature the overstable modes are shifting to higher frequencies. These results are not inconsistent with observed spectra (e.g. Michel *et al.* 1995). The blue edge of the instability domain is predicted to shift to higher effective temperatures with increasing radial order, in consistence with model calculations by other authors (e.g. Stellingwerf 1979, 1980; Dziembowski 1995). Through the inclusion of the turbulent flux perturbations in the stability analyses the computations predict well-defined red edges. The location and width of the instability domain are sensitive to the convection parameters and chemical composition of the models. This will be discussed in more detail in Section 4.3.2 for an evolving 1.7 $M_\odot$ δ Scuti star.

4.3.1. Overstable modes in FG Vir

Recent DSN[13] and WET[14] campaigns identified ten possible pulsation frequencies in the δ Scuti star FG Vir (Breger *et al.* 1995). Due to the large number of detectable modes and the relatively slow rotation FG Vir is one of the most promising of the ~ 370 known δ Scuti stars for seismic probing of stellar interior in distant stars. Tentative model calculations by Dziembowski were successful to match the observed frequency values (presented in Breger *et al.* 1995), suggesting three radial and four non-radial p modes as well as three g modes. Here, we present tentative linear damping rates for radial modes of FG Vir models assuming the model parameters of Guzik & Bradley (1995). They evolved stellar models of FG Vir similar to those of Dziembowski varying the effective temperature such till the radial modes matched those identified by Breger *et al.* as radial modes of FG Vir. Using their model parameters (see Fig. 4.16), we computed non-adiabatic radial eigenfunctions of model envelopes using Gough's non-local, time-dependent mixing-length theory. Assuming a heavy element abundance $Z = 0.02$ and mixing-length parameter $\alpha_c = 2.0$, our equilibrium model results predict a moderate surface convection zone with a maximum ratio of the convective to the total heat flux $F_c/F = 0.87$ at the depth of $\log T = 4.06$. Non-adiabatic effects due to the convective heat perturbation δF_c may therefore influence pulsational stability and should probably not be neglected in the stability analysis.

The damping rates for FG Vir models, using various values for α_c and Z as well as their dependence upon the convective dynamics and treatment of radiation are displayed in Fig. 4.16 as function of the radial order n. Reducing the mixing-length parameter has a predominant effect on the stability of high-order radial modes, whereas decreasing Z influences the stability of the fundamental radial mode. The high-order modes are found to be excited by the effects of the turbulent pressure fluctuations δp_t; if δp_t is neglected in the pulsation calculations only the first four radial modes are found to be overstable. These results are not in complete agreement with the radial mode identifications of Breger

[13] Delta Scuti Network
[14] Whole Earth Telescope

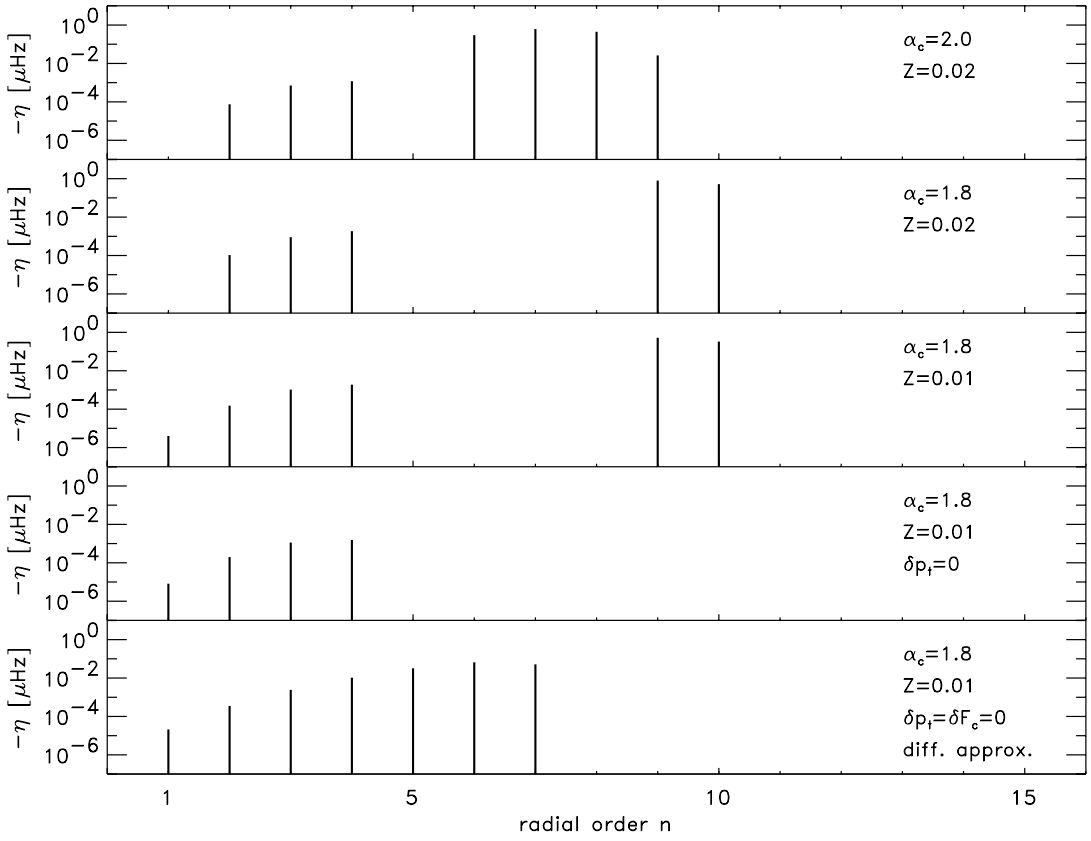

Figure 4.16: Theoretical damping rates versus radial order n for the δ Scuti star FG Vir assuming the model parameters according to Guzik & Bradley (1995): $M = 1.82\,M_\odot$, $T_{\rm eff}$=7458 K, $L/L_\odot$=13.43 X=0.7. The calculations were carried out using $a^2 = 900$ and $b^2 = 2000$ for the non-local mixing-length parameters.

et al., who found no evidence of an unstable mode of radial order $n = 2$. Interesting are the results if the turbulent flux variations are neglected in the stability computations and radiation is treated in the diffusion approximation (lowest panel in Fig. 4.16). For this case the fifth overtone is predicted to be overstable.

Since only envelope models are considered here, we are not able to compare our frequency predictions directly with those of Breger *et al.*. However, comparing the ratios of the pulsation periods of unstable radial modes may help constrain model parameters. In Table 4.3 the computed period ratios for our FG Vir models are depicted together with the observed values of Breger *et al.*. The model calculated with $Z = 0.005$ and $\alpha_{\rm c} = 1.8$ predicts the smallest residuals of the period ratios relative to the observations. Moreover, the results show a more distinctive dependence upon the heavy element abundance than on the mixing length. A similar behaviour of the period ratios upon Z were also found in double-mode Cepheids by Christensen-Dalsgaard & Peterson (1995).

Beside damping rates and periods, linear non-adiabatic pulsation analyses provide two additional quantities that may be compared with observations. These "*non-adiabatic observables*" are the amplitude ratio $f = (\delta L/L)/(\delta r/r)$ and phase shift $\varphi(f) = \varphi(\delta L/L) - \varphi(\delta r/r)$ between the luminosity and velocity variations which may be directly compared

Table 4.3: Comparison of radial period ratios for FG Vir with theoretical models assuming model parameters of Fig. 4.16 (Guzik & Bradley 1995) and various values for Z and α_c.

Period ratios	Obs.: Breger *et al.* (1995)	Model: $Z = 0.02$		Model: $Z = 0.01$	Model: $Z = 0.005$
		$\alpha_c = 2.0$	$\alpha_c = 1.8$	$\alpha_c = 1.8$	$\alpha_c = 1.8$
Π_2/Π_0	0.6255	0.6116	0.6115	0.6158	0.6203
Π_3/Π_2	0.8363	0.8285	0.8286	0.8311	0.8334

with those occurring in the Fourier decomposition of the observed light and radial velocity curve (see also Section 5). Balona & Stobie (1979) and Stamford & Watson (1981) introduced a method for radial and non-radial mode identification of low-amplitude pulsations based on a linearized analytical expression for the flux variations presented first by Dziembowski (1977). In this approach theoretical amplitude ratios and phases in different colours and light are compared with observational data obtained from two-color photometry. Watson (1988) further elaborated on this approach by deriving a linearized analytical expression for monochromatic flux variations for which the required parameters can be obtained from detailed static model stellar atmospheres (e.g. Kurucz 1992). Recently, Cugier *et al.* (1994) introduced an improved method for the evaluation of the flux variations using linearized non-adiabatic eigenfunctions obtained from pulsation models according to Dziembowski & Pamyatnykh (1993). Moreover, they demonstrated the determination of the radial order of unstable modes as well as the mean stellar parameters from their comparison of the non-adiabatic observables with data of β Cephei stars. Since convection in β Cephei stars is almost negligible they ignored convection dynamics entirely in their pulsation model ($\delta F_c = \delta p_t = 0$) and treated the radiative flux in the diffusion approximation. As already mentioned above such a treatment may induce large errors in the non-adiabatic observables for cooler stars such as FG Vir.

The effects of neglecting convection dynamics and using the diffusion instead of the Eddington approximation to radiative transfer upon the non-adiabatic observables are demonstrated in Fig. 4.17. A striking result is the difference in the phase shifts $\varphi(f)$ in the upper parts of the atmosphere, as depicted in the panels d & h. In the superadiabatic layers, where there is the transition between radiation and convection ($\log p \approx 4.3$), the diffusion approximation becomes invalid promoting a sudden change in the luminosity eigenfunctions (see panel e) and thus in the phases of f. Moreover, the distinction in $\varphi(f)$ between modes of different order n becomes less pronounced in the superficial layers, which may prevent radial mode identification by comparing the phases with observations.

Another interesting result of Fig. 4.17 is the nearly constant behaviour of the amplitude ratio $|f|$ in the upper layers of the atmosphere due to the much shorter radiative cooling time τ_R [cf. equation (3.13)] relative to the pulsation period Π. The magnitude variations in a particular colour can then be obtained by varying the input parameters $\log T_{\rm eff}$ and $\log g$ of an accurate static model atmosphere according to the variation in f (Cugier *et al.* 1994). Such a static model atmosphere approximately reflects the real physical conditions at every time instant during a pulsation cycle, since $\tau_R \ll \Pi$. A more accurate method was suggested by Frandsen (1996, personal communications) in which the mean stratification of a static model atmosphere is modified by the non-adiabatic linear eigenfunctions in order to compute the monochromatic flux perturbations in a particular photometric system.

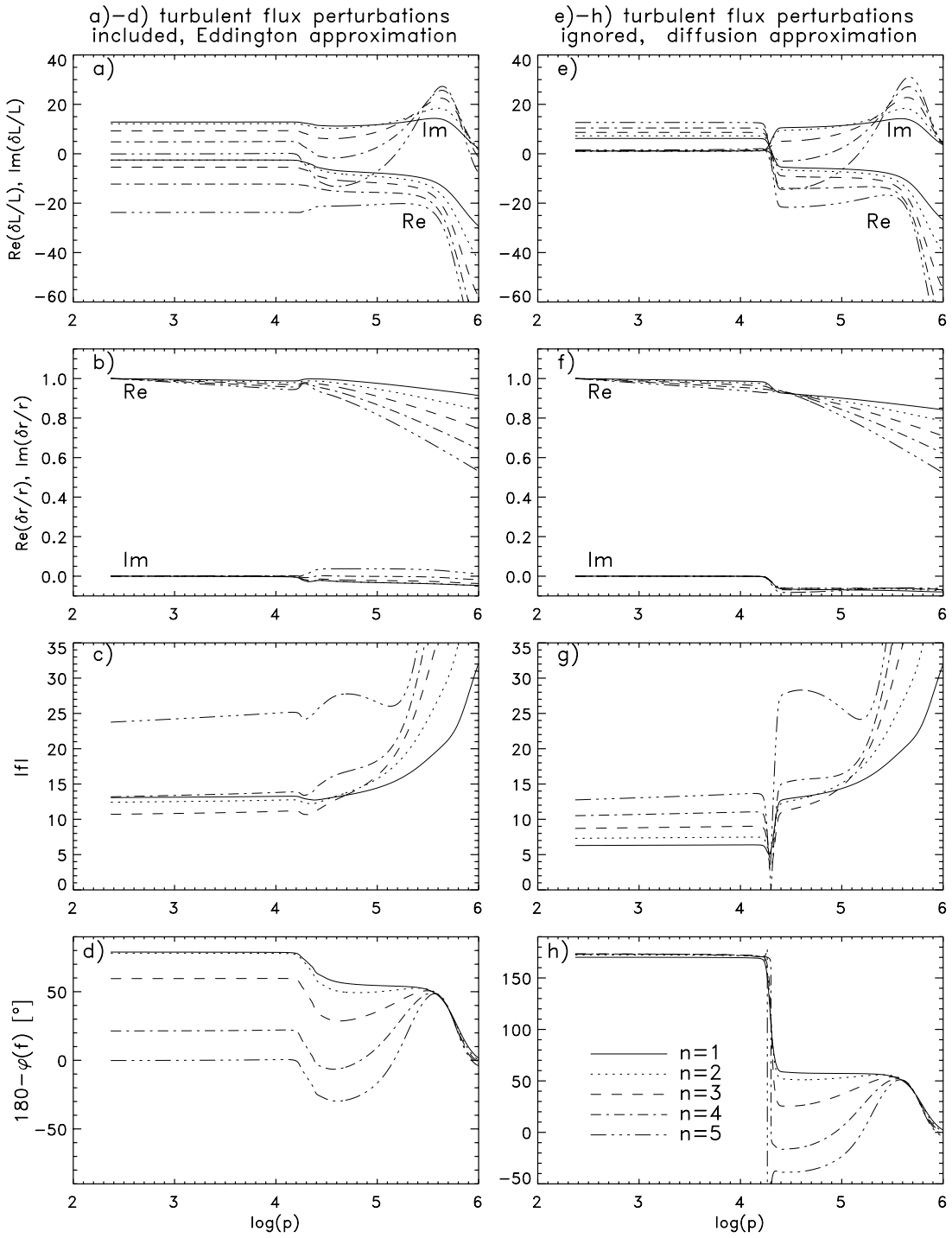

Figure 4.17: Non-adiabatic eigenfunctions and observables $|f|$ & $\varphi(f)$ of the first five radial oscillation modes for models of FG Vir plotted against the depth variable $\log p$. The computations were carried out with the model parameters from Fig. 4.16 assuming $Z = 0.01$ and $\alpha_c = 1.8$. Panel a) & b) show the luminosity and displacement eigenfunctions and panel c) & d) the norm of the amplitude ratio $f = (\delta L/L)/(\delta r/r)$ and its phase $\varphi(f) = \varphi(\delta L/L) - \varphi(\delta r/r)$ of a pulsation calculation with turbulent flux perturbations and the Eddington approximation to radiative transfer. Panel e) - h) show $\delta L/L$, $\delta r/r$, $|f|$ and $\varphi(f)$ of similar pulsation calculations in which the perturbation of the turbulent fluxes were omitted ($\delta F_c = \delta p_t = 0$) and the diffusion approximation to radiative transfer was assumed.

4.3.2. On the δ Scuti instability domain

At low surface temperatures stars exhibit distinctive surface convection zones, which influence non-adiabatic effects substantially and thus the mechanisms of excitation and damping of pulsations in these layers. Neglecting the interaction between convection and pulsation for these stars may therefore result in a failure to predict the proper sign of the mode damping rates. Solving numerically the non-linear hydrodynamic equations and using a time-varying eddy viscosity, Deupree (1977) has been successful in setting the cool boundary of the RR Lyrae instability strip, which has been also found by Baker & Gough (1979) using Gough's (1977) formulation of a time-dependent local mixing-length theory (cf. Section 2.3.2). Recently, Bono *et al.* (1995) investigated the dependence of the RR Lyrae fundamental red edge upon model mass and helium abundance assuming Stellingwerf's (1982) prescription of a non-linear, non-local, time-dependent treatment of convection. The red edge of δ Cephei stars has been successfully produced by Xiong (1980) using his own prescription of time-dependent convection and by Balmforth & Gough (1989) by means of Gough's (1977) local theory. Both calculations suggested that the inclusion of turbulent pressure may become important for stabilizing modes as lower surface temperatures are approached.

Theoretical investigations of radial pulsations of models in the δ Scuti strip have been carried out by several authors (e.g. Stellingwerf 1979 and references therein). These computations, however, ignored convection entirely or employed some form of mixing-length theory in the equilibrium model and then neglected the pulsationally induced perturbations in the turbulent fluxes in the stability analysis. Their results therefore failed to predict the return to stability at the cool boundary of the instability strip for low-order radial modes. Here we analyse the stability properties of an $1.7\,M_\odot$ δ Scuti star, using Gough's non-local mixing-length prescription for convection (cf. Section 2.4.2). In particular the separate contributions to the damping rates arising from the fluctuating Reynolds stresses and gas pressure, as well as their dependence upon the parameters of convection, the variation of the chemical composition and the choice of the opacity data, will be studied along the lower δ Scuti instability strip.

The model series with constant mass of $1.7\,M_\odot$ was calculated by specifying effective temperature and luminosity obtained from full evolution sequences by Christensen-Dalsgaard (1993). The modal damping rates, η, as function of effective temperature across the instability strip are portrayed in Fig. 4.18 for the radial modes of order $n = 1$ and $n = 2$, respectively. Additionally depicted are the contributions arising from the gas pressure fluctuations, $\eta_{\rm g}$, and the perturbation of the Reynolds stresses, $\eta_{\rm t}$, which both contribute to the work integral such that $\eta = \eta_{\rm g} + \eta_{\rm t}$. These results suggest that the return to stability at the cool boundary of the strip is exclusively through the fluctuations of the turbulent pressure that oscillates out of phase with the density fluctuations. Through the inclusion of $\delta p_{\rm t}$ in the stability analysis, the contribution of $\eta_{\rm g}$ to the work integral will be modified as a result of a change in the shape of the modal eigenfunctions. Thus by setting artificially $\delta p_{\rm t} = 0$ the resulting solution of the damping rates $\eta = \eta_{\rm g}$ (triple-dot dashed curve) displays different values relative to the $\eta_{\rm g}$ components of the full computations. The differences between these results, however, are rather small and demonstrates quite

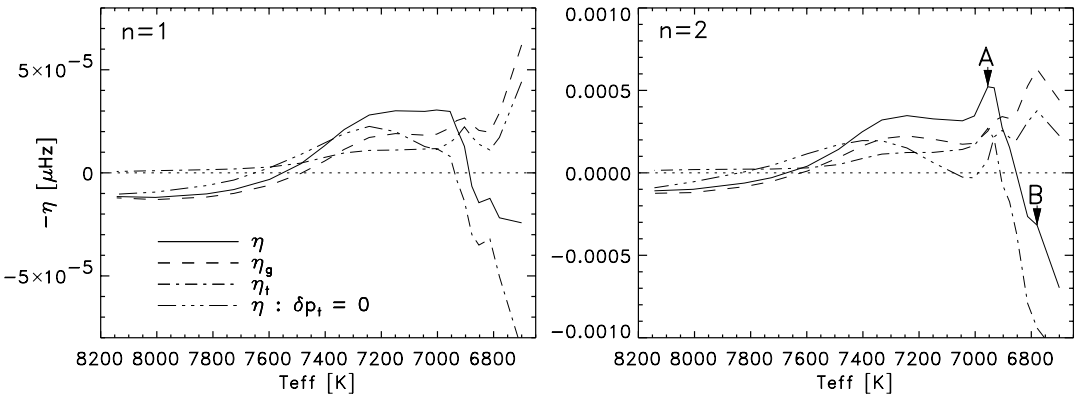

Figure 4.18: Theoretical damping rates η as function of effective temperature for the fundamental ($n = 1$) and first overtone ($n = 2$) radial mode. Computations were carried out for models assuming the convection parameters $\alpha_c = 2.0$, a^2=900 & b^2=2000 as well as $Z = 0.02$ for the heavy element abundance. The solid curve shows the results from the computations including the Lagrangian perturbations of the gas and turbulent pressure. The gas pressure contribution η_g and turbulent-pressure damping contribution η_t are indicated by the dashed and dot-dashed line, respectively. The triple-dot-dashed curve displays the results for the calculations in which turbulent pressure fluctuations were omitted, $\eta : \delta p_t = 0$.

obviously that without the inclusion of the turbulent pressure fluctuations the pulsation calculations fail to produce the red edge of the δ Scuti instability strip.

The location of the layers in which damping and driving take place can be studied by considering the spatial dependence of the work integrals W_g and W_t, which describe the portions of the mechanical work performed by the gas and turbulent pressure perturbations, respectively (cf. Section 3.4.5). For the models with an effective temperature of $T_{\rm eff}$=6955 K and $T_{\rm eff}$= 6799 K, as indicated by the labeled arrows A and B in Fig. 4.18, the accumulated work integrals for modes with radial order n=2 are depicted in Fig. 4.19. In regions where the accumulated work increases with radius, the modes are damped, and where it declines pulsation is locally excited. The principal driving sources contributing to W_g in the hotter model A are located in the HeII and HeI ionization zones, whereas in the cooler model B the driving layers are predominantly in the HeII ionization zone. Moreover, in the latter model W_g exhibits an oscillatory behaviour, arising from the pulsationally induced modulation of the convective heat flux F_c, which carries most of the total energy flux in these layers. The work accumulated from the perturbation of the momentum flux, W_t, experiences its largest contribution in the upper layers of the HeII ionization zone, destabilizing the mode in the hotter model A. In the cooler model B, however, W_t contributes significantly to the damping, which results in a stable mode. The shape of the accumulated work integral, W, for the models when δp_t is neglected in the computations, are not very different from the solution of W_g, when solving the full set of the pulsation equations. To estimate the effects of δF_c upon the mechanism of damping and driving, the variations of W, computed without the Lagrangian perturbations in the turbulent fluxes, are also indicated in Fig. 4.19 using, however, the diffusion approximation to radiative transfer. From these results it appears that δF_c has some stabilizing effect upon the modal damping rates in both models A and B.

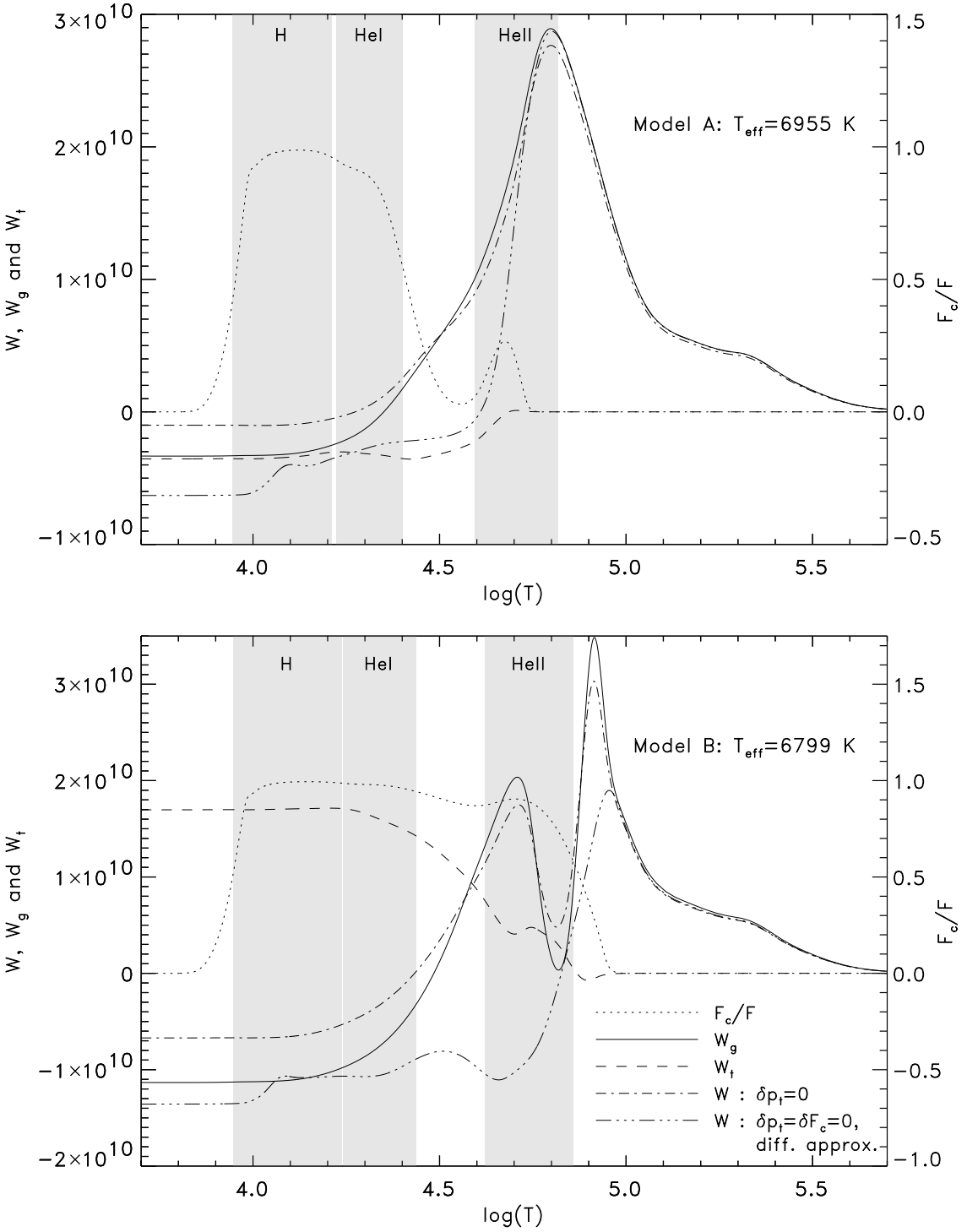

Figure 4.19: Accumulated work integrals as function of the depth co-ordinate log(T) for model A ($T_{\rm eff} = 6955\,K$) and model B ($T_{\rm eff} = 6799\,K$). The results are depicted for the first radial overtone and plotted in units of 10^{30} erg. The solid curve displays the work accumulated from the perturbation of the gas pressure, $W_{\rm g}$, and the dashed curve the work performed by the perturbation of the turbulent pressure, $W_{\rm t}$. The results of the calculations in which turbulent pressure fluctuations were omitted, $W : \delta p_{\rm t} = 0$, are indicated by the dot-dashed curve. The triple-dot-dashed line shows the result of the accumulated work when convection dynamics effects were ignored in the stability analysis, $W : \delta p_{\rm t} = \delta F_{\rm c} = 0$, and when radiation was treated in the diffusion approximation. The convection zone is marked by the ratio of the convective to the total heat flux $\rm F_c/F$ (dotted curve). The extents of the zones of ionization of H and He, from 5% to 95% ionization, are similarly indicated. For the model calculations the same parameters have been used as given in Fig. 4.18.

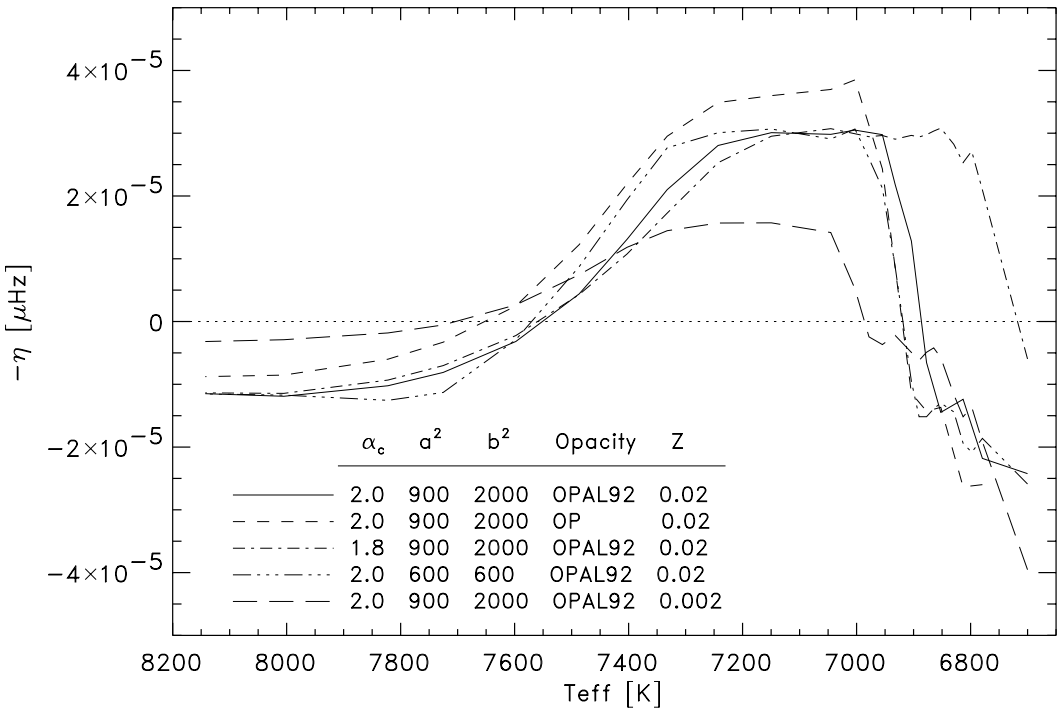

Figure 4.20: Calculated linear damping rates as function of effective temperature for the fundamental mode of radial pulsation. Results are displayed for model computations assuming different values for the heavy element abundance and parameters for convection, as well as opacity data from the OPAL and OP tables.

The sensitivity of the instability domain upon the mixing-length parameter α_c and upon the two non-local parameters is demonstrated in Fig. 4.20 for the fundamental radial mode. A decrease in α_c results in a significant shift of the cool boundary of the strip towards lower temperatures, whereas the blue edge is nearly unaltered. Surface convection in models with high effective temperatures is very inefficient and therefore less sensitive to variation in α_c than in cooler models. It appears that instability becomes less pronounced when the heavy element abundance Z is reduced, as indicated by the long-dashed curve. Moreover, the whole instability domain is shifted to higher temperatures. This effect may help constrain the model parameter Z by comparing the theoretical position of the strip with the observed one. Also indicated in Fig. 4.20 are the changes in η when using the OP (Seaton *et al.* 1994) instead of the OPAL92 opacities, promoting instability and leading to a shift of the whole strip towards higher temperatures.

5. Phase shifts and amplitude ratios in the solar atmosphere

5.1. Introduction

Through the improvement of observation techniques fairly accurate data now exist of amplitude ratios and phase shifts between different types of oscillation measurements. These measurements depend crucially on the properties of the oscillations just beneath and in the solar atmosphere. Hence they provide information about the damping and excitation processes within the photosphere. This can be used to improve our understanding of the underlying physics and help us to reconstruct the eigenfunctions at the top of the theoretical model. For the simple case of an adiabatic, isothermal atmosphere the phase shift between irradiance and velocity is 90°. However radiative damping as well as changes in the convective dynamics, i.e. perturbation of the convective heat flux δF_c and turbulent pressure δp_t and other non-adiabatic effects contribute to the phase shift giving a value different from 90°. Solar-like stars exhibit a distinctive convection zone, which influences the non-adiabatic effects substantially, particularly in the upper part of the convection zone, where the temperature gradient is extremely superadiabatic . Using a local, time-dependent mixing-length formalism for convection (Baker & Gough, 1979), which accounts for the interaction between convection and pulsation, Gough (1985) calculated phase shifts different from 90°, but still got an unsatisfactory agreement with the observations. However he used the diffusion approximation to radiative transfer, which insufficiently treats the radiation field in the super-adiabatic layers and in optical thin regions, where the pulsation induces large deviations from thermal equilibrium.

Here we investigate the oscillation properties by means of a non-local, time-dependent mixing-length theory and the Eddington approximation to radiative transfer in both the envelope and pulsation model. The calculated results of the amplitude ratios and phase shifts are compared with irradiance measurements from the IPHIR instrument on the PHOBOS 2 spacecraft and contemporaneous velocity measurements obtained from the Birmingham instrument at Tenerife (Schrijver, Jiménez & Däppen 1991). The height dependence of the phase shift between temperature and velocity fluctuations are compared with measurements derived from temporal line-profile variations formed at different heights in the solar atmosphere (Alamanni *et al.* 1990; Staiger *et al.* 1984). Finally we discuss the relative velocity phase and velocity amplitude as function of height in connection with observations by Stebbins & Goode (1987).

5.2. Results

In order to compare properly theoretical phase shifts and amplitude ratios with observations, it is necessary to understand exactly which quantities should be compared with the observations and at which height in the atmosphere. In our model calculations the

atmosphere was treated with a grey radiation, giving a bolometric value for the calculated luminosity fluctuations. Assuming that the luminosity perturbation experiences no further disturbance on the way from the point in the solar atmosphere where we applied the boundary conditions, the measured continuum luminosity fluctuation corresponds to the evaluated value at the outermost mesh-point of the model ($\Delta L_{\rm s}$, in the following the top of the atmosphere). However, most of the observational data available today are based on measurements of the Doppler displacements of line-profile variations (velocity) and monochromatic intensity fluctuations. A consistent comparison with such observations demands the calculation of the oscillatory spectral line profiles from the computed eigenfunctions solving the radiative transfer equations (Frandsen 1986).

Schrijver, Jiménez & Däppen (1991) derived phase delays and amplitude ratios from observations of continuum irradiance measurements at 500 nm in a broad-band continuum window (5 nm) and velocity data obtained in the neutral potassium line (769.9 nm). This line is formed at an optical depth of τ=0.013 (Christensen-Dalsgaard & Gough 1982), which corresponds to a height of h=200 km using a T-τ–relation derived from a model C of Vernazza, Avrett & Loeser (1981). The calculated luminosity amplitudes have been corrected for the measured irradiance wavelength of $\lambda = 500$ nm using the approximation

$$(\delta L/L)_\lambda = (\delta L/L)_{\rm bol} \frac{\lambda_{\rm bol}}{\lambda}\,, \tag{5.1}$$

where

$$\lambda_{\rm bol} = \frac{623\ \ {\rm nm}}{T_{\rm eff}/5777\ \ K}\,, \tag{5.2}$$

derived by Kjeldsen & Bedding (1995), which is accurate to a few percent for values of λ deviating less than $\pm 40\%$ for $\lambda_{\rm bol}$.

Fig. 5.1 shows the amplitude ratios of these observations together with our calculated results as function of frequency. Theoretical results for different heights (h) in the solar atmosphere are shown by different line-styles and for the luminosity perturbation the surface value $\Delta L_{\rm s}$ has been used. Observations with a coherence greater than 0.7 are represented through different symbols for the degree l. The thick solid line represents a running-mean average of the observational data with a width of 300 μHz. The velocity amplitude varies by about 15 % between the photosphere and the outer boundary conditions defined at the temperature minimum; the relative luminosity amplitude however, is roughly constant in this domain. The height dependence of the amplitude ratios for selected modes close to the 5 min oscillations are shown in Fig. 5.2. Modes of higher order exhibit a stronger dependence on height, particularly in the deeper layers of the photosphere.

The phase differences between luminosity and inward directed velocity as function of frequency are depicted in Fig. 5.3 together with the observational results from Schrijver, Jiménez & Däppen (1991). For frequencies larger than 2.5 mHz, the theoretical phases are bend to larger values, which is due to the mechanism arising from the interaction of the

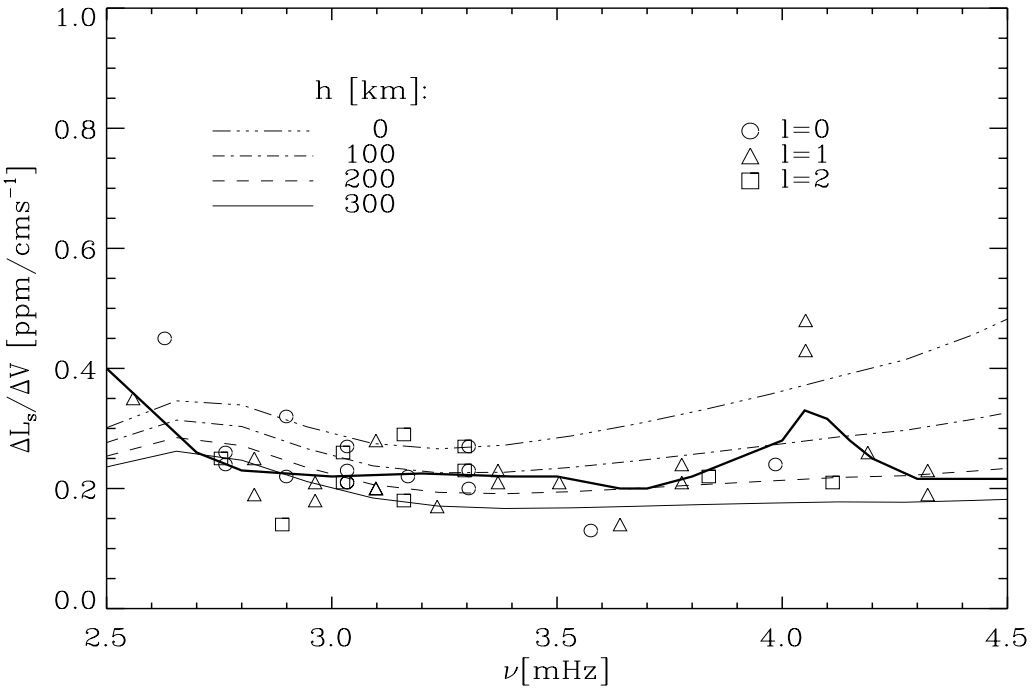

Figure 5.1: Theoretical amplitude ratios between surface luminosity $\Delta L_{\rm s}$ (outermost meshpoint of the model) and velocity versus frequency compared with observations by Schrijver, Jiménez & Däppen (1991). Computed results are depicted at different heights in the atmosphere assuming the mixing-length parameters $\alpha_c = 1.8$,a^2=600 and b^2=300. The zero height (h=0 km) corresponds to the level where the temperature is equal to $T_{\rm eff}$. The thick, solid line indicates a running-mean average of the observations.

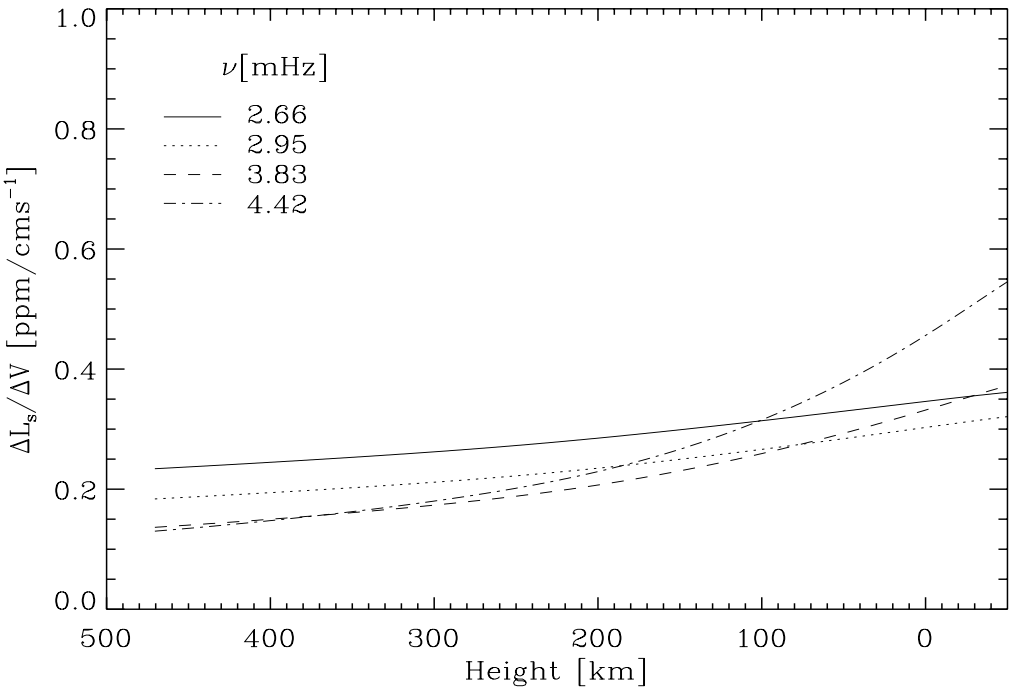

Figure 5.2: Calculated amplitude ratios between surface luminosity perturbation $\Delta L_{\rm s}$ and velocity as function of height in the solar atmosphere for modes in the 5 min range. The model parameters are the same as in Fig. 5.1.

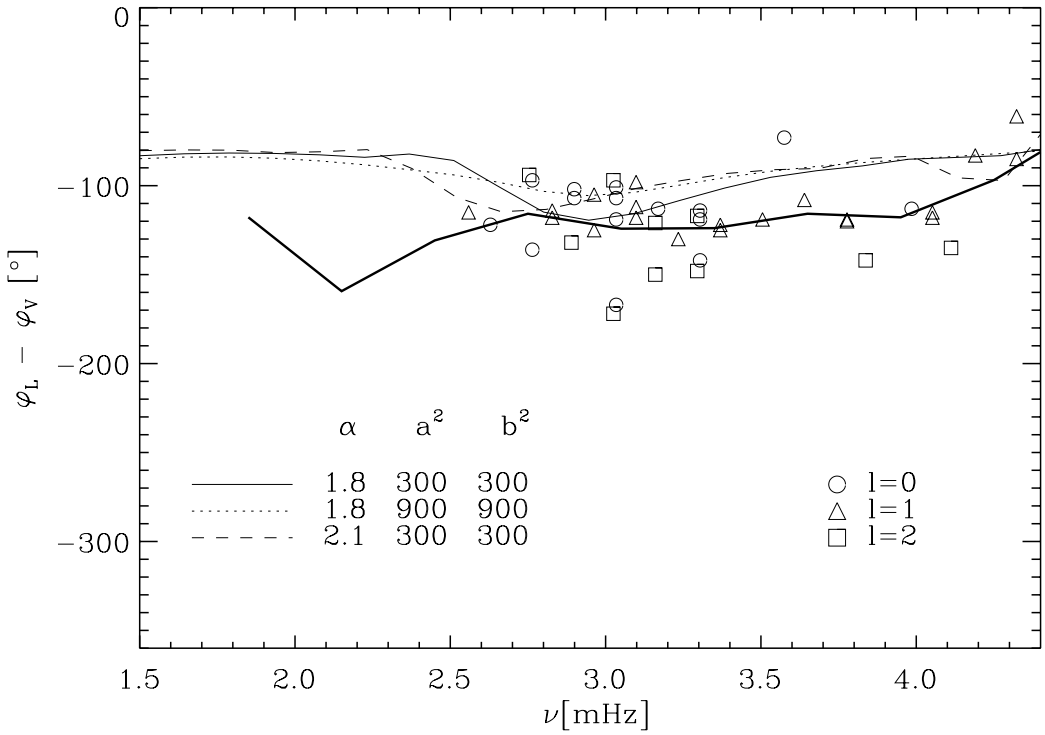

Figure 5.3: Calculated phase delays between surface luminosity ΔL_s and inward directed velocity as function of frequency for models with different mixing-length parameters. The theoretical results are depicted for a photospheric level of h=200 km, at which the velocity is measured by the observations in the potassium line. Observations of low degree-modes having a coherence greater than 0.7 are depicted as symbols (Schrijver, Jiménez & Däppen 1991). The thick, solid line represents a running-mean average of the observational data.

pulsation with the convection. These high-order modes sample the super-adiabatic layers with more detail and are therefore more sensitive to its structure.

In Fig. 5.4 & Fig. 5.5 we compare the height dependence in the photosphere of the phase delays between temperature and velocity with observations by Alamanni *et al.* (1990) and Staiger *et al.* (1984) respectively. Both observations are based on temporal line-profile variations in certain Fraunhofer lines. The measured irradiance phase is actually the ratio between line and continuum irradiance, which becomes very uncertain for values close to the continuum. The intensity perturbations can be described by the temperature fluctuations (assuming local thermodynamic equilibrium) as long as the contribution arising from the opacity perturbation can be neglected. At large optical depths the theoretical phase differences increase with height but still have a too small slope compared with the observations. At an optical depth τ=0 an additional continuum value from Fröhlich and van der Ray (1984) is depicted, which fit fairly well with theory. Christensen-Dalsgaard & Frandsen (1984) calculated phase shifts between temperature and velocity, using a quite sophisticated non-grey radiation field by means of opacity distribution functions (ODF), but neglecting the convective heat-flux perturbations. Their results, taken from Frandsen (1986), are depicted in Fig. 5.5. Higher up in the atmosphere their results agree quite well with the observations; however, approaching the bottom of the photosphere their phases

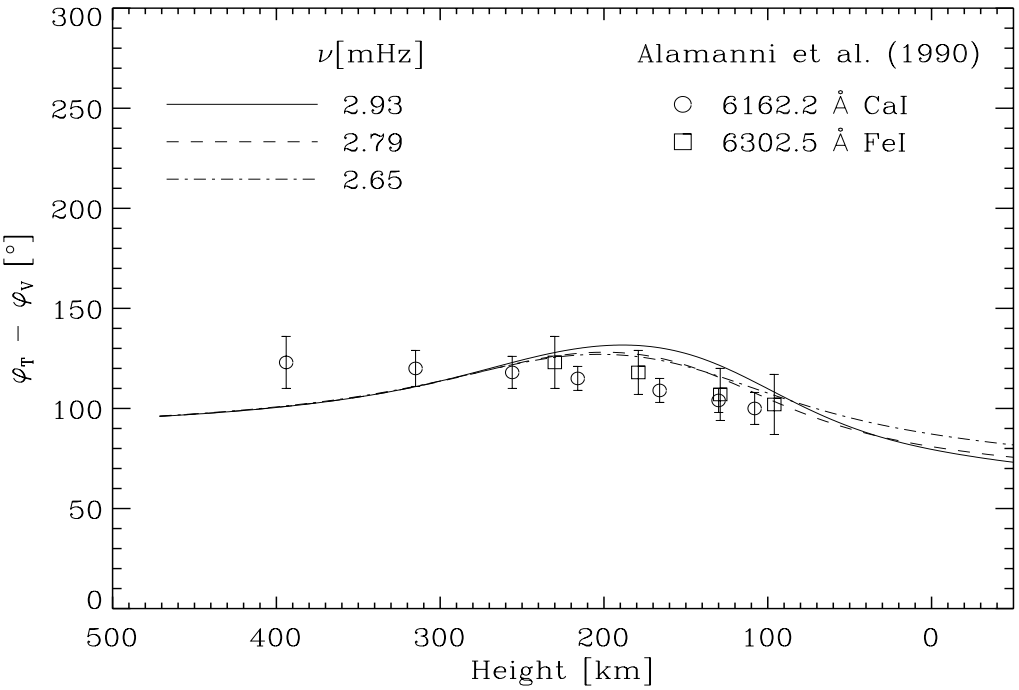

Figure 5.4: Phase differences between temperature and velocity (positive values corresponding to temperature leading velocity) compared with observations by Alamanni *et al.* (1990) based on spatio-temporal line-profile variations. They compared the oscillating power in the red and blue line flanks in order to derive the height dependence of the phases. For the model calculations the same parameters have been used as given in Fig. 5.1.

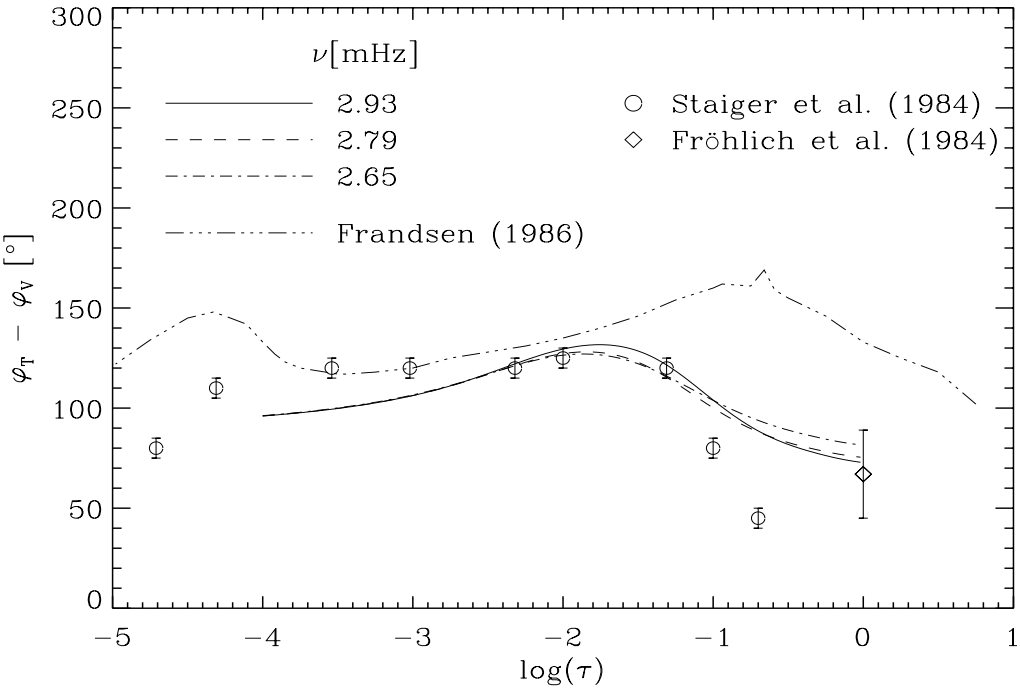

Figure 5.5: Phase differences between temperature and velocity as function of the optical depth τ. Calculated results for different modes using the model parameters from Fig. 5.1 are represented by solid, dashed and dot-dashed lines. Theoretical phase shifts calculated by Christensen-Dalsgaard & Frandsen (1984) who used non-grey opacities by means of opacity distribution functions but neglected convective dynamics are shown by the triple-dot-dashed line. Circles with error bars give the corresponding observed values from Staiger *et al.* (1984) and the diamond indicates a continuum value from Fröhlich & van der Raay (1984) (adopted from Frandsen 1986).

get larger. The inclusion of non-grey opacities significantly modifies the temperature perturbation, which directly feels the heat exchange associated with non-grey opacities and may also effect the phase differences.

The frequency-averaged velocity phase and amplitude as function of height in the photosphere is shown in Fig. 5.6 & Fig. 5.7 for models with different mixing-length parameters. Observational data by Stebbins & Goode (1987), which have been reduced by Marmolino & Stebbins (1989) are represented by symbols. They observed Doppler shifts in the highest-lying, nonmagnetic line, FeI 543.45 nm, using nine independent spectral samples representing different locations in the atmosphere. After identifying the velocity strings the data set was Fourier transformed in time and space and filtered to pass only power in the five-minute range. The amplitudes and phases of the grand average eigenfunctions (averaged in time and horizontal position) are then obtained by performing a Hilbert transform. In order to perform the comparison with the theory the nine spectral samples have to be related to the formation heights of the various spectral line depths, which are determined from non-LTE calculations by Altrock *et al.* (1975). The amplitude is normalized by its value at a height h=62 km and the velocity phase is given relative to its value at this level. There is a decent agreement between theory and observation for models including the time-dependent mixing-length theory and using the Eddington

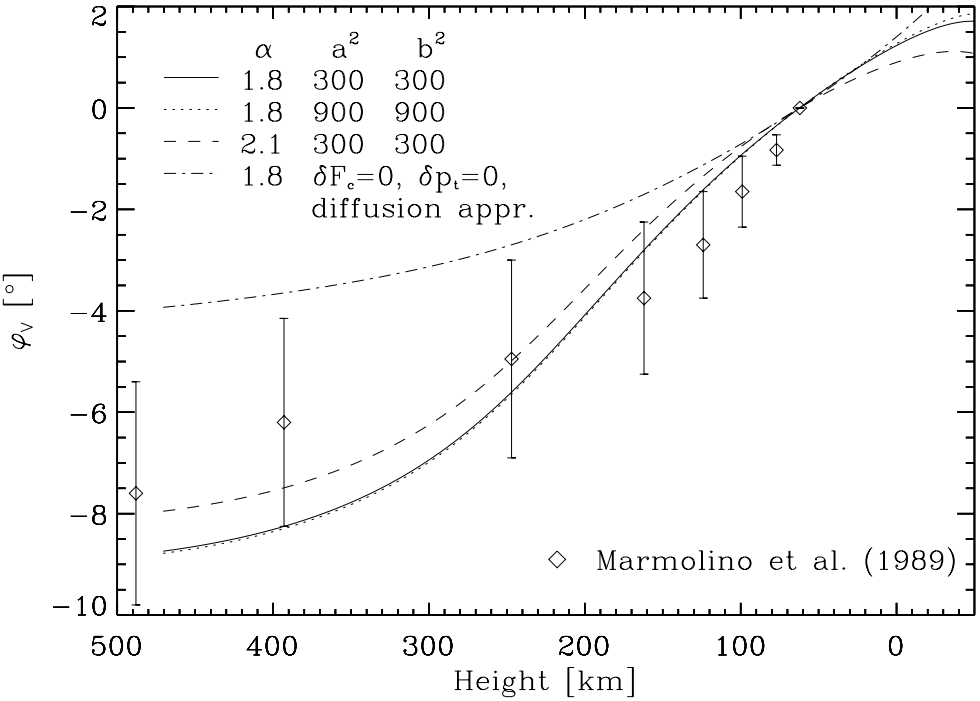

Figure 5.6: Relative velocity phase for models with different mixing-length parameters as function of height in the solar photosphere. The phases have been averaged over frequency for modes with a radial order between n=18 and n=31, and are given relative to their value at a height of h=62 km. The dot-dashed line gives the results for a model neglecting the convective dynamics and using the diffusion approximation to radiative transfer. Observations by Stebbins & Goode (1987) are depicted as diamonds (adopted from Marmolino & Goode 1989).

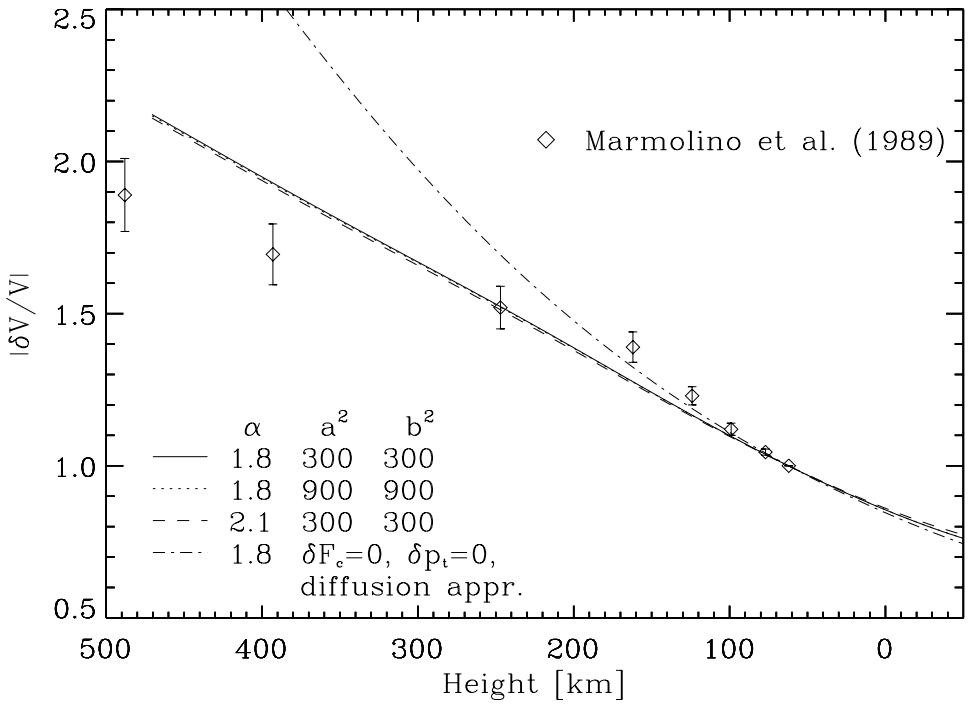

Figure 5.7: Frequency-averaged velocity amplitudes (for modes with a radial order between n=18 and n=31) as function of height in the solar photosphere for different models. The amplitudes have been normalized to their value at h=62 km. The diamonds give the corresponding observations from Stebbins & Goode (1987) reduced by Marmolino & Stebbins (1989).

approximation to radiative transfer. However there is a discrepancy at larger heights if the diffusion approximation is used and the convective dynamics are neglected.

6. Conclusion

The main purpose of this work has been to study theoretically the properties of radial oscillations, such as damping and excitation processes and the estimation of amplitudes of stochastically excited modes, in solar-like stars. The perhaps most important conclusion drawn from this survey is the support of the theory that oscillations in solar-like stars are intrinsically damped and stochastically driven by convection, explaining the comparatively low amplitudes of such modes. This view is also consistent with detailed hydrodynamical simulations by Stein & Nordlund (1991) for the solar case and by Trampedach (1996) for η Bootis and α Centauri.

One of the largest deficiencies in modelling more accurate eigenfunctions in stars with distinctive surface convection zones is the lack of a proper convection theory which can cope the interaction with pulsation in a realistic way. Although several attempts have been made in the last years to address this problem (for a review see Baker 1987) none of the proposed prescriptions seem to be considered as a complete theory. The time-dependent theory of Gough (1977) put much emphasis on the effects of the initial conditions under which each eddy is created, i.e. the phase of pulsation of the time-varying mean field at the birth of the eddy, whereas other prescriptions (e.g. Stellingwerf 1982; Kuhfuss 1986) considered the effects of the interactions with the turbulent small-scale motions in more detail. It was demonstrated by Balmforth (1992a), however, that mode stability in the solar case depends crucially on the initial conditions out of which eddies evolve and less on the effects associated with the dynamics by the small scale turbulence, when modelled by means of an enhanced viscosity ν_e [see equation (2.104)]. Extending Gough's time-dependent theory by means of a non-local treatment, as implemented by Balmforth (1992a) and reviewed in section 2.4.2, seems therefore one of the most promising prescription of convection in a pulsating envelope, available today. In a non-local treatment of the turbulent fluxes, the turbulent pressure and in particular its gradient can be implemented consistently in the computations. The effects of the turbulent pressure and its pulsationally induced fluctuations upon model results relevant to the field of helio- and asteroseismology were discussed in great detail.

The substantial contributions of the turbulent pressure gradient to the hydrostatic support has been demonstrated for models of the Sun and η Boo. In both models the changes in the mean stratification of the superadiabatic layers due to the inclusion of the mean turbulent pressure was such, that the discrepancy between observed and adiabatically computed oscillation frequencies was reduced. Non-adiabatic effects and turbulent pressure variations on the other hand suggest to increase the frequencies in the opposite sense to the observed discrepancy, implying that little correction is required to the frequencies obtained in the adiabatic approximation and in the absence of turbulent pressure. From these results we may conclude that turbulent pressure should be taken into account in the computations in order to reproduce more adequately the mean stratification of the convectively unstable boundary layers, which is also in agreement with the results obtained from hydrodynamical simulations (Rosenthal *et al.* 1995).

As noted by Balmforth (1992a) for the solar case, the perturbation in the momentum flux, $\delta p_{\rm t}$, or more precisely its phase relative to the density fluctuations, contribute

significantly to modal damping rates in solar-type stars. With its inclusion in the stability analysis, all modes were found to be stable for models with effective temperatures of roughly $\log T \lesssim 3.85$. For models with higher effective temperature the computations predict well-defined instability strips for the fundamental and higher-order modes, lying more or less in the δ Scuti range. Furthermore, it has been demonstrated, that the return to stability at the red edge of the lower δ Scuti instability domain is solely determined by the damping contributions associated with the variations in the momentum flux. However, it appears that the turbulent pressure fluctuations are also responsible for driving higher-order radial modes in stars lying in the lower δ Scuti instability strip, as discussed for the star FG Virginis. These results demonstrate quite obviously the importance of the momentum flux variations in pulsation calculations and hence, $\delta p_{\rm t}$ should not be neglected in the stability analysis.

Amplitudes of intrinsically damped and stochastically driven modes were estimated for stars evolving along the main-sequence. The computations suggest that the amplitudes increase quite steeply with increasing luminosity and that they appear to depend less on the model's effective temperature. For a $1.5\,\mathrm{M}_\odot$ star of spectral type F1 the predicted luminosity amplitude could reach values of ~ 78 ppm and hence, ~ 16 times larger than the values measured in the Sun. The estimated amplitudes obtained in this study, may help observers in the choosing process for targets stars and for deciding whether a given star is best observed in luminosity or velocity. The most promising evidence of solar-like oscillations in a star other than the Sun was proposed for η Boo by Kjeldsen *et al.* (1995), and for which the computed amplitude of ~ 36 ppm agree fairly well with the observations. However, for stars like Procyon and members of M67 no unambiguous detection of solar-like oscillations were found so far, although the predicted amplitude values are larger than the detection threshold of the used instrumentation. The convective velocities, computed according to mixing-length theory, might therefore still be overestimated for more massive stars, as it was noted before by Christensen-Dalsgaard & Frandsen (1983b). From the asteroseismological space project COROT one may hope to obtain accurate data of amplitudes on which one could apply at least a limited inversion, to obtain information about the properties of convection, such as the convective velocity field. Amplitudes obtained over a wide range of stellar parameters would therefore be very helpful to improve theories of stellar convection.

Beside data of line widths and amplitudes, additional information is available from observations of amplitude ratios and phase differences (the so called non-adiabatic observables) between different types of oscillation measurements. With the inclusion of convective dynamics in the pulsation calculations and using the Eddington approximation to radiative transfer, a decent agreement is obtained between theory and observations of amplitude ratios and phase shifts in the solar atmosphere. These non-adiabatic observables may also be used for radial and non-radial mode identification in classical pulsating stars, demanding accurate non-adiabatic eigenfunctions in the superficial layers. For cooler stars with surface convection zones accurate eigenfunctions may only be obtained with the inclusion of the turbulent flux perturbations in the model computations, as discussed for the δ Scuti star FG Vir.

Frequencies of gravity modes, which are believed to be already detected in some δ Scuti stars (e.g. Breger *et al.* 1995), provide strong constraints on conditions in the stellar core,

such as convective overshooting (Dziembowski & Pamyatnykh 1991; Audard, Provost & Christensen-Dalsgaard 1995). Overshoot from a convective core would have a very substantial effect on age determinations based in the location of clusters in the HR diagram. Moreover, the region just outside the convective stellar core is supposed to be superadiabatic, however, dynamically stabilized by the spatial gradient of the mean molecular weight (semi-convection). In this zone high order g modes appear to be excited by the Cowling mechanism (e.g. Unno *et al.* 1989). Measurements of g modes and comparing estimated amplitudes and phase shifts of non-radial oscillations with observations would provide additional constraints on the control parameters of stellar evolution theory (e.g. Brown *et al.* 1994). Thus one of the most important and promising tasks for the future study of pulsation properties in solar-type stars as well as in low-amplitude variables would therefore be the extension of Gough's time-dependent convection theory for non-radial modes.

A. Implementation Details

A.1. Equilibrium Model

A.1.1. Equations for the local Mixing-length Theory

The equations for hydrostatic equilibrium and continuity for a spherical shell with radius r enclosing the mass m are

$$\frac{dp}{dm} = -\frac{g}{4\pi r^2}\left[1 + (3-\Phi)\,\frac{p_\mathrm{t}}{\rho g r}\right], \tag{A.1}$$

and

$$\frac{dr}{dm} = \frac{1}{4\pi r^2 \rho}. \tag{A.2}$$

They are supplemented by an energy-equation, which may be written in the absence of any energy-producing layers due to nuclear reactions, in the following form

$$\rho\frac{\partial q}{\partial t} = -div\,\mathbf{F}, \tag{A.3}$$

The first law of thermodynamics provides the expression

$$dq = c_\mathrm{p} dT - \frac{\delta}{\rho} dp_\mathrm{g}, \tag{A.4}$$

providing the energy equation for a spherically symmetric envelope

$$c_\mathrm{p}\frac{\partial T}{\partial t} - \frac{\delta}{\rho}\frac{\partial p_\mathrm{g}}{\partial t} = -4\pi\,\frac{\partial}{\partial m}\left[r^2\,(F_\mathrm{r} + F_\mathrm{c})\right]. \tag{A.5}$$

In a static envelope, i.e., setting $\partial/\partial t = 0$, Eq. (A.5) has the first integral

$$4r^2\pi\,(F_\mathrm{r} + F_\mathrm{c}) = L. \tag{A.6}$$

Assuming the envelope to be in thermal equilibrium the luminosity L is constant outside the energy-producing core.

The system of equations is closed by providing proper expressions for the radiative and convective fluxes. Assuming the horizontally averaged integrated mean intensity J to be

equal to the mean Planck function B, the mean radiative transfer equation reduces to the diffusion approximation

$$F_{\rm r} \;=\; -\frac{4\,a_{\rm r}\,c\,T^3}{3\,\varkappa\,\rho}\frac{dT}{dr}\,. \tag{A.7}$$

The turbulent fluxes of heat, $F_{\rm c}$, and momentum, $p_{\rm t}$, are obtained according to the local mixing-length prescription of convection, described by the equations (2.78) and (2.79). The inclusion of the turbulent pressure, in particular its gradient in the equation for hydrostatic support, increases the order of the system of differential equations by one. For this case, the definition of the superadiabatic lapse rate β, provides an expression for the turbulent pressure gradient by inverting Eq. (2.25), yielding

$$\frac{dp_{\rm t}}{dr} \;=\; \frac{dp}{dr} - \frac{\rho c_{\rm p}}{\delta}\left(\beta + \frac{dT}{dr}\right)\,, \tag{A.8}$$

where $p = p_{\rm g} + p_{\rm t}$ is the total pressure. However, this equation possesses singular points at the edges of the convection zone (Gough 1976; Stellingwerf 1976) which complicates the numerical treatment substantially. This can be avoided by replacing the gas pressure gradient by the total pressure gradient in Eq. (2.25) which is equivalent to setting the left-hand side of Eq. (A.8) to zero. Hence, the order of the differential system is artificially reduced by one and the turbulent pressure can be found by iteration. This approximation has been employed in the computation with the local theory, which is not necessary to apply when using the non-local equations for convection.

In terms of the independent variable $\log p$, the equations for a steady mean envelope using the diffusion approximation to radiative transfer may be rewritten as

$$\frac{d\log m}{d\log p} \;=\; -\frac{4\pi r^2 p}{mg}\tilde{\mu}\,, \tag{A.9}$$

$$\frac{d\log r}{d\log p} \;=\; -\frac{p}{\rho g r}\tilde{\mu}\,, \tag{A.10}$$

$$\frac{d\log T}{d\log p} \;=\; -\frac{3\varkappa p L_{\rm r}}{16\pi r^2 a_{\rm r} c T^4 g}\tilde{\mu}\,, \tag{A.11}$$

where the function $\tilde{\mu}$ is given by

$$\tilde{\mu} \;=\; \left[1 + (3-\Phi)\,p_{\rm t}/\rho g r\right]^{-1}\,, \tag{A.12}$$

and describes the dynamical correction to the total pressure gradient due to the anisotropy of the Reynolds stresses.

The system of equations are solved as an initial value problem integrating from the surface inward. For the integration a fourth-order Runge-Kutta-Fehlberg scheme was employed.

A.1.2. Equations for the non-local Mixing-length Theory

In the upper layers of the convection zone, where there is the transition from convection to radiation, radiative equilibrium is no longer maintained, and the diffusion approximation, Eq. (A.7), becomes invalid. Out of equilibrium, the Eddington approximation is more general than the optically thick approximation. It describes in non-equilibrium situations the optically thick and thin limits ($\tau = 0$) exactly. However, above the convection zone, the mean radiation intensity J is equal to the Planck function B and hence, the Eddington approximation collapses back to the diffusion approximation. Since it is known, that the Eddington approximation produces solutions for the radiation field with an accuracy to about 10% in the optically thin regions, a $T - \tau$ relation, fitted to a model atmosphere, was chosen instead for the static mean atmosphere.

The radiative transfer equation for a grey, static and spherically symmetric atmosphere (e.g. Mihalas 1978) is given by

$$\mu \frac{\partial I}{\partial r} + \frac{1}{r}\left(1-\mu^2\right)\frac{\partial I}{\partial \mu} \;=\; \rho\varkappa\,(B - I)\;, \tag{A.13}$$

where μ is the direction cosine of the incident beam with respect to the radius vector. Following Eddington's approach, the zeroth moment is obtained by integrating Eq. (A.13) over all solid angles Ω

$$div\, F_{\rm r} \;=\; \frac{1}{r^2}\frac{\partial}{\partial r}\left(r^2 F_{\rm r}\right) \;=\; -4\pi\rho\varkappa\,(J - B)\;, \tag{A.14}$$

where the mean intensity and radiative flux are

$$J \;=\; \frac{1}{4\pi}\int I\, d\Omega \qquad \text{and} \qquad F_{\rm r} \;=\; \int \mu I\, d\Omega\,, \tag{A.15}$$

respectively. Since we are using a $T-\tau$ relation for describing the radiative transfer in the mean atmosphere, we implemented a spatially varying Eddington factor $f_{\rm eq}$ (Auer & Mihalas 1970) in the atmosphere in order to be consistent with the Eddington approximation employed in the pulsation calculation. With the definition for the Eddington factor

$$f_{\rm eq} \;=\; \frac{K}{J}\,, \tag{A.16}$$

where K denotes the second moment of the radiation field, the first moment of equation (A.13) becomes

$$\frac{\partial}{\partial r}\left(f_{\rm eq} J\right) + \frac{1}{r}\left(3 f_{\rm eq} - 1\right) J \;=\; -\frac{1}{4\pi}\rho\varkappa F_{\rm r}\,. \tag{A.17}$$

The second term of the left hand side of Eq. (A.17) may be considered as a measure of the "curvature" of the spherical geometry and is neglected for a plane parallel atmosphere.

For most of the stars, being in their main-sequence phase, the plane parallel atmosphere is an adequate assumption. However, the density in the outer regions of red super-giants, for example, are so small, that the atmosphere can cover up to 40% of the outer radius and a plane parallel atmosphere is no longer appropriate. Since we are mainly interested in solar-like stars, we consider here a plane-parallel atmosphere and the Eddington approximation is described by the two first-order, ordinary differential equations

$$\frac{d\ln J}{dm} = -\frac{\varkappa L_{\rm r}}{64\pi^3 r^4 (f_{\rm eq} J)} \left[1 + \frac{d\ln f_{\rm eq}}{d\ln J}\right]^{-1} , \tag{A.18}$$

and

$$\frac{dL_r}{dm} = 4\pi\varkappa (B - J) . \tag{A.19}$$

Because in a plane-parallel atmosphere, the radiative flux is constant (assuming the convective layers lying below the atmosphere), the independent variable can be changed to the optical depth τ. Using a detailed model atmosphere, the Eddington factor $f_{\rm eq}$ can be derived as

$$f_{\rm eq}(\tau) = \frac{1}{3}\left[\frac{\tau + q(2/3)}{\tau + q(\tau)}\right] , \tag{A.20}$$

where $q(\tau)$ is the Hopf function fitted to a model atmosphere

$$T^4 = \frac{3}{4} T_{\rm eff}^4 [\tau + q(\tau)] . \tag{A.21}$$

The functional form of $f_{\rm eq}(T)$ used in the computations was derived from a model C of Vernazza, Avrett & Loeser (1981).

For the pure isotropic case, $f_{\rm eq} = 1/3$ and hence, Eq. (A.18) simplifies to it's usual form

$$\frac{dJ}{dm} = -\frac{3\varkappa}{64\pi^3 r^4} L_{\rm r} . \tag{A.22}$$

For radiative equilibrium, where $J = B$, $dL_{\rm r}/dm$ becomes zero, and equations (A.19) and (A.18) are replaced by the single equation (A.11), i.e. the diffusion approximation.

In the mean static envelope the divergence of the total energy flux must vanish providing the expression

$$\frac{dL_r}{dm} = -\frac{dL_c}{dm} , \tag{A.23}$$

and thus the equality

$$\frac{a_r c T^4}{4\pi} = B = J - \frac{1}{4\pi\varkappa}\frac{dL_c}{dm}\,, \tag{A.24}$$

which is solved by iteration for the temperature.

An expression for the temperature gradient, $\nabla = d\ln T/d\ln p$, may be obtained from taking the first derivative of equation (A.24), which yields

$$\begin{aligned}\nabla &= \frac{1}{4B + \varkappa_{\rm T}\,(B-J)} \\ &\quad\times\left[J\frac{d\ln J}{d\ln p} + (B-J)\left(\frac{d\ln m}{d\ln p} - 4\frac{d\ln r}{d\ln p} - \varkappa_{\rm p}\frac{d\ln p_{\rm g}}{d\ln p}\right) + \frac{G}{4\pi r^2}\frac{m}{p\varkappa}\frac{d^2F_c}{d\ln p^2}\right]\,,\end{aligned} \tag{A.25}$$

where the dynamical correction factor for the pressure gradient, $\tilde{\mu}$, has been neglected and the relation

$$\frac{d\ln\varkappa(p_{\rm g},T)}{d\ln p} = \left(\frac{\partial\ln\varkappa}{\partial\ln T}\right)_{\rm p_g}\nabla + \left(\frac{\partial\ln\varkappa}{\partial\ln p_{\rm g}}\right)_{\rm T}\frac{d\ln p_{\rm g}}{d\ln p}\,, \tag{A.26}$$

has been applied. With the help of equation (A.25), the expression for the superadiabatic lapse rate, β [cf. equation (2.25)], can be defined as

$$\beta = -\frac{dT}{dr} + \left(\frac{dT}{dr}\right)_{\rm ad} = \frac{T}{H_{\rm p}}\nabla - \frac{\delta g}{c_{\rm p}\tilde{\mu}}\frac{dp_{\rm g}}{dp}\,, \tag{A.27}$$

where

$$H_{\rm p} = -\frac{d\,r}{d\ln p} = -\frac{p}{\rho g}\tilde{\mu}\,, \tag{A.28}$$

is the scale height of the total pressure. In contrast to the local mixing-length theory, the superadiabatic lapse rate in the non-local theory does not exhibit singular points at the edges of the convection zone and can therefore be computed consistently.

In section 2.4 we introduced the equations describing the non-local mixing-length theory according to Gough (1976). Assuming a plane parallel atmosphere and using the equations (2.92) and (A.28), the expressions for the convective heat-flux, Eq. (2.98), averaged superadiabatic lapse rate, Eq. (2.101) and turbulent pressure, Eq. (2.102), become

$$\frac{d^2F_c}{d\ln p^2} = \frac{a^2}{\alpha_{\rm c}^2}\left(F_c - \frac{1}{4}F_c^{\rm loc}\right)\,, \tag{A.29}$$

$$\frac{d^2\mathscr{B}}{d\ln p^2} = \frac{b^2}{\alpha_{\rm c}^2}\left(\mathscr{B} - \beta\right)\,, \tag{A.30}$$

and

$$\frac{d^2 p_\mathrm{t}}{d\ln p^2} = \frac{a^2}{\alpha_\mathrm{c}^2}\left(p_\mathrm{t} - p_\mathrm{t}^\mathrm{loc}\right), \tag{A.31}$$

where

$$F_c^\mathrm{loc} = \frac{1}{4}\frac{\rho c_p \Phi T}{g\delta}\sigma^3 \ell_\mathrm{c}^2, \tag{A.32}$$

and

$$p_\mathrm{t}^\mathrm{loc} = \frac{1}{4}\rho\sigma^2\ell_\mathrm{c}^2, \tag{A.33}$$

denote the source functions of the turbulent heat and momentum flux, obtained according to the local mixing-length formulation [cf. equation (2.78) and (2.79)].

The equations discussed above build a system of ninth order and are implemented in the following form

$$\frac{d\log m}{d\log p} = -4\pi r^2 \frac{p}{mg}\tilde{\mu}, \tag{A.34}$$

$$\frac{d\log r}{d\log p} = -\frac{p}{\rho g r}\tilde{\mu}, \tag{A.35}$$

$$\frac{d\log J}{d\log p} = \frac{\varkappa p L}{16\pi^2 r^2 g\,(f_\mathrm{eq} J)}\,(1-f)\,\tilde{\mu}\left[1 + \frac{d\ln f_\mathrm{eq}}{d\ln J}\right]^{-1}, \tag{A.36}$$

$$\frac{df}{d\log p} = \frac{z_f}{(\alpha_\mathrm{c}\log e)^2}, \tag{A.37}$$

$$\frac{dz_f}{d\log p} = a^2\left(f - f^\mathrm{loc}\right), \tag{A.38}$$

$$\frac{d\mathscr{B}}{d\log p} = \frac{z_\beta}{(\alpha_\mathrm{c}\log e)^2}, \tag{A.39}$$

$$\frac{dz_\beta}{d\log p} = b^2\left(\mathscr{B} - \beta\right), \tag{A.40}$$

$$\frac{d\nu_1}{d\log p} = \frac{z_t}{(\alpha_\mathrm{c}\log e)^2} - \frac{\nu_1}{\log e}, \tag{A.41}$$

$$\frac{dz_t}{d\log p} = a^2\left(\nu_1 - \nu_1^\mathrm{loc}\right) - \frac{z_t}{\log e}, \tag{A.42}$$

where $f = L_c/L$, $\nu_1 = p_\mathrm{t}/p$ and f^loc and ν_1^loc are the corresponding values obtained with the local mixing-length theory. The new introduced variables z_f, z_β and z_t are defined as

$$z_f \;=\; \frac{df}{d\log p}\,(\alpha_{\rm c}\log e)^2\;, \tag{A.43}$$

$$z_\beta \;=\; \frac{d\mathscr{B}}{d\log p}\,(\alpha_{\rm c}\log e)^2\;, \tag{A.44}$$

$$z_t \;=\; \frac{1}{p}\frac{dp_{\rm t}}{d\log p}\,(\alpha_{\rm c}\log e)^2\;. \tag{A.45}$$

The temperature gradient and the superadiabatic lapse rate are computed according to Eq. (*A*.25) and Eq. (*A*.27).

In order to solve the system of Eq. (*A*.34)–Eq. (*A*.42) we still need nine boundary conditions, where three of them are specified by the mass, radius and effective temperature of the model. The remaining six conditions are obtained from the fact that the locally computed source-functions in Eq. (*A*.38) and Eq. (*A*.42) appear to vanish at the boundaries of the convection zone. The second-order differential equation for the non-local turbulent fluxes may then be written in the general form

$$\frac{d^2}{d\log p^2}\psi \;=\; \alpha^2\psi\,, \tag{A.46}$$

where ψ is either of F_c, $\mathscr{B}$ or $p_{\rm t}$ and

$$\alpha^2 \;=\; \frac{a_i^2}{(\alpha_{\rm c}\log e)^2}\,, \qquad a_i \;=\; \{a\,,b\}\,, \tag{A.47}$$

with the general solution

$$\psi \;=\; Ae^{\pm\alpha\log p}\,. \tag{A.48}$$

The convective heat fluxes decay exponentially with $\log p$ in the convectively stable layers adjoining the overturning layers. The characteristic length-scale of the turbulent overshoot is determined by the value $\ell/a = (\alpha_{\rm c}/a)H_{\rm p}$. With typical values for $\alpha_{\rm c} = 2$ and $a^2 = 900$ the characteristic distance of the overshooting is 1/15 of the pressure scale-height. This is in fair agreement with other investigations (e.g. Latour, Toomre & Zahn 1981). Above the convection zone $\log p$ decreases to smaller values, providing a positive value for α, whilst below the convection zone $\log p$ increases, forcing α to be negative. With the relation

$$z_i \;=\; (\alpha_{\rm c}\log e)^2\,\frac{d\psi}{d\log p} \;=\; \pm\,(a_i\alpha_{\rm c}\log e)\,\psi\,, \qquad z_i \;=\; \{z_f\,,z_t\}\,, \tag{A.49}$$

the general expression for the boundary condition is given by

$$z_i \pm (a_i\alpha_{\rm c}\log e)\,\psi \;=\; 0\,, \tag{A.50}$$

which provides the four boundary conditions

$$\frac{dF_c}{d\ln p} = \pm\frac{aF_c}{\alpha_c}\,, \tag{A.51}$$

and

$$\frac{dp_t}{d\ln p} = \pm\frac{ap_t}{\alpha_c}\,. \tag{A.52}$$

Finally the last two boundary conditions are obtained from the requirement

$$\mathscr{B} \to \beta\,, \tag{A.53}$$

outside the overturning layers, yielding

$$\frac{dz_\beta}{d\ln p} = b^2\,(\mathscr{B}-\beta) = 0\,. \tag{A.54}$$

A.2. Pulsation Model

The calculation of the non-adiabatic eigenfunctions and eigenfrequencies are performed in three steps. In a first step the pulsation equations are solved in the adiabatic approximation providing a trial solution for the quasi-adiabatic approximation to the non-adiabatic equations (e.g. Däppen 1993). The latter equations are then solved using first the local mixing-length theory, followed by a re-integration process assuming the non-local formulation for convection.

A.2.1. Linear adiabatic radial oscillation

The solutions of the linearized oscillation equations do have exponentional time dependence yielding the following form for any mean variable such as the total pressure, for example

$$p\,(r,t) = p_0\,(r)\left[1 + \frac{\delta p}{p_0}\,(r)\,e^{i\omega t}\right], \tag{A.55}$$

where the subscript zero denotes the value in the equilibrium model and the quantity $\delta p/p_0$ represents the relative perturbation in a Lagrangian frame of reference; ω is the eigenfrequency, which is usually a complex quantity. In the adiabatic case one assumes that the mass elements in the star neither gain nor lose heat, *i.e.* the entropy s remains constant and the eigenfrequency ω becomes purely real. In this case the equation of state can be written in the form

$$\frac{\delta p_{\rm g}}{p_{\rm g0}} \;=\; \Gamma_1 \frac{\delta\rho}{\rho_0}\,, \tag{A.56}$$

where Γ_1 is the first adiabatic exponent as defined by the equation (3.42).

Perturbing the equations for momentum (A.1) and continuity (A.2), as well as using the relation (A.56) the adiabatic pulsation equations become to first order in the relative perturbations

$$\frac{\partial}{\partial \ln p_0}\left(\frac{\delta r}{r_0}\right) \;=\; \frac{p_0 r_0}{Gm\rho_0}\left(3\frac{\delta r}{r_0} \;+\; \tilde{\Gamma}_1^{-1}\frac{\delta p}{p_0}\right)\,, \tag{A.57}$$

$$\frac{\partial}{\partial \ln p_0}\left(\frac{\delta p}{p_0}\right) \;=\; -\frac{\delta p}{p_0} - \left(4 \;+\; \frac{\omega^2}{\Omega^2}\right)\frac{\delta r}{r_0}\,, \tag{A.58}$$

where

$$\Omega^2 \;=\; \frac{Gm}{r_0^3}\,, \tag{A.59}$$

and $\tilde{\Gamma}_1$ denotes the modified first adiabatic exponent if turbulent pressure $p_{\rm t}$, is considered in the model calculations [cf. equation (3.43)]. The dynamical correction factor to the pressure gradient, $\tilde{\mu}$, has been neglected in the momentum equation.

As reasonable general boundary conditions, one usually demands that all relative pulsation variables be regular both at the centre and surface of the star. At the base of the model envelope we impose a vanishing displacement

$$\frac{\delta r}{r_0} \;=\; 0\,. \tag{A.60}$$

At the surface the mechanical condition is that appropriate to an isothermal atmosphere. This is a reasonable approximation, since in a real atmosphere the temperature variation is much slower than the variation in pressure or density. In the upper part of the atmosphere (near the temperature minimum, *e.g.* at an optical depth $\tau \sim 10^{-4}$ in the solar case) the density is so low that the gas looses energy very inefficiently by radiation, and hence the motion is nearly adiabatic. Eq. (A.57) and Eq. (A.58) may be written as a single, second-order equation for the relative displacement $x = \delta r/r_0$

$$\frac{d^2x}{dr^2} \;-\; \left(\frac{3}{r_0} \;-\; \frac{1}{H_\rho}\right)\frac{dx}{dr} \;+\; \frac{1}{r_0 H_\rho}\left[\frac{1}{\Gamma_1}\left(4+\frac{\omega^2}{\Omega^2}\right) - 3\right]x \;=\; 0\,, \tag{A.61}$$

where $H_\rho = -d\,r/d\,\ln\rho$ denotes the scale height of the density (which is evidently equal to $H_{\rm p}$ for an atmosphere treating the gas as ideal with constant mean molecular weight).

If we assume that the thickness of the atmosphere is small compared with the radius R of the star, r_0 may be set to the constant value R wherever it appears in the coefficients. Hence, the first term in the coefficient of dx/dr can be neglected, and Eq. (A.61) exhibits constant coefficients and the solution may therefore be written as

$$x\,(r) \;=\; c_1\,\exp\left(\frac{r}{H_\rho}\lambda_+\right) \;+\; c_2\,\exp\left(\frac{r}{H_\rho}\lambda_-\right)\,, \tag{A.62}$$

where

$$\lambda_\pm \;=\; \frac{1}{2} \;\pm\; \frac{1}{2}\left\{1 \;-\; \frac{4H_\rho}{R}\left[\frac{1}{\Gamma_1}\left(4 \;+\; \frac{\omega^2}{\Omega^2}\right) \;-\; 3\right]\right\}^{1/2}\,. \tag{A.63}$$

Since the pulsational energy of the atmosphere must remain finite as r tends to infinity, only the λ_- solution has a physically reasonable meaning. Using Eq. (A.59), it can be shown that the term

$$\frac{4H_\rho r_0^2}{\Gamma_1 Gm}\omega^2 \;=\; \frac{\omega^2}{\omega_{\rm co}^2}\,, \tag{A.64}$$

where

$$\omega_{\rm co} \;=\; \frac{c_s}{2H_\rho}\,, \tag{A.65}$$

is the so called *acoustical cut-off frequency* (Lamb 1906), and Eq. (A.63) may be written in the form

$$\lambda_- \;=\; \frac{1}{2} \;-\; \frac{1}{2}\left[1 \;-\; \frac{4H_\rho}{R}\left(\frac{4}{\Gamma_1} \;-\; 3\right) \;-\; \frac{\omega^2}{\omega_{\rm co}^2}\right]^{1/2}\,. \tag{A.66}$$

Assuming $H_\rho/R \ll 1$ everywhere in the atmosphere, the middle term of the expression enclosed between the brackets may be neglected compared to 1 and the remaining expression of Eq. (A.66) may explain the physical meaning of $\omega_{\rm co}$. For $\omega < \omega_{\rm co}$, λ_- is real and the variation grows or decays exponentially; however, if $\omega > \omega_{\rm co}$, λ_- is complex and the motion corresponds to a propagating wave through the atmosphere. Hence, $\omega_{\rm co}$ represents the minimum frequency for propagating waves and the maximum frequency for reflecting p modes.

Applying the approximation $H_\rho/R \ll 1$ to Eq. (A.63), we have to first order

$$\lambda_- \;=\; \frac{H_\rho}{R}\left[\frac{1}{\Gamma_1}\left(4 \;+\; \frac{\omega^2}{\Omega^2}\right) \;-\; 3\right]\,. \tag{A.67}$$

Using the continuity equation Eq. ($A.2$) and the adiabatic equation of state Eq. ($A.56$), yields the expression

$$\frac{\delta p}{p_0} = -\Gamma_1 \left(3x + r_0 \frac{\partial x}{\partial r} \right) . \qquad (A.68)$$

Inserting solution ($A.62$) into Eq. ($A.68$), the mechanical boundary condition at the surface becomes with the help of Eq. ($A.67$)

$$\frac{\delta p}{p_0} = -\left(4 + \frac{\omega^2}{\Omega^2} \right) \frac{\delta r}{r_0} . \qquad (A.69)$$

Because of the linearity of the equations, the normalization of $\delta r/r_0$ is arbitrary and one usually chooses (e.g. Cox 1980)

$$\frac{\delta r}{r_0} = 1 . \qquad (A.70)$$

The boundary conditions ($A.69$) and ($A.70$) are applied at a suitable point in the atmosphere, such as the temperature minimum.

The equations ($A.57$) and ($A.58$) together with the boundary conditions ($A.60$), ($A.69$) and ($A.70$) form a *Sturm Liouville eigenvalue problem* for the eigenvalue ω and the eigenfunctions $\delta r/r_0$ and $\delta p/p_0$. The problem is solved numerically and provides the trial solution for the computation of the non-adiabatic pulsation equations using the local, time-dependent mixing-length theory according to Gough (1977).

A.2.2. Linear non-adiabatic radial oscillation using local MLT

The non-adiabatic eigenfunctions are computed first assuming the local, time-dependent formulation for convection, providing a trial solution for the pulsation equation appropriate to the non-local theory. The equations are obtained by perturbing the corresponding equations describing the equilibrium structure, Eq. ($A.9$)–($A.11$) and Eq. ($A.5$), with the terms non-linear in the fluctuations excluded. Using the equation of state written in the form

$$\frac{\delta \rho}{\rho} = \alpha_0 \frac{\delta p_{\rm g}}{p_{\rm g0}} - \delta_0 \frac{\delta T}{T_0} , \qquad (A.71)$$

the gas dynamic equations governing linear non-adiabatic radial pulsation are

$$\frac{\partial}{\partial \ln p_0} \left(\frac{\delta r}{r_0} \right) = \tilde{\mu} \frac{p_0 r_0}{G m \rho_0} \left(3 \frac{\delta r}{r_0} + \alpha_0 \frac{\delta p_{\rm g}}{p_{\rm g0}} + \delta_0 \frac{\delta T}{T_0} \right) , \qquad (A.72)$$

$$\frac{\partial}{\partial \ln p_0}\left(\frac{\delta p}{p_0}\right) = -\left\{\frac{\delta p}{p_0} + \left[3 + \tilde{\mu}\left(1 + \frac{\omega^2}{\Omega^2}\right)\right]\frac{\delta r}{r_0} + \tilde{\mu}\nu_1 \frac{p_0 r_0}{Gm\rho_0} \times \left[(3 - \Phi_0)\left(\alpha_0 \frac{\delta p_{\rm g}}{p_{\rm g0}} - \delta_0 \frac{\delta T}{T_0} - \frac{\delta p_{\rm t}}{p_{\rm t0}}\right) - \delta\Phi\right]\right\}, \tag{A.73}$$

$$\frac{\partial}{\partial \ln p_0}\left(\frac{\delta T}{T_0}\right) = \tilde{\mu}\frac{3\varkappa_0 L_{r0} p_0}{16\pi a_{\rm r} c G m T_0^4}\left[\frac{\delta L_{\rm r}}{L_{r0}} + \varkappa_{\rm p}\frac{\delta p_{\rm g}}{p_{\rm g0}} + (\varkappa_{\rm T} - 4)\frac{\delta T}{T_0} - 4\frac{\delta r}{r_0}\right], \tag{A.74}$$

$$\frac{\partial}{\partial \ln p_0}\left(\frac{\delta L}{L_0}\right) = i\omega\tilde{\mu}\frac{4\pi r_0^4 p_0 c_{\rm p0} T_0}{G m L_0}\left(\frac{\delta T}{T_0} - \nabla_{\rm ad}\frac{\delta p_{\rm g}}{p_{\rm g0}}\right), \tag{A.75}$$

using

$$\delta L = \delta L_{\rm r} + \delta L_{\rm c}, \tag{A.76}$$

and

$$\delta p = \delta p_{\rm g} + \delta p_{\rm t}, \tag{A.77}$$

and where $\varkappa_{\rm p} = (d\ln\varkappa_0/d\ln p_{\rm g0})_{T_0}$, $\varkappa_{\rm T} = (d\ln\varkappa_0/d\ln T_0)_{p_{\rm g0}}$.

The fluctuation in $F_{\rm c}$, $p_{\rm t}$ and shape factor Φ are computed according to the local time-dependent prescription of convection expressed by the equations (2.88), (2.89) and (2.90).

Outside the convection zones, the turbulent pressure becomes zero, yielding $\tilde{\mu} = 1$, and $\nu_1 = p_{\rm t}/p = 0$ and the momentum equation (*A*.73) reduces to (*A*.58).

The non-adiabatic pulsation equations are of fourth order requiring two more boundary conditions as in the adiabatic case. At the surface an additional condition may be obtained from perturbing the temperature-optical-depth relation for an Eddington atmosphere (Baker & Kippenhahn 1965)

$$T^4(\tau) = \frac{3}{4}T_{\rm eff}(\tau + 2/3), \tag{A.78}$$

providing the thermal condition

$$\frac{\delta L}{L_0} = 2(1 + f_\tau)\frac{\delta r}{r_0} + (4 - \varkappa_{\rm T} f_\tau)\frac{\delta T}{T_0} - \varkappa_{\rm p}\frac{\delta p}{p_0}, \tag{A.79}$$

where

$$f_\tau \;=\; \frac{\tau_0}{\tau_0 + 2/3}\,, \tag{A.80}$$

and τ_0 represents the unperturbed optical depth. Setting $\tau_0 = 0$ we obtain the usual condition

$$2\frac{\delta r}{r_0} + 4\frac{\delta T}{T_0} - \frac{\delta L_{\rm r}}{L_{\rm r0}} \;=\; 0\,. \tag{A.81}$$

At the bottom of the model envelope the pulsation-thermodynamics are assumed to be sufficiently adiabatic providing the condition

$$\nabla_{\rm ad}\frac{\delta p_{\rm g}}{p_{\rm g0}} - \frac{\delta T}{T_0} \;=\; 0\,. \tag{A.82}$$

The non-adiabatic pulsation equations (*A*.72)- (*A*.75), supplemented by the five boundary conditions (*A*.60), (*A*.69), (*A*.70), (*A*.79) and (*A*.82), describe a linear eigenvalue problem for the complex eigenfrequency ω. The real part of ω represents the pulsation period of the star and the imaginary part denotes the damping or excitation rate. The system of equations are solved by a second-order Newton-Raphson-Kantorovich algorithm, solving the eigenfunctions and eigenvalues simultaneously (Baker, Moore & Spiegel 1971; Cash & Moore 1980), which explains the need of the additional boundary condition (*A*.60). The starting solution for the iteration may be obtained from the quasi-adiabatic approximation to the non-adiabatic system. In this approximation the adiabatic eigenfunctions $\delta r/r_0$ and $\delta p/p_0$ are inserted into equation (*A*.82) providing an expression for the temperature fluctuation $\delta T/T_0$. The corresponding quasi-adiabatic eigenfunction of the luminosity fluctuation may then be obtained from equation (*A*.74) using the relation

$$\frac{\partial}{\partial \ln p_{\rm g0}}\left(\frac{\delta T}{T_0}\right) \;=\; \nabla_{\rm ad}\frac{\delta p_{\rm g}}{p_{\rm g0}} + p_{\rm g}\frac{\partial \nabla_{\rm ad}}{\partial \ln p_0}\,, \tag{A.83}$$

where

$$\frac{\partial \nabla_{\rm ad}}{\partial \ln p_{\rm g0}} \;=\; \left(\frac{\partial \nabla_{\rm ad}}{\partial \ln p_{\rm g0}}\right)_{\rm T} + \left(\frac{\partial \nabla_{\rm ad}}{\partial \ln T_0}\right)_{\rm p_g} \nabla\,. \tag{A.84}$$

A.2.3. Linear non-adiabatic radial oscillation using non-local MLT

The solutions of the eigenfunctions and eigenfrequencies discussed in the previous section are used as a trial solution for the computation of the linear stability analysis problem using the non-local, time-dependent mixing-length theory.

In order to be consistent with the computation in the equilibrium model, the treatment of radiation transfer has been employed in the Eddington approximation. The equations ($A.19$) and ($A.18$) become to first order in the perturbations

$$\frac{\partial J}{\partial m} = -\frac{\varkappa L_{\mathrm{r}0}}{64\pi^3 r_0^4 \left(f_{\mathrm{eq}} J_0\right)} \left(\frac{\delta L_{\mathrm{r}}}{L_{\mathrm{r}0}} - \frac{\delta\varkappa}{\varkappa_0} - 4\frac{\delta r}{r_0} - \frac{\delta J}{J_0} \right) , \tag{$A.85$}$$

and

$$\frac{\partial}{\partial m}\left(\delta L_{\mathrm{r}}\right) = 4\pi\varkappa_0 B_0 \left(4\frac{\delta T}{T_0} - \frac{\delta J}{B_0} \right) + 4\pi \left(B_0 - J_0\right) \delta\varkappa . \tag{$A.86$}$$

Similar as in the static case equation ($A.76$) provides the following expression for the temperature fluctuation

$$\begin{aligned} \frac{\delta T}{T_0} &= \left[4 + i\frac{\omega}{\omega_{\mathrm{R}}} + \left(1 - J_0/B_0\right) \varkappa_{\mathrm{T}} \right]^{-1} \\ &\quad \times \left\{ \frac{\delta J}{B_0} + \frac{1}{4\pi\varkappa_0 B_0} \frac{\partial}{\partial m}\left(\delta L_{\mathrm{c}}\right) + \left[i\frac{\omega}{\omega_{\mathrm{R}}} \nabla_{\mathrm{ad}} - \left(1 - J_0/B_0\right) \varkappa_{\mathrm{p}} \right] \frac{\delta p_{\mathrm{g}}}{p_{\mathrm{g}0}} \right\} , \end{aligned} \tag{$A.87$}$$

where

$$\omega_{\mathrm{R}} = \frac{4\pi\varkappa_0 B_0}{c_{\mathrm{p}0} T_0 \nabla_{\mathrm{ad}}} , \tag{$A.88$}$$

is the radiative relaxation rate, cf. equation (3.13).

The perturbation of the non-local turbulent fluxes and mathematically averaged superadiabatic gradient increase the order of the system of equations by six and may be written in the form such as for the convective heat flux, for example

$$\begin{aligned} &\frac{\alpha_{\mathrm{c}}^2}{a^2} \frac{\partial}{\partial \ln p_0} \left[\frac{\partial}{\partial \ln p_0}\left(\delta F_{\mathrm{c}}\right) - \frac{\partial}{\partial \ln p_0} \left(\frac{\delta p}{p_0} \right) \frac{\partial F_{\mathrm{c}}}{\partial \ln p_0} \right] = \\ &\qquad \delta F_{\mathrm{c}} - \delta F_{\mathrm{c}}^{\mathrm{loc}} + \left(F_{\mathrm{c}} - F_{\mathrm{c}}^{\mathrm{loc}} \right) \frac{\partial}{\partial \ln p_0} \left(\frac{\delta p}{p_0} \right) , \end{aligned} \tag{$A.89$}$$

where $F_{\mathrm{c}}^{\mathrm{loc}}$ represents the source function, computed according to the time-dependent, local mixing-length theory, and $\delta F_{\mathrm{c}}^{\mathrm{loc}}$ denotes the Lagrangian perturbation to it.

The system of equations defined above is of tenth order and is implemented as a system of first order differential equations in the following form

$$\frac{\partial}{\partial \ln p_0}\left(\frac{\delta r}{r_0}\right) = \tilde{\mu}\frac{p_0 r_0}{Gm\rho_0}\left[3\frac{\delta r}{r_0} + \frac{\alpha_0}{1-\nu_1}\left(\frac{\delta p}{p_0} - \frac{\delta p_\mathrm{t}}{p_0}\right) - \delta_0\frac{\delta T}{T_0}\right], \tag{A.90}$$

$$\begin{aligned}\frac{\partial}{\partial \ln p_0}\left(\frac{\delta p}{p_0}\right) = &-\frac{\delta p}{p_0} - \left[3 + \tilde{\mu}\left(1 + \frac{\omega^2}{\Omega^2}\right)\right]\frac{\delta r}{r_0} + \tilde{\mu}\nu_1\frac{p_0 r_0}{Gm\rho_0} \\ &\times\left\{(3-\Phi_0)\left[\delta_0\frac{\delta T}{T_0} - \frac{\alpha_0}{1-\nu_1}\left(\frac{\delta p}{p_0} - \frac{\delta p_\mathrm{t}}{p_0}\right) + \frac{1}{\nu_1}\frac{\delta p_\mathrm{t}}{p_0}\right] + \delta\Phi\right\},\end{aligned} \tag{A.91}$$

$$\begin{aligned}\frac{\partial}{\partial \ln p_0}\left(\frac{\delta J}{J_0}\right) = \tilde{\mu}\frac{\varkappa_0 p_0 (1-f) L_0}{16\pi^2 Gm\,(f_\mathrm{eq} J_0)}\Bigg[&\varkappa_\mathrm{T}\frac{\delta T}{T_0} + \frac{\varkappa_\mathrm{p}}{1-\nu_1}\left(\frac{\delta p}{p_0} - \frac{\delta p_\mathrm{t}}{p_0}\right) - 4\frac{\delta r}{r_0} \\ &- \frac{\delta J}{J_0} + \frac{1}{1-f}\left(\frac{\delta L}{L_0} - \frac{\delta L_\mathrm{c}}{L_0}\right)\Bigg],\end{aligned} \tag{A.92}$$

$$\frac{\partial}{\partial \ln p_0}\left(\frac{\delta L}{L_0}\right) = i\omega\tilde{\mu}\frac{4\pi r_0^4 p_0}{Gm}\frac{\delta_0 p_0}{\rho_0 L_0}\left(\frac{1-\nu_1}{\nabla_\mathrm{ad}}\frac{\delta T}{T_0} - \frac{\delta p}{p_0} + \frac{\delta p_\mathrm{t}}{p_0}\right), \tag{A.93}$$

$$\frac{\partial}{\partial \ln p_0}\left(\frac{\delta L_\mathrm{c}}{L_0}\right) = \frac{\delta z_\mathrm{L}}{L_0} + \frac{z_\mathrm{L}}{L_0}\frac{\partial}{\partial \ln p_0}\left(\frac{\delta p}{p_0}\right), \tag{A.94}$$

$$\frac{\partial}{\partial \ln p_0}\left(\frac{\delta z_\mathrm{L}}{L_0}\right) = \frac{a^2}{\alpha_\mathrm{c}^2}\left[f_\mathrm{L}(1-\varphi_\mathrm{L})\frac{\partial}{\partial \ln p_0}\left(\frac{\delta p}{p_0}\right) + \frac{\delta L_\mathrm{c}}{L_0} - f_\mathrm{L}\varphi_\mathrm{L}\left(\frac{\delta L_\mathrm{c}}{L_{\mathrm{c}0}}\right)^{\mathrm{loc}}\right], \tag{A.95}$$

$$\frac{\partial}{\partial \ln p_0}\left(\frac{\delta \mathscr{B}}{\mathscr{B}_0^{\mathrm{osc}}}\right) = \frac{\delta z_\beta}{\mathscr{B}_0^{\mathrm{osc}}} + \frac{z_\beta}{\mathscr{B}_0^{\mathrm{osc}}}\frac{\partial}{\partial \ln p_0}\left(\frac{\delta p}{p_0}\right), \tag{A.96}$$

$$\frac{\partial}{\partial \ln p_0}\left(\frac{\delta z_\beta}{\mathscr{B}_0^{\mathrm{osc}}}\right) = \frac{b^2}{\alpha_\mathrm{c}^2}\left[f_\beta(1-\varphi_\beta)\frac{\partial}{\partial \ln p_0}\left(\frac{\delta p}{p_0}\right) + \frac{\delta \mathscr{B}}{\mathscr{B}_0^{\mathrm{osc}}} - f_\beta\varphi_\beta\left(\frac{\delta\beta}{\beta_0}\right)\right], \tag{A.97}$$

$$\frac{\partial}{\partial \ln p_0}\left(\frac{\delta p_\mathrm{t}}{p_0}\right) = \frac{\delta z_\mathrm{t}}{p_0} - \frac{\delta p_\mathrm{t}}{p_0} + \frac{z_\mathrm{t}}{p_0}\frac{\partial}{\partial \ln p_0}\left(\frac{\delta p}{p_0}\right), \tag{A.98}$$

$$\frac{\partial}{\partial \ln p_0}\left(\frac{\delta z_\mathrm{t}}{p_0}\right) = \frac{a^2}{\alpha_\mathrm{c}^2}\left[\nu_1(1-\varphi_\mathrm{t})\frac{\partial}{\partial \ln p_0}\left(\frac{\delta p}{p_0}\right) + \frac{\delta p_\mathrm{t}}{p_0} - \nu_1\varphi_\mathrm{t}\left(\frac{\delta p_\mathrm{t}}{p_{\mathrm{t}0}}\right)^{\mathrm{loc}}\right] - \frac{\delta z_\mathrm{t}}{p_0}, \tag{A.99}$$

where

$$z_{\rm L} = \frac{\partial L_{\rm c}}{\partial \ln p_0}, \qquad f_{\rm L} = \frac{L_{\rm c0}}{L_0}, \qquad \varphi_{\rm L} = \frac{L_{\rm c0}^{\rm loc}}{L_{\rm c0}}, \tag{A.100}$$

$$z_\beta = \frac{\partial \mathscr{B}_0}{\partial \ln p_0}, \qquad f_\beta = \frac{\mathscr{B}_0}{\mathscr{B}_0^{\rm osc}}, \qquad \varphi_\beta = \frac{\beta_0}{\mathscr{B}_0}, \tag{A.101}$$

$$z_{\rm t} = \frac{\partial p_{\rm t}}{\partial \ln p_0}, \qquad \nu_1 = \frac{p_{\rm t0}}{p_0}, \qquad \varphi_{\rm t} = \frac{p_{\rm t0}^{\rm loc}}{p_{\rm t0}}, \tag{A.102}$$

and the constant value $\mathscr{B}_0^{\rm osc}$ denotes the peak to peak amplitude of the mathematically averaged superadiabatic lapse rate, defined as

$$\mathscr{B}_0^{\rm osc} = {\rm Max}\left[\mathscr{B}_0\left(p\right)\right] - {\rm Min}\left[\mathscr{B}_0\left(p\right)\right] . \tag{A.103}$$

The supplementary equation for the temperature fluctuation, equation (*A*.87), can be rewritten in terms of the dependent variables with the help of equations (*A*.76), (*A*.93) and (*A*.94). Neglecting the dynamical correction factor for the pressure gradient, $\tilde{\mu}$, in the continuity and momentum equations, the expression for $\delta T/T_0$ becomes

$$\begin{aligned}\frac{\delta T}{T_0} = & \left[4 + i\frac{\omega}{\omega_{\rm R}} + \left(1 - \frac{J_0}{B_0}\right)\varkappa_{\rm T}\right]^{-1} \left\{\frac{J_0}{B_0}\frac{\delta J}{J_0} + i\frac{\omega}{\omega_{\rm R}}\nabla_{\rm ad}\frac{1}{1-\nu_1}\left(\frac{\delta p}{p_0} - \frac{\delta p_t}{p_0}\right)\right. \\ & \left. + \left(1 - \frac{J_0}{B_0}\right)\left[\frac{\delta z_{\rm L}}{z_{\rm L}} - \left(4 + \frac{\omega^2}{\Omega^2}\right)\frac{\delta r}{r_0} - \frac{\delta p}{p_0} - \frac{\varkappa_{\rm p}}{1-\nu_1}\left(\frac{\delta p}{p_0} - \frac{\delta p_t}{p_0}\right)\right]\right\} . \end{aligned} \tag{A.104}$$

Similar as in the equilibrium model, the requirement of decaying solutions for the turbulent flux perturbations outside the overturning layers, provide us six additional boundary conditions. In a local theory for convection the turbulent fluxes and their pulsationally induced perturbations become instantaneously zero in the convectively stable layers adjoining the overturning layers. Thus at the boundaries of the convection zone $\varphi_{\rm L} \to 0$ and $\varphi_{\rm t} \to 0$ and the equations (*A*.95), (*A*.99), (*A*.38) and (*A*.42) are reduced to

$$\frac{\partial}{\partial \ln p_0}\left(\frac{\delta z_{\rm L}}{L_0}\right) = \frac{a^2}{\alpha_{\rm c}^2}\left[f_{\rm L}\frac{\partial}{\partial \ln p_0}\left(\frac{\delta p}{p_0}\right) + \frac{\delta L_{\rm c}}{L_0}\right] , \tag{A.105}$$

$$\frac{\partial}{\partial \ln p_0}\left(\frac{\delta z_{\rm t}}{p_0}\right) = \frac{a^2}{\alpha_{\rm c}^2}\left[\nu_1\frac{\partial}{\partial \ln p_0}\left(\frac{\delta p}{p_0}\right) + \frac{\delta p_{\rm t}}{p_0}\right] - \frac{\delta z_{\rm t}}{p_0} , \tag{A.106}$$

$$\frac{d^2 f_{\rm L}}{d \ln p^2} = \frac{a^2}{\alpha_{\rm c}^2} f_{\rm L} , \tag{A.107}$$

$$\frac{d^2\,\nu_1}{d\ln p^2} \;=\; \frac{a^2}{\alpha_{\rm c}^2}\left[\nu_1 - \frac{d\,\nu_1}{d\ln p}\right]\,. \tag{A.108}$$

Since Eq. (A.107) and Eq. (A.108) appear to have constant coefficients, their general solution may be written as

$$\psi \;=\; A\,e^{\lambda\ln p}\,, \tag{A.109}$$

where ψ is either of $f_{\rm L}$ or ν_1 and $\lambda = +a/\alpha_{\rm c}$ above the convection zone and $-a/\alpha_{\rm c}$ below it. Inserting solution (A.109) into the equations (A.94), (A.105), (A.98) and (A.106) and comparing the coefficients of the resulting expressions, the four additional boundary conditions become

$$\frac{a}{\alpha_{\rm c}}\,\frac{\delta F_{\rm c}}{L_0} \;=\; \pm\frac{\partial}{\partial\ln p_0}\left(\frac{\delta F_{\rm c}}{L_0}\right)\,, \tag{A.110}$$

and

$$\frac{a}{\alpha_{\rm c}}\,\frac{\delta p_{\rm t}}{p_0} \;=\; \pm\frac{\partial}{\partial\ln p_0}\left(\frac{\delta p_{\rm t}}{p_0}\right)\,. \tag{A.111}$$

Finally the remaining two boundary conditions are obtained from the requirement

$$\delta\beta \;=\; \delta\mathscr{B}\,, \tag{A.112}$$

above and below the overturning layers.

Thus the equations of the linear eigenvalue problem (A.90)-(A.99) can be solved numerically with subject to the boundary conditions (A.60), (A.69), (A.70), (A.79), (A.82), (A.110), (A.111) and (A.112).

B. Coefficients for Gough's time-dependent mixing-length equations

The coefficients of the linearized perturbations of the turbulent fluxes and shape parameter, as expressed by the equations (2.88), (2.89) and (2.90), are summarized below according to Gough (1977) and Baker & Gough (1979):

$$W_{10} = \frac{\delta g}{g_0} + \frac{\delta(\delta)}{\delta_0} + \frac{\delta(\Delta)}{\Delta_0} - \epsilon^2\kappa_{10} - \left(1-\epsilon^2\right)\mu_{10} + \frac{2i}{\tilde{\sigma}}\frac{(1+\epsilon)\,\mu_{11} - \epsilon\,(1-i\tilde{\sigma})\,\kappa_{11}}{2-i\tilde{\sigma}\,(1-\epsilon)} + 2\,(\Phi_0-1)\,\frac{\delta\chi}{\chi_0}\,, \tag{B.1}$$

$$W_{11} = -\frac{2i}{\tilde{\sigma}}\,\frac{(1+\epsilon)\,\mu_{11} - \epsilon\kappa_{11}}{2+i\tilde{\sigma}\,(1-\epsilon)}\,, \tag{B.2}$$

$$W_{12} = (1+\epsilon)\,\mu_{10} - \epsilon\kappa_{10}\,, \tag{B.3}$$

$$W_{21} = -2\left[\left(W_{11} - \frac{\delta\ell}{\ell_0}\right)\left(1+i\frac{\omega}{\tilde{\sigma}}\right)^{-1} - \frac{\delta r}{r_0}\right], \tag{B.4}$$

$$\Theta_{10} = W_{10} + W_{12} + \Phi_{10}\,, \tag{B.5}$$

$$\Theta_{11} = (1+i\tilde{\sigma})\,W_{11} + \Phi_{11} + \frac{\delta T}{T_0} - \left(\frac{\delta g}{g_0}\right) - \frac{\delta(\delta)}{\delta_0} - i\tilde{\sigma}\Phi_0^{-1}\left(\frac{\delta\rho}{\rho_0} + 2\frac{\delta r}{r_0}\right), \tag{B.6}$$

$$\Theta_{12} = W_{12}\,, \tag{B.7}$$

$$\Phi_{10} = -2\left(1-\Phi_0^{-1}\right)\left(3\frac{\delta r}{r_0} + \frac{\delta\rho}{\rho_0} + \Phi_0\frac{\delta\chi}{\chi_0}\right), \tag{B.8}$$

$$\Phi_{11} = 2\left(1-\Phi_0^{-1}\right)\left(3\frac{\delta r}{r_0} + \frac{\delta\rho}{\rho_0}\right), \tag{B.9}$$

where

$$\frac{\delta g}{g_0} = -\left(2 + \frac{\omega^2 r^3}{G\,m}\right)\frac{\delta r}{r_0}\,, \tag{B.10}$$

$$2\mu_{10} = -\Phi_{10}\,, \tag{B.11}$$

$$2\mu_{11} = \delta_p\frac{\delta p}{p_0} + (\delta_T - 1)\,\frac{\delta T}{T_0} - \Phi_0^{-1}\tilde{\sigma}\,(1+\epsilon)^{-1}\left[\tilde{\sigma}\,(1-\epsilon) - 2i\epsilon\right]\left(\frac{\delta\rho}{\rho_0} + 2\frac{\delta r}{r_0}\right) - 2\left(1-\Phi_0^{-1}\right)\left(\frac{\delta\rho}{\rho_0} + 3\frac{\delta r}{r_0}\right) + \frac{\delta\beta}{\beta_0} + \frac{\delta g}{g_0}\,, \tag{B.12}$$

$$2\mu_{12} = \frac{\delta g}{g_0} + \frac{\delta(\delta)}{\delta_0} + \frac{\delta\beta}{\beta_0} - \frac{\delta T}{T_0} + 2\,(\Phi_0-1)\,\frac{\delta\chi}{\chi_0}\,, \tag{B.13}$$

$$\kappa_{10} = -2\phi_0 \left[\left(2 - 3\Phi_0^{-1}\right) \frac{\delta r}{r_0} + \left(1 - \Phi_0^{-1}\right) \frac{\delta \rho}{\rho_0} + \frac{\delta H_\mathrm{p}}{H_{\mathrm{p}0}} - \frac{\delta \chi}{\chi_0} \right], \tag{B.14}$$

$$\begin{aligned} \kappa_{11} = {} & 2\phi_0 \left[\left(2 - 3\Phi_0^{-1}\right) \frac{\delta r}{r_0} + \left(1 - \Phi_0^{-1}\right) \frac{\delta \rho}{\rho_0} \right] + 3\frac{\delta T}{T_0} + (1 - 2\phi) \frac{\delta \varkappa}{\varkappa_0} \\ & - \frac{\delta c_\mathrm{p}}{c_{\mathrm{p}0}} + i\tilde{\sigma} \left(\epsilon^{-1} - 1\right) / 2 \left[(1 - \delta + c_{p_T}) \frac{\delta T}{T_0} - \delta_T \frac{\nabla_{ad}}{1 - \nu_1} \frac{\delta p}{p_0} - \frac{\delta g}{g_0} \right. \\ & \left. - \frac{\delta(\delta)}{\delta_0} + 2\left(3 - 4\Phi_0^{-1}\right) \frac{\delta r}{r_0} + \left(2 - 3\Phi_0^{-1}\right) \frac{\delta \rho}{\rho_0} \right], \end{aligned} \tag{B.15}$$

$$\kappa_{12} = 3\frac{\delta T}{T_0} - 2\phi \left(\frac{\delta \ell}{\ell_0} + \frac{\delta \rho}{\rho_0} - \frac{\delta \chi}{\chi_0} \right) + (1 - 2\phi) \frac{\delta \varkappa}{\varkappa_0} - \frac{\delta c_\mathrm{p}}{c_{\mathrm{p}0}}, \tag{B.16}$$

$$\frac{\delta(\Delta)}{\Delta_0} = \frac{\delta \ell}{\ell_0} + \frac{\delta \beta}{\beta_0} - \frac{\delta T}{T_0} + \epsilon(1 - \epsilon)(\mu_{12} - \kappa_{12}), \tag{B.17}$$

$$\begin{aligned} \frac{\delta \chi}{\chi_0} = {} & \frac{1}{8} \left[\frac{\delta(\delta)}{\delta_0} - \left(2 + \frac{\omega^2}{\Omega^2}\right) \frac{\delta r}{r_0} + 2\left(\frac{\delta c_\mathrm{p}}{c_{\mathrm{p}0}} - \frac{\delta \varkappa}{\varkappa_0} \right) + 4\left(\alpha_0 \frac{\delta p_\mathrm{g}}{p_{\mathrm{g}0}} - \delta_0 \frac{\delta T}{T_0} \right) \right. \\ & \left. + 4\frac{\delta \ell}{\ell_0} + \frac{\delta \beta}{\beta_0} - 7\frac{\delta T}{T_0} \right], \end{aligned} \tag{B.18}$$

$$\begin{aligned} \frac{\delta \beta}{\beta_0} = {} & \left(1 + \frac{\delta_0 g_0}{\tilde{\mu} \beta_0 c_{\mathrm{p}0}}\right) \left(2\frac{\delta r}{r_0} + \alpha_0 \frac{\delta p_\mathrm{g}}{p_{\mathrm{g}0}} - \delta_0 \frac{\delta T}{T_0} \right) + \frac{\delta_0 g_0}{\tilde{\mu} \beta_0 c_{\mathrm{p}0}} \left\{ \left(\frac{\rho_0 c_{\mathrm{p}0} T_0}{\delta_0 p_0} \nabla + \nu_2 \delta_0 \right) \frac{\delta T}{T_0} \right. \\ & + \frac{\rho_0 c_{\mathrm{p}0} T_0}{\delta_0 p_0} \frac{\partial}{\partial \ln p_0} \left(\frac{\delta T}{T_0} \right) + (1 - \nu_2) \left(\frac{\delta c_\mathrm{p}}{c_{\mathrm{p}0}} - \frac{\delta(\delta)}{\delta_0} \right) + \tilde{\mu} \left(2 + \frac{\omega^2}{\Omega^2}\right) \frac{\delta r}{r_0} \\ & \left. + \nu_1 \frac{\partial}{\partial \ln p_0} \left(\frac{\delta p_\mathrm{t}}{p_{\mathrm{t}0}} \right) + \nu_2 \left(\frac{\delta p_\mathrm{t}}{p_{\mathrm{t}0}} - \alpha_0 \frac{\delta p_\mathrm{g}}{p_{\mathrm{g}0}} \right) \right\} \\ & - \frac{\nu_1 \delta_0 p_0}{\beta_0 \rho_0 c_{\mathrm{p}0} r_0} \left[(3 - \Phi_0) \left(\frac{\delta p_\mathrm{t}}{p_{\mathrm{t}0}} - \alpha_0 \frac{\delta p_\mathrm{g}}{p_{\mathrm{g}0}} + \delta_0 \frac{\delta T}{T_0} - \frac{\delta r}{r_0} \right) - \delta\Phi \right], \end{aligned} \tag{B.19}$$

$$\begin{aligned} \frac{\delta H_\mathrm{p}}{H_{\mathrm{p}0}} = {} & \frac{\delta p}{p_0} - \tilde{\mu} \left\{ \alpha_0 \frac{\delta p_\mathrm{g}}{p_{\mathrm{g}0}} - \delta_0 \frac{\delta T}{T_0} - \left(2 + \frac{\omega^2}{\Omega^2}\right) \frac{\delta r}{r_0} \right. \\ & \left. + \nu_1 \frac{p_0 r_0}{G m \rho_0} \left[(3 - \Phi_0) \left(\frac{\delta p_\mathrm{t}}{p_{\mathrm{t}0}} - \frac{\delta r}{r_0} \right) - \delta\Phi \right] \right\}, \end{aligned} \tag{B.20}$$

and where $\epsilon = (1 + \eta_0^2 S)^{-1/2}$, cf. equation (2.70), $\tilde{\sigma} = \omega/\sigma$, $\nu_1 = p_\mathrm{t}/p$, $\nu_2 = d\,p_\mathrm{t}/d\,p$ and $\delta\ell \sim \alpha_\mathrm{c} \delta H_\mathrm{p}$.

The remaining functional expressions $\mathscr{F}, \mathscr{G}$, and $\mathscr{H}$ appearing in equations (2.88), (2.89) and (2.90) are defined as

$$\mathscr{F} \;=\; \mathscr{I}\Gamma\left(2 - i\tilde{\sigma}\right) , \tag{B.21}$$

$$\mathscr{G} \;=\; \mathscr{J}/\mathscr{I} + \digamma\left(2 - i\tilde{\sigma}\right) , \tag{B.22}$$

$$\begin{aligned}\mathscr{H} \;=\; & \left[2\frac{\delta r}{r_0} + \left(1+\epsilon\right)\mu_{12} - \epsilon\kappa_{12}\right]\mathscr{F} \\ & - \left(2 - i\tilde{\sigma}\right)\left(W_{10} - W_{12}\right)\mathscr{F} - W_{12}\mathscr{F}\left[1 + \left(2 - i\tilde{\sigma}\right)\mathscr{G}\right] ,\end{aligned} \tag{B.23}$$

where

$$\mathscr{I} \;=\; 107\{E_1\left[2.88\left(1 + i\tilde{\sigma}\right)\right] - 320E_1\left[2.88\left(3 + i\tilde{\sigma}\right)\right]\} , \tag{B.24}$$

$$\mathscr{J} \;=\; i\frac{d\mathscr{J}}{d\tilde{\sigma}} \;=\; \frac{12}{\left(1 + i\tilde{\sigma}\right)\left(3 + i\tilde{\sigma}\right)}\left(\frac{5^{1/2}s}{2}\right)^{i\tilde{\sigma}} , \tag{B.25}$$

and where Γ, $\digamma$, and E_1 denote the gamma function, digamma function, and exponential integral of first order, and $s = 0.05$.

C. Opacity Interpolation

C.1. Introduction

The opacity calculation is far too complicated to be performed within stellar evolution programmes. Consequently, the opacity is found by interpolation in precomputed tables; hence, we are faced with the choice of a suitable interpolation procedure. In this Appendix we discuss the accuracy of interpolation methods and its influence on the results of stellar model calculations.

In our survey, we consider three interpolation schemes. The first method uses splines under tension (Cline 1974), which has been used so far in several evolution and envelope calculation programmes (e.g. Christensen-Dalsgaard 1982). The second scheme is based on birational splines which we have implemented according to Späth (1991). And finally the third method uses a C^1 interpolant defined over triangles, which enables us to interpolate data given on an irregular grid (Montefusco & Casciola 1989).

In a first step we compared these methods with an analytical formula derived by Stellingwerf (1975). This formula is a fit to the Cox-King tables using proper exponential functions and rational fractions. In order to emphasize the impact of the table grid-spacing on the interpolation errors, the comparison has been carried out with different mesh points in $\log(T)$ according to the OPAL92 (Iglesias, Rogers & Wilson 1992) and OPAL95 tables (Iglesias & Rogers 1996). In a next step we compared the opacity between model envelopes, calculated with the above introduced interpolation schemes for the solar case and a 1.5 $M_\odot$ ZAMS star. The resulting changes in the temperature gradient and velocity of sound of the model envelopes will be discussed.

C.2. Methods

In the OPAL tables the opacity is tabulated as a function of temperature, log(R), (where $R=\rho^3/T_6$, ρ being the density and $T_6 = 10^{-6}T$), and the chemical composition which can be specified by the mass-fractions of hydrogen (X) and of the heavy elements (Z). The opacity (κ) is found by interpolation in the four-dimensional space, normally using a bivariate method in the $\log(T)$–log(R) plane and applying a univariate scheme in X and Z, respectively. The following methods have been considered for interpolating the opacity in the temperature–density space:

C.2.1. Splines under tension

The geometry of the $\log(\kappa)$–surface is often such that use of the commonly applied cubic spline interpolation may give rise to large artificial variations between the grid points. Cline (1974) was guided by the physical notion of an elastic band passing through rings at the interpolation points, and which can be pulled by its ends to eliminate all unnecessary wiggles. This introduces the additional requirement that the quantity $f'' - \sigma^2 f$ varies

linearly between the given grid points, where f is the resulting piecewise interpolant with continuous first and second derivatives. Here the parameter σ determines the amount of the "tension". A small value of σ gives essentially a cubic spline behaviour, whereas a large value results in a linear interpolant f between the mesh points.

C.2.2. Rational splines

In this method rational fractions are used for the nonlinear terms of the piecewise interpolating function defined as

$$f_k(x) = a_k u + b_k t + c_k \frac{u^3}{pt+1} + d_k \frac{t^3}{pu+1}; \quad t = \frac{x - x_k}{\Delta x_k}; \quad u = 1 - t, \tag{C.1}$$

where a_k, b_k, c_k, d_k are the spline-coefficients. The coefficients are determined for the given function values defined at the grid points x_k. The parameter p specifies the pole of the rational function and defines the curvature of $f_k(x)$. The value $p = 0$ leads to the well-known cubic spline interpolant in Eq. (C.1).

C.2.3. Minimum-norm interpolation in triangles

One of the disadvantages of using spline-based interpolation methods is that the given table points have to be defined on a rectangular and regular grid. Here we introduce a scheme which interpolates arbitrarily scattered data in the plane. The interpolated value is computed in three steps. First a triangulation of the given table points is carried out, using the max–min angle optimization criterion due to Lawson (1977). In the next step, the first partial derivatives are evaluated, solving the following minimization problem

$$\text{Min} \sum_n \int_{e_i} \left[\frac{\partial^2 F}{\partial e_i^2} \right]^2 ds_i, \tag{C.2}$$

where F is an element from the set of interpolating cubic Hermite polynomials, defined on all edges e_i, $i = 1 \ldots n$, of the triangulation, and ds_i being the element of arc-length along e_i. The interpolated value is then found by the triangular blending method due to Nielson (1983) using certain minimum-norm properties, which results in an interpolant of second-order accuracy with continuous first derivatives.

C.3. Results

The relative opacity differences between the minimum-norm interpolation scheme and Stellingwerf's analytical fit to the Cox-Tabor tables are depicted in Fig. C.1 as a contour plot in the log(R)–log(T) space for different grid-spacings in temperature. Using the OPAL92 grid spacing (top panel) we encounter a local maximum of the interpolation errors in the order of 1% at a temperature of $\log(T) \approx 5.2$. They occur at a point where

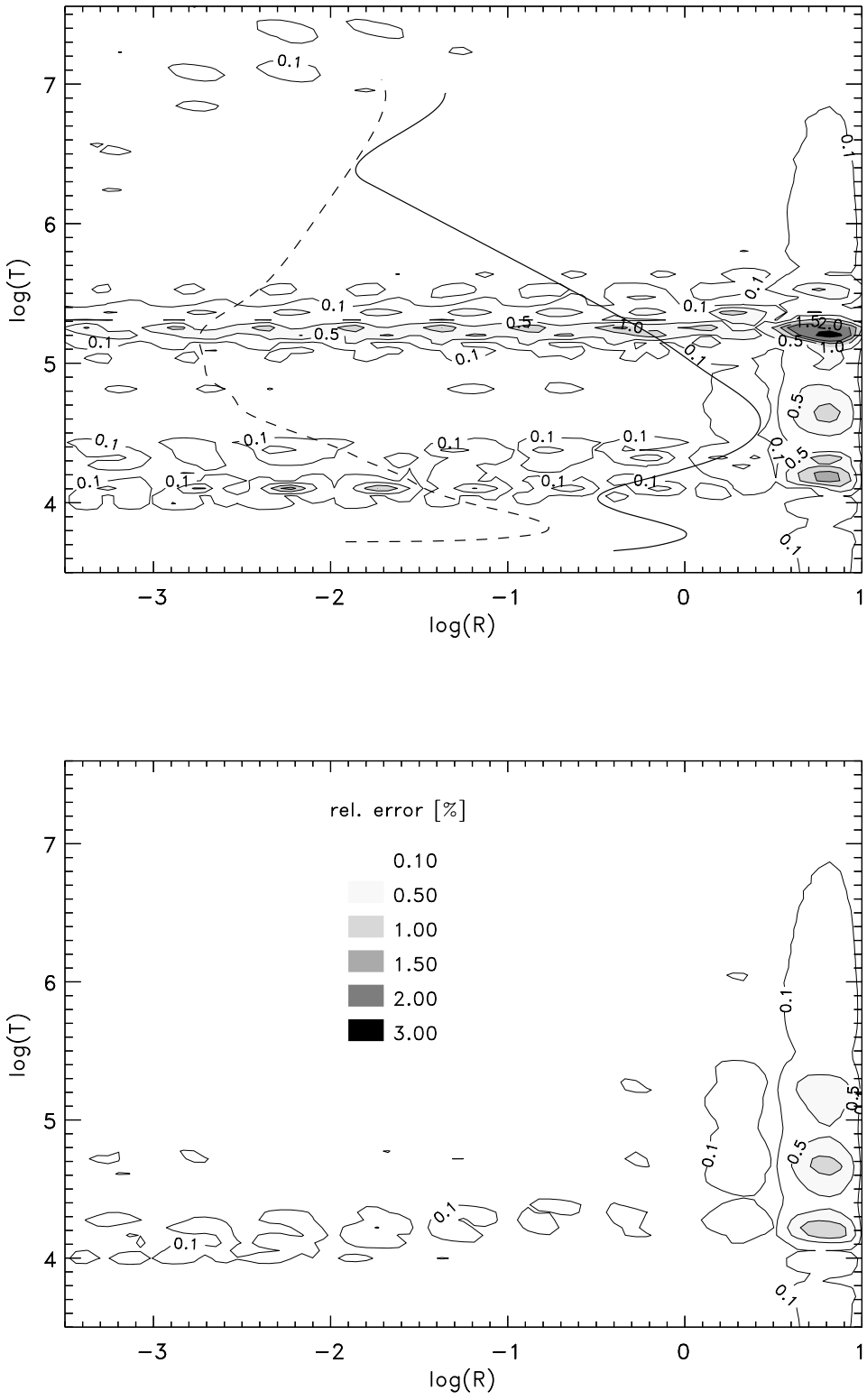

Figure C.1: Relative interpolation errors between minimum-norm scheme and Stellingwerf's analytical formula, using the grid spacing of the OPAL92 (top) and OPAL95 (bottom) tables. In the top panel the opacity tracks of model envelopes for the Sun (solid line) and a 1.5 $M_\odot$ ZAMS star (dashed line) are depicted.

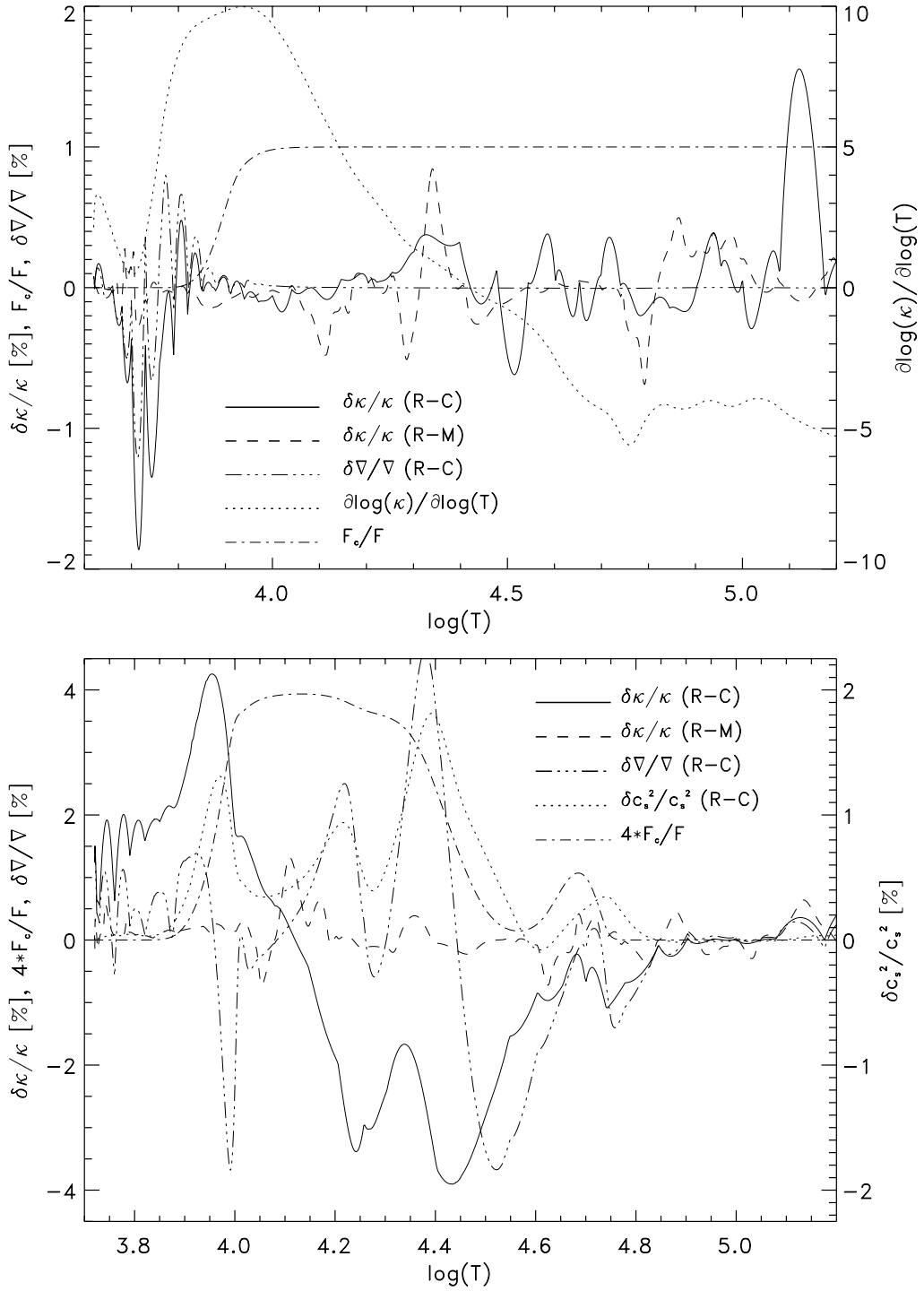

Figure C.2: Relative differences of the opacity (κ) and temperature gradient (∇) between model envelopes calculated with the rational splines scheme and Cline's spline under tension (R-C), and between the rational splines and minimum-norm method (R-M) for the solar case (top panel) and a 1.5 $M_\odot$ ZAMS star (bottom panel). In both panels the ratio between the convective to the total flux (F_c/F) is depicted. Additionally, the upper panel shows the temperature derivative of the opacity and the bottom panel the differences in the velocity of sound (c_s). For the interpolation parameters σ and p values of 0.005 and 0.1 has been used, respectively.

there is a local maximum in the step-size of the temperature grid which coincides with the falling edge of the opacity–bump at this particular temperature. The steepness of this edge increases with density or R, resulting in an absolute maximum error in the opacity of 3.4% at log(R) $\approx$ 0.8. The opacity tracks of model envelopes for the Sun and a 1.5 $M_{\odot}$ ZAMS star indicate their expected magnitude and location of interpolation errors.

Suggestions have been made (e.g. Moskalik & Dziembowski 1992) that interpolation might be improved by the inclusion of additional grid points. In the bottom panel of Fig. C.1 the results are displayed for the grid used in the OPAL95 tables, which do have a finer mesh in the temperature, revealing substantially smaller errors. The maximum value has been reduced to 1.5%, and occurs at the same R-value previously found in the OPAL92 tables.

In Fig. C.2 the opacity differences are depicted as a function of temperature between model envelopes calculated with the three interpolation schemes for the Sun and a 1.5 $M_{\odot}$ ZAMS star. For the solar case (top panel) we encounter at $\log(T) \approx 5.1$ a difference in the opacity of 1.5% between the rational splines method and Cline's splines under tension (R-C). Fortunately this occurs in the convection zone, indicated by the ratio of the convective to the total flux (F_c/F). However in the radiative atmosphere at $\log(T) \approx 3.7$ the differences exhibit a value of up to 2% , whereas the changes between the rational splines and the minimum-norm method (R-M) are substantially smaller. At this $\log(T)$ value the temperature derivative of the opacity exhibits a rapid change in a small interval, where Cline's interpolant seems to display artificial variations. The differences in the opacity for the R-C comparison became even more significant for the 1.5 $M_{\odot}$ star (bottom panel of Fig. C.2) where we found values larger than 4%.

In regions where radiation contributes to the total flux and coincides with the opacity changes, the differences in the temperature gradient are in the order of 1% for the solar case and larger than 4% for the 1.5 $M_{\odot}$ star. The resulting changes in the velocity of sound for the 1.5 $M_{\odot}$ star are in the order of up to 2% and less than 0.1% for the Sun. The implications from these results on the adiabatic frequencies are rather negligible, yielding a maximum change of less then 1 μHz. However the impact on the nonadiabatic frequencies might be more severe, since nonadiabaticity is also confined in a small domain in the upper part of the convection zone.

References

Alamanni N., Bertello L., Cavallini F., Ceppatelli G., Righini A., 1990 A&A 231, 518.

Altrock R.C., November L.J, Simon G.W., Milkey R.W., Worden S.P., 1975, SPh 43, 33.

Ando H., Osaki Y., 1975, PASJ 27, 581.

Ando H., Osaki Y., 1977, PASJ 29, 221.

Antia H.M., Chitre S.M., Narasimha D., 1982, SPh 77, 303.

Antia H.M., Chitre S.M., Gough D.O., 1988, in: Proc. IAU Symp. 123: Advances in Helio- and Asteroseismology, Christensen-Dalsgaard J., Frandsen S. (eds.), Dordrecht, p. 371.

Antia H.M., Basu S., 1996, in: Proc. SCORE'96: Solar Convection and Oscillations and their Relationship, Pijpers F.P., Christensen-Dalsgaard J., Rosenthal C.S. (eds.), Kluwer, *in press*.

Audard N., Provost J., & Christensen-Dalsgaard J., 1995, A&A 297, 427.

Auer L.H., Mihalas D., 1970, MNRAS 149, 65.

Baker N.H., 1987, in: Physical Processes in Comets, Stars and Active Galaxies, Hillebrandt W., Meyer-Hofmeister E., Thomas H.-C. (eds.), Springer-Verlag, New York, p. 105.

Baker N.H., Kippenhahn R., 1962, Zs. f. Ap. 54, 114.

Baker N.H., Kippenhahn R., 1965, ApJ 142, 868.

Baker N.H., Moore D.W., Spiegel E.A., 1971, Q. J. Mech. Appl. Math. 24, 391.

Baker N.H., Gough D., 1979 ApJ, 234,232.

Balmforth N.J., 1990, Ph.D. Thesis, University of Cambridge.

Balmforth N.J., 1992a, MNRAS 255, 603.

Balmforth N.J., 1992b, MNRAS 255, 632.

Balmforth N.J., 1992c, MNRAS 255, 639.

Balmforth N.J., Gough D.O., 1989, in: Seismology of the Sun and Sun-like Stars, Domingo V., Rolfe E. (eds.), ESA SP-286, Noordwijk, p. 47.

Balmforth N.J., Gough D.O., 1990a, SPh 128, 161.

Balmforth N.J., Gough D.O., 1990b, ApJ 362, 256.

Balona L.A., Stobie R.S., 1979, MNRAS 189, 649.

Basu S., Christensen-Dalsgaard J., Schou J., Thompson M.J., Tomczyk S., 1996, Bull. Astr. Soc. India 24, 147.

Batchelor G.K., 1956, The theory of homogeneous turbulence, Cambridge University Press.

Batchelor G.K., 1967, An Introduction to Fluid Dynamics, Cambridge University Press.

Bedding T.R., Kjeldsen H., Reetz J, Barbuy B., 1996, MNRAS 280, 1155.

Biermann L., 1932, Zs. f. Ap. 5, 117.

Biermann L., 1937, Astron. Nachr. 264, 361.

Biermann L., 1943, Zs. f. Ap. 22, 244.

Böhm-Vitense E., 1958, Zs. F. Ap. 46, 108.

Bogdan T.J., 1989, ApJ 339, 1132.

Bono G., Caputo F., Castellani V., Marconi M., Staiano L., Stellingwerf R.F., 1995, ApJ 442, 159.

Boussinesq J., 1877, Mém. pres. par div. savants a l'Academie Sci. Inst. France 23, 1.

Boussinesq J., 1903, Théorie analytique de la chaleur, Tome II, Gauthier-Villars, Paris.

Breger M., Handler G., Nather R.E., Winget D.E., Kleinman S.J., Sullivan D.J., Zhi-ping Li, Solheim J.E., Shi-Jang J., Zong-Li Liu, Wood M.A., Watson T.K., Dziembowski W.A., Serkowitsch E., Mendelson H., Clemens J.C., Krzesinski J., Pajdosz G., 1995, A&A 297, 473.

Brown T.M., 1996, in: Proc. 4th SOHO Workshop: Helioseismology, Hoeksema, J.T., Domingo V., Fleck B., Battrick B. (eds.), ESA SP-376, vol.2, ESTEC, Noordwijk, p. 177.

Brown T.M., Gilliland R.L., 1990, ApJ 350, 839.

Brown T.M., Gilliland R.L., 1994, ARA&A 32, 27.

Brown T.M., Gilliland R.L., Noyes R.W., Ramsey L.W., 1991, ApJ 368, 599.

Brown T.M., Christensen-Dalsgaard J., Weibel-Mihalas B., Gilliland R.L., 1994, ApJ 427, 1013.

Burden A.D., 1991, in: Advances in Turbulence 3, Johansson A.V., Alfredsson P.H. (eds.), Springer-Verlag, Berlin, p. 387.

Canuto V.M., 1992, ApJ 392, 218.

Canuto V.M., 1993, ApJ 416, 331.

Canuto V.M., Mazzitelli I., 1991, ApJ 370, 295.

Catala C. and the COROT team, 1995, in: Proc. GONG'94: Helio- and Astero-seismology from Earth and Space, Ulrich R.K., Rhodes Jr E.J., Däppen W. (eds.), PASPC 76, San Francisco, p. 426.

Cash J.R., Moore D.R., 1980, BIT 20, 44.

Chan K.-L., Sofia S., 1987, Science 235, 465.

Chandrasekhar S., 1950, Radiative Transfer, Clarendon Press, Oxford.

Chandrasekhar S., 1961, Hydrodynamics and Hydromagnetic Stability, Clarendon Press, Oxford.

Christensen-Dalsgaard J., 1982, MNRAS 199, 735.

Christensen-Dalsgaard J., 1986, in: Seismology of the Sun and Distant Stars, Gough D.O. (ed.), Reidel, Dordrecht, p. 23.

Christensen-Dalsgaard J., 1988, in: Proc. IAU Symp. 123: Advances in Helio- and Asteroseismology, Christensen-Dalsgaard J., Frandsen S. (eds.), Dordrecht, p. 295.

Christensen-Dalsgaard J., 1989, in: Multimode Stellar Pulsations, Kovács G., Szabados L., Szeidl B. (eds.), Konkoly Observatory, Kultura Press, Budapest, p. 153.

Christensen-Dalsgaard J., 1993, in: Inside the Stars, Weiss W.W., Baglin A. (eds.), PASPC 40, p. 483.

Christensen-Dalsgaard J., 1994, Lecture notes on Solar Oscillations (Third Edition), D.f.I. Print, Aarhus University.

Christensen-Dalsgaard J., 1995, Lecture notes on Stellar Structure and Evolution (Fourth Edition), D.f.I. Print, Aarhus University.

Christensen-Dalsgaard J., 1996, in: The Structure of the Sun, VI Canary Islands Winter School of Astrophysics, Roca Cortés T., Sánchez F. (eds.), Cambridge University Press, p. 47.

Christensen-Dalsgaard J., Gough D.O., 1976, Nature 288, 544.

Christensen-Dalsgaard J., Gough D.O., 1982, MNRAS 198, 141.

Christensen-Dalsgaard J., Frandsen S., 1983a, SPh 82, 165.

Christensen-Dalsgaard J., Frandsen S., 1983b, SPh 82, 469.

Christensen-Dalsgaard J., Frandsen S., 1984, Mem. Soc. Astron. Ital. 55, 285.

Christensen-Dalsgaard J., Berthomieu G., 1991, in: Solar Interior and Atmosphere, Cox A.N., Livingston W.C., Matthews M. (eds.), Space Science Series, University of Arizona Press, p. 401.

Christensen-Dalsgaard J., Däppen W., 1992, A&AR 4, 267.

Christensen-Dalsgaard J., Peterson J.O., 1995, A&A 299, L17.

Christensen-Dalsgaard J., Thompson M.J., 1996, MNRAS, *in press.*

Christensen-Dalsgaard J., Gough D.O., Libbrecht K.G., 1989, ApJ 341, L103.

Christensen-Dalsgaard J., Gough D.O., Thompson M.J., 1991, ApJ 378, 413.

Christensen-Dalsgaard J., Bedding T.R., Kjeldsen H., 1995, ApJ 443, L29.

Christensen-Dalsgaard J., Monteiro M.J.P.F.G., Thompson M.J., 1995, MNRAS 276, 283.

Christensen-Dalsgaard J. and the GONG team, 1996, Science 272, 1286.

Claverie A., Isaak G.R., McLeod C.P., van der Raay H.B., Roca Cortés T., 1979, Nature 282, 591.

Cline A.K., 1974, Comm. of the ACM 4, 218.

Collins G.W.II, 1978, The Virial Theorem in Stellar Astrophysics, Pachart Publishing House, Tucson Ariz.

Cox J.P., 1980, Theory of Stellar Pulsation, Princeton University Press.

Crighton D.G., Dowling A.P., Ffowcs Williams J.E., Heckl M., Leppington F.G., 1992, Modern Methods in Analytical Acoustics, Springer-Verlag, London.

Cugier H., Dziembowski W.A., Pamyatnykh A.A., 1994, A&A 291, 143.

Däppen W., 1993, in: Gong 1992: Seismic Investigation of the Sun and Stars, Brown T. (ed.), PASPC 42, San Francisco, p. 317.

Däppen W., Dziembowski W.A., Sienkiewicz R., 1988, in: Proc. IAU Symp. 123: Advances in Helio- and Asteroseismology, Christensen-Dalsgaard J., Frandsen S. (eds.), Dordrecht, p. 233.

Deubner F.-L., 1975, A&A 44, 371.

Deupree R.G., 1977, ApJ 211, 509.

Duvall T.L., Harvey J.W., 1983, Nature 302, 24.

Duvall T.L., Harvey J.W., 1984, Nature 310, 19.

Dziembowski W.A., 1977, Acta Astron. 27, 203.

Dziembowski W.A., in: 1988, Multimode Stellar Pulsations, Kovács G., Szabados L., Szeidl B. (eds.), Konkoly Observatory, Kultura, Budapest, p. 127.

Dziembowski W.A., 1995, in: Proc. GONG'94: Helio- and Astero-seismology from Earth and Space, Ulrich R.K., Rhodes Jr E.J., Däppen W. (eds.), PASPC 76, San Francisco, p. 586.

Dziembowski W.A., Pamyatnykh A.A., 1991, A&A 248, L11.

Dziembowski W.A., Pamyatnykh A.A., 1993, MNRAS 264, 204.

Eddington A.S., 1926, The internal Constitution of the Stars, Cambridge University Press.

Eggleton P., Faulkner J., Flannery B.P., 1973, A&A 23, 325.

Elsworth Y., Isaak G.R., Jefferies S.M., McLeod C.P., New R., Pallé P.L., Régulo C., Roca Cortés T., 1990, MNRAS 242, 135.

Elsworth Y., Howe R., Isaak G.R., McLeod C.P., Miller B.A., New R., Speake C.C., Wheeler S.J., 1994, ApJ 434, 801.

Elsworth Y., Howe R., Isaak G.R., McLeod C.P., Miller B.A., Wheeler S.J., New R., 1995a, in: Proc. GONG'94: Helio- and Astero-seismology from Earth and Space, Ulrich R.K., Rhodes Jr E.J., Däppen W. (eds.), PASPC 76, San Francisco, p. 318.

Elsworth Y., Howe R., Isaak G.R., McLeod C.P., Miller B.A., New R., Wheeler S.J., 1995b, in: Proc. 4th SOHO Workshop: Helioseismology, Hoeksema J.T., Domingo V., Fleck B., Battrick B. (eds.), ESA SP-376, vol.2, ESTEC, Noordwijk, p. 335.

Finger J.E., Schmidt H., 1986, Beitr. Phys. Atmosph. 59, 505.

Frandsen S., 1986, in: Seismology of the Sun and the Distant Stars, Gough D. (ed.), Reidel, Dordrecht, p. 73.

Frandsen S., 1992, in: Inside the Stars, Weiss W.W., Baglin A. (eds.), PASPC 40, p. 679.

Fridlund M., Gough D.O., Jones A., Appourchaux T., Badiali M., Catala C., Frandsen S., Grec G., Roca Cortés T., Schrijver K., 1995, in: Proc. GONG'94: Helio- and Astero-seismology from Earth and Space, Ulrich R.K., Rhodes Jr E.J., Däppen W. (eds.), PASPC 76, San Francisco, p. 416.

Fröhlich C., van der Raay H.B., 1984, in: The Hydromagnetics of the Sun, Noordwijk, ESA SP-220, p. 17.

Gabriel A.H. and the GOLF team, 1991, Adv. Space Res., vol. 11, No. 4, 103.

Gilliland R.L., 1995, in: Proc. GONG'94: Helio- and Astero-seismology from Earth and Space, Ulrich R.K., Rhodes Jr E.J., Däppen W. (eds.), PASPC 76, San Francisco, p. 578.

Gilliland R.L., Brown T.M., Kjeldsen H., McCarthy J.K., Peri M.L., Belmonte J.A., Vidal I., Cram L.E., Palmer J., Frandsen S., Parthasarathy M., Petro L., Schneider H., Stetson P.B., Weiss W.W., 1993, AJ 106, 2441.

Goldreich P., Keeley D.A., 1977a, ApJ 211, 934.

Goldreich P., Keeley D.A., 1977b, ApJ 212, 243.

Goldreich P., Kumar P., 1990, ApJ 363, 694.

Goldreich P., Kumar P., 1991, ApJ 374, 366.

Goldreich P., Murray N., 1994, ApJ 424, 480.

Goldreich P., Murray N., Kumar P., 1994, ApJ 423, 466.

Goode P.R., Strous L.H., 1996, Bull. Astr. Soc. India 24, 223.

Gough D.O., 1965, Geophys. Fluid Dyn. II (Woods Hole Oceanographic Institution), p. 49.

Gough D.O., 1969, J. Atmos. Sci. 26, 448.

Gough D.O., 1976, in: Problems of stellar convection, Spiegel E., Zahn J.-P. (eds.), Springer-Verlag, Berlin, p. 15.

Gough D.O., 1977, ApJ 214, 196.

Gough D.O., 1978, in: Proc. Workshop on Solar Rotation, Belvedere G., Paternó L. (eds.), p. 337.

Gough D.O., 1980, in: Nonradial and Nonlinear Stellar Pulsation, Hill H.A., Dziembowski W.A. (eds.), Springer-Verlag, Berlin, p. 273.

Gough D.O., 1984, Adv. Space Res. 4, 85.

Gough D.O., 1985, in: Proc. ESA Workshop on Future Missions in Solar, Heliospheric and Space Plasma Physics. Noordwijk, ESA SP-235, p. 183.

Gough D.O., 1995, in: Proc. GONG'94: Helio- and Astero-seismology from Earth and Space, Ulrich R.K., Rhodes Jr E.J., Däppen W. (eds.), PASPC 76, San Francisco, p. 551.

Gough D.O., Weiss N.O., 1976, MNRAS 176, 589.

Gough D.O., Novotny E., 1990, SPh 128, 143.

Gough D.O., Toomre J., 1991, ARA&A 29, 627.

Grec G., Fossat E., Pomerantz M., 1980, Nature 288, 541.

Grec G., Fossat E., Pomerantz M., 1983, SPh 82, 55.

Guenther D.B., 1994, ApJ 422, 400.

Guenther D.B., Demarque P., 1995, ApJ 456, 798.

Guzik J.A., Cox A.N., 1993, ApJ 411, 394.

Guzik J.A., Bradley P.A., 1995, Baltic Astron. 4, 442.

Guzik J.A., Cox A.N., Swenson F.J., 1996, Bull. Astr. Soc. India 24, 161.

Hanjalic K., Launder B.E., 1976, J. Fluid Mech. 74, 593.

Henyey L., Vardya M.S., Bodenheimer P., 1965, ApJ 142, 841.

Iglesias C.A., Rogers F.J., Wilson B.G., 1992, ApJ 397, 717.

Iglesias C.A., Rogers F.J., 1996, ApJ 464, 943.

Isaak G.R., McLeod C.P., Pallé P.L., van der Raay H.B., Roca Cortés T., 1989, A&A 208, 297.

Jefferies S.M., Pallé P.L., van der Raay H.B., Régulo C., Roca Cortés T., 1988, Nature 333, 646.

Jones W.P., Launder B.E., 1972, Int. J. Heat Mass Transfer 16, 1119.

Keller L., Friedmann A., 1924, in: Proc. First Intern. Congress Appl. Mech., Delft, p.395.

Kennely E.J., 1995, in: Proc. GONG'94: Helio- and Astero-seismology from Earth and Space, Ulrich R.K., Rhodes Jr E.J., Däppen W. (eds.), PASPC 76, San Francisco, p. 568.

Kidman R.B., Cox A.N., 1984, in: Solar Seismology from Space, Ulrich R.K., Harvey J., Rhodes E.J., Toomre J. (eds.), NASA Publ. 84, p. 335.

Kim Y.-C., Fox P.A., Sofia S., Demarque P., 1995, ApJ 442, 442.

Kjeldsen H., Bedding T.R., 1995, A&A 293, 87.

Kjeldsen H., Bedding T.R., Viskum M., Frandsen S., 1995, AJ 109, 1313.

Kosovichev A.G., 1995, in: Proc. 4th SOHO Workshop: Helioseismology, Hoeksema, J.T., Domingo V., Fleck B., Battrick B. (eds.), ESA SP-376, vol.2, ESTEC, Noordwijk, p. 165.

Kosovichev A.G., 1996, in: Proc. IAU Symp. 181: Sounding Solar and Stellar Interiors, Schmider F.-X., Provost J. (eds.), Nice Observatory, *in press.*

Kraichnan R.H., 1962, The physics of the fluids vol. 5, No. 11, 1374.

Kuhfuss R., 1986, 160, 116.

Kuhn J.R., 1996, in: The Structure of the Sun, VI Canary Islands Winter School of Astrophysics, Roca Cortés T., Sànchez F. (eds.), Cambridge University Press, p. 231.

Kumar P., Goldreich P., 1989, ApJ 103, 331.

Kurucz R.L., 1991, in: Stellar Atmospheres: Beyond Classical Models, Crivellari L., Hubney I., Hummer D.G. (eds.), Kluwer, Dordrecht, p. 441.

Kurucz R.L., 1992, Rev. Mex. Astron. Astrofis. 23, 187.

Lamb H., 1909, Proc. London Math. Soc. 7, 122.

Latour J., Toomre J., Zahn J.-P., 1981, ApJ 248, 1081.

Launder B.E., 1978, in: Turbulence, Bradshaw P. (ed.), Springer-Verlag, Berlin.

Launder B.E., Reece G.J., Rodi W., 1975, J. Fluid Mech. 68, 537.

Lawson C.L., 1977, in: Mathematical Software III, Rice J.R. (ed.), Academic Press, p. 161.

Ledoux P., Walraven T., 1958, in: Handbuch der Physik, Flügge S. (ed.), Springer-Verlag, New York, vol. 51, p.353.

Ledoux P., Schwarzschild M., Spiegel E.A., 1960, ApJ 133, 184.

Leibacher J., Stein R.F., 1971, ApJ 7, L191.

Leighton R.B., Noyes R.W., Simon G.W., 1962, ApJ 135, 474.

Libbrecht K.G., 1988, ApJ, 334, 510.

Libbrecht K.G., Woodard M.F., 1991, Science 253, 152.

Libbrecht K.G., Woodard M.F., Kaufman J.M., 1990, ApJS 74, 1129.

Libbrecht K.G., Popp B.D., Kaufman J.M., Penn M.J., 1986, Nature 323, 235.

Lighthill M.J., 1952, Proc. Roy. Soc. London A211, 564.

Lighthill M.J., 1954, Proc. Roy. Soc. London A222, 1.

Ljuboja M., Rodi W., 1981, ASME J. Heat Transfer 103, 343.

Mangeney A., Däppen W., Praderie F., Belmonte J.A., 1991, A&A 244, 351.

Marmolino C., Stebbins R.T., 1989, SPh 124, 23.

Mihalas D., 1978, Stellar Atmospheres (Second Edition), Freeman and Company, San Francisco.

Millionschikov M., 1941, Dokl. Akad. Nauk. SSSR 32, 611.

Michel E., Chevreton M., Goupil M.J., Belmonte J.A., Jiang S.Y., Alvarez M., Suran M., Soufi F., Auvergne M., Baglin A., Liu Y.Y., Vidal I., Hernandez M., Fu J.N., 1995, in: Proc. 4th SOHO Workshop: Helioseismology, Hoeksema, J.T., Domingo V., Fleck B., Battrick B. (eds.), ESA SP-376, vol.2, ESTEC, Noordwijk, p. 533.

Montefusco L.B., Casciola G., 1989, ACM TOMS 15, 365.

Monteiro M.J.P.F.G., Christensen-Dalsgaard J., Thompson M.J., 1994, A&A 283, 247.

Monteiro M.J.P.F.G., Christensen-Dalsgaard J., Thompson M.J., 1996, A&A 307, 624.

Moore, D.W., Spiegel E.A., 1964, ApJ 139, 48.

Moskalik P., Dziembowski W.A., 1992, A&A 256, L5.

Murray N., 1993, in: Gong 1992: Seismic Investigation of the Sun and Stars, Brown T. (ed.), PASPC 42, San Francisco, p. 3.

Musielak Z.E., Rosner R., Stein R.F., Ulmschneider P., 1994, ApJ 423, 474.

Nielson G.M., 1983, J. Math. Comp. 40, 253.

Öpik E.J., 1950, MNRAS 110, 559.

Orszag S.A., 1977, in: Fluid dynamics, Balian R., Peube J.-L. (eds.), Gordon and Breach.

Osaki Y., 1990, in: Progress of Seismology of the Sun and Stars, Osaki Y., Shibahashi H. (eds.), Springer-Verlag, Berlin, p. 145.

Pallé P.L., 1996, in: Proc. IAU Symp. 181: Sounding Solar and Stellar Interiors, Schmider F.-X., Provost J. (eds.), Nice Observatory, *in press*.

Prandtl L., 1925, Zs. f. angew. Math. Mech. 5, 136.

Prandtl L., 1932, Beitr. z. Phys. d. freien Atm. 19, 188.

Reif F., 1985, Fundamentals of Statistical and Thermal Physics, McGraw Hill, Singapore.

Rodi W., 1976, ZAMM 56, T219.

Rosenthal C.S., 1996, in: Proc. SCORE'96: Solar Convection and Oscillations and their Relationship, Pijpers F.P., Christensen-Dalsgaard J., Rosenthal C.S. (eds.), Kluwer, *in press*.

Rotta J., 1951, Z. Phys. 129, 547.

Scherrer P.H., Hoeksema J.T., Bush R.I., 1991, Adv. Space Res., vol. 11, No. 4, 113.

Schrijver C.J., Jiménez A., Däppen W., 1991, A&A 251, 655.

Scuflair R., Gabriel M., Noels A., Boury A., 1975, A&A 45, 15.

Seaton M.J., Yan Y., Mihalas D., Pradhan A.K., 1994, MNRAS 266, 805.

Shaviv G., Chitre S.M., 1968, MNRAS 140, 61.

Siedentopf H., 1933, Astron. Nachr. 247, 297.

Siedentopf H., 1935, Astron. Nachr. 255, 157.

Späth H., 1991, Zweidimensionale Spline Interpolations Algorithmen, Oldenburg, Munich.

Spiegel E., 1962, J. Geophys. Res. 67, 3063.

Spiegel E., 1963, ApJ 138, 216.

Spiegel E., 1966, in: Stellar Evolution, Stein R.F., Cameron A.G. (eds.), Plenum Press, New York, p. 143.

Spiegel E.A., Veronis G., 1960, ApJ, 131, 442.

Staiger J., Schmieder B., Deubner F.-L., Mattig W., 1984, Mem. Soc. Astron. Ital. 55, 147.

Stamford P.A., Watson R.D., 1981, AP&SS 77, 131.

Stebbins R.T., Goode P., 1987, SPh 110, 237.

Stein R.F., 1967, SPh 2, 385.

Stein R.F., 1968, ApJ 154, 297.

Stein R.F., Nordlund Å., 1989, ApJ 342, L95.

Stein R.F., Nordlund Å., 1991, in: Challanges to Theories of the Structure of Moderate Mass Stars, Gough D.O., Toomre J. (eds.), Springer-Verlag, Heidelberg, p. 195.

Stellingwerf R.F., 1975, ApJ 195, 441.

Stellingwerf R.F., 1976, ApJ 206, 543.

Stellingwerf R.F., 1979, ApJ 227, 935.

Stellingwerf R.F., 1980, in: Nonradial and Nonlinear Stellar Pulsation, Hill H.A., Dziembowski W.A. (eds.), Springer-Verlag, Berlin, p. 50.

Stellingwerf R.F., 1982, ApJ 262, 330.

Tassoul M., 1980, ApJS 43, 469.

Taylor G.I., 1915, Phil. Trans. A 215, 1.

Taylor G.I., 1932, Proc. Roy. Soc. A, 135, 685.

Taylor P.A., Gent P.R., 1974, Boundary Layer Met. 7, 349.

Tooth P.D., Gough D.O., 1989, in: Seismology of the Sun and Sun-like Stars, Domingo V., Rolfe E. (eds.), Noordwijk, ESA SP-286, p. 463.

Toutin T., Fröhlich C., 1992, A&A 257, 287.

Trampedach R., 1996, in: Proc. SCORE'96: Solar Convection and Oscillations and their Relationship, Pijpers F.P., Christensen-Dalsgaard J., Rosenthal C.S. (eds.), Kluwer, *in press.*

Tripathy S.C., Christensen-Dalsgaard J., 1996, Bull. Astr. Soc. India 24, 129.

Ulrich R.K., 1970a, ApJ 162, 993.

Ulrich R.K., 1970b, Ap&SS 7, 71.

Unno W., 1964, Trans. Int. astr. Un. XII(B), 555.

Unno W., 1967, PASJ 19, 140.

Unno W., Kato S., 1962, PASJ 14, 416.

Unno W., Spiegel E.A., 1966, PASJ 18, 85.

Unno W., Osaki Y., Ando H., Saio H., Shibahashi H., 1989, Nonradial Oscillations of Stars (Second Edition), University of Tokyo Press.

Vitense E., 1953, Zs. f. Ap., 32, 135.

Vernazza J.E., Avrett E.H., Loeser R., 1981, ApJS 45, 635.

Watson R.D., 1988, Ap&SS 140, 255.

White F.M., 1991, Viscous Fluid Flow (Second Edition), McGraw-Hill, New York.

Woodard M, Hudson H., 1983a, Nature 305, 589.

Woodard M, Hudson H., 1983b, SPh 82, 67.

Xiong D., 1980, Scientia Sinica XXIII 9, 1139.

Xiong D., 1986, A&A 167, 239.

Yamaguchi S., 1963, PASJ 15, 412.

References associated to the Thesis

List of publications with the author of this thesis as co-author or author and which have been published during the PhD project on subjects associated to this thesis.

Christensen-Dalsgaard J., Bedding T., Houdek G., Kjeldsen H., Rosenthal C.S., Trampedach R., Monteiro M.J.P.F.G., Nordlund, Å., 1995, in: Proc. IAU Colloq. 155: Astrophysical Applications of Stellar Pulsation, Stobie R.S., Whitelock P.A. (eds.), PASP 83, p. 447.

Houdek G., 1997, in: Proc. IAU Symp. 181: Sounding Solar and Stellar Interiors, Schmider F.-X., Provost J. (eds.), Nice Observatory, Poster Volume, p. 227

Houdek G., Rogl J., 1996, Bull. Astr. Soc. India 24, 317.

Houdek G., Balmforth N., Christensen-Dalsgaard J., 1995, in: Proc. 4th SOHO Workshop: Helioseismology, Hoeksema, J.T., Domingo V., Fleck B., Battrick B. (eds.), ESA SP-376, vol.2, ESTEC, Noordwijk, p. 447.

Houdek G., Rogl J., Balmforth N., Christensen-Dalsgaard J.,1995, in: Proc. GONG'94: Helio- and Astero-seismology from Earth and Space, Ulrich R.K., Rhodes Jr E.J., Däppen W. (eds.), PASPC 76, San Francisco, p. 641.

Rosenthal C.S., Christensen-Dalsgaard J., Houdek G., Monteiro M.J.P.F.G., Nordlund Å., Trampedach R., 1995, in: Proc. 4th SOHO Workshop: Helioseismology, Hoeksema, J.T., Domingo V., Fleck B., Battrick B. (eds), ESA SP-376, vol.2, ESTEC, Noordwijk, p. 459.

Zusammenfassung

Die Entdeckung der Variabilität der Sonne mit Perioden um 5 Minuten zu Beginn der 60-er Jahre (Leighton *et al.* 1962) und deren Identifikation als globale nicht-radiale Oszillationen (Deubner 1975) war eine der wichtigsten Entwicklungen in der Geschichte der Sternenphysik. In den letzten 25 Jahren wurden massive Anstrengungen unternommen, die diesen beobachteten Schwingungen zugrundeliegende Physik, zu verstehen. Es entstand eine neue Disziplin der Astrophysik, die *Helioseismologie*. Mit Hilfe dieser neuen Methode konnten zahlreiche, detaillierte Informationen über die Eigenschaften der Sonne und ihrer Physik im Inneren gewonnen werden. Diese Informationen stellen ferner einen wichtigen Beitrag zur Verbesserung der Theorie über den Aufbau der Sonne und ihrer Entwicklung dar. Trotz der enormen Fortschritte in der Helioseismologie gibt der Mechanismus, der für die Anregung von sonnenähnlichen Schwingungen verantwortlich ist, Anlaß für zahlreiche Diskussionen. Im Gegensatz zu den klassischen Variablen, z.B. den Cepheiden, zeigen sonnenähnliche Sterne, sowie Rote Riesen, ausgeprägte Konvektionszonen in den äußeren Schichten des Sternes auf. Um den Energieaustausch zwischen der Pulsation und der Konvektion einerseits und dem Strahlungsfluß andererseits beschreiben zu können, wird eine zeitabhängige Konvektionstheorie sowie eine genaue Beschreibung des Strahlungsfeldes (z.B. Eddington Approximation) benötigt. Zeitabhängige Konvektionstheorien, die die Kopplung der Oszillationen mit dem turbulenten Geschwindigkeitsfeld beschreiben, stehen derzeit nur näherungsweise zur Verfügung. Mit Hilfe der Konvektionstheorie von Gough (1976, 1977) wurde von Balmforth (1992a,c) die Annahme erhärtet, daß die Oszillationen in der Sonne intrinsisch gedämpft und stochastisch angeregt sind. Die stochastische Anregung der beobachteten Pulsation in der Sonne wird durch die Emission von Schallwellen der turbulenten Multipol-Quellen verursacht (Goldreich & Keeley 1977b). Ferner konnte Balmforth mit dieser Theorie die Geschwindigkeits-Amplituden der Sonnenschwingungen abschätzen, die in guter Übereinstimmung mit den beobachteten Daten stehen.

Die derzeit einzigen Amplituden-Berechnungen von sonnenähnlichen Schwingungen in anderen Sternen wurden von Christensen-Daalsgard & Frandsen (1983b) veröffentlicht, die eine sehr vereinfachte Beschreibung der Kopplung zwischen Pulsation und Konvektion verwendeten. Es ist das Hauptziel dieser Dissertation, die Schwingungseigenschaften von Hauptreihensternen mit Hilfe der nichtlokalen, zeitabhängigen Mischungswegtheorie von Gough zu untersuchen, sowie die Geschwindigkeits- und Leuchtkraftamplituden von stochastisch angeregten Schwingungen in Sternen zu berechnen.

Eine Methode für das Testen von Konvektionstheorien ist der Vergleich von berechneten und beobachteten Pulsationsfrequenzen. Es konnte für die Sonne und für den Hauptreihenstern η-Bootis gezeigt werden, daß der Beitrag des turbulenten Druckgradienten zum hydrostatischen Gleichgewicht die vorhandene Diskrepanz zwischen theoretischen und beobachteten Frequenzen deutlich reduziert. Diese Ergebnisse sind auch in guter Übereinstimmung mit den Resultaten von Rosenthal *et al.* (1995), die mit Hilfe von hydrodynamischen Simulationen erzielt wurden. Der Einfluß nicht-adiabatischer Effekte sowie der Fluktation des tubulenten Druckes (Impulsflusses) führten jedoch zu einer Vegrößerung der obigen Diskrepanz zwischen berechneten und beobachteten Frequenzen.

Die Fluktation des Impulsflusses stellt jedoch den wichtigsten Beitrag zur Dämpfung der Oszillationen in sonnenähnlichen Sternen dar. Ohne ihre Berücksichtigung in der

Stabilitätsanalyse würden fast alle Pulsationsmoden überstabil sein, wie es Balmforth (1992a) für die Sonne berichtete. Für Sternmodelle mit einer Effektivtemperatur von $\log T \lesssim 3.85$ wurden ausgeprägte Instabilitätsstreifen für die fundamentale radiale Schwingung und deren höheren Ordnungen gefunden. Darüber hinaus konnte gezeigt werden, daß die Rückkehr zur Stabilität am roten Rand des unteren δ Scuti Instabilitätsstreifens ausschließlich durch die Variation des Impulsflusses erfolgt.

Die berechneten Amplituden von stochastisch angeregten radialen Oszillationsmoden in Hauptreihensternen, in denen alle Schwingungen stabil sind, vergrößern sich mit Alter und Masse der Sterne. Für einen $1.5\,M_\odot$ Stern vom Spektraltyp F1 wird eine Leuchtkraftamplitude voraus gesagt, die ~ 16 mal größer ist als jener Wert, der für die Sonne gemessen und berechnet wird. Die derzeit einzige Beobachtung von möglichen sonnenähnlichen Oszillationen in anderen Sternen wurde von Kjeldsen *et al.* (1995) für η Boo berichtet, für welchen die berechneten Amplituden in guter Übereinstimmung mit der Beobachtung sind. Die hier berechneten Amplituden stellen unter anderem eine große Hilfe für die Selektion von 'Targetsternen' dar und für die Entscheidung, ob die Schwankungen in der Leuchtkraft oder in der Geschwindigkeit eines bestimmten Sternes optimal beobachtet werden können (solche Informationen sind nicht nur für erdgebundene Beobachtung von Bedeutung, sondern auch für Weltraumprojekte, wie z.B. COROT, das Pulsationsfrequenzen, Amplituden und andere Oszillationseigenschaften in mehreren sonnenähnlichen Sternen messen wird).

Durch die rasante Entwicklung in der Beobachtungstechnologie und durch den Einsatz von Satelliten stehen sehr genaue Beobachtungsdaten von Phasenverschiebungen zwischen verschiedenen Oszillationsarten schon heute für die Sonne zur Verfügung. Diese Beobachtungsdaten geben Auskunft über die komplizierte Oberflächenstruktur der Sonne sowie deren Effekte auf die seismische Qualität der globalen Oszillationen. Mit Hilfe der nichtlokalen, zeitabhängigen Mischungswegtheorie wurden Berechnungen von Phasenverschiebungen zwischen verschiedenen Arten von radialen Eigenfunktionen in der Sonnenatmosphäre durchgeführt und die Modellresultate mit den IPHIR Beobachtungsdaten verglichen. Mit diesen Simulationsrechnungen konnte gezeigt werden, daß durch die Berücksichtigung der dynamischen Effekte der Konvektion (Fluktationen des turbulenten Druckes sowie des konvektiven Flusses), eine wesentlich bessere Übereinstimmung mit den Beobachtungen erreicht werden kann. Phasenverschiebungen und Amplitudenverhältnisse zwischen Oszillationen in verschiedenen Farben und im integrierten Licht können auch für die Identifikation von radialen und nicht-radialen Pulsationsmoden in anderen Sternen, wie z.B. vom Typ δ Scuti, von großer Hilfe sein. Für den relativ kalten δ Scuti Stern FG Vir wurde der Einfluß der dynamischen Effekte der Konvektion auf die Form der Eigenfunktionen diskutiert und aufgezeigt, daß diese Effekte für die Modellierung von genaueren Eigenfunktionen von großer Wichtigkeit sind.

Eines der großen Ziele für die zukünftige Verbesserung von Sternmodellen und der zugrundeliegenden Physik wäre die Möglichkeit, die theoretischen Pulsationseigenschaften von nicht-radialen Schwingungen mit Daten von einer großen Anzahl von Sternen zu vergleichen, die mit netzwerkweiten Beobachtungs-Kampagnen oder mit Satelliten gewonnen wurden. Mit Hilfe einer zeitabhängigen Konvektionstheorie für nicht-radiale Oszillationen (z.B. durch Erweiterung der obigen Mischungswegtheorie von Gough) könnten dann weitere Erkenntnisse über den turbulenten Energietransport in Sternen erworben werden.

Acknowledgements

The last years have been an exciting time for me not only in the specific aspect related to my scientific work, but also due to the wonderful experience of having met many people associated directly or indirectly with the astronomical community and from whom I have gained invaluable knowledge and wisdom in every respect of daily life. It is therefore a great pleasure having the possibility to express my special thank to all the people and organizations who have helped to make this work possible.

My deepest gratitude I would like to express to Jørgen Christensen-Dalsgaard for his invaluable help and scientific advice during the last few years and for the assistance and guidance in the preparation of this thesis. Many thanks also for the wonderful time I had the pleasure and privilege to work with him during my visits to Aarhus and for the many enlightening discussions which contributed crucially to my understanding in this scientific field.

The door to the world of astrophysics has been opened for me by the pleasurable and inspiring lectures of Werner Däppen during his stay in Vienna at the Institute for Astronomy and which I have since come to appreciate. My greatest thanks also for the encouragement and the help in so many ways to my career as an Astronomer.

I am indebted to Werner Weiss, my advisor in Vienna, for pointing me to the interesting subject of this project, for contacts with people in Denmark and USA and for helpful discussions in many aspects related to this work.

Also thanks to Michel Breger for revealing me some of the mysteries associated with the observation of δ Scuti stars and pointing me to helpful references.

I am very grateful to Neil Balmforth for providing me all the programmes and related informations for this project and for enlightening discussions.

Special thanks to Søren Frandsen and Hans Kjeldsen for many helpful conversations, to Poul Erik Nissen for showing me one of the most beautiful landscapes of Jutland and to all my colleagues and friends at the astronomy department in Aarhus, especially Nathalie Audard for the exciting trips with the motor bike, Sarbani Basu for the pleasure we had in solving problems for the exercise classes, Colin Rosenthal for his contribution to my understanding of stellar convection, Regner Trampedach for hospitality and Michael Viskum for enjoyable discussions. Also thanks to Helene Nielsen, Anette Skovgaard and Susanna Toldi for the help with dealing in many practicalities during my stays in Aarhus.

At my home institute in Vienna I am thankful to Fritz Kupka for explaining me many issues of the newest theories of turbulent convection and for help of Michael Gelbmann, Ulrike Heiter, Rainer Kuschnig, Ernst Paunzen and Günter Wuchterl.

Finally, my deepest thanks to Jadzia Donatowicz for being such good company during the last years and for all her encouragement and invaluable help and support in many moments of my life.

For financial support, I would like to thank the Fonds zur Förderung der Wissenschaftlichen Forschung for travel support, the Austrian Department for Science and Research, the Institut for Fysik og Astronomi at the Aarhus University and the Danmarks Grundforskningsfond through the establishment of the Theoretical Astrophysics Center.

Contents

List of Figures

List of Tables